RESULTS OF GROUND MOTION AND AIRBLAST MEASUREMENTS, PROJECT ESSEX 1, PHASE 1, VOLUMES 1 AND 2

L. J. Vortman, et al

Sandia Laboratories

Prepared for:

Atomic Energy Commission
Defense Nuclear Agency

November 1974

Issued by Sandia Laboratories, operated for the United States Atomic Energy Commission by Sandia Corporation.

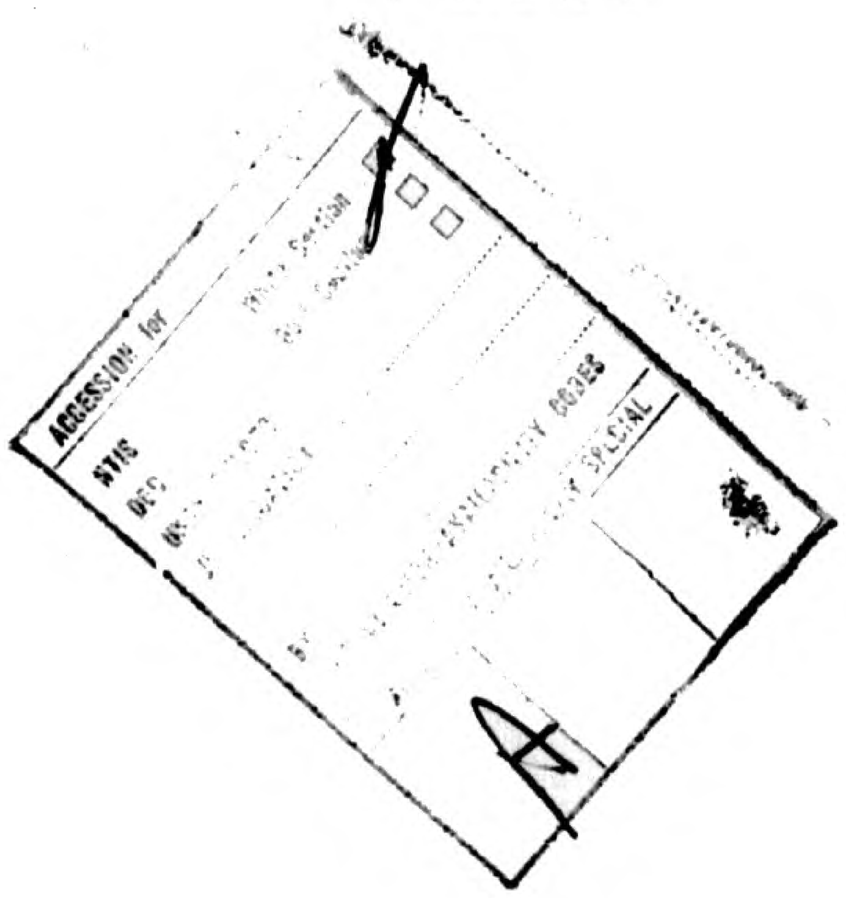

SLA-73-0918
DNA PR 0006
Unlimited Release
Printed November 1974

RESULTS OF GROUND MOTION AND AIR BLAST MEASUREMENTS, PROJECT ESSEX I, PHASE 1

Volume I of 2

L. J. Vortman
Underground Physics Division

J. A. Beyeler
Measurements Development Division I

Sandia Laboratories
Kirtland AFB East
Albuquerque, New Mexico 87115

ABSTRACT

Four high-explosive charges were detonated in saturated soil to simulate employment of atomic demolition munitions. Two 10-ton charges were buried 12 meters deep, one stemmed and one with a small open hole; one 10-ton stemmed charge and one 8.5-ton unstemmed charge were at 6 meters. On each shot instruments measured shock propagation above the charge, shock stress and ground acceleration at one position at half-shot depth and at three shot-depth positions, ground-surface acceleration at four to five positions, shock pressure in the open holes of the unstemmed shots, and above-ground airblast at several distances. Ground-surface displacement was measured with high-speed photography. Peak stresses ranged from 0.05 to 3 kilobars. These measurements were made to provide information on effects of charge burial depth and stemming, as well as physical data that could be used to verify the hydrodynamic codes being used for numerical simulation of ADM explosions. An internally consistent set of measurements of all parameters was obtained on each shot. The measurements were especially well suited to the objectives but heterogeneity of the soil obscured subtle effects of stemming differences and detracted from the precision with which codes can be verified from the measured data. Suppression of airblast was found to be a reasonable analogue of nuclear radioactivity suppression and a promising alternative to the use of a radioactivity simulant for that purpose. Airblast measurements on five 1,000-pound surface and near-surface detonations showed that differences in meteorology on the different days the shots were fired obscured the subtle differences that could be attributed to charge position.

ACKNOWLEDGMENTS

Project Essex I, Phase 1 was undertaken by the U.S. Army Engineer Waterways Experiment Station, Explosive Excavation Research Laboratory (EERL), Livermore, California, was supported by the Defense Nuclear Agency, and was designed to develop techniques for simulating nuclear cratering using chemical explosives, with special emphasis on atomic demolition munitions. Particular attention was given to stemming effects. Because Sandia Laboratories (SL) has an interest in earth-penetrating weapon systems, SL funded EERL for the instrumentation of a partially stemmed shot in the series to represent the stemming that would occur naturally behind an earth penetrator. In addition to funding the instrumentation for that event, SL also funded half the cost of the instrumentation described in this report for the corresponding fully stemmed shot, on the basis that the results of comparable instrumentation for that shot and the partially stemmed shot were necessary for proper evaluation of the latter. The balance of the instrumentation described in this report was funded on a reimbursable basis by EERL.

The authors express their appreciation to CPT. W. T. Harvey and MAJ. G. M. Miller, Jr., for their cooperation in the planning and execution of the project, and to C. W. Moses, SL Albuquerque, for his technical liaison between EERL and SL. Special acknowledgment is made for those whose field work, and support of it, made the experiment such a remarkable success.

The lithium-niobate gages, used for the first time in a field operation on Project Essex I, were developed by R. P. Reed, assisted in assembly, testing, and installation by R. W. Morris and O. J. Birdsong. Other end instruments were installed by G. W. Burnside, C. B. Kinabrew, and S. A. Winters. Recording was done by B. C. Holt and R. G. Oliveira, assisted by R. Griffin of Bell & Howell, Albuquerque. D. L. Fastle and W. G. Foy did the technical photography. B. O. Shaw provided administrative support in the field. D. K. Overmier advised on accelerometer technology, and R. C. Bass and H. M. Miller on Slifers. The latter were assisted in Slifer assembly by M. E. Gilmer and in field installation by A. J. Brouillard. Data were reduced by R. J. Beyatte, assisted by G. L. Riggins. W. B. Miller reduced photographic data. J. W. Long assisted in data analysis and preparation of published records. P. L. Mead edited the report.

CONTENTS

CONTENTS (cont)

CONTENTS (cont)

NOTE: The following Appendices appear in Volume II

A

TABLE 3.4

Summary of Acceleration Measurements at Shot Depth and
ESSEX I 12 MS 23 August 1973
21,594 Pounds Nitromethane Buried 12 Meters Deep, Ful

Accelerometer Designation	Accelerometer Orientation	Distance (m)	Depth (m)	Gage Range	Gage Limit (g's)	Gage Sensitivity	Calibration Step (g's)	Arrival Time* (msec)	Peak Acc (g'
6-6 AR-LO	Radial	6	6	Low	10,000	High	2,000	(4.7) ~6.96	>3,
				Low	10,000	Low	2,000	~7.0	6,
6-6 AR-HI	Radial	6	6	High	20,000	High	5,016	~7.0	6,
				High	20,000	Low	5,016	~7.0	6,
12-12 AH-LO	Horizontal	12	12	Low	5,000	High	497	4.53	>
				Low	5,000	Low	497	4.60	>2,
12-12 AH-HI	Horizontal	12	12	High	10,000	High	1,355	4.55	>2,
				High	10,000	Low	1,355	4.63	>6,
24-12 AH-LO	Horizontal	24	12	Low	200	High	70	10.38 ~33	>
				Low	200	Low	70	10.39 ~33	>
24-12 AH-HI	Horizontal	24	12	High	1,000	High	200	10.38 ~33	>
				High	1,000	Low	200	10.58 ~33	1,
24-12 AV	Vertical	24	12		200	High	69	10.43 ~28	>
					200	Low	69	10.39 ~28	
24-12 AT	Tangential (Horizontal)	24	12		200	High	71	10.33 33.5	>
					200	Low	71	10.35 33.5	
36-12 AH-LO	Horizontal	36	12	Low	200	High	20	16.15 35.7	
				Low	200	Low	20	16.24 36	>
36-12 AH-HI	Horizontal	36	12	High	200	High	64	16.11 36	
				High	200	Low	64	16.2 36	
36-12 AV	Vertical	36	12		200	High	19	16.7 34.3	
					200	Low	19	16.92 34.5	
36-12 AT	Tangential (Horizontal)	36	12		200	High	19	16.25 35	
					200	Low	19	16.9 35	

*Time resolution limited to 0.02
(L) Peak Limited
(a) Peak reconstructed
(b) Gage or cable failed at 9.54 msec.
(c) Gage or cable failed 0.27 msec after arrival.
(d) Direct signal
(e) Reflected Signal

TABLE 3.4

asurements at Shot Depth and Half Shot Depth
12 MS 23 August 1973
e Buried 12 Meters Deep, Fully Stemmed

Arrival Time* (msec)	Peak Acceleration (g's)	Time of Peak* (msec)	Peak Velocity (m/sec)	Time of Peak* (msec)	Peak Displacement (cm)	Time of Peak* (msec)	Remarks
(4.7)	100						(b)
~6.96	>3,000 (L)		>34.5	>9.54			(b)
~7.0	6,500	8.71	>51	>9.5	>6	>9.5	(b)
~7.0	6,540	8.90	>56	>9.5	>4.2	>9.5	(b)
~7.0	6,500	8.73	>53	>9.5	>4.0	>9.5	(b)
4.53	>500 (L)						(c)
4.60	>2,250 (L)						(c)
4.55	>2,000 (L)						(c)
4.63	>6,500 (L)						(c)
10.38	>100 (L)	~11.4					(d)
~33	>100 (L)						(e)
10.39	>200 (L)	~11.45	>1.5				(d)
~33	190	~35					(e)
10.38	>300 (L)	11.11					(d)
~33	162	~35					(e)
10.58	1,400 (a)	11.04	4.9	11.6			(d)
~33	170	~35	3.85	36.9	~21	120	(e)
10.43	>100 (L)						(d)
~28	100 (L)						(e)
10.39	540 (a)	11.73	3.84	12.5			(d)
~28	287	~35	3.40	36.1	+0.96, -1.97	15, 34.6	(e)
10.33	>100 (L)	~11.					(d)
33.5	>-100 (L)						(e)
10.35	277	11.50	+0.25, -0.5	11.2, 13.1			(d)
33.5	-122	~35	-0.64	35.1			(e)
16.15	>30 (L)						(d)
35.7	>30 (L)						(e)
16.24	>100 (L)						(d)
36	63	41.8					(e)
16.11	>92 (L)						(d)
36	53	41.1					(e)
16.2	550 (a)	17.5	2.05	17.9			(d)
36	48	41.9	1.82	42.6	7	130	(e)
16.7	>28 (L)						(d)
34.3	>28 (L)						(e)
16.92	510 (a)	17.7	2.05	18.0			(d)
34.5	50	47.0	1.75	48.0	1.2	120	(e)
16.25	>29 (L)						(d)
35	21.6	36.7					(e)
16.9	-215	17.5	+0.17, -0.177	17.4, 17.9			(d)
35	-21, +21	35.8, 36.6	-0.22	36.3	-0.027, -0.1	19.8, 50	(e)

The first velocity pulse was outward, as would have been expected. The second pulse also was outward, as would be expected if there was a reflection from a high-impedance stratum below the shot. A pulse returning from the surface would be a rarefaction wave that would tend to decrease in outward velocity. Increasing outward velocity from a surface rarefraction wave could be possible if the material was under compression from the expanding cavity gas pressure and was given the opportunity for further outward motion by the rarefaction wave having decreased resistance to compression.

The vertical acceleration measurement at the 24-meter station had positive and negative peaks for both pulses that were beyond band edge on the high-sensitivity channel (Fig. B-8). This was as expected for the accelerations observed, because the range had purposely been set low in case vertical motions turned out to be small. This record, however, is especially good for determining pulse arrival times.

The low-sensitivity record for the vertical component (Fig. B-9) had a first positive peak that was beyond both band edge and gage range. Actually, the value read at band edge was 296 g's, well beyond the 200-g range of the gage used, and the portion of the pulse over 200 g's may be in a nonlinear region of gage response. The positive peak of the second pulse does not appear to be limited by band edge, although the peak (290 g's) was essentially the same as the first pulse peak. Even though not limited by band edge, some portion of the record over 200 g's may be in a nonlinear region. Negative peaks of both pulses were within both band edge and gage range.

Let us assume that the positive peak of the second pulse remained in a linear region. Then all the residual negative (downward) velocity after the second pulse, when most motion should have ceased, can be attributed to the loss in integration of the first acceleration peak. The record can be adjusted at the first peak velocity by adding the amount of residual velocity at the peak and to all the record subsequent to it. This allows velocity to return to zero after the second pulse and provides a displacement-time record that becomes constant at a residual displacement of 0.6 cm. The result is shown in Fig. B-10.

The horizontal tangential gage at 24 meters gave a record (Fig. B-11) for the high-sensitivity channel that had excursions beyond band edge on both the clockwise and counterclockwise peaks for the first pulse and on the counterclockwise peaks of the second pulse. Here again the record provides accurate arrival-time even though peaks are limited.

The low-sensitivity channel gave a record (Fig. B-12) that was slightly limited on a clockwise peak of the first pulse by an amount that would add less than 3% to the corresponding velocity peak. In the second pulse there is a strong counterclockwise excursion that appears to be a temporary electrical dropout or a spurious gage response. Nothing similar is observed from the tangential measurement at the 36-meter station. When this portion is removed, an extension of time beyond that shown in Fig. B-13 shows that the velocity returns to nearly zero at about 110 msec. After 110 msec, however, the counterclockwise velocity increases irregularly at rates inconsistent with any reasonable pattern of ground motion and the record is not considered valid after that time.

RESULTS OF GROUND MOTION AND AIRBLAST MEASUREMENTS,

PROJECT ESSEX I, PHASE 1

CHAPTER I

INTRODUCTION AND OBJECTIVES

The effectiveness of atomic demolition munitions (ADM)[1] and small-yield nuclear weapons in creating obstacles and barriers to mobility[2,3] depends on the sizes and shapes of the craters formed. Damage to underground or surface targets by buried detonations is dependent on resulting ground motion. Collateral damage from airblast and residual radioactivity is a strong function of charge burial depth and stemming. Crater size and shape, as well as ground motion, are also dependent upon the depth of charge burial, the way the charge is stemmed, the geology, and the explosive yield. For a given yield and medium, the stemming and depth of charge burial are the principal determinants of crater size and shape, as well as ground motion. Emplacement holes can be either unstemmed or stemmed (usually with earth or water), or partially stemmed (having a small-diameter open hole), as would be the case with earth-penetrator emplacement.[4-7]

Since the problem being addressed involves nuclear explosive applications under conditions proscribed by the Limited Test Ban Treaty of 1963, an experimental approach using nuclear explosives is ruled out. The recourse is to calculate nuclear ground motion and craters by using available hydrodynamic codes. The accuracy of such calculations is governed by how adequately the codes that treat mathematically the conservation of mass, momentum, and energy represent the phenomena of stress-wave propagation in a real medium. Their adequacy also depends on how well the equation of state of the medium is known. For typical media this involves how well a few finite samples of the medium, from which the equation of state is determined, represent the macroscopic structure of the medium.

One way to evaluate the adequacy of hydrodynamic codes in calculating response to nuclear explosions is to use them to predict response to a chemical explosion of comparable energy, then to produce such a chemical explosion, and to measure the response to permit comparison of calculation with measurement. This method is the essence of the Essex I program and of the measurements described in this report.

Certain caveats must be interjected with respect to comparing the results of calculation and measurement. First, confidence in calculated response decreases as distance from the explosion increases and as stress levels correspondingly decrease. Confidence in measurement, on the other hand, tends to decrease as the explosion is approached and stress levels increase, until a point is reached when the survival of both the measuring instrument and its signal cable are challenged. The philosophy behind the measurements described in this report is to have them span the region from small distances where survival of measuring equipment is highly uncertain (but not impossible) to where survival and confident measurements are assured.

Second, where there is a difference between calculated and measured response, fair evaluation requires an assessment of how much of a difference can be attributed to the code, how much to the equation of state, and how much to measurement factors such as gage and recording equipment response, and accuracy of gage calibration. To the latter end, most measurements described in this report were backed up with a second instrument of either like or different kind.

The four shots of the Essex I program are summarized in Table 1.1.

TABLE 1.1

SUMMARY OF ESSEX I SHOTS

Charge Burial Depth (m)	Type of Stemming	Shot Code	Charge Weight (lb) [c]	Agency Responsible for Calculations	Shot Date and Time [d]	
12	Fully Stemmed	12MS	20,000	Lawrence Livermore Laboratory	08/23/73	12:43 p. m.
12	Partially Stemmed [a]	12MPS	20,000	Sandia Laboratories Albuquerque	09/20/73	11:15 a. m.
6	Fully Stemmed	6MS	20,000	Systems, Science and Software	10/03/73	11:15 a. m
6	Unstemmed [b]	6MU	16,000	Systems, Science and Software	10/24/73	11:15 a. m.

(a) 7-inch (17.8-cm)-diameter open hole.

(b) 1.8-meter-diameter open hole.

(c) Charge weight is in terms of TNT equivalent. The 20,000-pound equivalent charges consisted of 21,594 pounds of liquid nitromethane; 2,482 pounds of sand for the radioactive tracer simulation experiment; and 745 pounds of gelling agent. For the 16,000-pound charge the weights were 17,275, 1,986, and 576 pounds, respectively.

(d) Central Daylight Time.

Measurement Plan

The basic philosophy behind the measurement plan was one of triple redundancy. Since end-instrument and cable costs are the smaller part of the expense of a project like Essex I, the added insurance provided by this philosophy is warranted. The first redundancy was to use two gages at each location wherever reasonable. This provided a means of checking on the accuracy and stability of gage calibration, and gage response to the entire waveform. Where two gages were used, one was in a high- and one in a low-range mode. The second redundancy was to split the signal at the recording trailer through two voltage-controlled oscillators to record the signal at two sensitivities that generally differed by a factor of three. The third redundancy was to record all information on two separate tapes. This not only protected against tape-machine failure, but allowed one tape to be used for field playback while the other was preserved for final data reduction.

The use of the first two redundancies is best explained by reference to Table 1.2, using as an example a stress gage to be located where expected stress was 3 kilobars. For each channel, the stress level shown in the table was adjusted to represent 80% of bandwidth. Using the example of the table, if the peak stress was actually 3 kilobars, the high-sensitivity channel of the low-range gage would be beyond band edge, and good signal would be recorded on the low and high sensitivities of the high-range gage. This permits comparison of the output of two different gages subjected to the same shock environment. The low sensitivity of the high-range gage would give a signal that would be adequate but would usually have a smaller signal-to-noise ratio. If the peak stress were actually 1 kilobar or less, all channels would have adequate records, but the high sensitivity of the low-range gage would have the most favorable signal-to-noise ratio. If the peak stress were actually 5 kilobars, only the low sensitivity of the high-range gage would give an adequate signal, and the others would be beyond band edge. For the second shot the set ranges were modified on the basis of the results of the first shot. The modifications can be recognized by comparing Table 3.1 with Table 4.1. In addition to set-range modifications to reduce the number of channels going beyond band edge, all set ranges were changed to 60% of bandwidth rather than 80%.

TABLE 1.2

APPLICATION OF GAGE REDUNDANCY

	Low Sensitivity	High Sensitivity
Low-Range Gage	3	1
High-Range Gage	9	3

The essence of the foregoing is that for each gage, two records were obtained. In the appendices, where copies of the records are reproduced, first and second integrations of acceleration records showing velocity and displacement have been included. Occasionally the integrations have been omitted where the quality of the acceleration record did not warrant them.

CHAPTER 2

INSTRUMENTATION

The most desirable parameters for comparing measured with calculated values are arrival time, stress-time as a function of distance, and velocity-time as a function of distance. Arrival times were obtained from vertical Slifers between the charge and the ground surface. Stress-time was measured using ytterbium and lithium-niobate gages. There are no proven velocity-time gages for close-in regions where most of the measurements were desired. In lower-velocity regimes there has been considerable success in using velocity-time obtained by integrating the acceleration-time output of accelerometers. The decision was made to obtain velocity-time in that manner in recognition of the fact that success in the closer region could be less than at the greater distances. This decision introduced another difficulty. Before gages can be selected to make such measurements, there must be some prediction of the acceleration to be expected. Peak accelerations come from hydrodynamic code calculations as the differential of the velocity-time function between arrival and peak velocity. Since essentially all codes use an artificial viscosity to prevent the wave from shocking up, the rate of rise, and hence peak acceleration, is strongly dependent on the way the artificial viscosity and other parameters are handled in the code.

Instruments were arranged along a line extending from ground zero to a radius of 36 meters as shown in Figs. 3.1, 4.1, 5.1, and 6.1.

Weatherproof terminal boxes were located near an extension of this line at a radial distance of approximately 60 meters. These boxes housed calibration and bridge-completion resistors, batteries, and signal-conditioning circuitry required by the various transducers. From this point, buried signal and control cables were run to a recording trailer. The boxes were protected with shock-mitigating foam, plywood, and sand bags, so that they could be recovered and reused for each succeeding shot.

The buried portions of signal cables from accelerometer canisters and pressure gages were protected with lengths of hydraulic hose (Aeroquip Part No. 1503-20) which extended approximately 3 meters beyond the ground surface. These signal cables were cut 15 meters longer than required to reach the signal conditioning boxes so they could be serpentined along the ground. This minimized strain on signal cables during early ground motion, thereby prolonging useful recording time.

End Instruments

Slifer -- The Slifer[8] is an electrical transmission line used as the inductive element of an oscillator, the frequency of which indicates the position along the line at which the shock wave has shorted the line. This gives an FM signal of shock-wave position vs time.

All Slifers were made with a 40-foot (12.2 m) sensing cable. With this length of cable, the frequency limits of oscillation were approximately 800 kHz with cable intact and 1200 kHz with the cable shorted next to the oscillator canister.

A total of 8 Slifers were installed on the 4 Essex shots, as shown in Figs. 3.1, 4.2, 5.1, and 6.2. Note that at least one Slifer cable on each shot was placed in the explosive itself, giving a measure of burn rate in the gelled nitromethane.

Each oscillator unit was calibrated with a cable which had holes drilled through its shield at regular intervals. The recording frequency of oscillation as a shorting pin was sequentially inserted in these holes provided a frequency-vs-position curve for that unit.

High-Pressure Airblast Gages -- Measurement of pressure-time in the open holes of the unstemmed and partially stemmed shots (6MU and 12 MPS) was made with PCB Piezotronics Model 109A, 109M13, and 109M14 transducers. The 109M13 and 109M14 are modified versions of the 109A and were manufactured expressly for the high pressure ranges expected on Essex.

These gages are flush diaphragm type with a quartz crystal sensor, and contain a built-in MOSFET source-follower circuit with 100 ohms output impedance. The gages were flush-mounted on the circumference of the open holes, two feet below the surface, as shown in Figs. 2.1 and 2.2.

Both static and dynamic calibrations were performed by Division 9486 at Sandia's Menaul facility using the same circuitry as was later fielded with the gages. A block diagram of the pressure-gage setup is shown in Fig. 2.3.

Two gages were mounted in a shock tube in the laboratory to check rise-time characteristics. The rise time was 5 μs, using 6000 feet of cable. This was the maximum length of signal cable used on Essex (6MU). The gage itself has a rise time of 1 μs.

A field modification was made to the 12 MPS installation. It was found that water seeped into the 8-inch open hole to within 10 feet of the surface, and at a rate that precluded pumping the hole dry and removing the pump just before shot time. Sections of aluminum tubing were therefore welded together, and a disc welded across the bottom, to form a 7-inch-ID by 1/8-inch-wall "dry well" which was lowered to the surface of the nitromethane explosive charge. Figs. 2.4 and 2.5 show this assembly before and after installation. The projection from the bottom of the assembly seen in Fig. 2.4 consists of the initiating booster charge and the LLL rate stick measurements.

Slots 2 inches wide and 6 feet long were cut near the upper end of the 7-inch pipe at the location of the air-pressure gages which had already been grouted in place. The slots extended two feet above and four feet below the gage locations.

Ytterbium Stress Gage -- The ytterbium stress gages[9] fielded in Essex I by Sandia were Model SP-12 "Paddle" gages made by Pulsar, Inc., of Redwood City, California. These gages consist of a thin piezoresistive ytterbium foil grid, encapsulated between two 1/16 in.-thick printed circuit boards with epoxy resin (see Fig. 2.6). The assembled unit is 1-3/4 in. wide by 10 in. long. RG-122 signal cable was run from the sensor assembly to the surface in 5/16-OD aluminum tubing. The tubing also served as an insertion tool.

The sensing elements of these gages were wired in a Wheatstone bridge configuration, as shown in Fig. 2.7. Calibration resistor values were calculated using a stress-resistance loading curve published by Ginsberg.[10] The portion of this curve pertinent to the stresses encountered on Essex I is reproduced in Fig. 2.8.

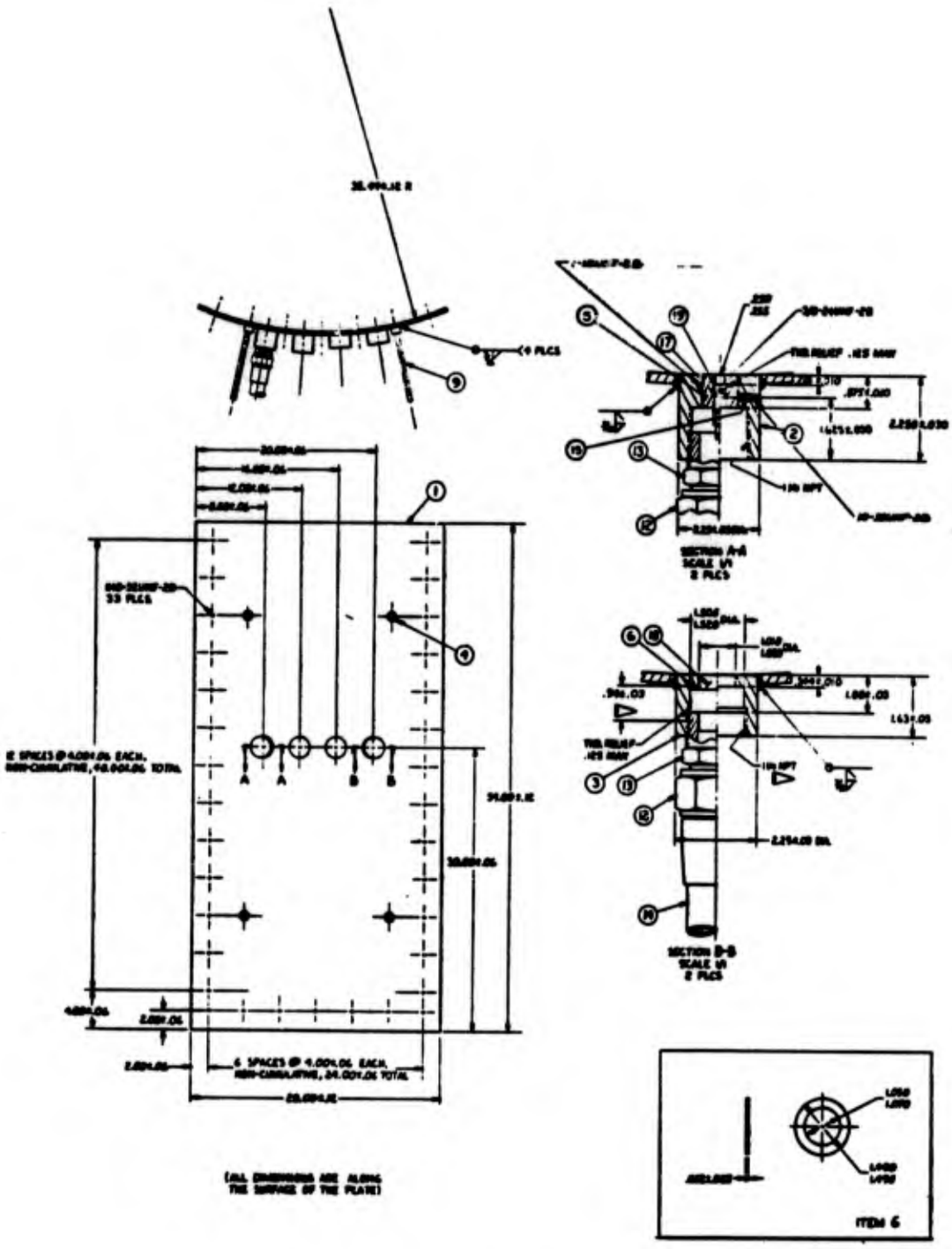

Fig. 2.1. Pressure Gage Mount, 6MU

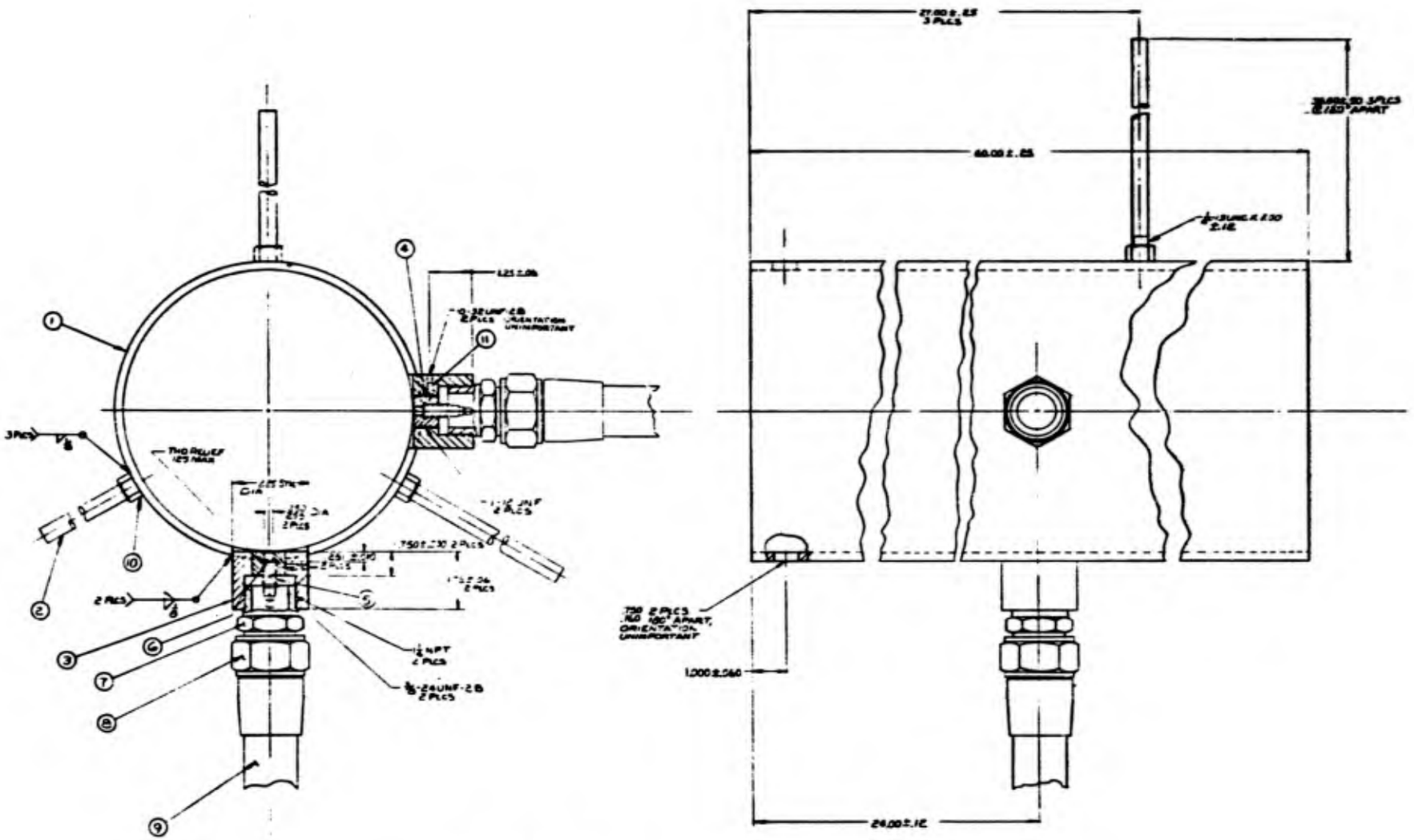

Fig. 2.2. Pressure Gage Mount, 12 MPS

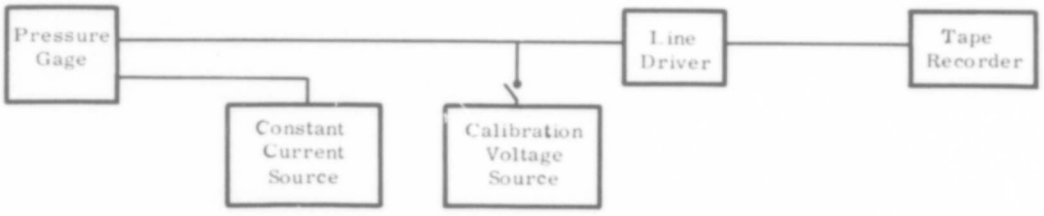

Fig. 2.3. Essex Pressure Gage System

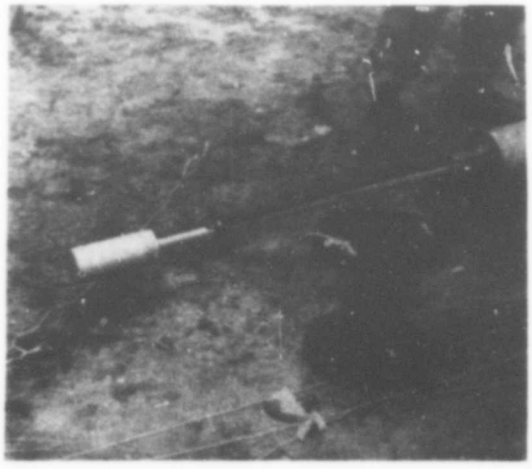

Fig. 2.4. Dry Well Assembly Before Installation

Fig. 2.5. Dry Well Assembly After Installation

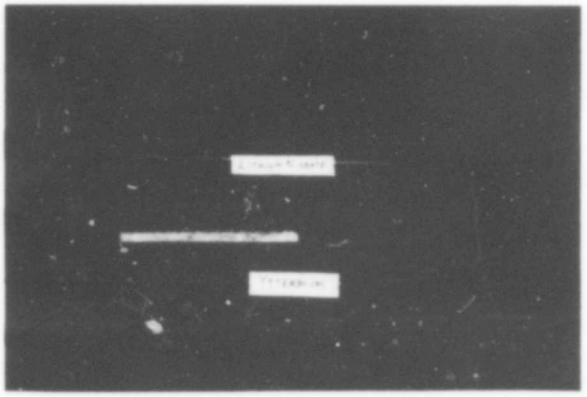

Fig. 2.6. Ytterbium and Lithium-Niobate Stress Gages

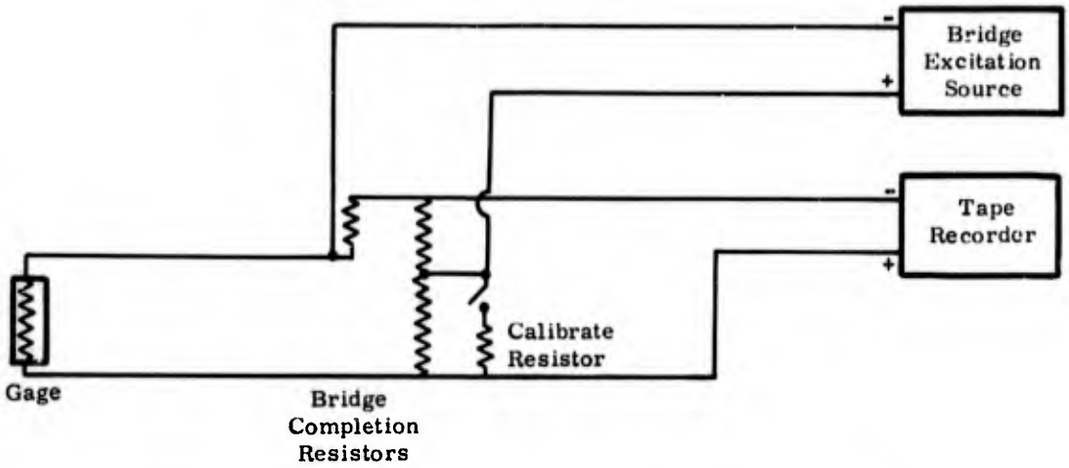

Fig. 2.7. Recording Configuration for Ytterbium Stress Gages and Piezoresistive Accelerometers

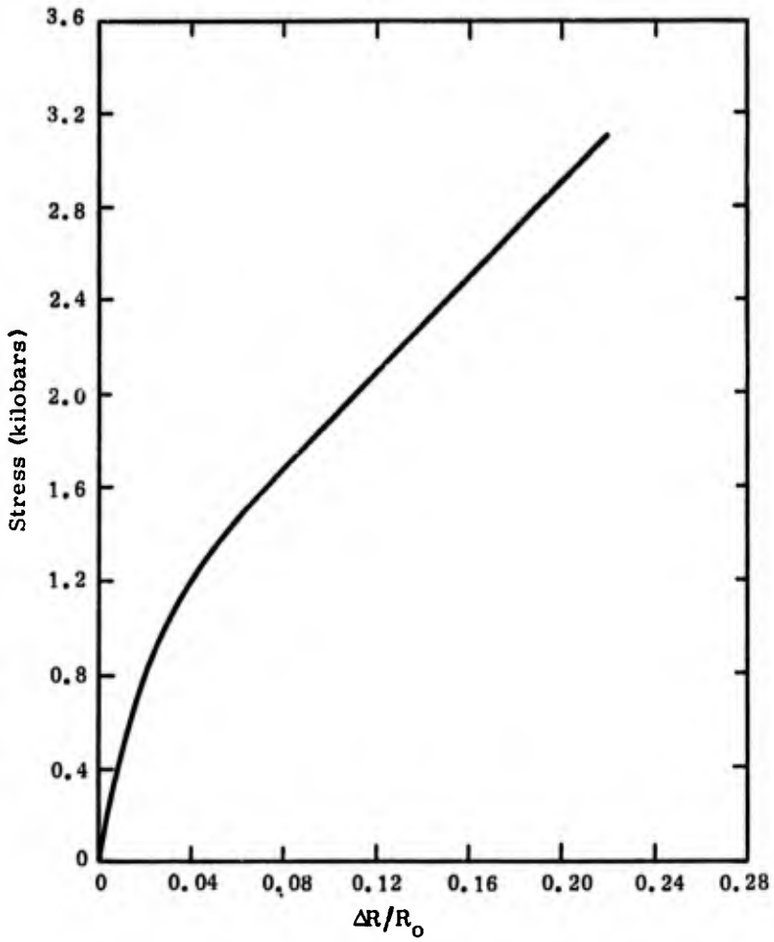

Fig. 2.8. Stress-Resistance Curve for Ytterbium (Per Ginsberg)

An undesirable characteristic of ytterbium is hysteresis between the loading and unloading portions of the stress-resistance curve.[10]

Lithium-Niobate Stress Gage -- This gage makes use of the pressure dependence of the piezoelectric polarization of Z-cut lithium niobate. Graham[11,12,13] determined the linear hydrostatic piezoelectric constant for lithium niobate, and its first application in gages as a measuring device was in the shots of the Essex I series. This gage has two distinct advantages over ytterbium gages in that the material exhibits no hysteresis upon reduction of pressure and it has a strong electrical output. Because of the high output of the lithium-niobate gages, they were earmarked for use at the 12- and 24-meter ranges. Later in the program additional gages became available, and both lithium niobate and ytterbium stress gages were emplaced in the same holes for comparison at several locations.

Since this was the first time the former had been used in the field, and they were to be compared with the latter, the lithium-niobate units were made to resemble ytterbium gage assemblies as closely as practicable (Fig. 2.6).

A capacitor was placed across the output of the sensor to reduce the voltage of the gage to a value suitable for driving an electrometer, as shown in Fig. 2.9.

Risetime of this system, with 6000 feet of cable, was less than 4 μs going into the recorder. Gages were calibrated in a hydraulic pressure vessel at Sandia Laboratories, Albuquerque.

Accelerometers -- All accelerometers fielded on this project by Sandia were manufactured by Endevco Corp., Pasadena, California. Four models were used: the 2261A, 2262C, 2264A, and 2291. Model 2291 is a 100-kg piezoelectric gage with a quartz-crystal transducer. All other models are piezoresistive and were wired in a four-arm bridge configuration, as shown in Fig. 2.7. The two piezoelectric gages were wired as shown in Fig. 2.10.

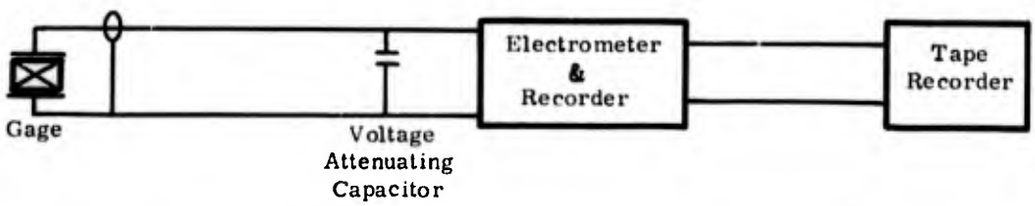

Fig. 2.9. Lithium Niobate Stress Gage System

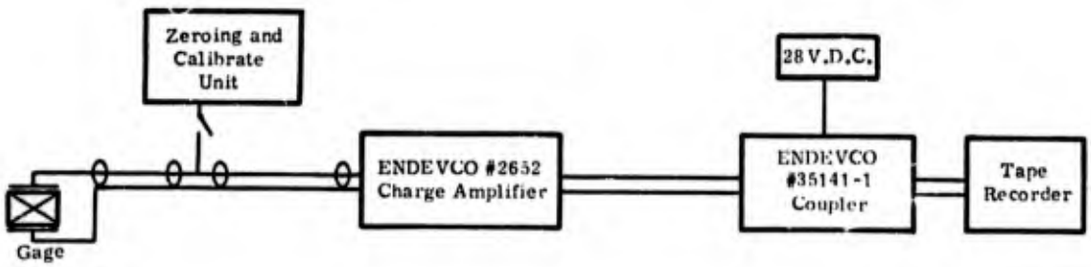

Fig. 2.10. Piezoelectric Accelerometer Recording System

Accelerometers were mounted on a tapered aluminum block drawn tightly into an aluminum canister shell, which was machined with a matching taper. This formed a rigid assembly that minimized spurious low-frequency resonances from the mounting structure. Figs. 2.11 and 2.12 show details of the internal structure and a view of the assembled canister.

Calibration was done at Sandia Laboratories' Albuquerque Menaul facility. For shallow holes such as those used on Essex, the hydraulic hose used for signal cable protection, when held in axial tension, has sufficient torsional rigidity to be used both as an installation and alignment fixture. Alignment between the accelerometer mounting plug and canister body was established by an alignment pin. A reference mark on the canister body defined the ground zero direction.

The canister assembly, with the hydraulic hose attached, was placed horizontally on the floor of an assembly building. The alignment fixture (Fig. 2.13) was attached using the nonsymmetrical canister-lid hole pattern. When it was so attached, the gage axis that would be radial was approximately horizontal. Leveling legs on the fixture permitted this axis to be precisely adjusted to the horizontal using a carpenter's level. With the assembly still on the floor, a sighting fixture (Fig. 2.14) was clamped to the hydraulic hose (again using a carpenter's level) a few feet above the point where the hose would be at ground level when the assembly was lowered to its proper depth. After the canister assembly was down-hole, sighting along the fixture to ground zero was used to orient the accelerometers to the proper azimuth. The canister assembly was then clamped in place until the grout had set. Lead weights were suspended below the canister with 1/8-inch nylon cord to insure proper location and alignment by keeping the installation under tension.

Low-Pressure Airblast Gages -- Either bonded strain gage Dynesco Type 85B or unbonded strain gage Statham Type PN283TC were used for the three low-pressure stations. At each station, two gages were enclosed in a single canister. Each station contained a canister, battery power, a telemetry transmitter, and an antenna with mast (Figs. 2.15 and 2.16). One of the two gages in each canister accommodated a low set range and the other a high set range. The low-range gage was used in such a manner that it could record 3 to 4 times the expected overpressure without exceeding telemetry band edge. The other gage accommodated a high set range equal to 5 times the expected overpressure, but was recorded in such a way that an overpressure of 1.5 times the high set range could be accommodated without exceeding band edge.

Recording

Data were recorded in trailer B-23. Equipment included two Consolidated Electrodynamics Model VR 3700 and 3 Ampex CP-100 tape recorders with associated amplifiers and multiplexing modules, a transceiver system for data reception and control of the low-pressure air-blast gages, a CEC 5-133 paper recorder used for playback and real-time quick-look at selected data channels at shot times, and a termination card for each data channel.

Timing and control signals were generated by the trailer programmer, referenced to master signals received from the control point.

Each Slifer signal was recorded on a VR-3700 direct-record channel with a frequency response capability of 2 MHz.

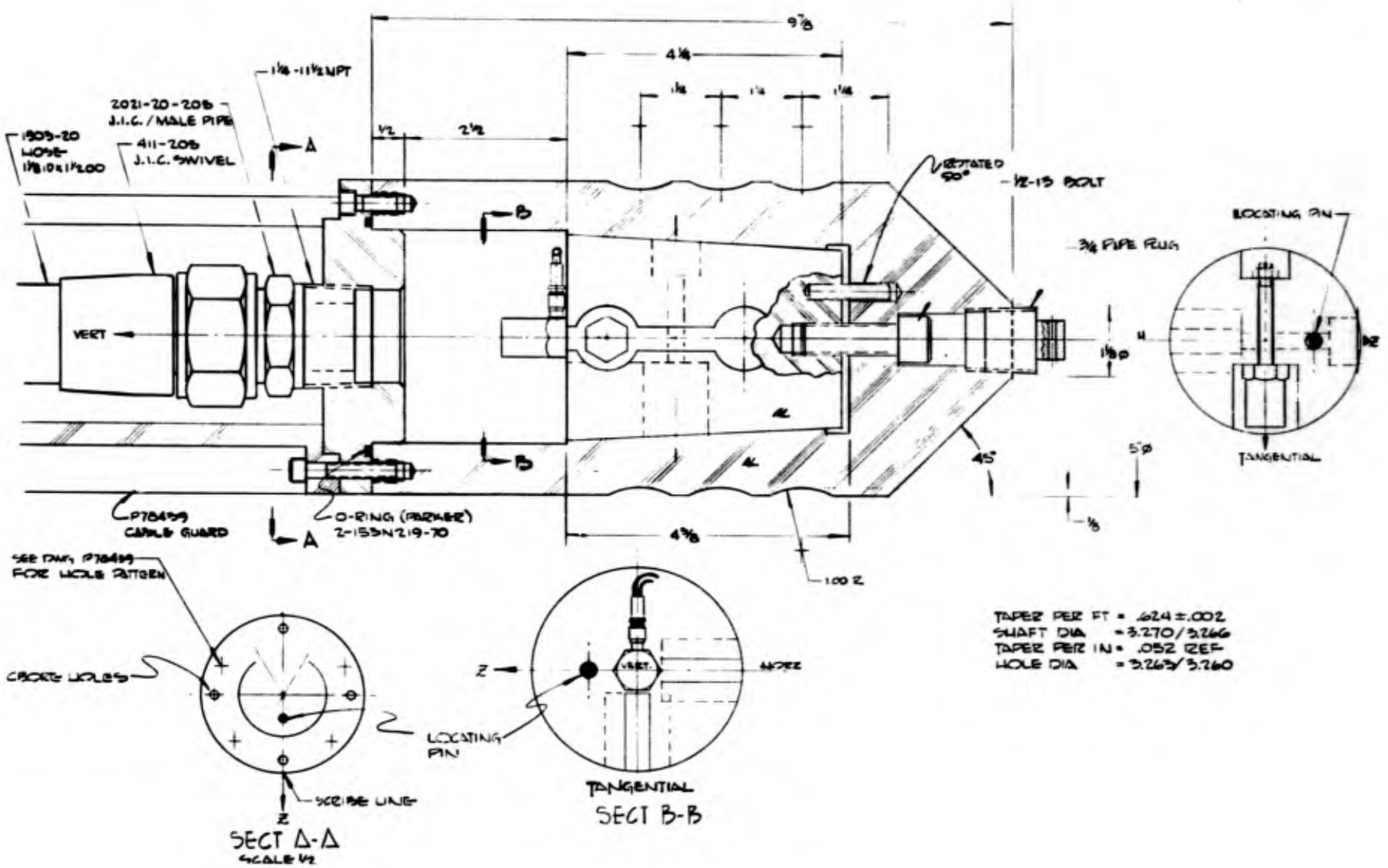

Fig. 2.11. Accelerometer Canister

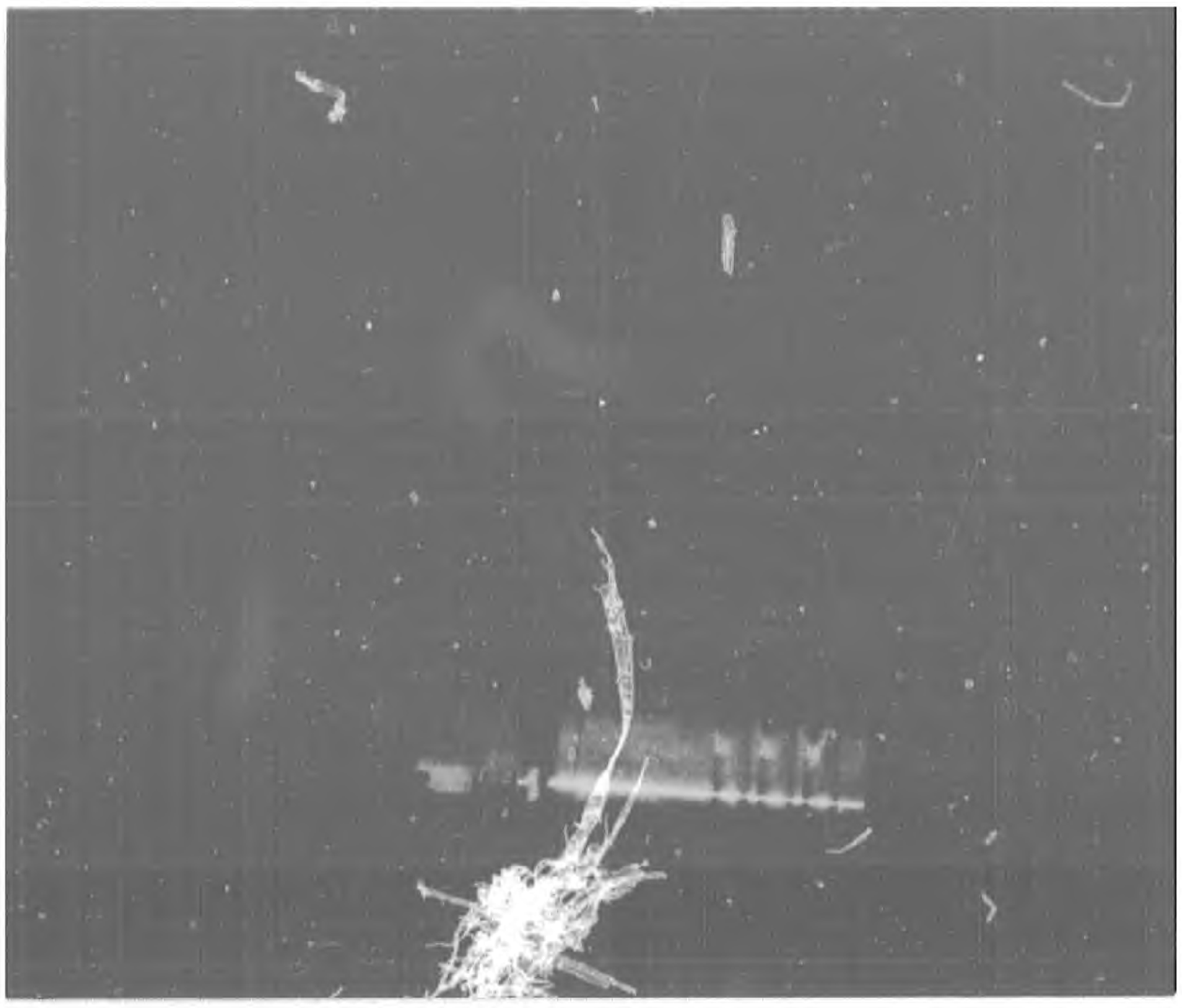

Fig. 2.12. Assembled Accelerometer Canister

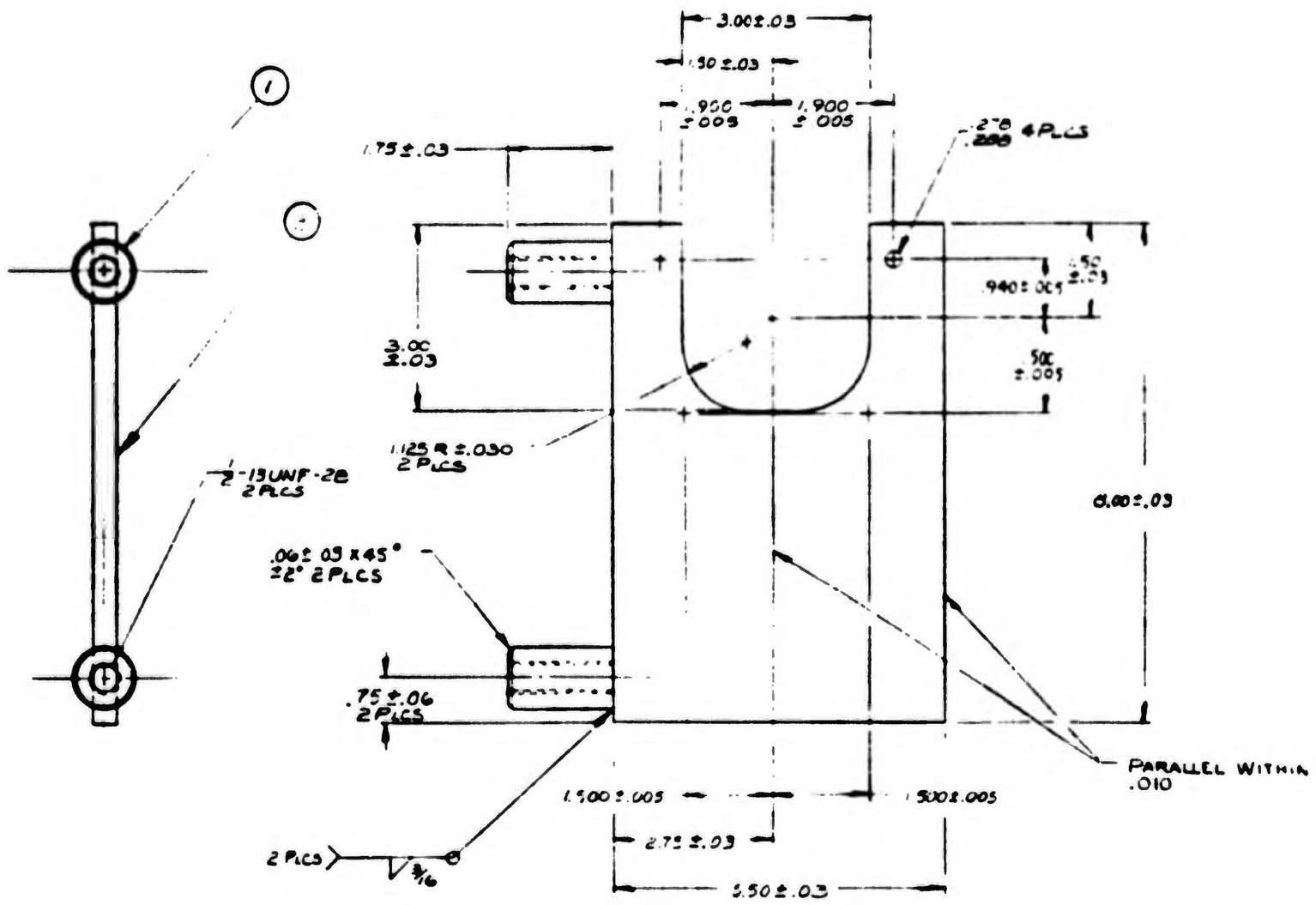

Fig. 2.13. Canister Leveling Plate

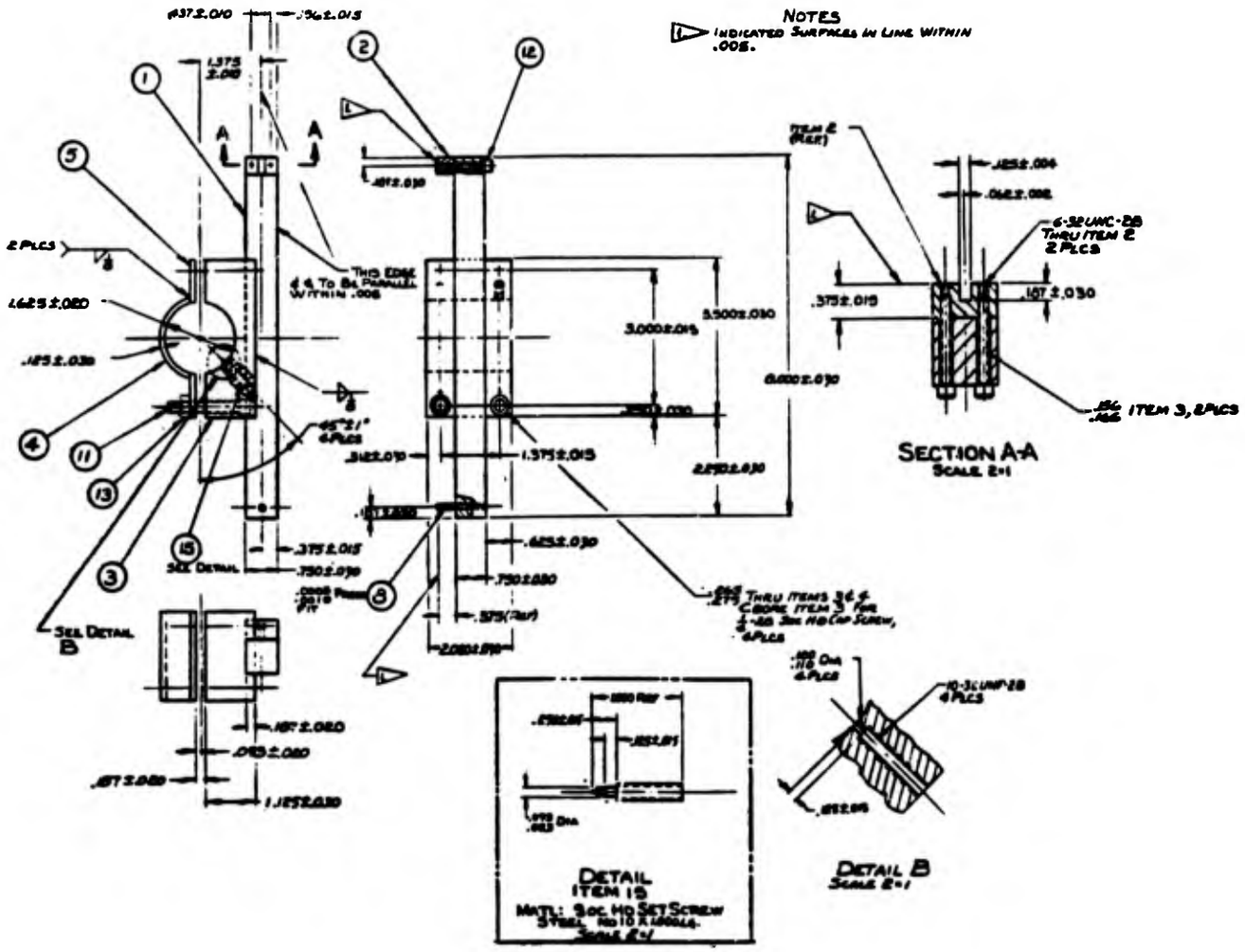

Fig. 2.14. Sighting Fixture

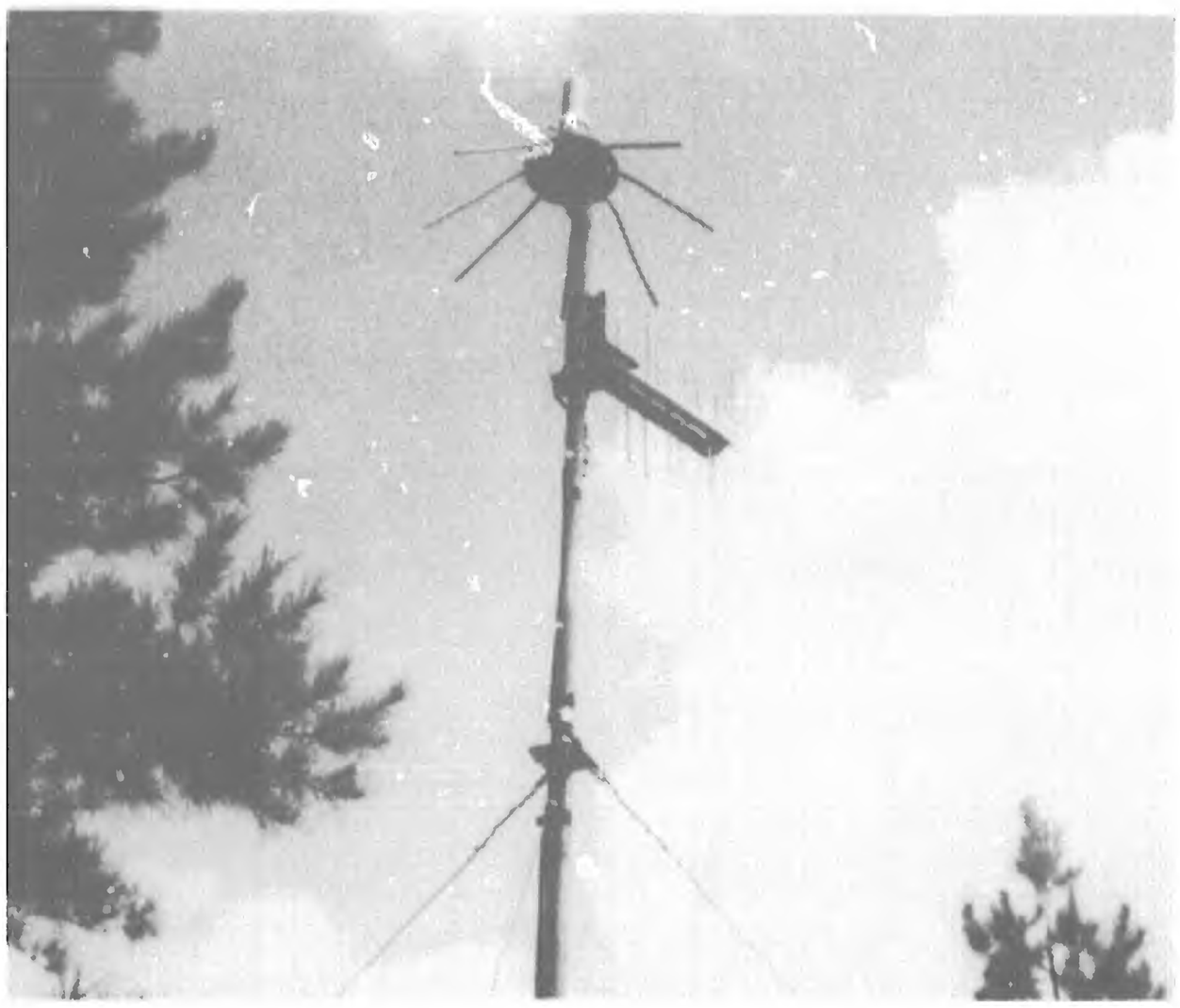

Fig. 2.15. Antenna for Airblast Station

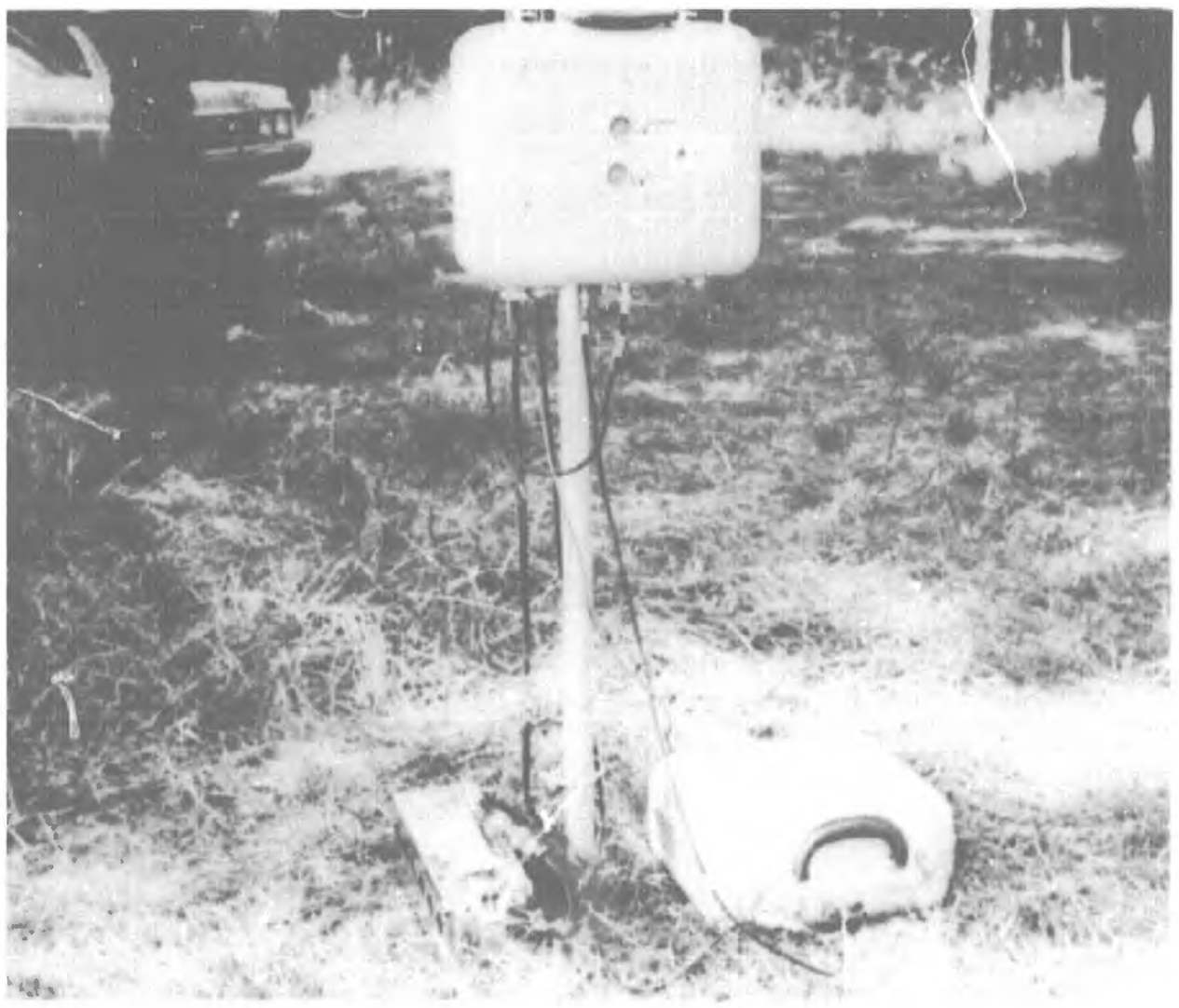

Fig. 2.16. Remote Airblast Station

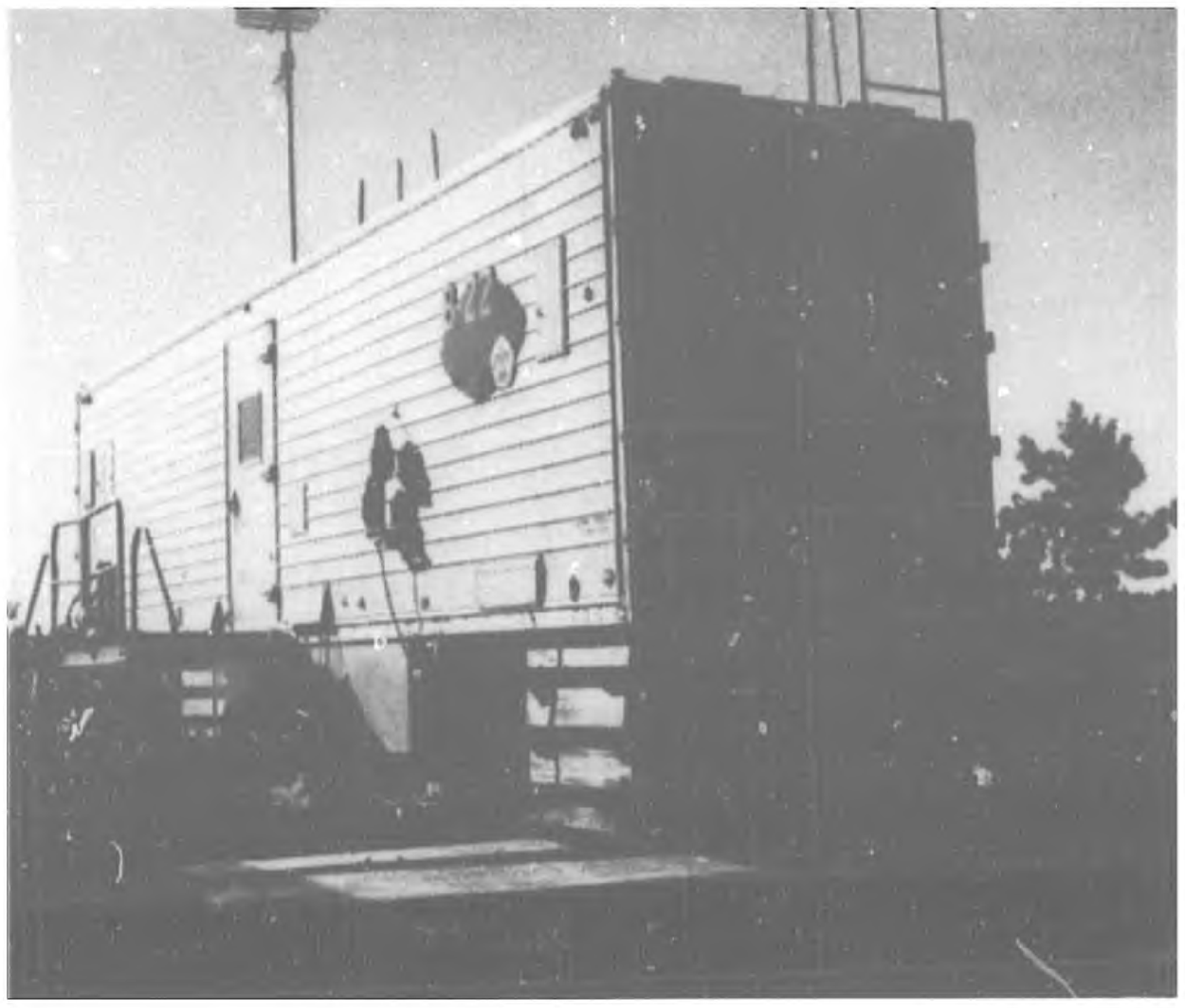

Fig. 2.17. External View of Recording Trailer

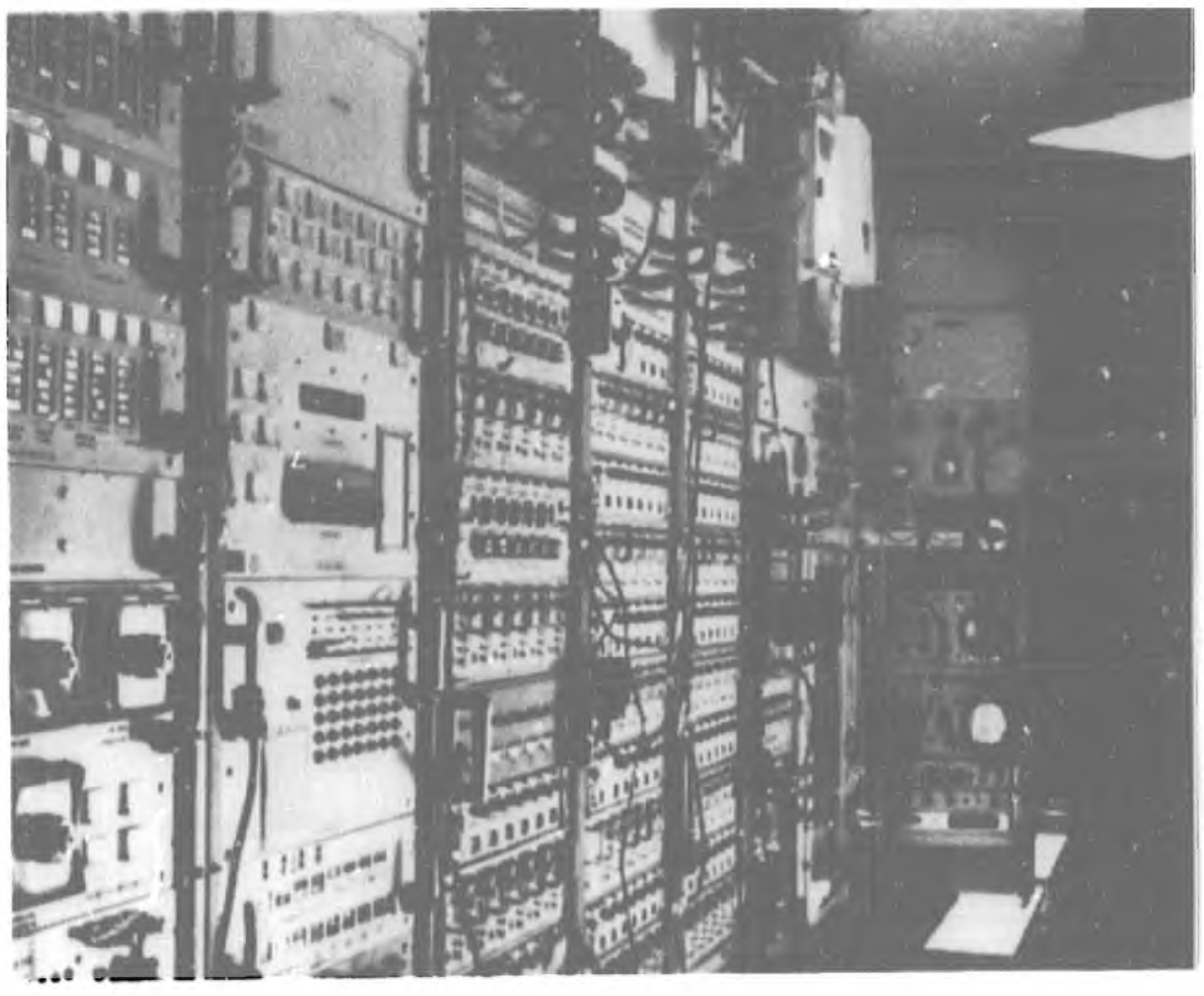

Fig. 2.18. Internal View of Recording Trailer

Signals from the high-pressure airblast gages were terminated in 50 ohms, fed through a CEC Model 173581-0104 wide-band amplifier, and recorded on a VR 3700 in the wide-band FM mode.

Piezoelectric accelerometers and lithium niobate stress-gage signal lines were terminated at the trailer with 50 ohms, ytterbium stress gages with 1000 ohms, and the piezoresistive accelerometers with 5000 ohms.

All accelerometer and stress-gage signals were multiplexed in groups of up to 6 gage channels per tape channel. The VCO center frequencies used were 200, 500, 850, 1200, 1550, and 1900 kHz. VCO frequency response was 20 kHz for the 200-kHz channel and 50 kHz or better for the other 5 channels.

Each multiplexed group of 6 data channels was recorded on a VR 3700 tape track in the direct-record mode.

Calibration steps were automatically applied to each channel at minus two minutes on command from the trailer program timer. A zero-time fiducial derived from the shot firing signal, and an IRIG timing channel, were recorded on each tape.

External and internal views of the recording trailer are shown in Figs. 2.17 and 2.18.

Data Playback and Digitizing

Stress measurements were played back through 20-kHz filters and digitized at a rate of 400,000 points per second. Acceleration records were first played back for 0.1 second through 40-kHz filters and digitized at the same rate. Later selected records were played back for ±3 seconds through 1-kHz filters at a rate of 5,000 points per second. Sandia airblast, which was recorded on the slower system, was played back through 330-Hz filters and digitized at a rate of 2000 points per second. Digitizing rates and filtering for BRL airblast was 20,000 points per second and 5 kHz for Station 1, 5,000 and 1 for Station 2, and 2,000 and 0.45 for Station 3.

Adjustments to Data

Where necessary, all stress, acceleration, and airblast data have been processed using methods developed at Sandia Laboratories, Albuquerque.[14] Digital smoothing was applied to noisy records, typically those of the high-range, low-sensitivity measurements where the signal-to-noise ratio was expected to be small if the signal was appreciably below that expected. Acceleration records that gave suitable data were singly and doubly integrated to give velocity and displacement as functions of time. Baseline shifts were removed to provide acceleration and velocity plots that returned to zero at late times, and displacement plots that showed a constant residual displacement. Near-surface gages that were in a ballistic trajectory at late times were adjusted only to the extent that the baseline shift affected integration before signal arrival on the assumption that the shift remained constant through the signal. In certain cases, special treatment was given to first integrations in order to recover valid velocity peaks.

CHAPTER 3

RESULTS OF THE 12-METER STEMMED EVENT

On the 12-meter stemmed shot, 35 gages were emplaced by SL and signals were obtained from 34 of these, as well as from 6 gages emplaced by BRL. Excellent results were obtained from Slifer time-of-arrival measurements, from 7 of 8 stress measurements, and from airblast measurements. Surface-motion measurements were also excellent except for the small signal-to-noise ratios from some channels at the greater distances. Only a few channels were limited in amplitude by bandwidth of the subcarrier. For subsurface acceleration measurements, bandwidth limitations were more common because acceleration attenuated with distance at a slower rate than was expected from pre-shot information. At two locations, either the gages or their signal cables did not survive long enough for their integrals to provide a peak velocity, although at one location the loss could not have degraded the peak appreciably.

Gage Range and Set Range

In making measurements of the kind reported here it is necessary to have some preconception of the levels to be measured, first so that instruments capable of measuring those levels can be procured, and second, so that appropriate levels can be set within the recording frequency band. Table 3.1 summarizes the set ranges for the low- and high-sensitivity gages and indicates the expected level. Note that where possible the expected level was used for the low-sensitivity set range of the low-range gage, and for the high sensitivity of the high-range gage. Expected stress levels were provided by LLL, and, as will be seen, were close to the levels measured. They also provided, with some reservation, expected levels for free-field radial peak accelerations. The authors' own reservations result from the fact that hydrodynamic codes do not calculate peak accelerations directly. Rather, most are capable of calculating particle velocity versus time, the differential of which is acceleration. The peak acceleration is the steepest slope on the rise of the particle velocity-time curve. Since the tendency of calculated shock waves is to move toward an infinite rate of rise, most codes contain artificial terms to prevent this from occurring. Peak accelerations predicted from such calculations, then, are strongly dependent on these terms.

For the 12 MS shot it will be seen that these predictions were reasonable for close stations, but were considerably lower than measured values at the farther stations.

Hydrodynamic calculations based on a single homogeneous medium show that particle motions in directions perpendicular to a radius will be zero until there are returns from the surface. Since there was no experience or guidance from calculation, the authors selected set ranges approximately equal to the low-range gage levels for radial acceleration.

TABLE 3.1

Planned Set Ranges Based on Expected Ground Motion and Stresses for 12MS

12 METER STEMMED

Gage	R Meters	DOB Meters	Expected	Low Sensitivity	High Sensitivity
σ	6	6	2 (kb)	2 (kb)	0.7 (kb)
σ	6	6	2	6	2
σ	6	12	3	3	1
σ	6	12	3	9	3
σ	12	12	0.5	0.6	0.2
σ	12	12	0.7	2.0	0.6
σ	24	12	0.2	0.3	0.1
σ	24	12	0.5	1.0	0.3
a_h	12	12	1500 (g)	1500 (g)	500 (g)
a_h	12	12	1500	5000	1500
a_h	24	12	100	200	70
a_h	24	12	500	1000	200
a_v	24	12	100	200	70
a_t	24	12	100	200	70
a_t	36	12	50	150	20
a_h	36	12	50	60	20
a_h	36	12	50	150	60
a_v	36	12	50	150	20
a_r	6	6	5000	5000	2000
a_r	6	6	5000	15000	5000
a_v	2/3	2/3	3000	3000	1000
a_v	2/3	2/3	3000	10000	3000
a_v	9	2/3	2200	6000	600
a_v	12	2/3	1500	3000	300
a_h	12	2/3	750	1500	150
a_v	18	2/3	1000	3000	300
a_v	24	2/3	750	1500	150
a_h	24	2/3	500	1000	100

Slifer	1 channel
Sandia airblast	6 channels
BRL airblast	6 channels

Gages between lines were in a single hole.

There was also guidance from calculation for surface accelerations. Those at surface zero were chosen to be twice the free-field radial values. Those at other surface stations were chosen by extrapolating from the surface-zero station using rates of attenuation observed photographically on cratering shots in other media.[15,16,17] It will be seen that measured attenuation rates were greater than this prediction.

Measurement Locations

Figure 3.1 shows the locations of the Slifer, near-surface, and subsurface stress and acceleration measurements made by SL.

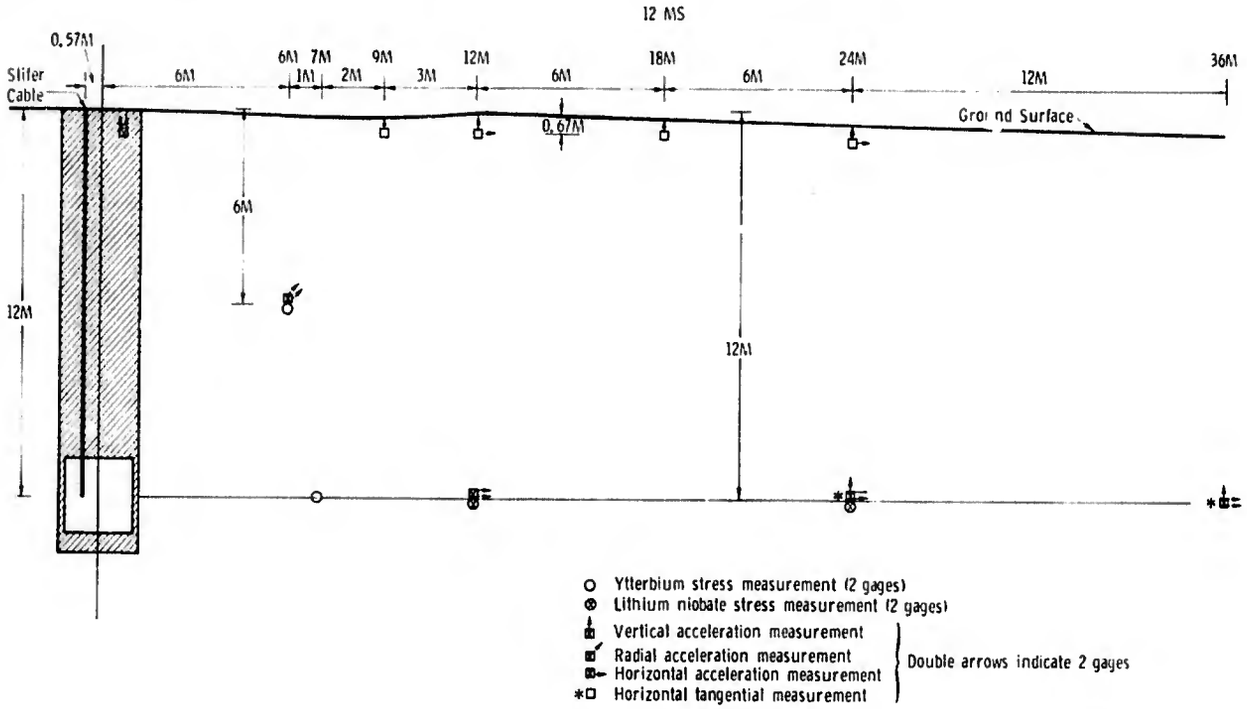

Figure 3.1 Location of instrumentation for 12MS

Slifer Time of Arrival

The record of frequency versus time as measured by the Slifer cable is shown in Fig. 3.2. Figure 3.3 is the calibration curve of frequency versus cable length used to make the conversion to time of arrival versus distance shown in Fig. 3.4. The ordinate in Fig. 3.4 is the radial distance from the charge center to the point activated on the Slifer, taking into account the geometry occasioned by the fact that the vertical axis of the Slifer was displaced 22.5 inches (0.571 meter) from the axis of the charge.

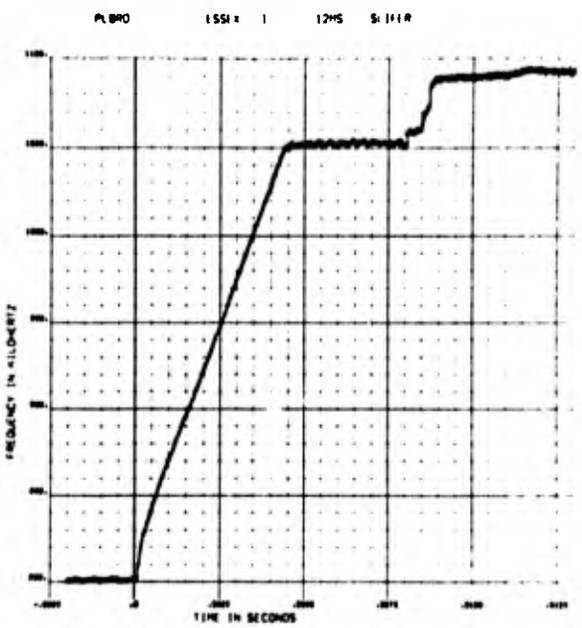

Figure 3.2 Frequency versus time for Slifer time of arrival measurement

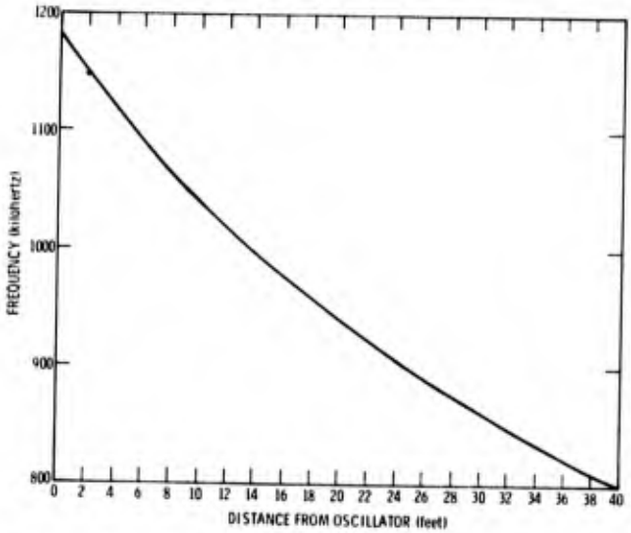

Figure 3.3 Slifer time-of-arrival calibration curve

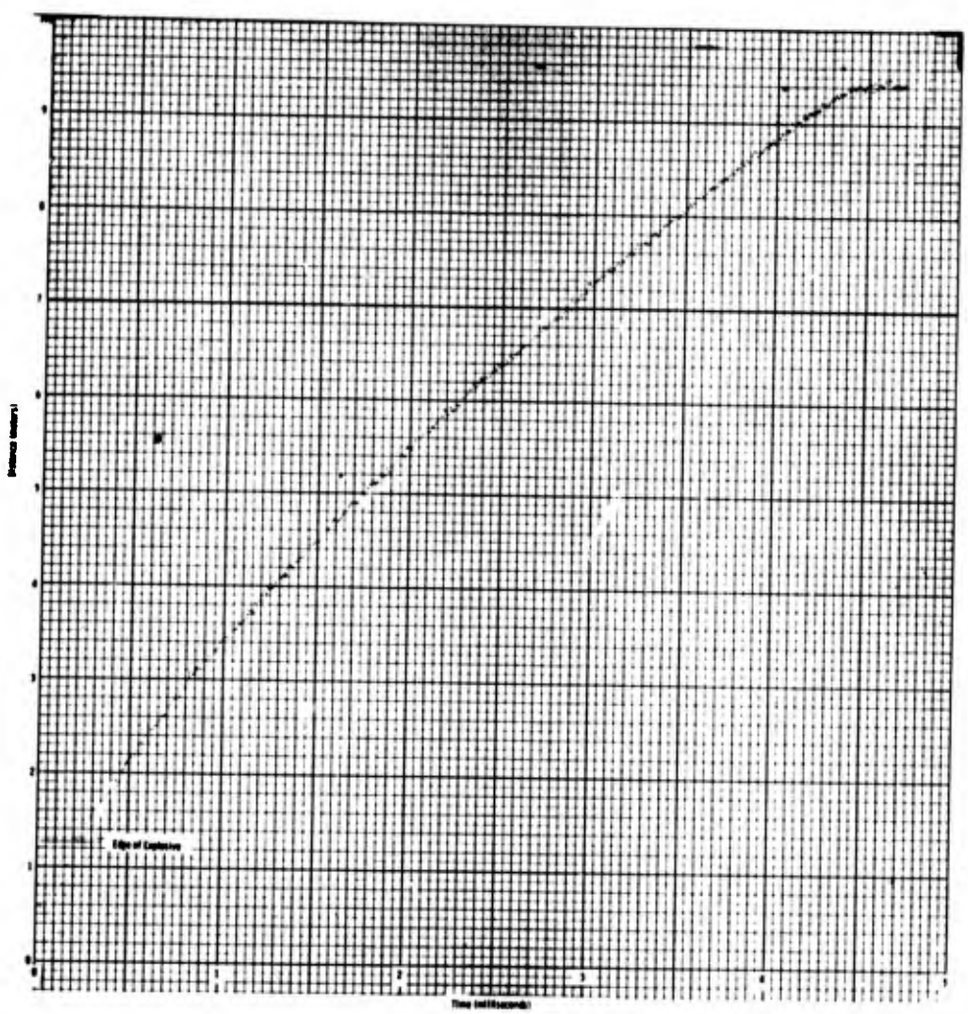

Figure 3.4 Time of arrival versus distance from Slifer measurement

Arrival Times at all Instrument Stations

In Fig. 3.5, arrival time as measured in the grout by the Slifer is compared with arrival times at the other stations. These times are cited in the subsequent summary tables, which are in turn supported by records in the appendices. From the Slifer measurement at 9 meters, the velocity has been extended according to the sonic velocities of 1.48 to 1.75 m/msec, as reported by Mather[18] for the grout used for stemming. Sonic velocities in the medium at shot depth were notably greater than in the grout, ranging from 2.35 m/msec between 7 and 12 meters to just over 2 m/msec between 12 and 36 meters.

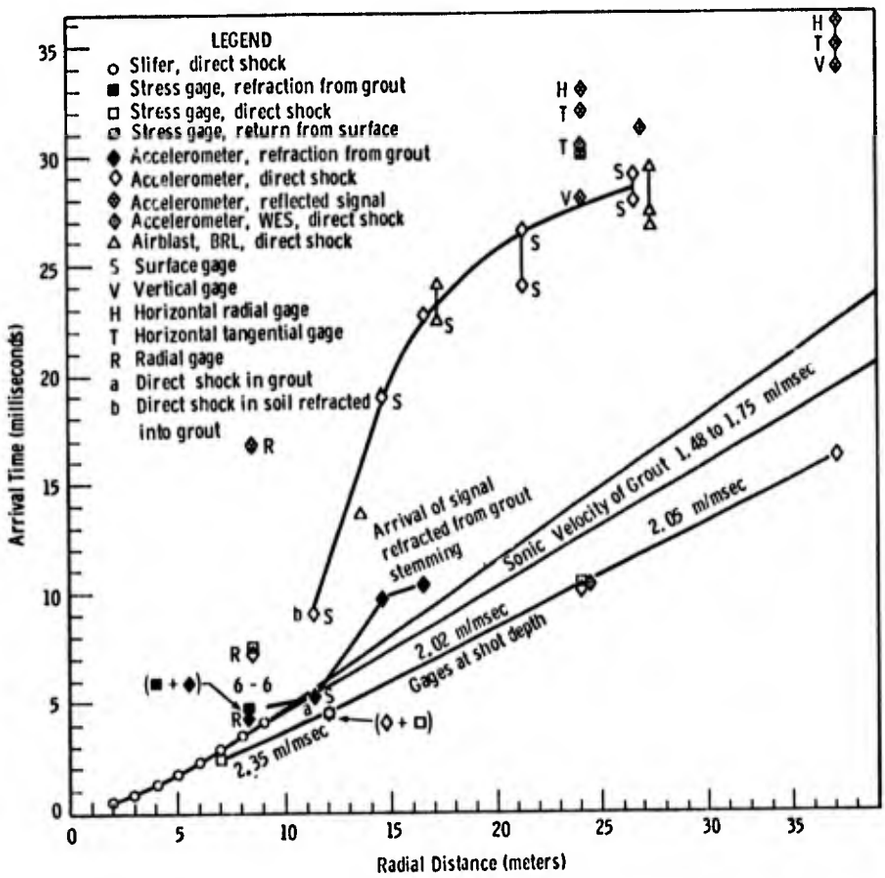

Figure 3.5 Summary plot of arrival time versus distance at all stations

The direct shock arrived at the surface stations much slower, as shown in Table 3.2. Average velocities increase from a minimum of 0.73 m/sec for the station 12 meters from surface zero to 0.93 at 24 meters, indicating a refracted signal traveling through the higher-velocity material closer to shot depth. The fact that average velocity to the near-surface-zero station is higher can be accounted for by the higher velocity in the grout.

TABLE 3.2

Arrival Times at Surface Stations

Radial Distance from Surface Zero (m)	Slant Distance from Detonator (m)	Arrival Time (msec)	Apparent Average Velocity Detonator to Gage (m/msec)	Apparent Average Velocity Over Incremental Distance (m/msec)
0	11.35	9.18	1.23	
9	14.47	18.92	0.76	0.25
12	16.51	22.65	0.73	0.55
18	21.27	26.5	0.80	1.24
24	26.54	28.15	0.93	2.64

The observation that the principal signal arrived at the near-surface-zero accelerometer at 9.18 msec, while an extension of the Slifer data indicated an arrival of about 5.5 msec, led to re-examination of the acceleration record. Close scrutiny showed a small (100-g) pulse arriving at 5.3 msec. Integrated, that small pulse gave a particle velocity of about 1.2 m/sec. Using measured particle velocity and shock velocity, together with Mather's value of 1.94 gm/cc for density of the stemming grout,[18] a peak stress of 20 bars was determined. If the rate of stress attenuation with distance of $R^{-3.9}$ calculated by Bryan and Burton[19] for this stress region in the medium is the same in the grout, and if it is used to extrapolate from 11.33 meters to 9.4 meters, where the Slifer stopped recording arrival, a peak stress of 40 bars is indicated. Slifer cables typically start crushing at static stresses as low as 75 bars, with the dynamic crushing margin estimated[20] to be 50 percent higher, or about 110 bars. Thus, the stress derived above is considerably below the expected crushing limit.

This reasoning leads to the conclusion that the 100-g pulse arriving at the surface-zero station is, in fact, the pulse to which the Slifer is responding. The low stress level can be accounted for only by refraction into the surrounding lower-velocity medium as the pulse propa gates up the grout column. Similarly, arrival of the principal pulse at the surface-zero station at 9.18 msec must be accounted for by refraction from the lower-velocity medium into the grout column. Just as the arrival at 5.3 msec is consistent with the Slifer data, so also is the later arrival at 9.18 consistent with arrival of the main pulse at other surface stations. The records show an insignificant pulse at the 9- and 12-meter surface stations ahead of the main pulse. This early arrival is interpreted also as a refraction from the grout column, greatly attenuated by the medium.

At the 6-meter-radius, 6-meter-deep station the main arrival at about 7 msec is preceded at 4.8 msec by a weak signal that also is interpreted as being refracted from the grout column. This station, we well as the 24- and 36-meter stations at shot depth, show arrival of a wave returning from the surface. These also are shown in Fig. 3.5.

Arrival time of the airblast measured by the BRL gages has been added to Fig. 3.5 These ground-shock-induced arrival times are consistent with those of other surface-level measurements. Arrival time at a WES accelerometer on the surface at 24 meters also is consistent.

Stress Measurements

Stress records are reproduced in Appendix A; principal parameters are summarized in Table 3.3.

TABLE 3.3

Summary of Stress Measurements
ESSEX I 12 MS 23 August 1973
21,594 Pounds Nitromethane Buried 12 Meters Deep, Fully Stemmed

Gage Type		Distance (m)	Depth (m)	Gage Range	Gage Sensitivity	Calibration Step (kbar)	Arrival Time* (msec)	Peak Stress (kbar)	Time of Peak* (msec)
Ytterbium	SY-1	6	6	Low	High	0.7	7.27 (a)	(b)	10.40
				Low	Low	0.7	7.26 (a)	1.03	10.40
	SY-2	6	6	High	High	2.0	7.26 (a)	1.07	10.43
				High	Low	2.0	7.24 (a)	1.07	10.06
	SY-3	7	12	Low	High	1.0	2.42	(c)	
				Low	Low	1.0	2.42	(c)	
	SY-4	7	12	High	High	3.0	2.458	2.93	2.580
				High	Low	3.0	2.448	2.95	2.563
Lithium Niobate	SL-1	12	12	Low	High	0.2	4.55	(c)	
				Low	Low	0.2	4.54	(c)	
	SL-2	12	12	High	High	0.6	4.50	0.85	5.17
				High	Low	0.6	4.60	0.85	5.11
	SL-3	24	12	Low	High	0.1	(d)	(d)	(d)
				Low	Low	0.1	(d)	(d)	(d)
	SL-4	24	12	High	High	0.3	10.52	0.144	11.59
							35	0.075	36.2 (e)
				High	Low	0.3	10.56	0.147	11.53
							35	0.070	36.5 (e)

*Reading accuracy for time is ±0.01 millisecond.
(a) Arrival time of precursor; shock estimated at 8.6 - 9.2 msec.
(b) Limited at 1 kbar.
(c) Limited.
(d) Lost.
(e) Reflected signal.

At 6 meters depth and 6 meters distance the wave (Figs. A-1 and A-2) shows what appears to be an elastic precursor. Since no precursor is evident at 12 meters depth and 7 meters radius (Figs. A-3 and A-4), it is suggested that the interpretation of an elastic precursor be viewed with some skepticism, especially in view of refractions from the grout column.

The first ytterbium gage (SY-1) gave a very good record on the low-sensitivity channel, while the high-sensitivity channel exceeded band edge (Fig. A-1). The second ytterbium gage (SY-2) reproduced the wave form reasonably well but was low in amplitude throughout (Fig. A-2). Figure 3.6 shows the records for the low-sensitivity channels for SY-1 and SY-2 plotted to the same scale. SY-2 is higher than SY-1 at the toe of the rise.

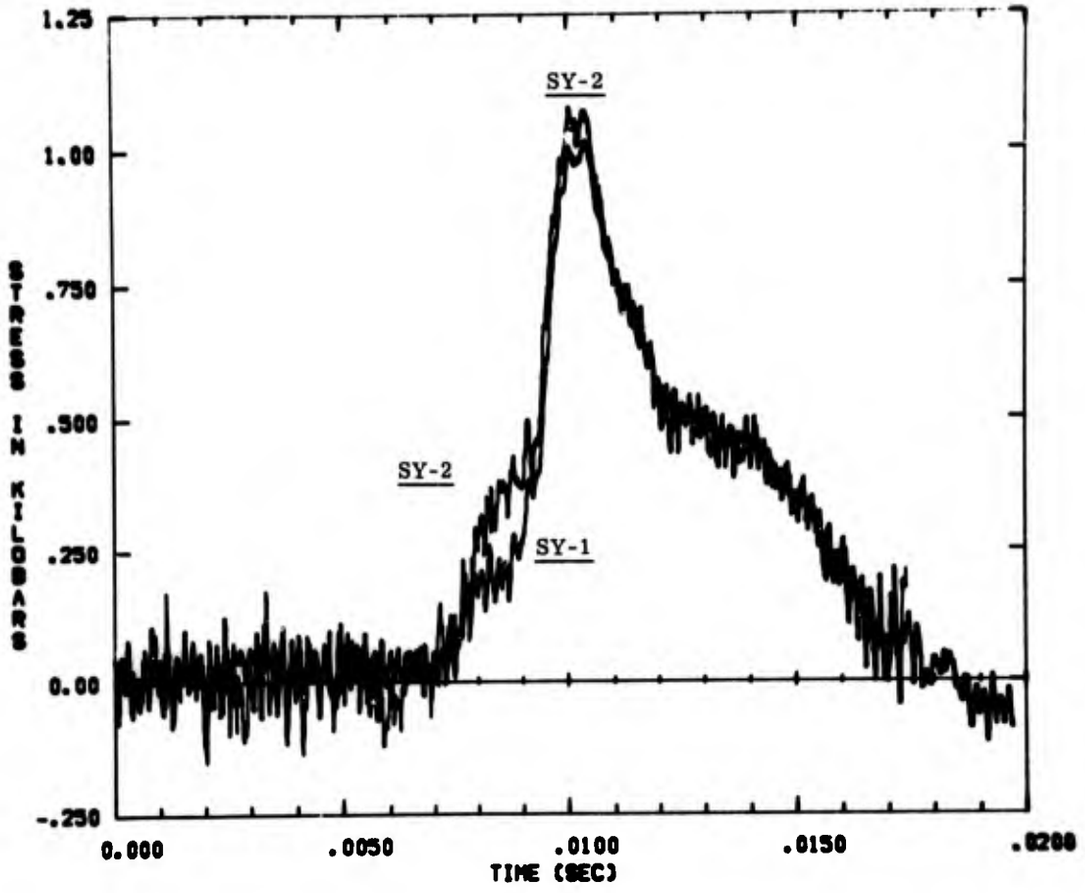

Figure 3.6 Comparison of records from SY-1 and SY-2

At the station 12 meters deep and at 7 meters radius the record was beyond band edge on both the high and low sensitivities of SY-3 (Fig. A-3). SY-4 (Fig. A-4) gave a good record on both sensitivities until the gage or cable failed at 2.65 msec. At the station 12 meters away at shot depth the first lithium niobate gage (SL-1) gave a record that was limited by band edge for both sensitivities. Whereas the ytterbium gages exhibited only a very small signal from the electromagnetic pulse, the lithium niobate gage shows a pronounced negative excursion at zero time, followed by a positive departure as the circuit picked up a charge that remained for a time long compared with the duration of the stress wave (see Fig. A-5, which shows the records at two different time scales). Consequently, peak stress was read from the breakaway rather than from the zero-stress baseline.

The other gage (SL-2) had no evidence of an EM signal, nor did the circuit pick up a charge (Fig. A-6).

SL-3, at shot depth at the 24-m station, was the only gage on the shot that returned no record. The reason is not known. The other gage (SL-4) gave an excellent record (Fig. A-7), the peak of the main shock being limited slightly by band edge. The record shows a pronounced negative EM spike at zero time, then a strong positive excursion as the circuit again took on a charge. Following the initial positive response to the EM pulse is a second positive pulse that also must be EM since its arrival at 5 msec is too early to be attributed to ground motion. The record also shows an apparent refracted signal at about 35 msec. The records for SL-1 and -2 were reexamined, and no comparable signal was found there at that time. The possibility that the signal is a return from the surface is less credible in view of the fact that the excursion is positive rather than negative, as it should be for a tensile wave reflected from the surface. A more reasonable explanation is a refracted or reflected return from a high-impedance layer. Assuming a sonic velocity of 1.5 m/msec, a reflecting layer would have to be at about 23 meters to account for the arrival time of the signal. A seismic refraction survey along the S-3, S-4 line shows a discontinuity of from 1.46 to 1.8 m/msec at 22 meters. Survey along the S-9, S-10 line that passes through the 12-MS location shows a discontinuity of from 0.61 to 1.58 at 9.4 meters, and one from 0.79 to 1.55 m/msec at 10.4 meters. The harder layer along the S-9, S-10 line is verified by the boring log and penetration tests; the one at or near 22 meters was not seen on the logs.

In Fig. 3.7 the measured peak radial stresses have been compared with those calculated by Bryan and Burton.[15] The short-dashed line represents a fit to the measurements made at shot depth.

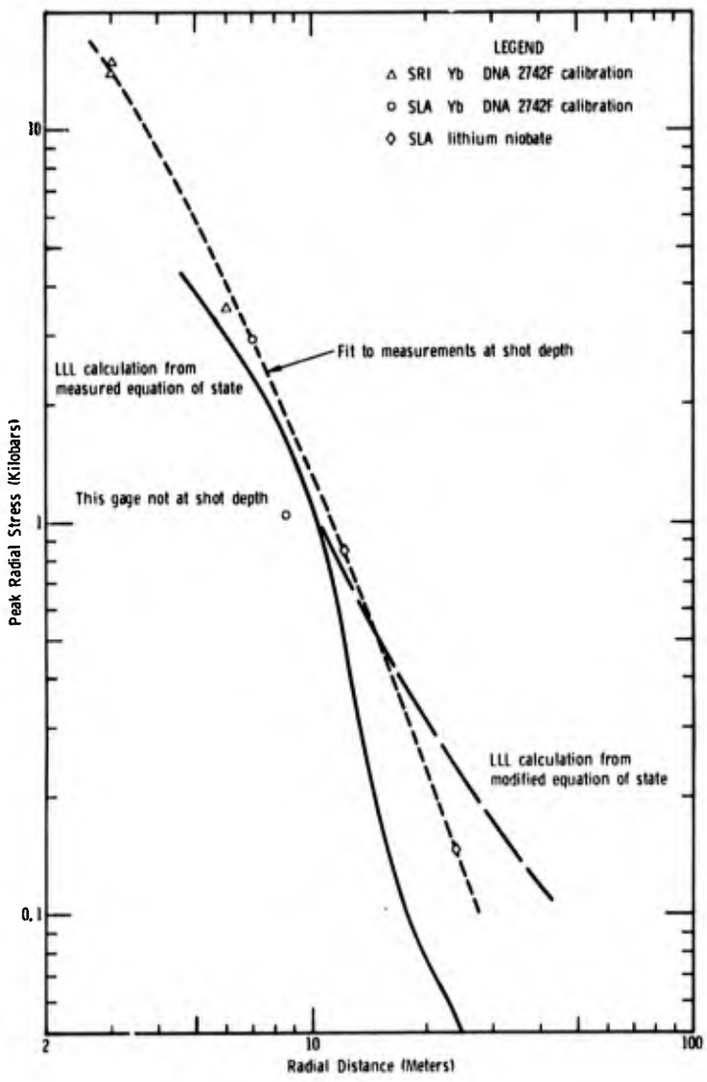

Figure 3.7 Comparison of measures and calculated peak radial stress

Free-Field Ground Motion

Table 3.4 summarizes results of the free-field ground-motion measurements made at shot depth and half-shot depth. Records of the measurements, together with velocity-time plots obtained from first integrations and displacement-time plots from second integrations, are reproduced in Appendix B.

Some discussion of the records from each station is in order.

The radial acceleration measurements 6 meters deep and at 6 meters radius (Figs. B-1 and B-2) gave peak accelerations greater than 6000 g's on three of the records. That of the other (6-6 AR-LO, high sensitivity) exceeded recording band edge. At 9.5 msec either the gages or the cables failed and no further information was recorded. At that time the acceleration level had not yet returned to zero, so the true peak velocity is greater than would be obtained by integrating the acceleration record to the time of failure. Similarly, full displacement occurs well after failure time and is greater than is shown to the time of failure.

Two accelerometers 12 meters from the charge at shot depth, measuring horizontal radial acceleration, underwent gage or cable failure at about 0.25 msec after signal arrival (Fig. B-3). The record of the high-range, low-sensitivity gage shows that peak acceleration at that station was in excess of 6500 g's, considerably more than the 1500 predicted (Table 3.1). Because full acceleration was beyond recording band edge, and the full pulse duration was not measured, all that can be concluded is that peak particle velocity at this station was greater than 11 meters per second.

There were also two accelerometers measuring horizontal radial motion 24 meters from the charge at shot depth. At this station two distinct pulses were recorded, one at about 10 msec and the other at about 34 msec. The high-sensitivity channel of the low-range gage (Fig. B-4) has excursions beyond band edge on the positive and negative peak accelerations of the first pulse and on the positive peak of the second pulse. The low-sensitivity channel was beyond band edge on the positive and negative peaks of the first pulse (Fig. B-5). The high-range gage (Fig. B-6) had the same limitations for the first pulse on the high-sensitivity channel, as would be expected, since set ranges were the same.

The low-sensitivity channel (Fig. B-7) had only the first acceleration peak at band edge. The region of the peak was hand-plotted above 400 g's at a greatly expanded time scale (1 inch = 0.1 msec), and the rising portion of the peak was extrapolated to meet a backward extrapolation of the declining portion at an apex. This apex was at 1400 g's, only 100 g's above the 1300-g peak recorded. The integral of the difference would have added only 0.15 m/sec to the velocity peak, and it is concluded that any effect of band edge was indeed quite small. There is a decrease in velocity between the two pulses and after the second pulse, as there would be if the outward forcing function was decreasing with time. This would be the case if the outward forcing function were reducing cavity gas pressure. Although it is not shown in the figure, the velocity became negative at about 120 msec and remained so until cable failure at about 450 msec. A peak outward displacement of about 21 cm was observed at 120 msec.

Without doubt, one of the most important findings from the 12 MS event was the larger-than-expected nonradial motion. To explore this finding further, the velocity-time functions for horizontal radial motion from Fig. B-7, the adjusted velocity-time for vertical motion from Fig. B-10, and the adjusted velocity-time for horizontal tangential motion from Fig. B-13 were combined to provide a velocity vector sum as a function of time. The result is shown in Fig. 3.8.

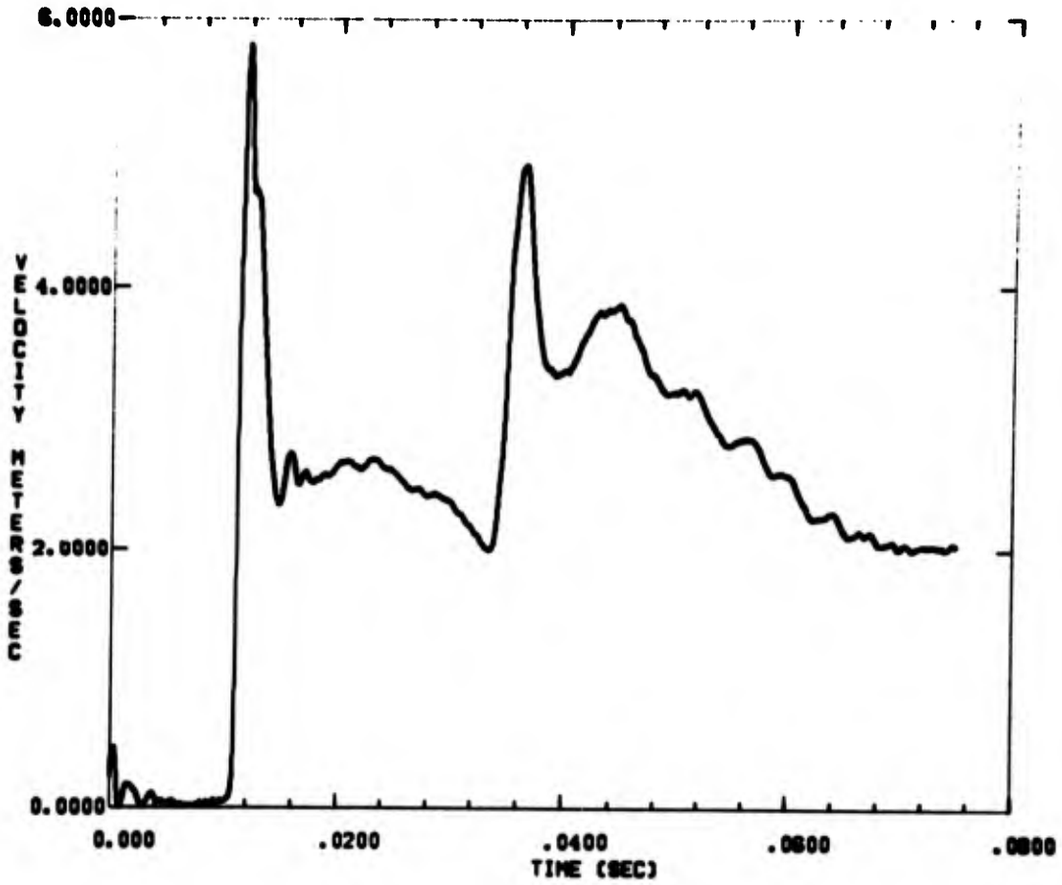

Figure 3.8 Vector sum of radial, vertical, and tangential components of velocity as a function of time at the 24-meter station

When ground motions in a homogeneous medium are calculated using hydrodynamic codes, only radial motions are observed, vertical motion appearing at late times as a result of the signal returning from the free surface. For structured or layered media, vertical and tangential components may be observed. The Essex site medium is not homogeneous, and certainly some of the vertical and tangential motions observed are a result of the inhomogeneities. The point to be made here is that the velocity vector of Fig. 3.8 is probably a more appropriate parameter to compare with calculated radial velocity than is the measured velocity.

At the 36-meter station at shot depth, both channels of the low-range horizontal gage were limited at band edge (Figs. B-14 and B-15). Positive and negative peaks of both first and second pulses were limited on the high-sensitivity channel, as were the positive and negative peaks of the first pulse on the low-sensitivity channel. The high-range horizontal gage (Fig. B-16) also was

limited on the positive and negative peaks of the first pulse on the high-sensitivity channel, as it should be, since band edge was the same. The low-sensitivity channel (Fig. B-17) gave a record with only the positive peak limited, and the negative peak unlimited. That peak was restored between 17.38 and 17.85 msec, adding 1.0 m/sec to the positive-peak velocity. The result of the velocity adjustment is shown in Fig. B-18. The velocity reached a final peak at about 60 msec, thereafter returning to zero at about 130 msec, at which time the peak displacement was 7 cm (Fig. B-24).

The vertical accelerometer at 36 meters gave a high-sensitivity record that was severely limited on most of the positive and negative peaks (Fig. B-19). The low-sensitivity record was limited by band edge on only the first positive peak (Fig. B-20). That peak was restored between 17.45 and 17.96 msec, adding 0.94 m/sec to the velocity peak. The result of the adjustment is reproduced as Fig. B-21. The adjusted record is questionable if the high frequency immediately following entry into a region of negative acceleration (Fig. B-20) is not valid data.

The tangential accelerometer at 36 meters also gave a high-sensitivity record (Fig. B-22) that was severely limited on most of the positive and negative peaks of the first pulse. The low-sensitivity channel gave records that were not limited (Fig. B-23). From the first pulse there was a peak clockwise velocity of 0.17 m/sec and a counterclockwise peak of 0.18. There was a subsequent counterclockwise peak of 0.22 m/sec associated with the train of waves returning from the surface. Residual counterclockwise displacement of about 0.1 cm occurred after about 50 msec.

As with the velocity-time records from the 24-meter station, those from the 36-meter station were used to determine velocity vector sums as a function of time. Used for the plot were the adjusted horizontal radial velocity-time of Fig. B-18, the adjusted vertical of Fig. B-21, and the unadjusted horizontal tangential of Fig. B-23. The result of the vector sum is shown in Fig. 3.9. Again, the vector sum may be better compared with calculated particle velocity than the radial measurement.

In Fig. 3.10, peak accelerations have been plotted versus range. There is not a single attenuation rate, and since the station at 6 meters depth and range (8.5 meters radial) was shallower and in a medium with lower sonic velocity, the different rate may be explained by those differences. The peak particle velocities (Fig. 3.11) agree well with Bryan and Burton's calculation. At the 24- and 36-meter locations, circles indicate the vector-sum peak velocities. Although the measured horizontal radial peaks agree well with the calculation and the vector sum falls higher, it does not seem possible to conclude that the former rather than the latter is the parameter with which calculated peak velocities should be compared.

Using the simple relation $P = \rho_o Uu$, peak radial stress was determined from the measured density at shot depth (1.986 gm/cc), the measured shock velocity (1.18 m/msec for the 6-6 station, and 2.03 for the 24- and 36-meter stations), and the particle velocities of Table 3.4. Peak stresses

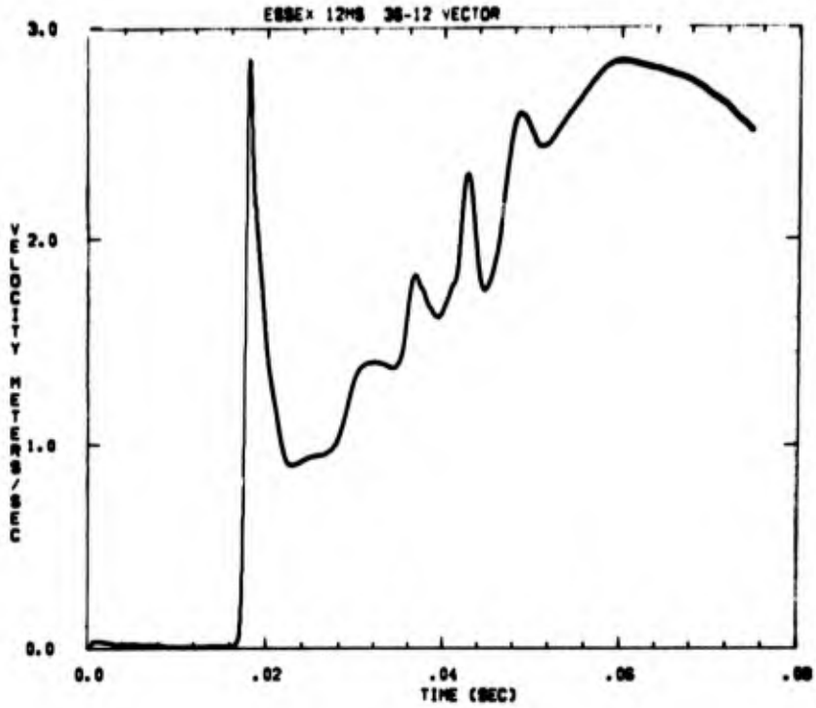

Figure 3.9 Vector sum of radial, vertical, and tangential components of velocity as a function of time at the 36-meter station

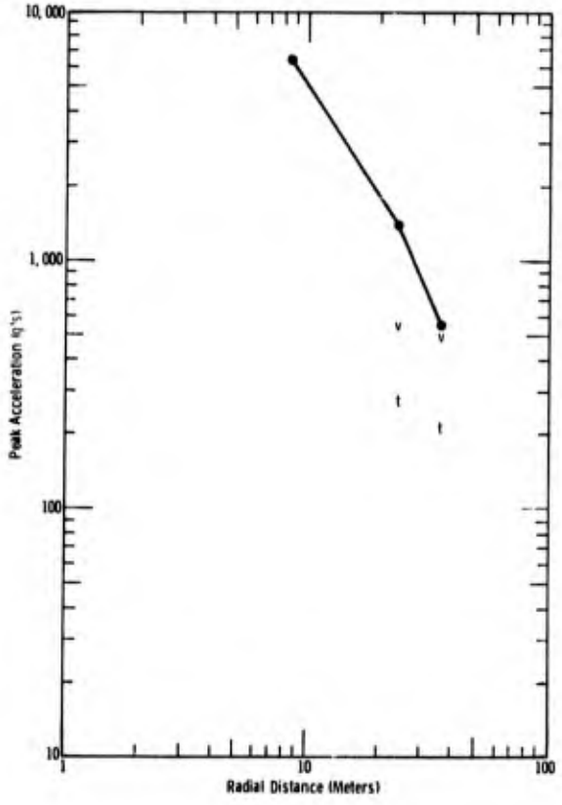

Figure 3.10 Peak acceleration versus radial distance for measurements at shot depth and half shot depth

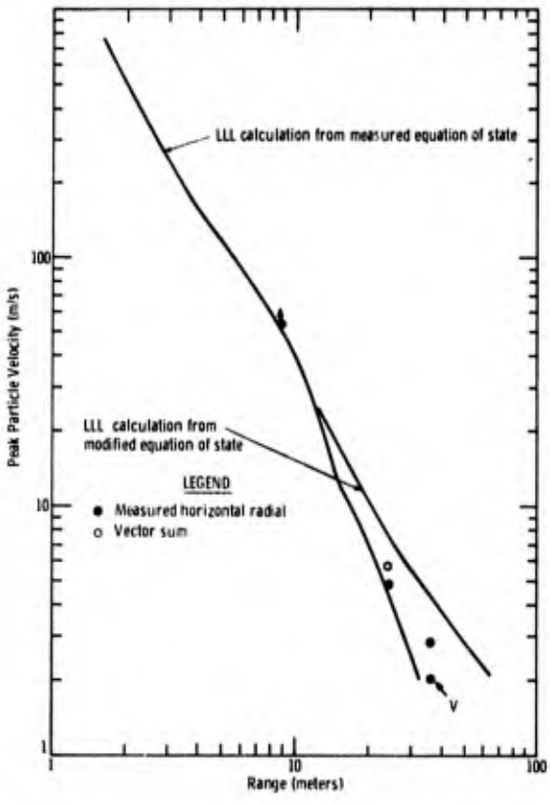

Figure 3.11 Peak particle velocities measured compared with those calculated

were derived by using both the radial and vector sum of the three measured components. In Fig. 3.12 these stresses have been added to the measured stresses of Fig. 3.7. At the 6-6 and 24-meter stations stresses determined as above are higher than the measured values. The half-shot-depth station was also supposed to have been in Unit 5, yet shock arrival times (see Table 3.3 and Fig. 3.5) indicate a shock velocity significantly below that at shot depth. If shock velocity at the 6-6 meter station is taken into account, the peak stress determined from peak radial acceleration could fall below the direct measured stress value.

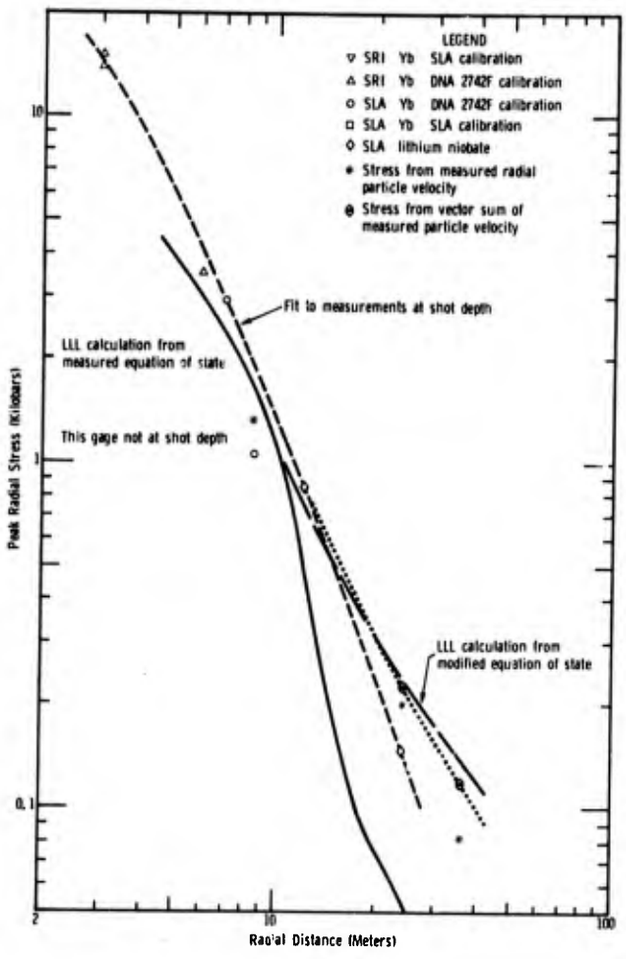

Figure 3.12 Comparison of measured peak stress and stress derived from particle velocity

The authors have indicated by a dotted line their interpretation of the stress-distance obtained by measurement, which should be compared with calculated results. The interpretation applies only at shot depth. The medium at the 6-6 meter station is sufficiently different from the medium at shot depth that stresses measured there should not be compared with those measured at shot-depth stations.

Surface-Motion Instrumentation

Results of surface-motion acceleration measurements are summarized in Table 3.5. Records of the gages, together with their first and second integrations, are reproduced in Appendix C.

The near-surface-zero station had peaks beyond band edge for the high-sensitivity channel of the low-range gage (Fig. C-1). The other three channels at this station gave records (Figs. C-2 to C-4) that are in good agreement for acceleration, velocity, and displacement. Results illustrated in Figs. C-3 and C-4 are essentially identical since they were from the same gage, split through different voltage-controlled oscillators to give the two sensitivities. Calibration step and signal amplitude were a smaller percentage of band edge for the low-sensitivity record; hence comparison is an evaluation of data-recording and reduction techniques. Figure C-2 is from an entirely different gage in the same canister and at 30 msec shows a velocity of 45 m/sec versus 50 for the other gage, and a displacement of 71 cm versus 80.

A small signal, which can be seen in the record from the most sensitive channel at about 5 msec, was mentioned in a previous section in connection with different arrival times of an early wave in the grout column and a later, larger pulse refracted from the medium into the grout column. That portion of the record has been expanded, digitally smoothed, and integrated, and is shown in Fig. 3.13 to support the discussion in the section on arrival times.

The principal acceleration pulse in Fig. C-4 is quite complex and in Fig. 3.14 it, together with its integral, has been expanded to reveal detail. The gage, or more probably the cable, failed at about 420 msec. The records of the low-range and high-range gages (low-sensitivity only) are shown to 400 msec in Fig. C-5. At 400 msec the velocities were 97 and 80 m/sec and displacements were 30 and 27 meters respectively. In the next section these displacement-time records will be compared with those measured photographically. At 400 msec the mound center (actually the grout plug) was still growing, although velocity was close to a peak. It is remarkable that the cable lasted as long as it did in view of the approximately 90 feet of vertical mound growth before failure. That the record is credible to those times will be shown in the next section, where these displacements are compared with those obtained photographically.

At the 9-meter near-surface vertical station the record was obtained for more than one second. In Fig. C-6 the results are reproduced to 40 and 100 msec. Note the small signal at about 10 msec, which is attributed to the refracted wave from the grout column. In Fig. C-7 the results are portrayed to 0.4 and 1.6 second. There it is seen that a peak velocity of nearly 30 m/sec is reached between 250 and 350 msec, and that at the end of the record, displacement has reached 33.5 meters and was continuing. Figure C-8 shows 40 msec of the low-sensitivity record from the same gage. Because the gage range was set for much larger accelerations, the signal-to-noise ratio is small. In the lower half of the figure is shown the record for 1.6 seconds. The peak velocity is about the same as for the high-sensitivity channel, but the peak occurs slightly earlier, and thereafter the velocity decreases at a much more rapid rate than in the record of the other channel.

A

TABLE 3.5

Summary of Surface Accelerati
ESSEX I 12 MS 23 A
21,594 Pounds Nitromethane Buried 12 M

Accelerometer Designation	Accelerometer Orientation	Distance (m)	Depth (m)	Slant Distance** (m)	Gage Range	Gage Limit (g's)	Gage Sensitivity	Calibr Step (
0-0 AV-LO	Vertical	2/3	2/3	11.33	Low	10,000	High	97
					Low	10,000	Low	97
0-0 AV-HI	Vertical	2/3	2/3	11.33	High	20,000	High	3,00
					High	20,000	Low	3,00
9-0 AV	Vertical	9	2/3	14.22		10,000	High	62
						10,000	Low	62
12-0 AV	Vertical	12	2/3	16.38		5,000	High	29
						5,000	Low	29
12-0 AH	Horizontal	12	2/3	16.38		1,000	High	14
						1,000	Low	14
18-0 AV	Vertical	18	2/3	21.07		1,000	High	31
						1,000	Low	31
24-0 AV	Vertical	24	2/3	26.32		1,000	High	16
						1,000	Low	16
24-0 AH	Horizontal	24	2/3	26.32		1,000	High	10
						1,000	Low	10

*Time resolution limited to 0.02 msec.

**Corrected for surface elevation

(L) Peak Limited

(a) Values poorly defined because of poor signal-to-noise ratio.

TABLE 3.5

of Surface Acceleration Measurements
ESSEX I 12 MS 23 August 1973
romethane Buried 12 Meters Deep, Fully Stemmed

Gage Sensitivity	Calibration Step (g's)	Arrival Time* (msec)	Peak Acceleration (g's)	Time of Peak* (msec)	Velocity (m/sec)	Time of Velocity* (msec)
High	979	5.34	96.5	6.47	1.21	8.7
		9.18	1,286 (L)			
Low	979	5.30	95	6.3	1.21	8.7
		8.70	3,500	10.22	45.7	30
High	3,000	5.30	Small	6.5	1.3	
		9.20	3,110	10.34	50	30
Low	3,000	5.30	Small	6.5		
		9.65	3,680	10.20	51.5	30
					80 (Peak)	400
High	628	9.74	Small			
		18.92	510	20.96	30 (Peak)	320-410
Low	628	9.70	Small			
		18.75	380 (a)	20.40	35	500
High	298	10.40	Small			
		20	260	28	19.7	280-320
Low	298	20	256	26.88	18	200
High	148	24	182	26.6	3.3 (Peak)	29.5
					12.9 (Peak)	1,000
Low	148	22.65	157	25.97	3.2 (Peak)	28.8
High	319	24	88	31.31	10 (Peak)	80
Low	319	26.5	85	31	10 (Peak)	80
High	161	28	21	36.70	4.6	52
			38	58.24	6.1 (Peak)	85
Low	161	29	20.7	36.31	(a)	(a)
			36.8	57.95	(a)	(a)
High	101		14	56.63	4	200
Low	101	(a)	(a)	(a)	(a)	(a)

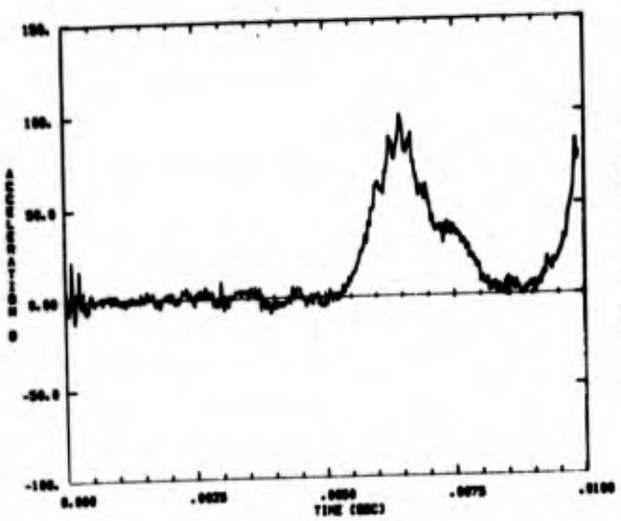

Figure 3.13a

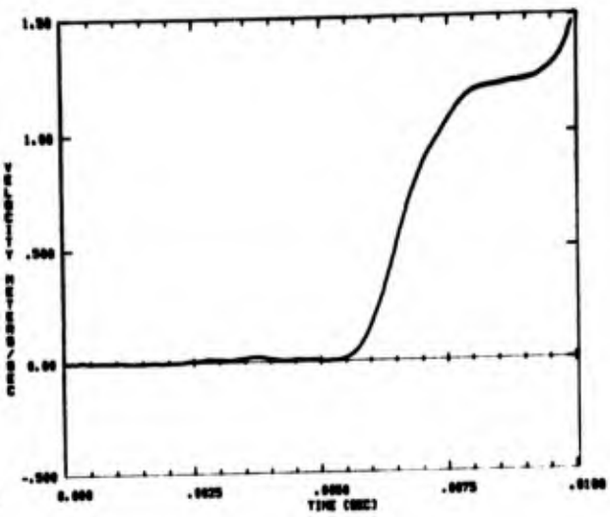

Figure 3.13b

Figure 3.13 Time and amplitude expansion of the signal propagated through the grout column

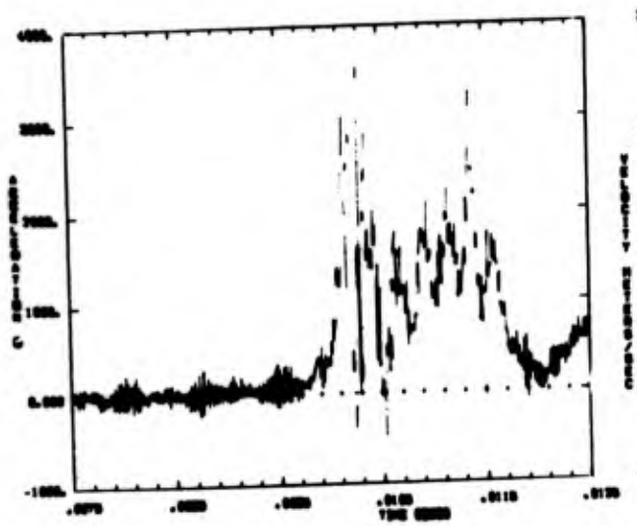

Figure 3.14a

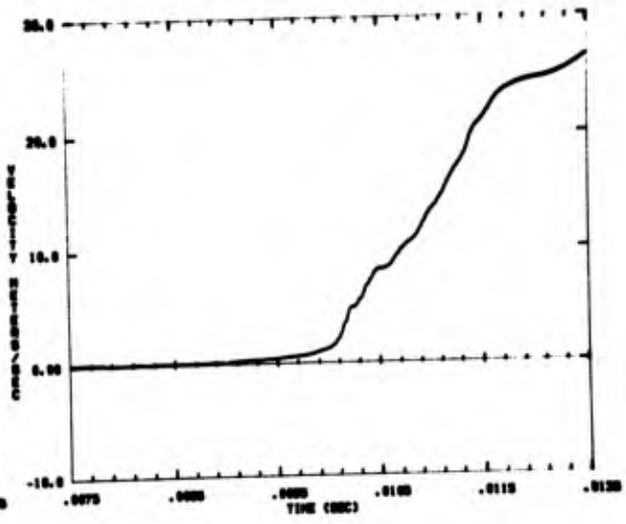

Figure 3.14b

Figure 3.14 Time and amplitude expansion of the principal signal at the top of the grout column

Since baselines were determined over a 3-sec interval for both channels (see Appendix R), the difference is attributed to differences in stability with time of recording-equipment components. The record from the high-sensitivity channel is considered the more credible.

At the 12-meter station, both vertical and horizontal components were measured. Figure C-9 shows the record from the high-sensitivity vertical channel to 0.05 and 2.4 seconds. A peak velocity of 17.8 m/sec occurred around 200 msec, and vertical displacement was 21.4 meters at 2.4 seconds. Figure C-10 shows the results for low sensitivity at the same time scales. Differences are for the reason given above, and again the high-sensitivity channel gave the record judged the more credible.

Records from the high-sensitivity channel of the horizontal gage at 12 m are shown in Fig. C-11 for the first 0.05 and 2.4 sec. Whereas vertical motion at this and the closer stations made essentially no acceleration excursion into the negative range, the horizontal shows a marked negative phase, causing a decrease of about half the peak velocity immediately following a peak velocity of 3.3 m/sec. This dip was followed by a period of increasing velocity to a relatively constant velocity of about 13 m/sec from 0.6 to 1 sec. This in turn was followed by another decrease. The horizontal displacement at 1 sec was about 10.6 m, and at cable failure at 2.4 sec was 28 m.

If the canister had remained in a vertical orientation, its displacement trajectory would be as shown by the circles in Fig. 3.15. However, it is certain that during this time the canister underwent some rotation. If the rotation were known, the trajectory could be corrected for it, but since no direct measurement was made, the rotation must be approximated. One method of doing this would be to assume that the axis of the canister remained normal to the ground surface as the mound grew. This requires determination of the slope of the mound from high-speed photography, but there was no marker that would clearly identify the surface intercept of the 12-m station.

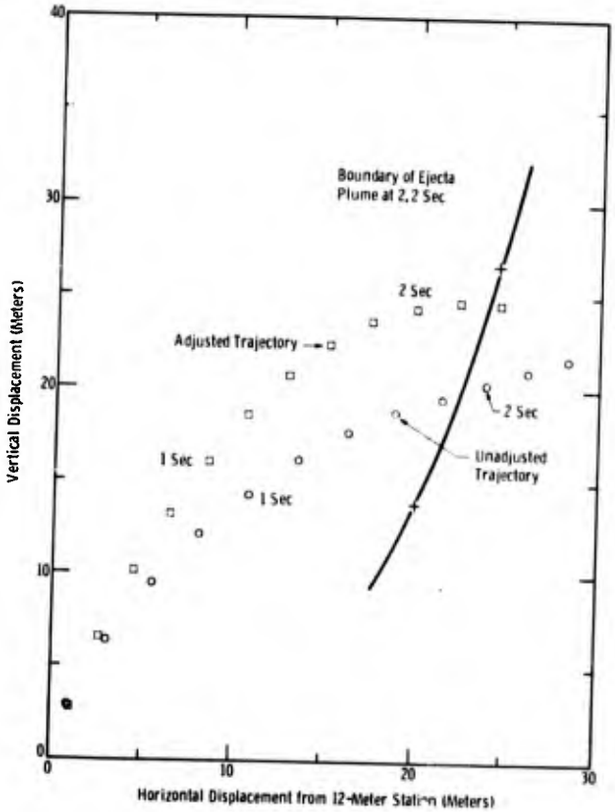

Figure 3.15 Horizontal displacement from 12-meter station (meters)

The procedure used was the following. The canister is assumed to follow a ballistic trajectory. An initial ballistic trajectory angle was obtained from the position of the canister during the interval from 0.3 to 0.4 sec when its vector velocity was maximum. (Both measured and ballistic trajectories were obtained at

0.1-sec intervals.) This assumes that there had been little tilt to the canister up to that time. The initial velocity for the ballistic trajectory was chosen as that which would give the measured maximum velocity during the interval from 0.3 to 0.4 sec. For each 0.1-sec interval the vertical and horizontal components of the incremental displacement, ΔV_1 and ΔH_1, were adjusted according to $\Delta V_2 = \Delta V_1 \cos \varphi - \Delta H_1 \sin \varphi$ and $\Delta H_2 = \Delta H_1 \cos \varphi + \Delta V_1 \sin \varphi$, where $\varphi = \theta_b - \theta_1$, where θ_b and θ_1 were the slopes of the ballistic and unadjusted trajectories, respectively, during each 0.1-sec increment, and where subscript 2 indicates the adjusted component of the incremental displacement. The adjusted trajectory obtained in this manner is shown by the squares in Fig. 3.15.

The results of the low-sensitivity record from the horizontal gages are shown in Fig. C-12 for 0.04 and 2.4 sec. Again, the long-term integration of the low-sensitivity channel is considered less reliable.

In Fig. C-13 the records from the high-sensitivity channel of the single vertical gage at 18 meters are shown for 0.1 and 2.2 sec. The records for the low-sensitivity channel are shown in Fig. C-14 for the same times. In this case the low-sensitivity channel gave the record considered the most credible. A peak vertical velocity of 10 m/sec at about 0.8 sec and a peak displacement of 12.4 m at 2.2 sec were observed.

It is worth noting that the apparent crater radius was 18.6 m for this shot. Thus, the gage at the 18-m station was barely inside the crater.

At the 24-meter station both vertical and horizontal components were measured. Using only the high-sensitivity channels, the records for the vertical component are shown in Fig. C-15, and those for the horizontal in Fig. C-16. Vertical velocity peaked at over 6 m/sec at about 85 msec. Vertical displacement peaked at about 1.5 meters at around 0.6 second. Horizontal velocity peaked at about 4 m/sec at a later time than the vertical (around 200 msec), and displacement peaked at 2.36 meters at around 1.0 second. The fact that a maximum displacement was observed is consistent with a location beyond the crater radius.

A signal occurs at about 1.8 seconds that is quite distinct on the vertical record and less distinct on the horizontal. Since this occurs at about the time the velocity becomes zero and displacement becomes constant, it is interpreted as the slap when the upthrust crater lip outside the crater falls back upon the supporting material beneath. At least two subsequent smaller signals can be observed, and are possibly reverberations of the one at 1.8 sec.

Figure 3.16 shows the canister trajectory for the 24-meter surface station, together with its post-shot location. The record from the two gages stopped short at about 3 seconds, presumably from a broken cable. Also, there is some question about the validity of the records after 2 seconds, although some relaxation of the ground at later times should be expected. Whether further relaxation would have brought the trajectory closer to the residual surveyed position of the canister can only be speculated. Also, since the ejecta over the canister was removed by a road grader there is a possibility that its residual position in the horizontal plane was disturbed.

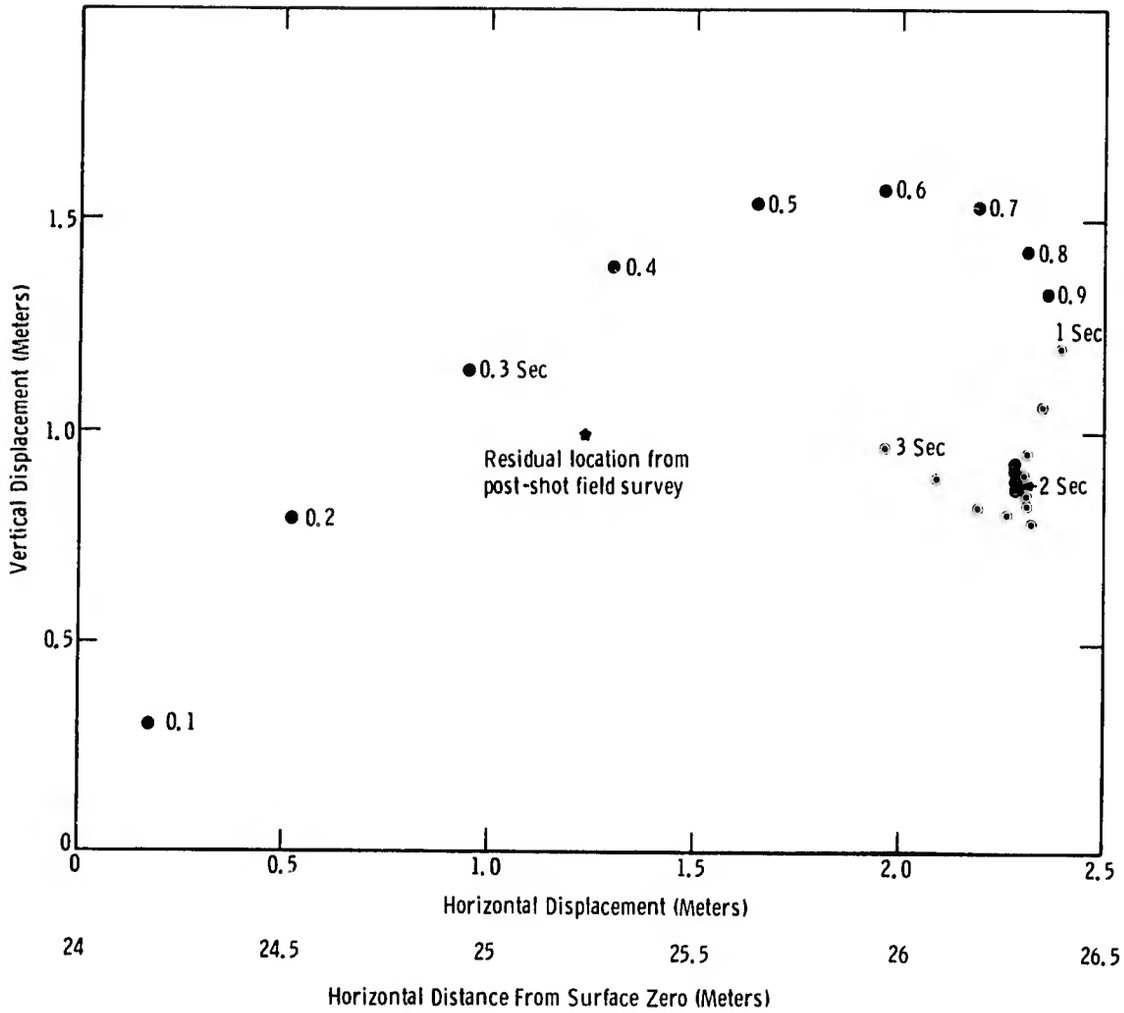

Figure 3.16 Canister trajectory for the 24-meter surface station

If the displacement-time functions for the vertical near-surface canisters are used to plot mound profile as a function of time, the results are as shown by the circles in Fig. 3.17 for the times given. If, in the case of the 12-meter station, the horizontal displacement is taken into account, the trajectory is as shown by the squares. Had horizontal components been measured at each station, the true trajectory would have permitted construction of more accurate profiles. The x's and +'s are data from the right and left sides, respectively, of the mound profile at 0.3 second as recorded by Camera 6. (See following section for other results of high-speed photography.) At the 12-meter station the profile from photography is in excellent agreement with the trajectory from the vertical and horizontal gages, even though it is above the value from the vertical gage alone. In the following section it will be seen that at surface zero the heights from photography are consistently below heights determined from the accelerometers.

In Fig. 3.18 peak acceleration has been plotted versus radial distance and an "eyeball" fit drawn to the data. Attenuation rate with distance is $R^{-4.8}$. That the near-surface-zero accelerations are greater can be attributed to the grout being more dense than the surrounding medium.

At the 24-meter station the two values are for the separate peaks. It was surprising to find horizontal acceleration peaks nearly as large as vertical peaks. Peak velocity data (Fig. 3.19) show a similar trend, with an approximate $R^{-2.8}$ attenuation rate with distance.

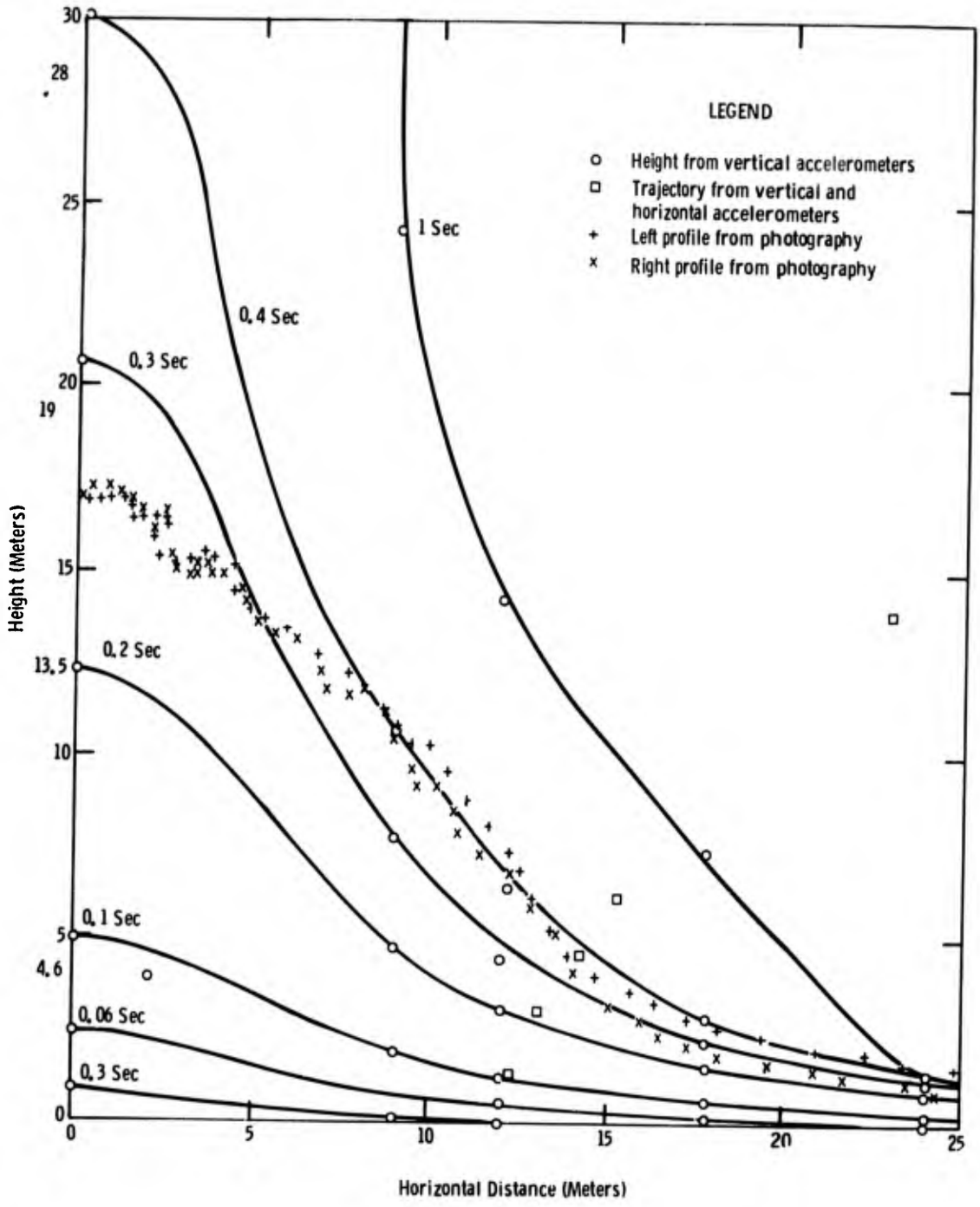

Figure 3.17 Mound profile; 12 MS

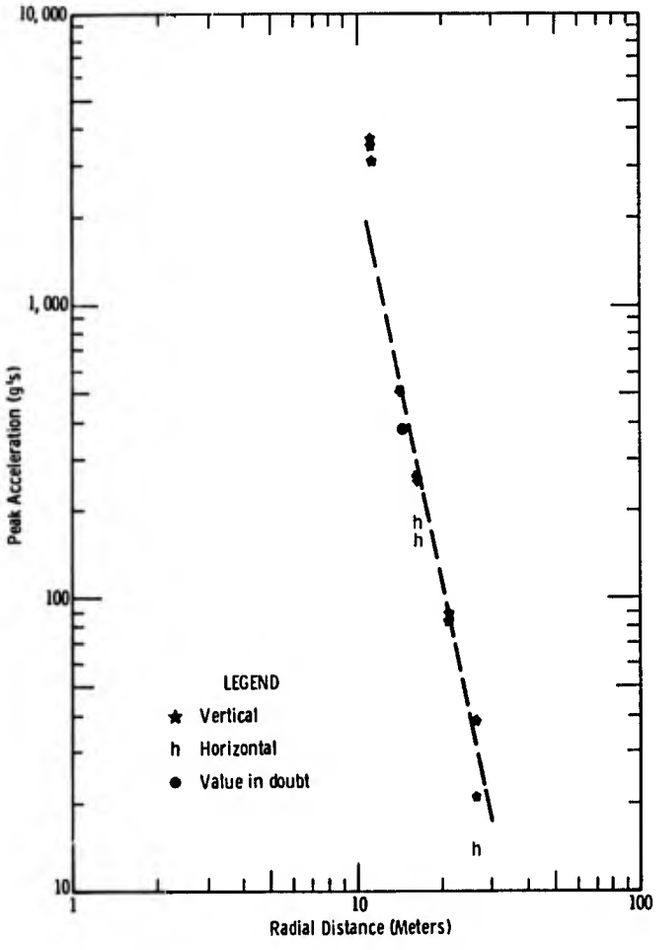

Figure 3.18 Peak vertical surface acceleration versus distance

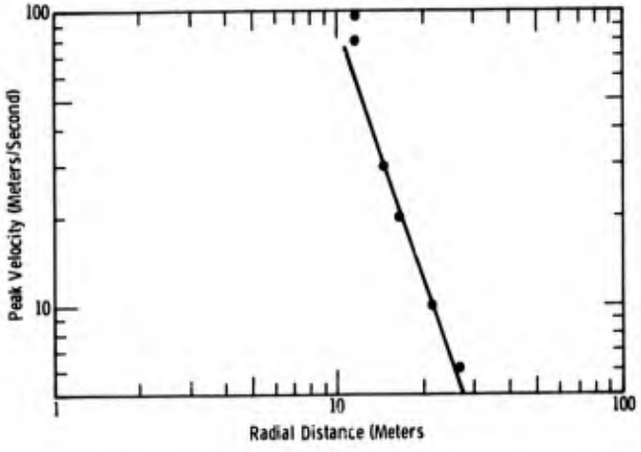

Figure 3.19 Peak vertical surface velocity versus radial distance

Surface Displacement from Photography

High-speed motion-picture cameras recorded surface motion. Cameras were chosen to provide different film speeds and fields of view; generally the higher frame rates were associated with smaller fields of view. Table 3.6 summarizes information on the cameras used.

TABLE 3.6

Summary of Camera Coverage - 12 MS

Camera	Timing (cps)	Camera Speed (fps)	Lens	Film	Field of View				f Stop
					Height		Width		
					(ft)	(meters)	(ft)	(meters)	
(1) Fastax 16 mm	1000	4000	10 in	2479	20.4	6.2	28.2	8.6	4.5
(2) Fastax 16 mm	1000	4000	10 in	2479	20.4	6.2	28.2	8.6	4.5
(3) Fairchild 16 mm	1000	1000	3 in	2496	68.2	20.8	93.9	28.6	5.6
(4) Fastax 16 mm	1000	1000	4 in	2496	51.1	15.6	70.4	21.5	5.6
(5) Fastax 16 mm	1000	4000	2 in	EF	102.2	31.2	140.8	43.0	2.8
(6) Milliken 16 mm	100	128	1 in	EF	204.5	62.3	281.7	85.8	11
(7) Milliken 16 mm	100	128	10 mm	EF	519.4	158.3	715.4	218.0	11
(8) Fastax 8 mm	1000	10000	6 in	2475	17.0	5.2	46.9	14.3	2.7
(9) Milliken 16 mm	100	128	1 in	EF	204.5	62.3	281.7	85.8	11

Figure 3.20 is a plan view of the camera station and reference markers with respect to surface ground zero.

Surface motion was read frame-by-frame in a telereader along a vertical line through surface ground zero- 9, 12, 18, and 24 meters. Since no photo targets were located at these points, the motion read is the intersection of the mound surface with a vertical line at each of the five distances. This result is slightly different from that recorded by the accelerometers, which observe a horizontal component of motion at all but the surface-ground-zero stations.

The motion pictures show (Fig. 3.21) that the grout plug is displaced vertically ahead of the surrounding surface at an early time and retains the lead thereafter (Fig. 3.22).

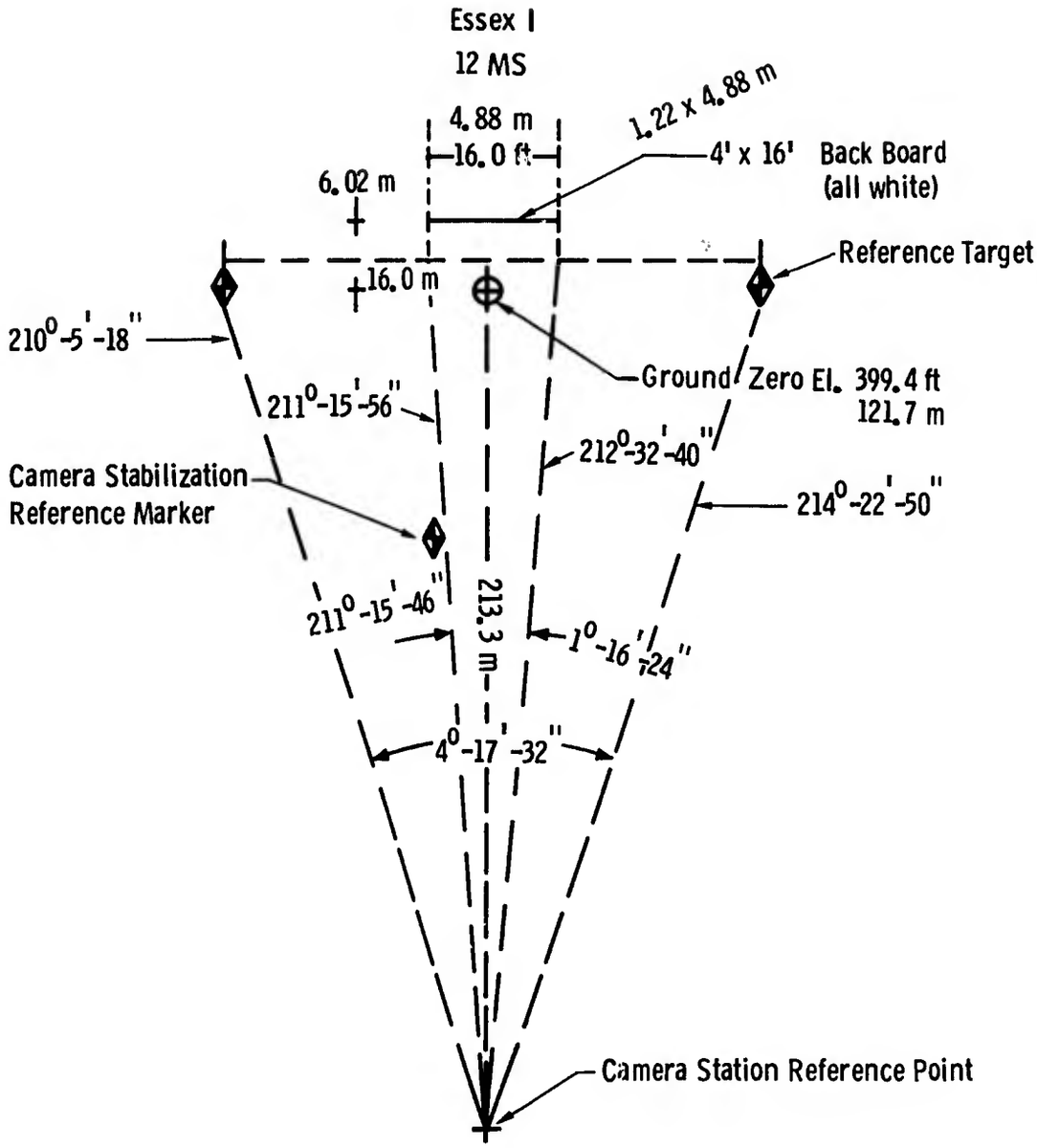

Figure 3.20 Plan view of camera layout

Figure 3.21 Grout plug advancing ahead of surrounding surface

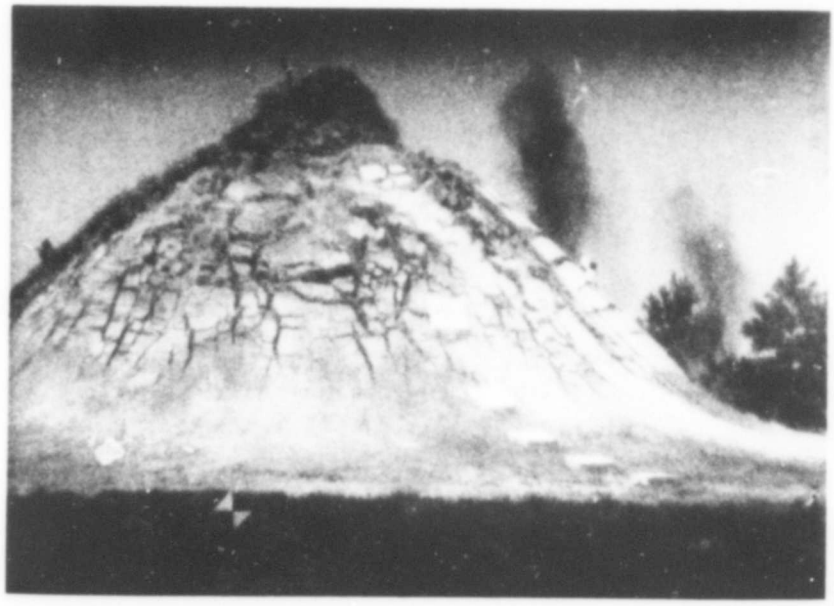

Figure 3.22 Grout plug remaining ahead of surrounding surface

In Fig. 3.23, displacement as a function of time recorded by the two accelerometers at the surface-ground-zero station is compared with that observed by Cameras 1 and 2 to 100 msec and by Camera 6 to 400 msec. Early-time differences between instrumented and photographed displacements could be explained if the stemming grout plug in which the instruments were placed was about 20 cm below the surrounding ground or if the surface-zero region was 20 cm below the camera horizon. Either would account for the photographed displacements lagging instrumented displacements. Agreement is still sufficiently good to give credence to displacements obtained by double integration of acceleration records.

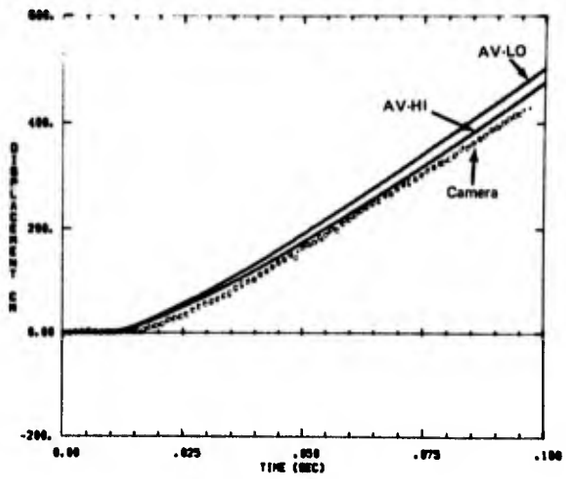

Figure 3.23a

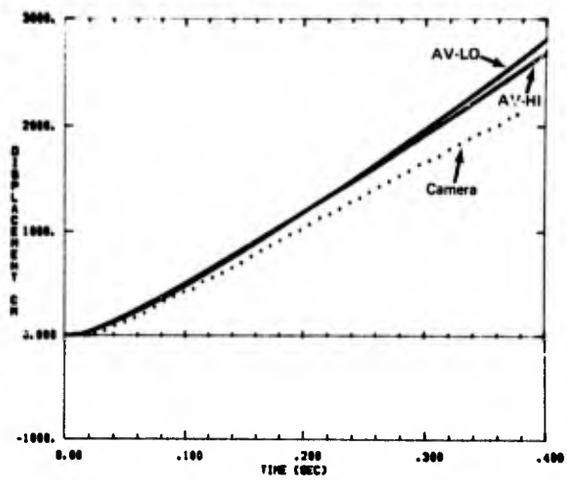

Figure 3.23b

Figure 3.23 Comparison of surface-zero displacements from photography with those from accelerometers

The difference between displacements derived from double integration of the acceleration records and those from photography can also be due to small baseline shifts in the acceleration record. In Fig. 3.23, the displacement derived from the record of one accelerometer is 4.13 m above that obtained photographically at 0.4 sec, and 5.43 m from the record of the other. This amounts to a baseline shift in the acceleration record of 2.1 g's in one case and 2.77 g's in the other. Since the peak acceleration at this location was 3500 g's, such baseline shifts represent less than a tenth of one percent of the peak acceleration. This is well within manufacturers' specifications for either the gages or the recording system.

In Fig. 3.24 the same comparison is made for the 9- and 12-meter stations. Agreement is quite good until about 200 msec. Thereafter, displacement recorded photographically increases faster with time than that recorded by the accelerometer. This can be accounted for by the slope of the mound at those stations after 200 msec. Because of the slope, and because material closer than 9 meters has a horizontal component that moves it across the 9-meter vertical line, the intercept rises faster than would be the case if one were following a single point at each station. This

can be seen in Fig. 3.17, where a profile at 300 msec from the photography has been added to those constructed by interpolating between accelerometer-deduced displacements.

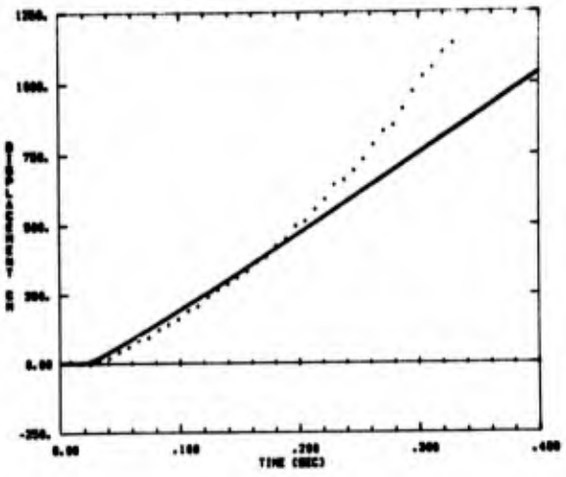

Figure 3.24a

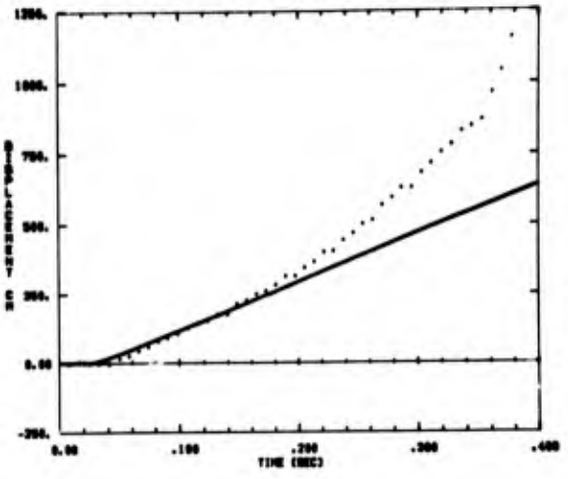

Figure 3.24b

Figure 3.24 Comparison of surface motion at 9 and 12 meters from photography with that from accelerometers

Figure 3.25 shows a similar comparison at the 18- and 24-meter stations. Agreement is good at the 18-meter station throughout the 400-msec interval. It is not so good at the 24-meter station after about 200 msec, primarily because of difficulty in defining the ground surface after that time in a region where displacements are small and the field-of-view of Camera 6 is relatively large.

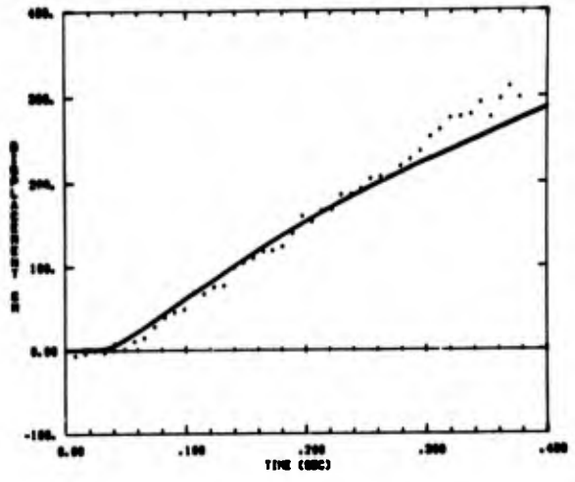

Figure 3.25a

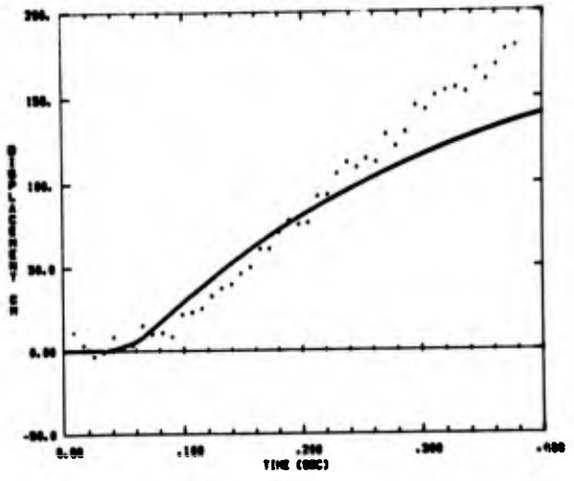

Figure 3.25b

Figure 3.25 Comparison of surface motion at 18 and 24 meters from photography with that from accelerometers

The results of the displacements derived from the photographs compare sufficiently well with those from the accelerometers that measured surface motion can be used with confidence for comparison with two-dimensional calculations of surface motion.

Airblast Measurements

Results of airblast measurements are summarized in Tables 3.7 and 3.8, and the records are reproduced in Appendix D. SL made measurements at three stations generally east of the shot at distances of 903, 2283, and 5417 m. SL also recorded airblast from gages installed by BRL at three stations 20, 40, and 80 feet (6.1, 12.2, and 24.4 m) from surface ground zero along an azimuth of 140°.

At the closest Sandia station a surface-wave-induced train preceded the ground-shock-induced pulse, and the latter was followed by a negative phase. The waveforms for the other two stations were essentially the same except that the surface-wave train preceded ground shock by a greater amount. The two closer stations recorded a barely perceptible signal that may be attributed to the direct ground shock. In Chapter 7 the results of airblast from all the shots are compared and the effects of stemming on airblast assessed.

Cables to the three BRL stations failed at 0.32, 1.55, and 12.9 sec respectively. At the closer station only the ground-shock-induced pulse was recorded before cable failure (Fig. D-4). At the 12.2-m station both the ground-shock-induced pulse and the full negative phase following it were recorded (Figs. D-5 and D-6). At the 24.4-m station (Figs. D-7, -8, and -9), that negative phase was followed by a train of pulses that preceded gas-venting-pulse arrival at 3 sec. The pulse train could result either from separate venting of gases at several points in the mound before the principal eruption, or from minor ground motions. Only the fast-rising signal at about 2 sec can be attributed to a ground motion identifiable on the acceleration record from the 24-m station. In Figs. D-8 and D-9 the ground-shock-induced and gas-venting pulses have been expanded to show the detail of the wave forms.

A

TABLE 3.7

Summary of Airblast Measu
(Metric Units)
ESSEX I 12 MS 23 Augus
21,594 Pounds Nitromethane Buried 12 Mete

Gage Designation	SLA 1-LO	SLA 1-HI	SLA 2-LO	SLA 2-HI	SLA 3-LO	S
Gage Range	Low	High	Low	High	Low	H
Gage Sensitivity	High	Low	High	Low	High	L
Distance (m)	903.	903.	2283.	2283.	5417.	5
Azimuth (rad)	1.962	1.962	1.602	1.602	1.616	1
Time of Arrival of Ground-Shock Induced Pulse (s)	1.200-2.486	1.172-2.483	4.108-6.485	4.078-6.484	11.360-15.463	1
Ground-Shock-Induced Pressure (Pa)	91.01	88.94	29.23	28.96	8.343	8
Time of Ground-Shock-Induced Peak Pressure (s)	2.602	2.602	6.542	6.542	15.540	1
Time of Crossover (s)	2.937	2.935	6.874	6.876	15.875	1
Ground-Shock-Induced Impulse (Pa-s)	9.791	9.515	3.640	3.689	1.262	1
Negative Peak Pressure (Pa)	53.78	53.78	21.86	21.51	8.343	8
Time of Negative Peak Pressure (s)	3.140	3.136	7.062	7.062	16.070	1
Time of Crossover (s)	3.362	3.348	7.266	7.270	16.358	1
Negative Impulse (Pa-s)	12.96	12.62	5.337	5.157	2.082	2
Gas Venting Peak Pressure (Pa)	37.23	37.92	15.24	15.38	5.006	5
Time of Gas Venting Peak Pressure (s)	3.717	3.704	7.656	7.656	16.661	1
Time of Crossover (s)	4.220	4.220	8.151	8.150	17.155	1
Gas Venting Impulse (Pa-s)	10.27	9.928	4.357	4.275	1.620	1

B

TABLE 3.7

Summary of Airblast Measurements
(Metric Units)
ESSEX I 12 MS 23 August 1973
itromethane Buried 12 Meters Deep, Fully Stemmed

SLA 3-LO	SLA 3-HI	BRL-1	BRL-1A	BRL-2	BRL-2A	BRL-3	BRL-3A
Low	High	Low	High	Low	High	Low	High
High	Low	High	Low	High	Low	High	Low
5417.	5417.	6.096	6.096	12.192	12.192	24.384	24.384
1.616	1.616	2.2689	2.2689	2.2689	2.2689	2.2689	2.2689
11.360-15.463	11.352-15.466	.0132	.0133	.0238	.0241	.0293	.0293
8.343	8.412	8067.	9239.	5985.	6564.	3344.	3427.
15.540	15.541	.0147	.0150	.0339	.0339	.0703	.0828
15.875	15.876						
1.262	1.282						
8.343	8.274						
16.070	16.074						
16.358	16.355						
2.082	2.103						
5.006	5.081					4220.	4095.
16.661	16.652					3.200	3.198
17.155	17.156						
1.620	1.634						

A

TABLE 3.8

Summary of Airblast Measure
(English Units)
ESSEX I 12MS 23 August
21,594 Pounds Nitromethane Buried 12 Meters

Gage Designation	SLA 1-LO	SLA 1-HI	SLA 2-LO	SLA 2-HI	SLA 3-LO	SLA
Gage Range	Low	High	Low	High	Low	High
Gage Sensitivity	High	Low	High	Low	High	Low
Distance (Ft)	2963.	2963.	7490.	7490.	17772.	177
Azimuth (Degrees)	112.4	112.4	91.8	91.8	92.6	92.6
Time of Arrival of Ground-Shock-Induced Pulse (Sec)	1.200-2.486	1.172-2.483	4.108-6.485	4.078-6.484	11.360-15.463	11.3
Ground-Shock-Induced Peak Pressure (PSI)	.0132	.0129	.00424	.00420	.00121	.000
Time of Ground-Shock-Induced Peak Pressure (Sec)	2.602	2.602	6.542	6.542	15.540	15.5
Time of Crossover (Sec)	2.937	2.935	6.874	6.876	15.875	15.(
Ground-Shock-Iriuced Impulse (PSI-Sec)	.00142	.00138	.000528	.000535	.000183	.000
Negative Peak Pressure (PSI)	.0078	.0078	.00317	.00312	.00121	.000
Time of Negative Peak Pressure (Sec)	3.140	3.136	7.062	7.062	16.070	16.(
Time of Crossover (Sec)	3.362	3.348	7.266	7.270	16.358	16.3
Negative Impulse (PSI-Sec)	.00188	.00183	.000774	.000748	.000302	.000
Gas Venting Peak Pressure (PSI)	.0054	.0055	.00221	.00223	.000726	.000
Time of Gas Venting Peak Pressure (Sec)	3.717	3.704	7.656	7.656	16.661	16.4
Time of Crossover (Sec)	4.220	4.220	8.151	8.150	17.155	17.1
Gas Venting Impulse (PSI-Sec)	.00149	.00144	.000632	.000620	.000235	.000

B

TABLE 3.8

of Airblast Measurements
(English Units)
12MS 23 August 1973
ne Buried 12 Meters Deep, Fully Stemmed

3-LO	SLA 3-HI	BRL-1	BRL-1A	BRL-2	BRL-2A	BRL-3	BRL-3A
	High	Low	High	Low	High	Low	High
	Low	High	Low	High	Low	High	Low
2.	17772.	20.	20.	40.	40.	80.	80.
	92.6	130.0	130.0	130.0	130.0	130.0	130.0
50-15.463	11.352-15.466	.0132	.0133	.0238	.0241	.0293	.0293
21	.00122	1.17	1.34	.868	.952	.485	.497
40	15.541	.0147	.0150	.0339	.0339	.0703	.0828
75	15.876						
183	.000186						
21	.00120						
0	16.074						
8	16.355						
02	.000305						
26	.000737					.612	.594
1	16.652					3.200	3.198
5	17.156						
35	.000237						

CHAPTER 4

RESULTS OF THE 12-METER PARTIALLY STEMMED EVENT

As noted in the Acknowledgments, SL sponsored a 12-meter partially stemmed (MPS) event to simulate penetrator emplacement of an explosive. On the Middle Course II series (Shot M-16), in a scaled experiment, use was made of a 1-ton charge and an open hole 4 inches (10.2 cm) in diameter. That shot indicated that the hole pinched off very early. Similar results were indicated by unpublished hydrodynamic code calculations at SL. The essence of the information from the 12 MPS shot is that if the hole does pinch off early, there will be little difference in the size or shape of the crater, regardless of whether the shot is fully or partially stemmed, and radioactivity vented to the atmosphere in a partially stemmed nuclear explosion will be different from a fully stemmed one primarily in that the radioactivity is limited to that contained in the very short burst of explosion gases escaping up the hole before pinch-off. It is even possible that the fraction vented at that time is offset in whole or in part by a decrease in the quantity of radioactivity in the gases that vent later when the cavity erupts. That is to say, the fraction of radioactivity out is essentially the same--only areal distribution on the ground would be different. Thus, the 20.4-cm-diameter open hole chosen for the 12 MPS event was critical to the objectives of the shot.

Cylindrical-fiber concrete-column forms had been used successfully for the M-16 shot of the Middle Course II series to form the 4-inch (10.2-cm) diameter open hole in the grout and earth used to stem the balance of the charge emplacement hole. The same material was specified for the 20.3-cm-diameter open hole of the 12 MPS event. Either because the wall of the cylinder was relatively weaker in the 20.3-cm configuration, because the hydrostatic pressure of the grout was greater for the 12-meter shot than for the 6.1-meter-deep M-16 shot, or because of improper handling by the contractor, the cylinder buckled and could not be used. Instead, an 8-inch outside diameter (20.3-cm) steel pipe was imbedded in the grout and withdrawn after the grout set up. Since the grout was installed in two separate pours and the pipe was withdrawn each time, alignment in the two pours was not precisely the same.

The natural watertable was approximately 3 meters below surface ground zero (SGZ). This, together with rains after charge emplacement and grouting, caused the open hole to fill with water to essentially the watertable. A waterfilled hole would not permit objectives of the experiment to be met. When the water was bailed out of the hole, it was discovered that permeability of the grout allowed the hole to refill with water at a rate of about 1.8 meters per hour. Since volunteers could not be found to bail out the hole to H minus 1 second, an alternate solution was sought. An interim answer was a small siphon pump at the bottom of the hole, operated from the surface with two lengths of 1-1/2-inch (3.8-cm) polyvinyl chloride tubing to the pump. This was an undesirable solution because of the presence of the pump and tubing in the region where the hole was expected

to pinch off, and because of the possibility that the first jet of gas up the hole before pinch-off would pack the tubing at some point along the length of the hole. The preferred solution and the one actually used was installation of an aluminum tube with a 1/8-inch base plate and a 1/8-inch (0.32 cm) wall at the bottom to exclude water. This solution necessitated reduction of the inside diameter of the open hole from 8 to 7 inches (20.3 to 17.8 cm). This meant that there was a water-filled gap 0.95 cm wide between the grout and the aluminum tube. It was concluded that this amount of water and the wall of the aluminum tubing would be less detrimental to experiment objectives than a pump and tubing in the pinch-off region.

Signals were obtained from all 41 gages installed by Sandia and from all but one of the five airblast gages installed by BRL. Records from all three Slifers were excellent except for damage during construction that made the first 4.4 meters of the closest Slifer inoperable. Gages or cables failed at shock arrival at the closest stress station, and no peak stress was recorded on the three gages. (Others gave records, two of which were limited.) Subsurface acceleration measurements were good except at the two closest stations. At the 24-m station, records from the two horizontal gages were questionable, and records from the tangential gage were limited. Surface acceleration measurements were quite good, although one of two gages at the surface-zero station or its cable failed shortly after 7.7 msec, and the vertical acceleration record at 9 meters was limited. The number of excursions beyond band edge was less than for the first shot. Excellent records were obtained from one of the two ported-pressure measurements in the open hole, and from all the Sandia and one of the BRL surface airblast gages.

Gage Range and Set Range

It was intended that the two 12-meter shots would be instrumented as nearly alike as possible to facilitate direct comparison. Ranges for all gages at comparable points were alike for both shots. Since so many of the accelerometers at shot depth and half-shot depth had been beyond set-range on the first shot, set-ranges for the second shot were increased as much as gage range would permit. Accelerations on the second shot turned out to be equal to or less than those expected for the first shot. As will be seen, the media at the two shot locations were so different that direct comparison was not possible. Where surface accelerations on the first shot had attenuated rapidly with distance, set-ranges for the most distant gages were lowered drastically for the second shot, and the set-ranges were often a small part of gage range. Table 4.1 summarizes the set-ranges for low- and high-sensitivity channels and indicates the peak values expected. Comparison of the table with Table 3.1 will show the changes made. For some of the gages at 24 and 36 meters at shot depth, the set-range was beyond the range of the 200-g gages installed. This was deliberate to make gage range rather than band edge the limiting parameter.

Measurement Locations

Figure 4.1 shows the location of the near-surface and sub-surface stress and acceleration measurements on the partially stemmed shot. Locations of Slifer and pressure measurements ported into the open hole are shown in Fig. 4.2.

TABLE 4.1 PLANNED SET RANGES BASED ON EXPECTED GROUND MOTION AND STRESSES FOR 12-MPS

12 METER PARTIALLY STEMMED

Gage	R meters	DOB meters	Expected	Low Sensitivity	High Sensitivity
σ - SY-1	6	6	1.3 (kb)	1.5 (kb)	1.0 (kb)
σ - SY-2	6	6	1.3	3.0	1.5
σ - SY-3	6	12	3	3	2
σ - SY-4	6	12	3	6	3
σ - SL-5	6	12	3	6	3
σ - SL-1	12	12	0.6	0.6	0.4
σ - SL-2	12	12	0.6	1.2	0.6
σ - SY-5	12	12	0.6	1.2	0.6
σ - SL-3	24	12	0.15	0.15	0.12
σ - SL-4	24	12	0.15	0.15	0.15
a_h	12	12	2100 (g)	2500 (g)	1500 (g)
a_h	12	12	2100	5000	2500
a_h	24	12	1500	500	500
a_h	24	12	1500	3000	1500
a_v	24	12	300	500	250
a_t	24	12	300	500	250
a_t	36	12	75	200	60
a_h	36	12	250	250	150
a_h	36	12	250	500	250
a_v	36	12	250	500	200
a_r	6	6	6500	6500	5000
a_r	6	6	6500	10000	6500
a_v	2/3	2/3	3500	3500	2500
a_v	2/3	2/3	3500	8000	3500
a_h	2/3	2/3	1500	4000	1000
a_v	9	2/3	500	1000	400
a_v	12	2/3	300	600	250
a_h	12	2/3	200	400	150
a_v	24	2/3	15	1-0	20
a_h	24	2/3	40	200	50

Pressure in Open Hole	2 channels
Slifer	3 channels
Sandia Airblast	6 channels
BRL Airblast	5 channels

Gages between lines were in a single hole

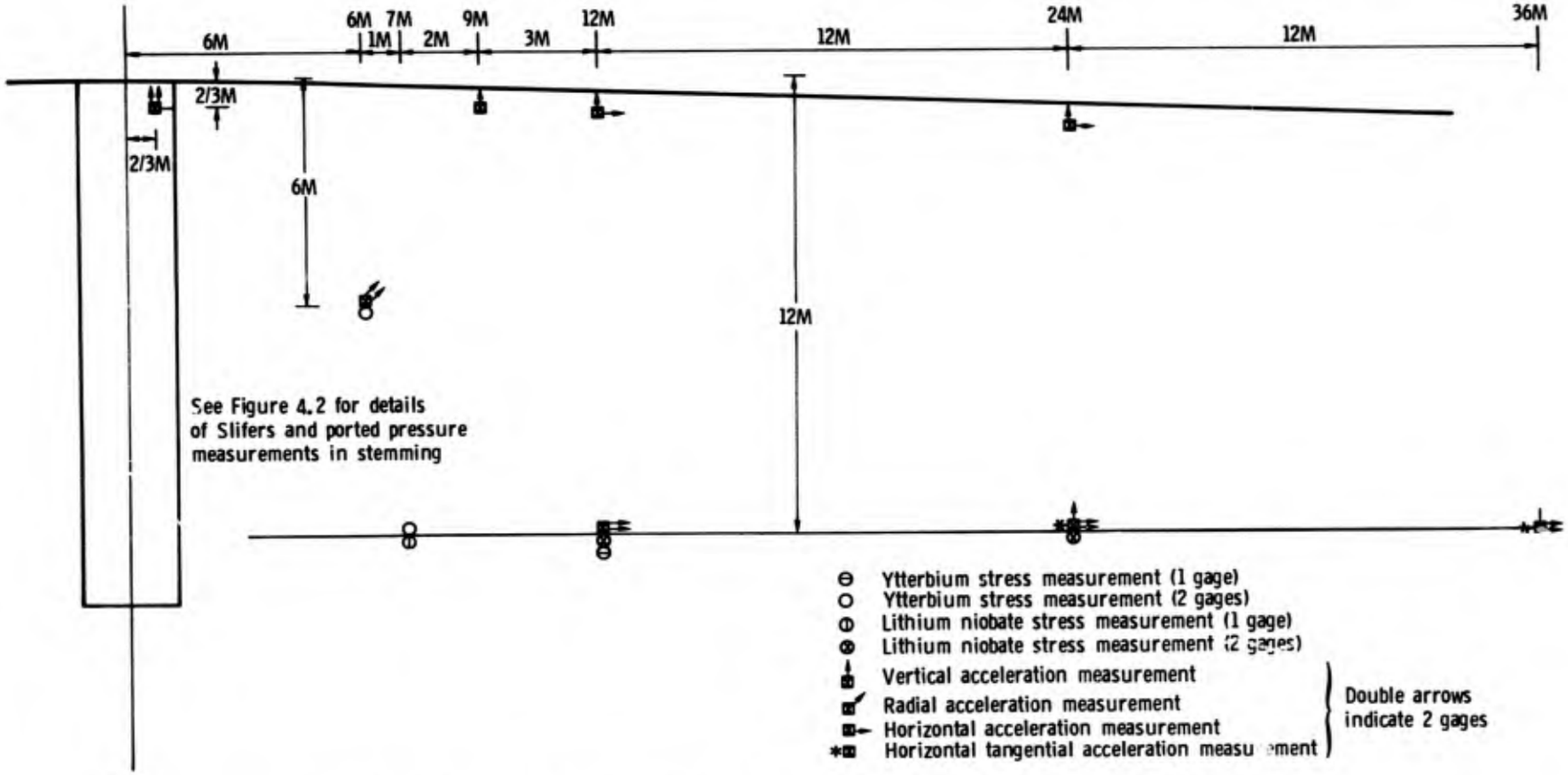

Figure 4.1 Location of new-surface and sub-surface stress and acceleration measurements on partially stemmed shot

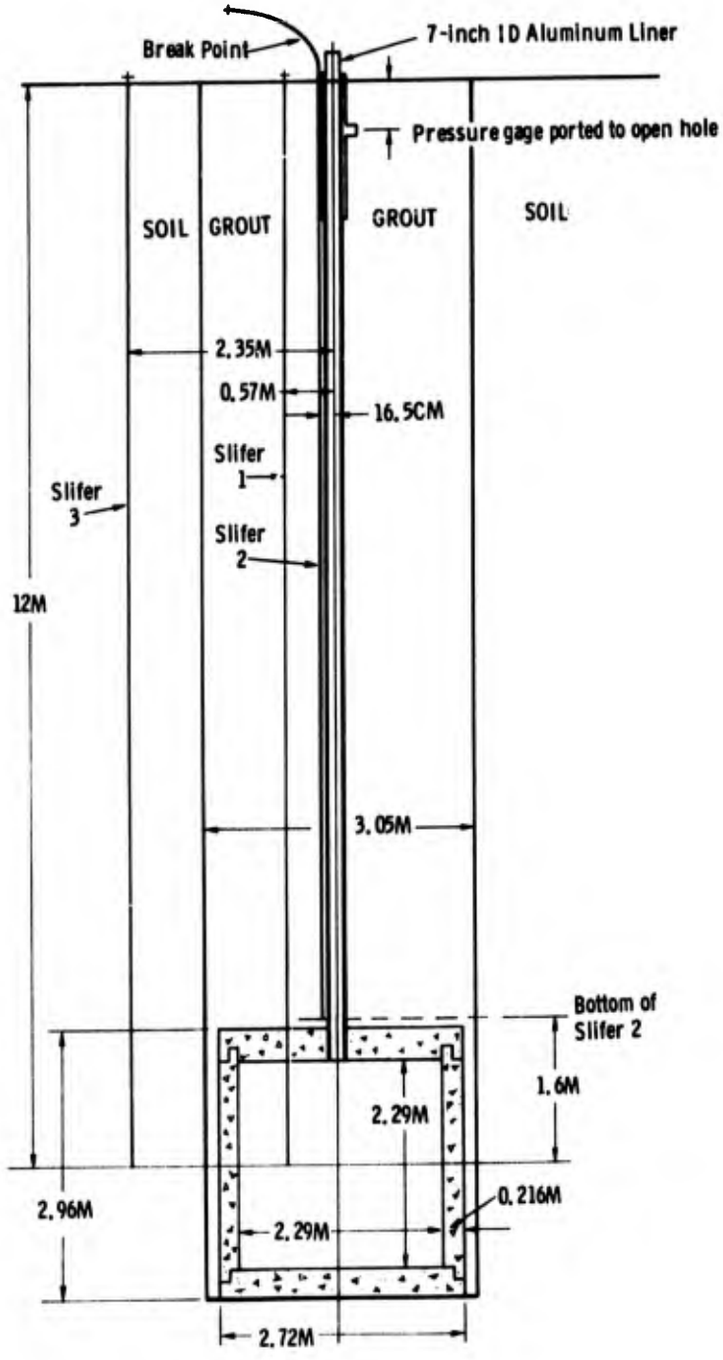

Figure 4.2 Location of Slifer and ported pressure measurements for the 12-meter partially-stemmed event

Slifer Time of Arrival

Figures 4.3 through 4.11 show, in order for Slifers 3, 1, and 2, plots of frequency versus time, calibration curves of frequency versus cable length, and conversion into radial distance versus time. The records for Slifers 3 and 1 are excellent (Figs. 4.5 and 4.8), while that for Slifer 2 (Fig. 4.11) appears at first glance to be invalid. Actually, it too is excellent, portraying

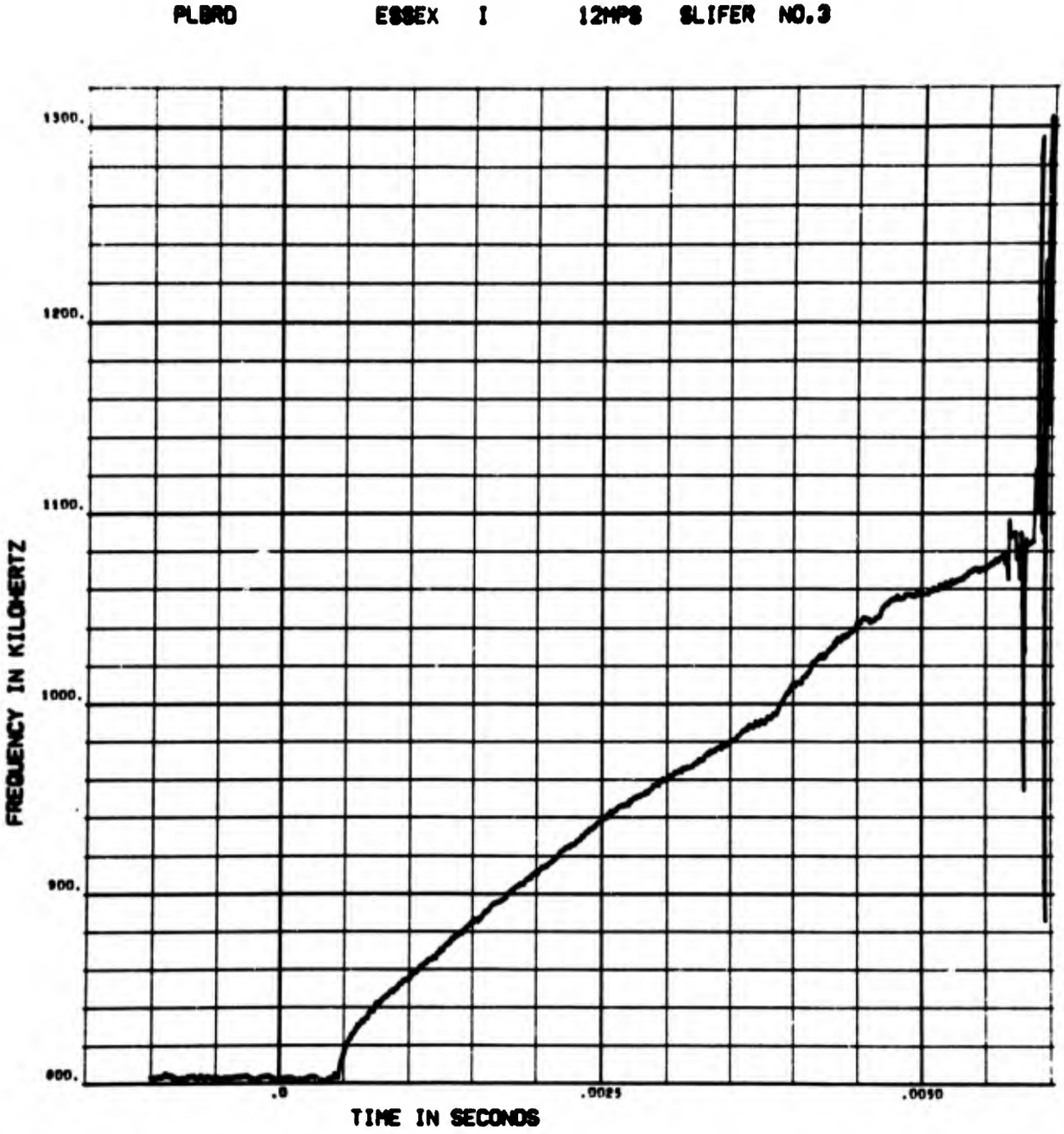

Figure 4.3 Frequency versus time for Slifer 3 time of arrival measurement

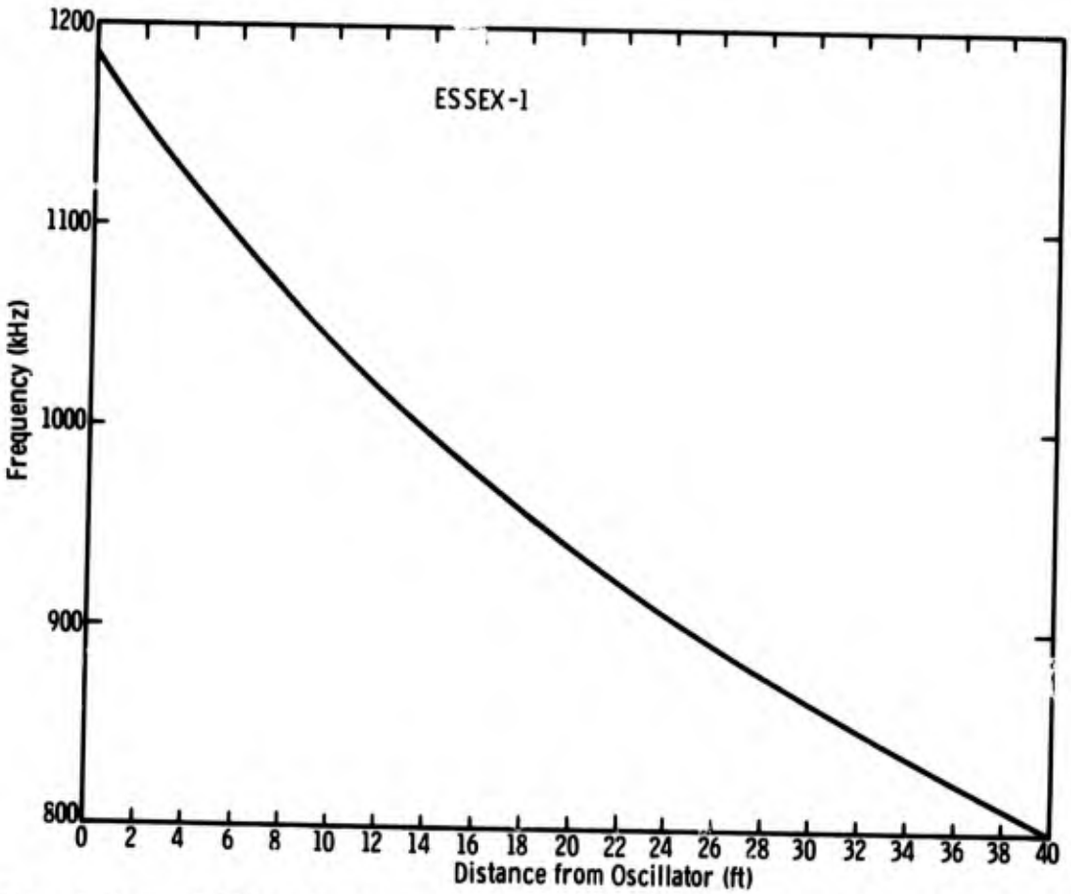

Figure 4.4 Calibration curve for Slifer 3 time of arrival measurement

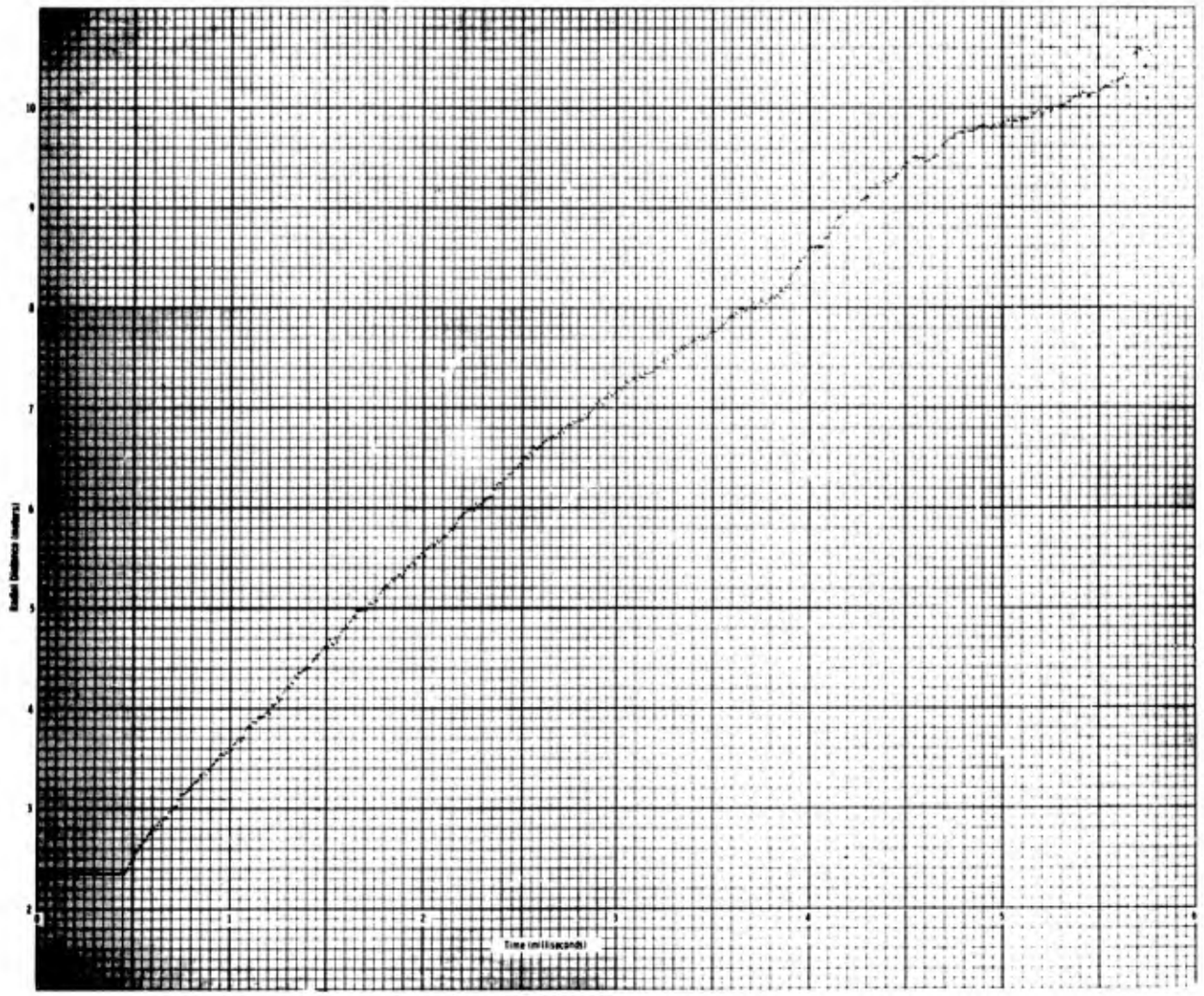

Figure 4.5 Time of arrival versus distance for Slifer 3 time of arrival measurement

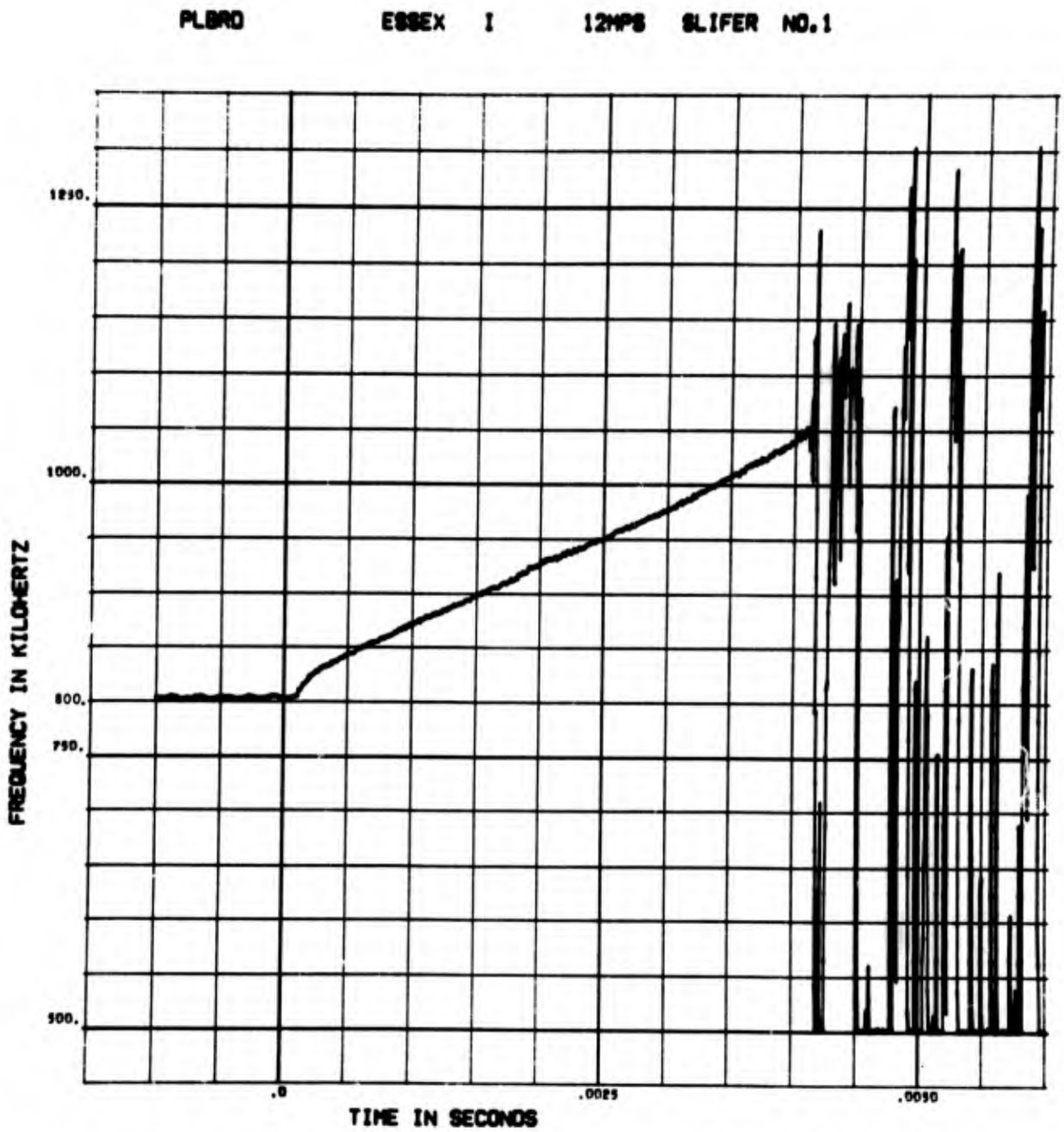

Figure 4.6 Frequency versus time for Slifer 1 time of arrival measurement

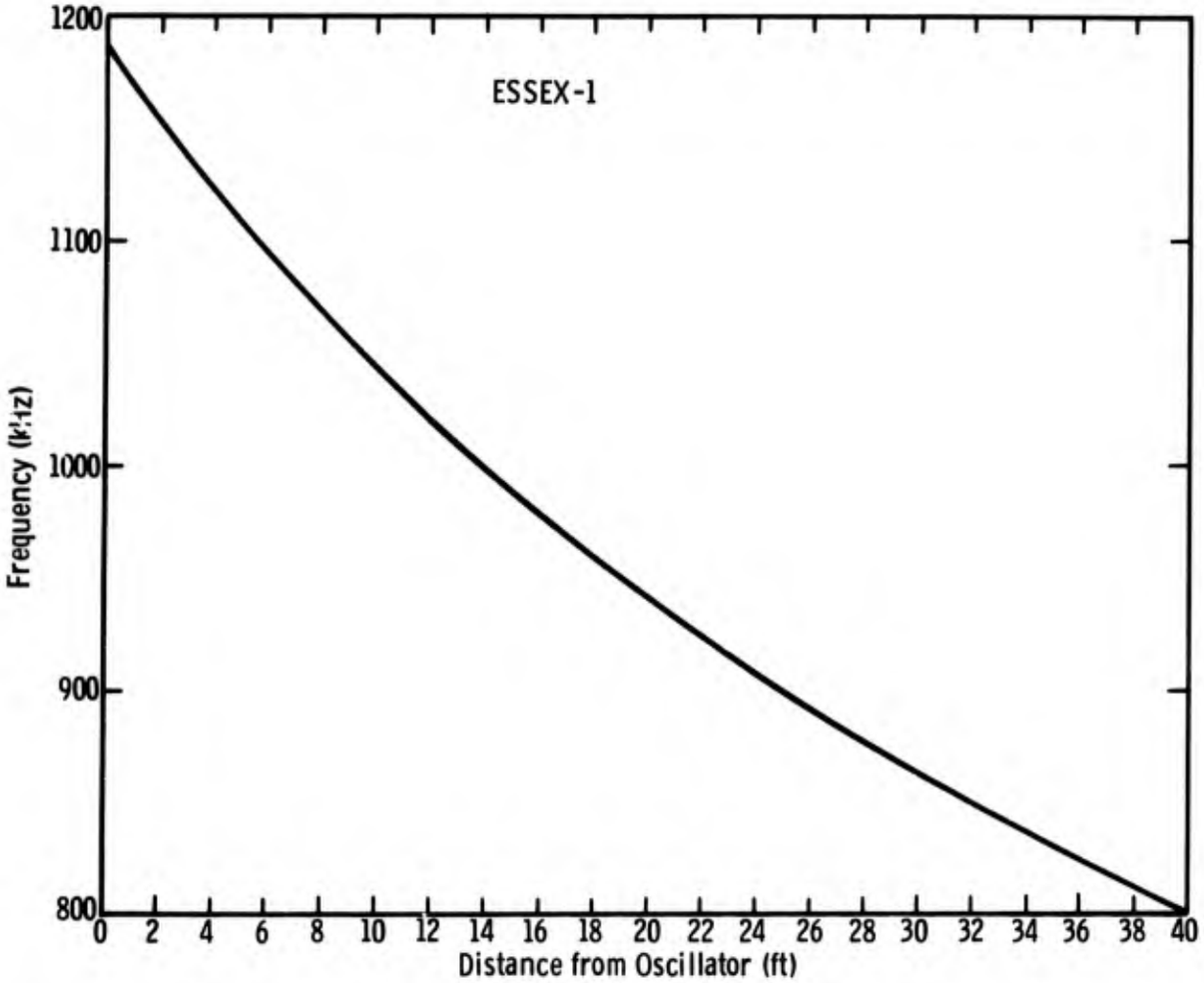

Figure 4.7 Calibration curve for Slifer 1 time of arrival measurement

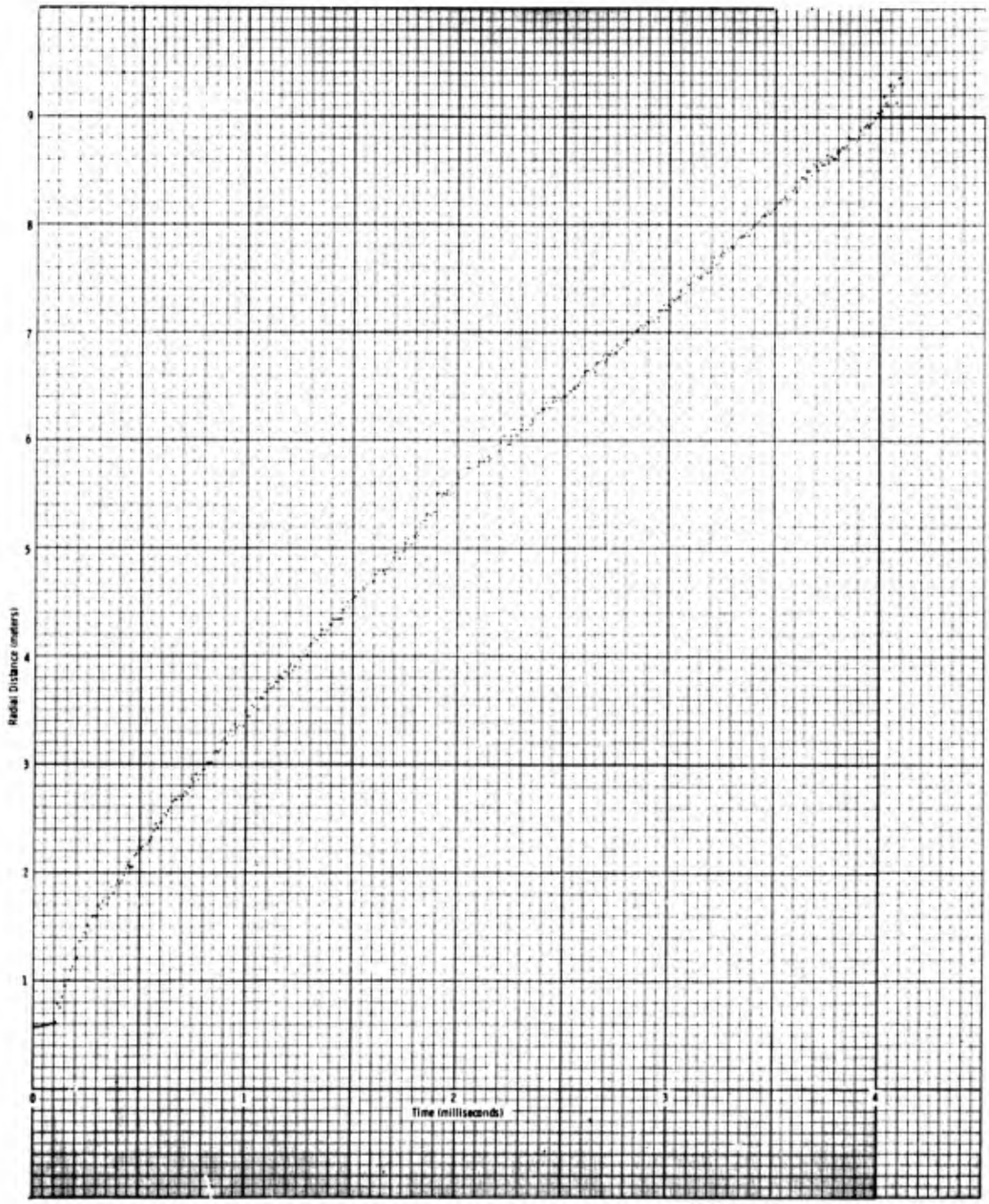

Figure 4.8 Time of arrival versus distance for Slifer 1 time of arrival measurement

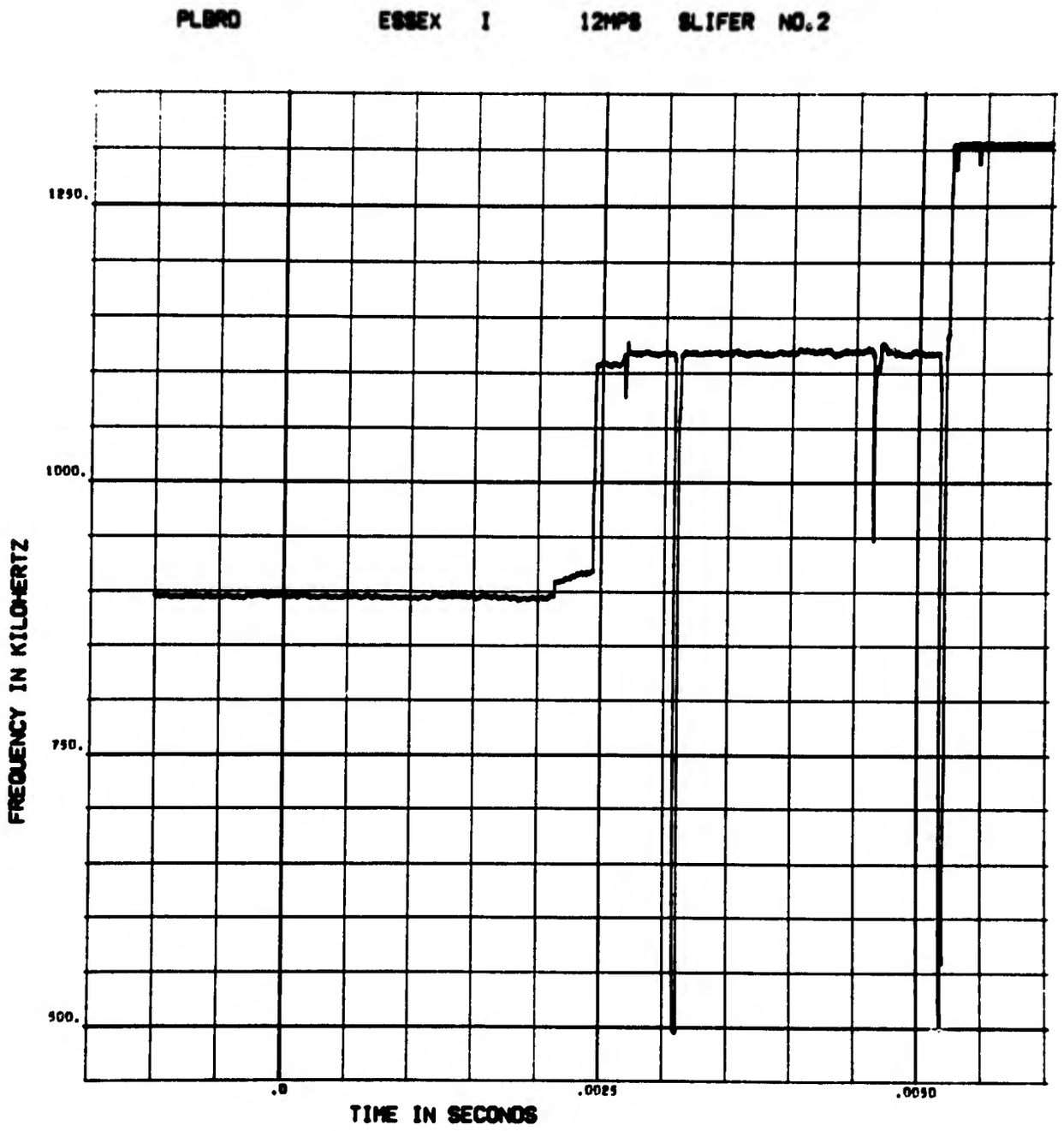

Figure 4.9 Frequency versus time for Slifer 2 time of arrival measurement

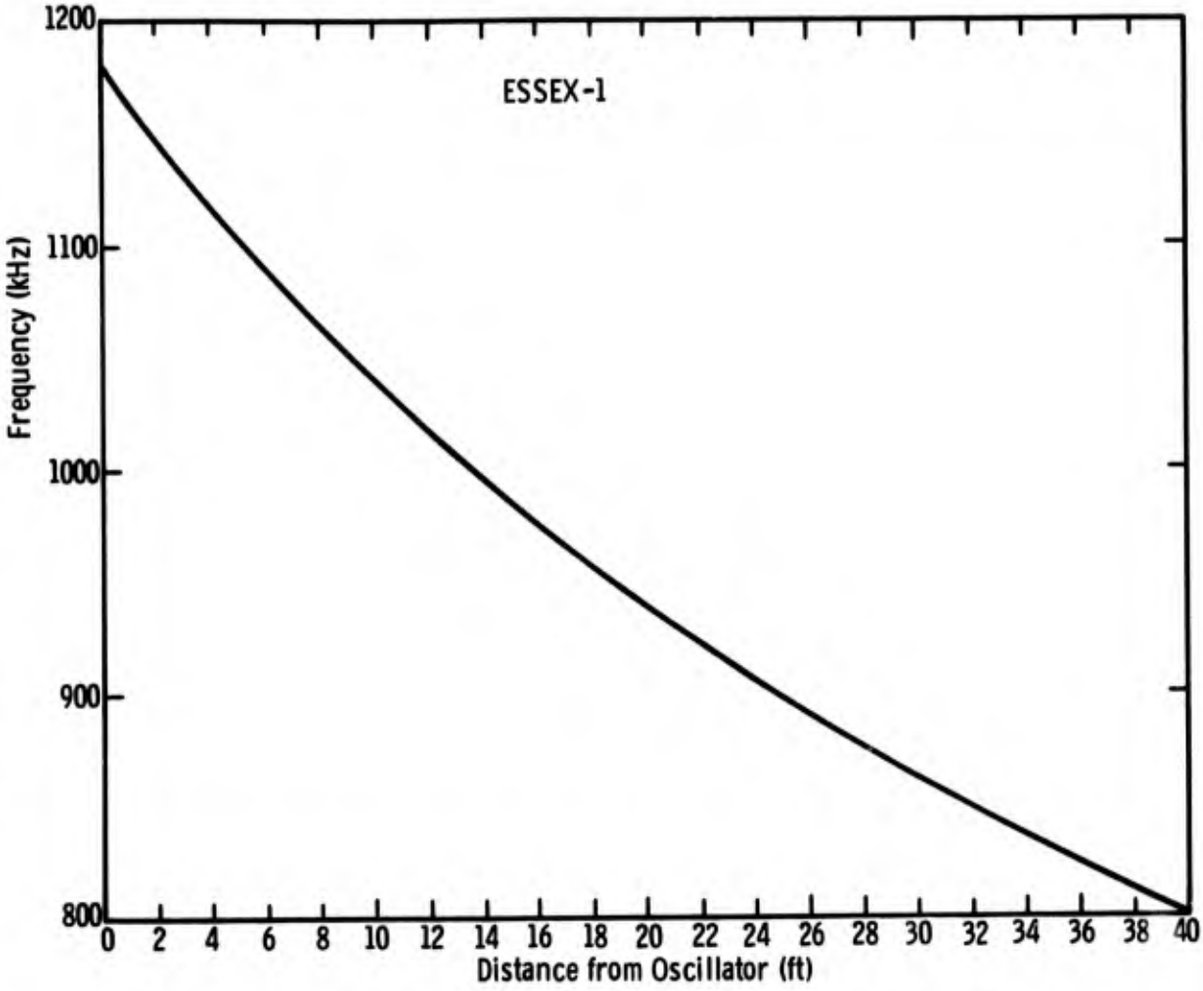

Figure 4.10 Calibration curve for Slifer 2 time of arrival measurement

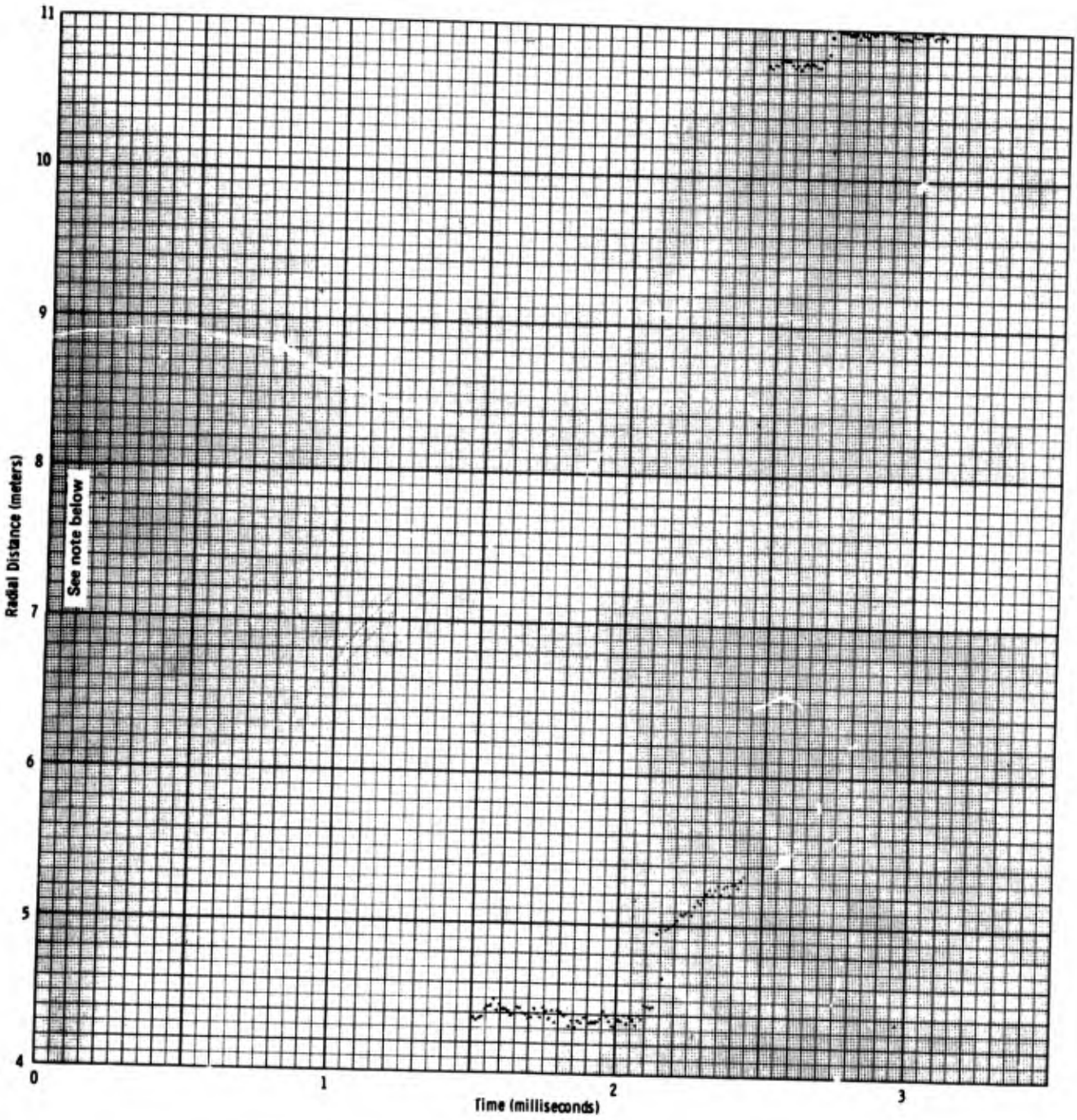

Figure 4.11 Time of arrival versus distance for Slifer 2 time of arrival measurement
Note: Scale shown is radial distance from end of Slifer. Radial distance from charge center is 1.6 meters greater. See Fig. 4.2 for Slifer location.

the situation that existed close to the open hole. The record shows an initial frequency of about 895 kHz, rather than the approximately 800-kHz unloaded frequency of the other two. This initial frequency corresponds to 4.4 m from the end of the Slifer or, adding the distance between the end of the Slifer and the charge center, to 6.0 m from the charge center. The Slifer was not functioning below that point.

In reviewing the sequence of construction events related to stemming of the hole, it was noted that about the first 5.7 m of stemming was p ured using the fiberboard tube for the open hole. When the tube buckled, it was removed after the grout had set and was replaced with an 8-inch (20.3-cm) OD steel pipe as a form for the open hole. During emplacement of the pipe into the first grout pour, a chain used in handling the pipe fell to the top of the grout and struck the Slifer, crushing it about a foot above the grout. At 2.13 msec the record takes a sharp jump from 6 to 6.55 m, thereafter arrival times parallel those of the other two Slifers until 2.44 msec. The reason for the st p at 2.13 msec is not clear, but it could be provided only by something preventing crushing between 6 and 6.55 m. Water inside the hollow portion of the cable through a slow leak at the 6-m level could conceivably prevent sufficient crushing to achieve electrical contact over the 0.55-m interval while remaining shorted at the 6-m level.

After a valid record from the main shock wave over a distance from 6.55 to 6.90 m and a time of 2.13 to 2.44 msec, the signal at that later time takes a jump to 12.35 m, a point 0.35 m above the ground surface. The break at that point is attributed either to the flare emerging from the open hole and spreading laterally, or to a piece of shrapnel from the aluminum tube from the top of the hole (see Fig. 4.12). As will be shown in the next section, the flare traveling up the pipe arrived at 11.44 m at 2.03 msec for an average velocity of 5.64 m/msec. The same average velocity to 12.35 m would indicate an arrival time of 2.19 msec. Allowing some time for the

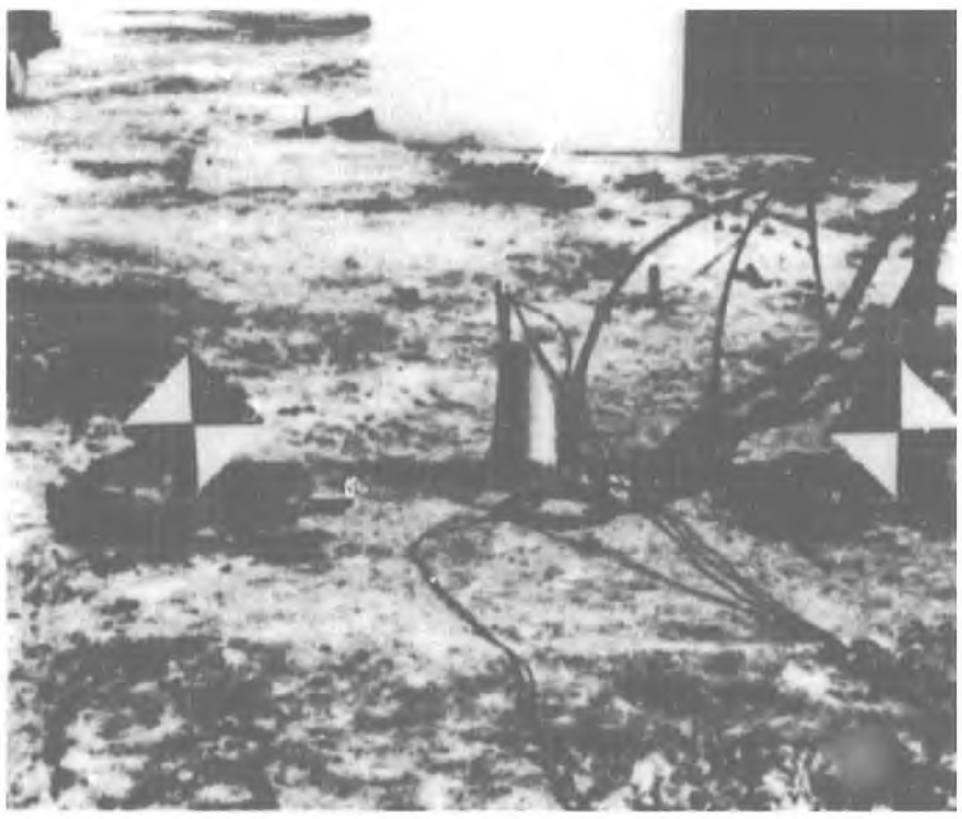

Figure 4.12 Installation of Slifer 2 adjacent to aluminum tube which may have provided shrapnel for crushing the Slifer

expanding flare outside the hole to rise to a pressure sufficient to crush the cable makes this explanation credible. At 2.7 msec the flare crushed the Slifer at 12.55 meters and did no further damage, presumably because of rapid lateral attenuation of pressure in the flare. This latter point was 1.05 meters from the end of the Slifer.

In Fig. 4.13 the profile of the advancing shock front is shown. The effect of the open hole is especially noticeable between 6 and 7 meters from the charge center.

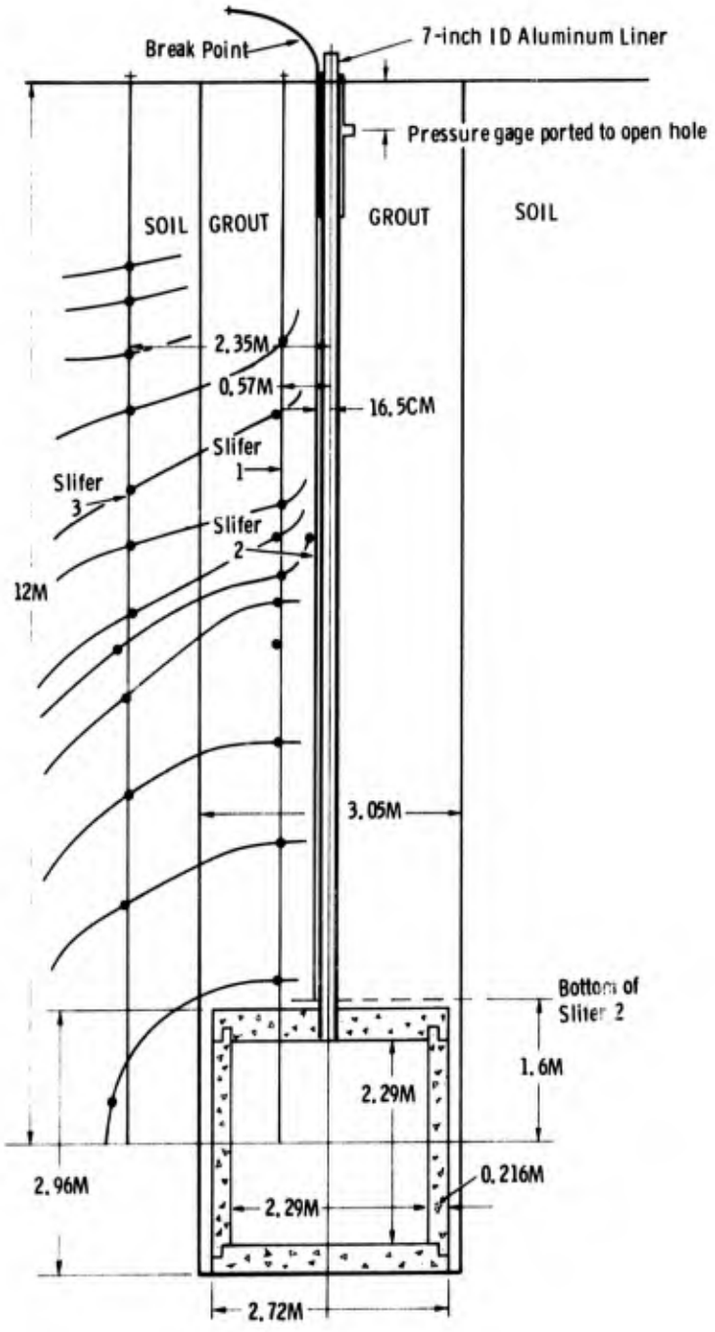

Figure 4.13 Advance of shock wave as determined from Slifer measurements

Arrival Times at All Instrument Stations

Arrival time as measured by the three Slifers is compared with arrival times at the other instrument stations in Fig. 4.14. The pattern is considerably simpler than for the fully stemmed shot, obviously because the medium at shot depth more nearly matched preshot predictions and grout specifications. Also, because of the higher water table at the 12-MPS site, arrivals at the near-surface stations were earlier than for the fully stemmed shot. Average shock velocities between stations at shot depth were 1.73, 1.59, and 1.45 m/msec in the intervals from 7 to 12, 12 to 24, and 24 to 36 m, respectively.

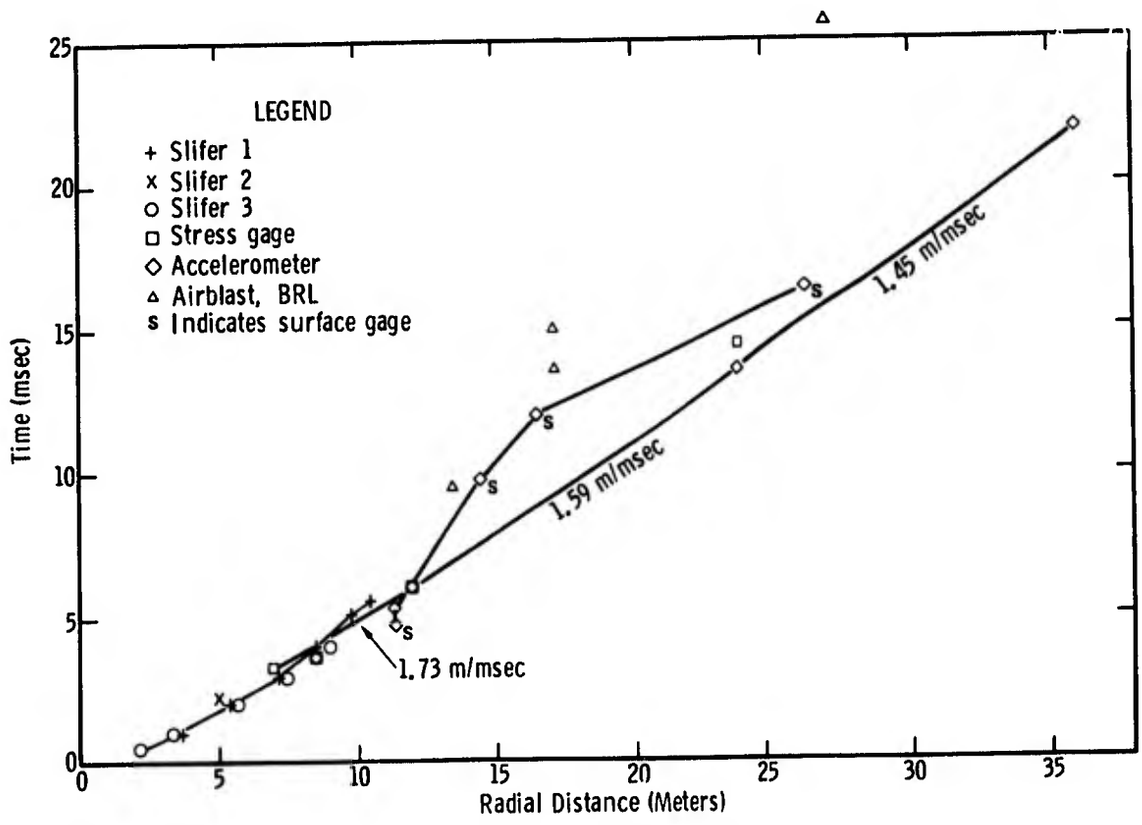

Figure 4.14 Summary plot of arrival times at all stations

Arrival times at the near-surface stations show that at the 24-m station the first arrival was from a refracted signal from deeper strata rather than from a direct path. At the near-surface-zero station the principal rise occurs at 5.35 msec, which is in good agreement with Slifer data, but there is a gradual breakaway preceding that rise by nearly 0.6 msec.

At the 24-m station at shot depth, arrival times for the four accelerometers differ by 1 msec from arrival times at the two stress gages. Both were played back from the analog tape for high resolution and the difference was confirmed. Arrival times at the accelerometers are consistent with those from stations at 12 and 36 meters. Arrival times at the stress gages are consistent with their being emplaced at 25.4 rather than 24 m. This could have come about as a result of a hole that was inclined 1.4 meters away from the charge, or as a result of separate holes.

Comparison of Fig. 4.14 with Fig. 3.5 provides the first of several demonstrations of the great differences between the media in which 12 MPS and 12 MS were fired. It is these differences that prevent direct comparison of the results of the two shots in assessing the effects of the open hole on 12 MPS. Differences attributable to the open hole would be expected to be subtle, and detecting them is precluded by gross distinctions attributable to medium variances at the two sites.

Ported Pressure Measurements in Open Hole

Chapter 2 included a description of the gages used to measure pressure as a function of time up the open 7-inch (17.8 cm) ID hole, together with a description of gage installation. The purpose of the measurements was to determine whether the open hole pinched off enough to stop the upward flow of explosion gases.

Records from the two gages are shown in Figs. 4.15 and 4.16. Both gages saw an EM signal at zero time, and the signal from flow up the open hole at 2.03 msec. Pulse duration was only 0.4 msec. The peaks on the low-range gage were limited. The high-range gage recorded a peak of 557 bars (8380 psi) at 2.05 msec, followed by a second peak of 475 bars (7000 psi) at 2.1 msec. There is disparity between the two records following the pulse. The low-range gage showed pressure going negative at about 2.6 msec to -15 to -20 bars until gage or cable failure just after 3 msec. Because of the large negative pressure, the record is suspect. The high-range gage maintained a positive pressure of about 50 bars during the time the other gage record was negative.

Arrival at the gage indicates an average velocity of 5.587 m/msec from the top of the explosive to the gage. Assuming a similar velocity for the front from the gage to the top of the hole and for rarefaction from the top to the gage, a rarefaction would be expected at the gage 0.2 msec after shock arrival. Actually the time would be longer because the rarefaction is moving against flow in the pipe.

The region after the initial pulse, during which pressure is sustained for about 3 msec at about 50 bars, could be attributed to hole collapse propagating up the pipe, driving air ahead of the pinch-off in the way that toothpaste is squeezed out of a tube.

Two additional pressure spikes over 410 bars (6000 psi) occur at about 6.5 and 7.7 msec. There are acceleration spikes at the nearby accelerometer at about 5.6 and 6.7 msec. Since there is no evidence of a ground-motion pulse at 7.7 msec, and since manufacturer's specifications indicate the acceleration sensitivity of the pressure gage is only 4 psi (0.27 bar) per 1000 g's, the signals can hardly be attributed to ground motion. Temperature sensitivity of the gage (0.03 % per degree Fahrenheit) is also ruled out on the basis of the fast rise and fall of the signals. The possibility is left that the pipe opened after having been pinched off in the region closer to the charge, and that the later pressures are related to cavity gas pressure coming up the hole. Hydrodynamic calculations show cavity pressures of 400 bars between 4 and 5 msec, and half that at the time of the 6.5- and 7.7-msec spikes.

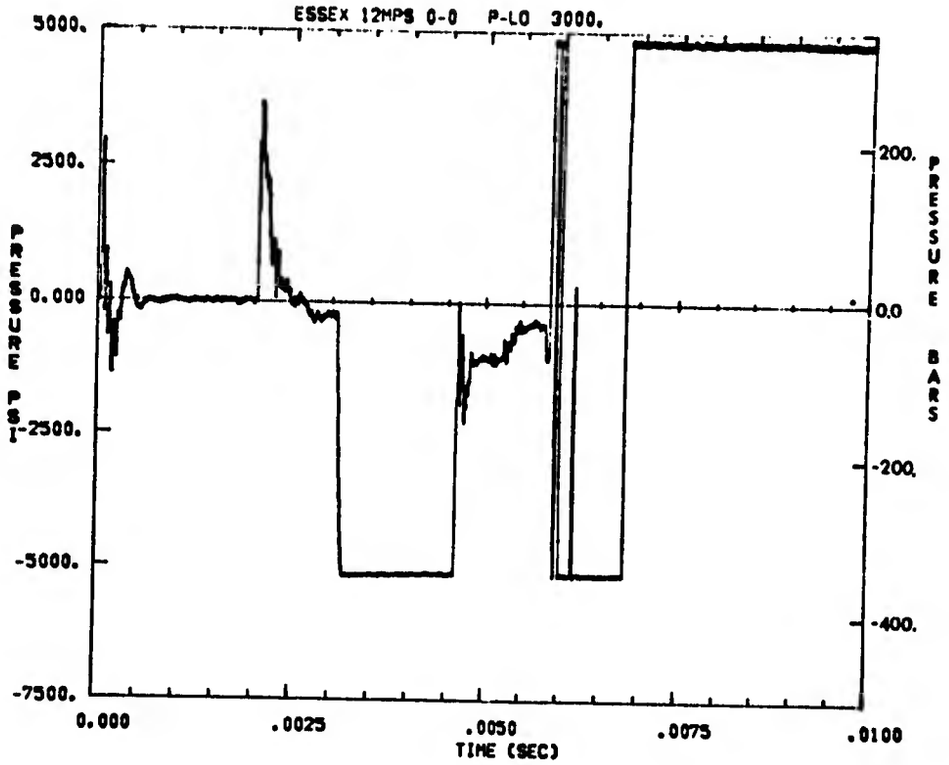

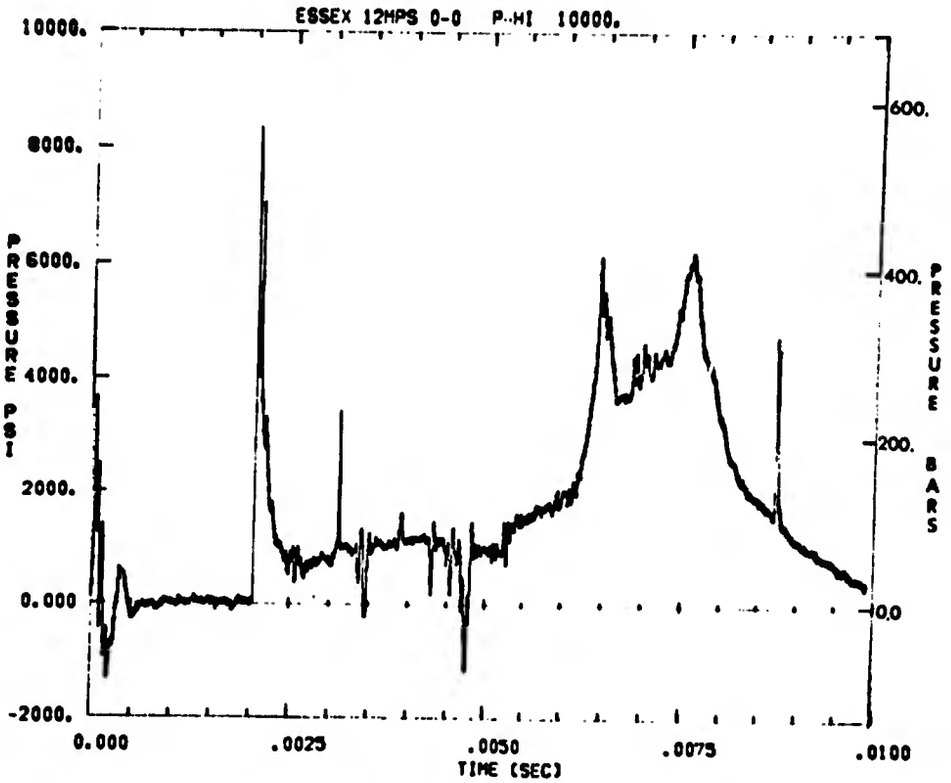

Figure 4.15 Records from two ported pressure gages

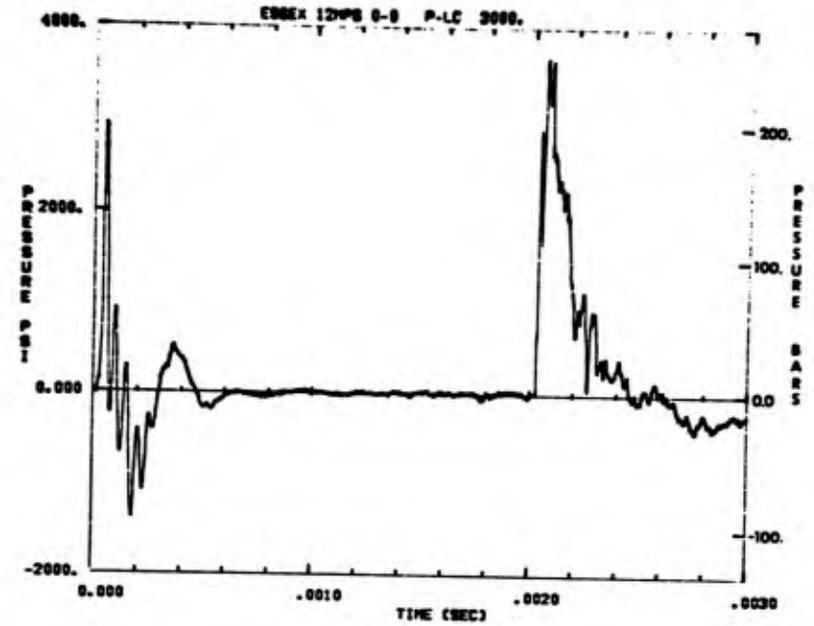

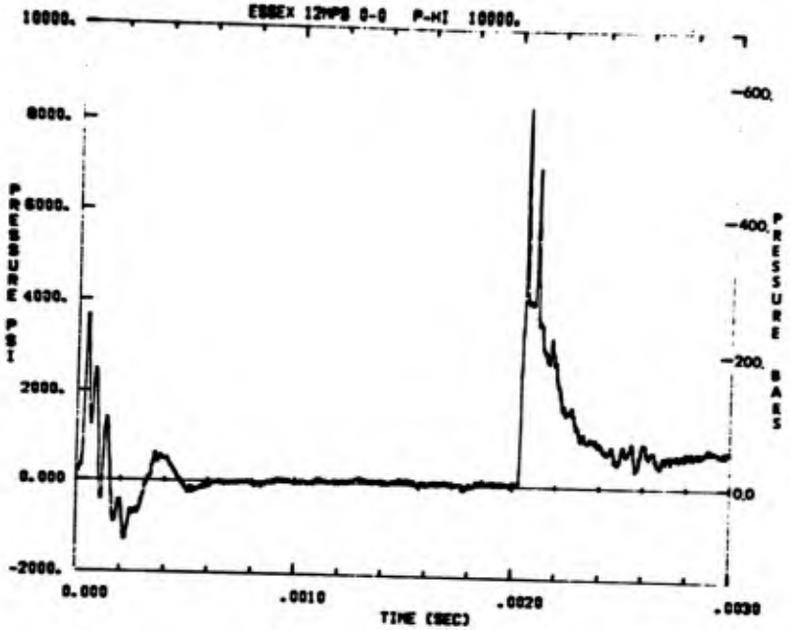

Figure 4.16 Expansion of records from two ported pressure measurements

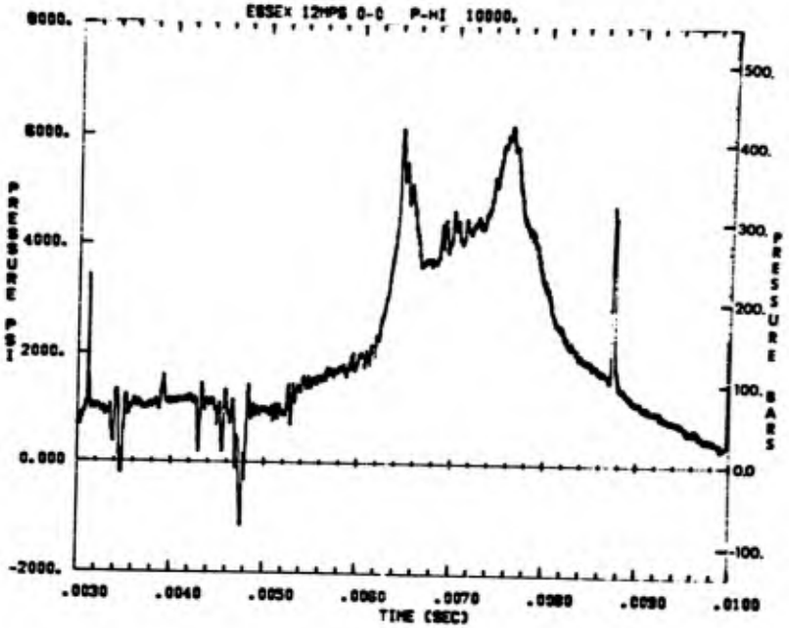

There is one other possibility that is impossible to verify--that of the aluminum tubing moving vertically to where the slot for the pressure gage prevented gas pressure being measured, but to where water being compressed between the tubing and the collar acted against the gage diaphragm.

Stress Measurements

Records obtained from stress measurements on the partially stemmed shot are reproduced in Appendix E; principal parameters are summarized in Table 4.2. The layout and gages were the same as for the fully stemmed shot except that another ytterbium gage was added to the 7-meter station and a lithium-niobate gage was added to the 12-meter station. This provided three gages at these two stations and gave the opportunity for direct comparison of measurements made by the two types of gages.

Of the 10 stress gages installed (20 records), three (SY-3, SY-4, and SL-5), all at 7 meters at shot depth and subjected to the harshest environment, gave records indicating that either the gage or the cable failed before peak stress was reached (see Figs. E-3, 4, and 5). One low-range gage (SY-1) gave a record (Fig. E-1) limited by band edge. A good record was obtained by the high-range gage at the same location. Another low-range gage (SL-1) gave a flat-topped record (Fig. E-6) which at first glance appears to have been limited, but at a value so far below band edge that the record must be discredited. Here again good records were obtained by the two high-range gages at the same location. One of these was ytterbium, the other lithium niobate, providing another chance for direct comparison of the two gages. Both recorded a quite similar waveform with minor differences in shape. There is a significant difference in amplitude, the record from the lithium niobate gage being much lower. In Fig. 4.17 the two plots have been overlaid after the amplitude of the ytterbium gage record was multiplied by 0.5. Here the minor differences in wave shape are more obvious.

At the 24-meter station both lituium niobate gages (SL-3 and SL-4) gave identical records (Figs. E-9 and E-10).

In Fig. 4.18 measured peak stresses are plotted versus distance for comparison with a pre-shot Chart-D calculation by Tyler[21] using the WES equation of state for the shot-depth medium (Unit 6). Later, Bass[20] made a similar calculation using an equation of state for a typical wet dirt, with no intention of exactly reproducing the characteristics of the Fort Polk medium. Results of that calculation are shown in the figure also. The latter calculation agrees with measured results above 5 kilobars, but departs increasingly from measured values below that stress level. A long dashed line has been drawn through measured data at shot depth. The line avoids the 8.5-m data (which were obtained at a zenith angle of 45° from the other measurements--6 m deep and 6 m from the avertical axis of the charge). The medium is most certainly different. That at 6 m was characterized by WES as Unit 5, the same as the shot-depth medium for 12 MS, whereas, the shot point for 12 MPS was on the boundary between Units 5 and 6. Stress measured at 12 m by the ytterbium gage is also above the line drawn through the rest of the data. The reason for the larger value is not known.

A

TABLE 4.2

Summary of Stress Me
ESSEX I 12 MPS 20 Sep
21,594 Pounds Nitromethane Buried 12 Met

Gage Type		Distance (m)	Depth (m)	Gage Range	Gage Sensitivity
Ytterbium	SY-1	6	6	Low Low	High Low
	SY-2	6	6	High High	High Low
	SY-3	7	12	Low Low	High Low
	SY-4	7	12	High High	High Low
Lithium Niobate	SL-5	7	12	High High	High Low
Lithium Niobate	SL-1	12	12	Low Low	High Low
Ytterbium	SY-5	12	12	High High	High Low
Lithium Niobate	SL-2	12	12	High High	High Low
	SL-3	24	12	Low Low	High Low
	SL-4	24	12	High High	High Low

*Reading accuracy for time is ± 0.01 millisecond.
(a) Limited
(b) Gage or cable failed

B

TABLE 4.2

Summary of Stress Measurements
X I 12 MPS 20 September 1973
thane Buried 12 Meters Deep, Partially Stemmed

Gage Positivity	Calibration Step (kbar)	Arrival Time* (msec)	Peak Stress (kbar)	Time of Peak (msec)*	Remarks
High	1.0	3.61			(a)
Low	1.0	3.60			(a)
High	1.5	3.63	1.88-2.10	3.84	
Low	1.5	3.62	1.88-2.33	3.85	
High	2.0	3.17	>1.10		(b)
Low	2.0	3.32	>1.10		(b)
High	3.0	3.13	>1.18		(b)
Low	3.0	3.32	>1.32		(b)
High	0.6	3.14	>0.78		(b)
Low	0.6	3.16	>0.94		(b)
High	0.4	6.05	>0.064		(a)
Low	0.4	6.16	>0.064		(a)
High	0.6	6.03	0.77	11.19	
Low	0.6	6.19	0.77	11.17	
High	0.6	6.05	0.393	11.25	
Low	0.6	6.14	0.414	11.09	
High	0.12	14.37	0.049	36.56	
Low	0.12	14.31	0.049	35.17	
High	0.15	14.54	0.049	36.41	
Low	0.15	14.57	0.051	36.06	

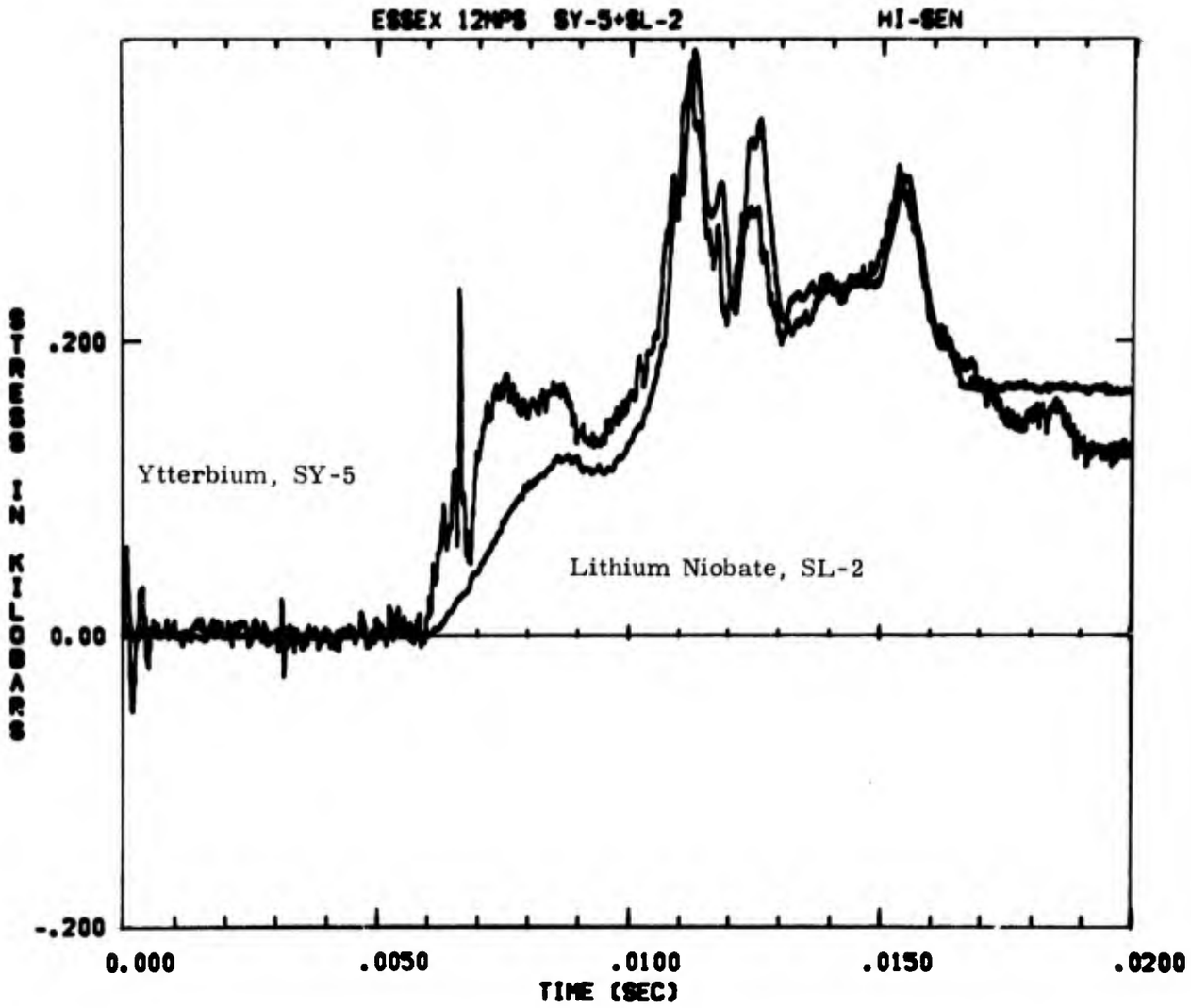

Figure 4.17 Comparison of record from lithium niobate gage with record from ytterbium gage at the same location after the amplitude of the ytterbium gage record was multiplied by 0.5

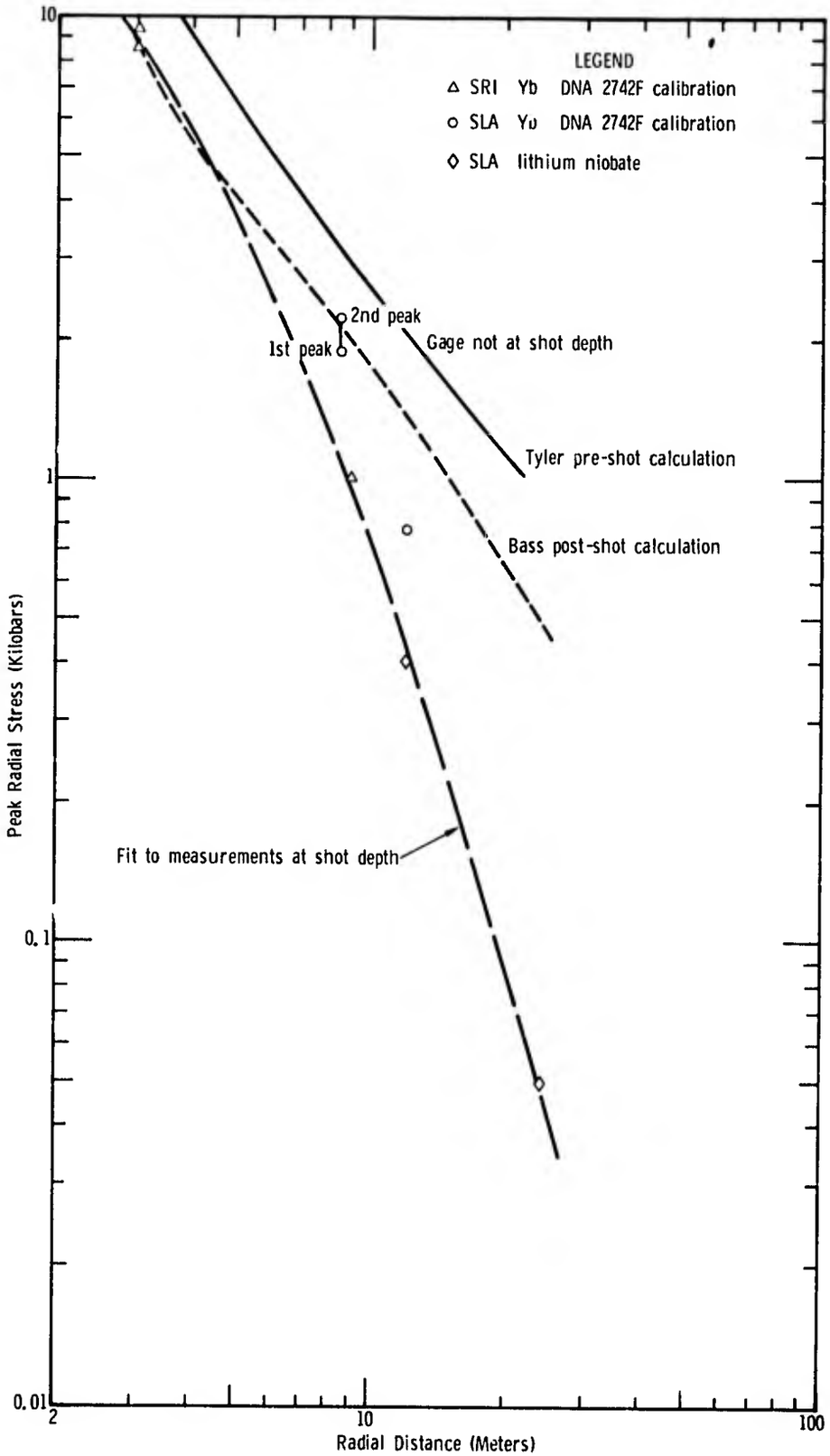

Figure 4.18 Comparison of peak radial stress measured on 12 MPS with pre-shot calculated stresses

Since the shot point was at the boundary between Units 5 and 6, it is interesting to compare the measured peak stress values with those of the calculation for 12 MS (Fig. 3.7), which was in Unit 5. This comparison is made in Fig. 4.19. Stresses recorded on 12 MPS by the lithium niobate gages are in agreement with the LLL calculation using the WES equation of state, and at 24 meters fall well below those measured on 12 MS. It is interesting to note that the line drawn through the 12 MPS data is about 40 % below the line through 12 MS data in the region above 2 kilobars, and that the difference increases to 60 % at about 0.1 kilobar and lower.

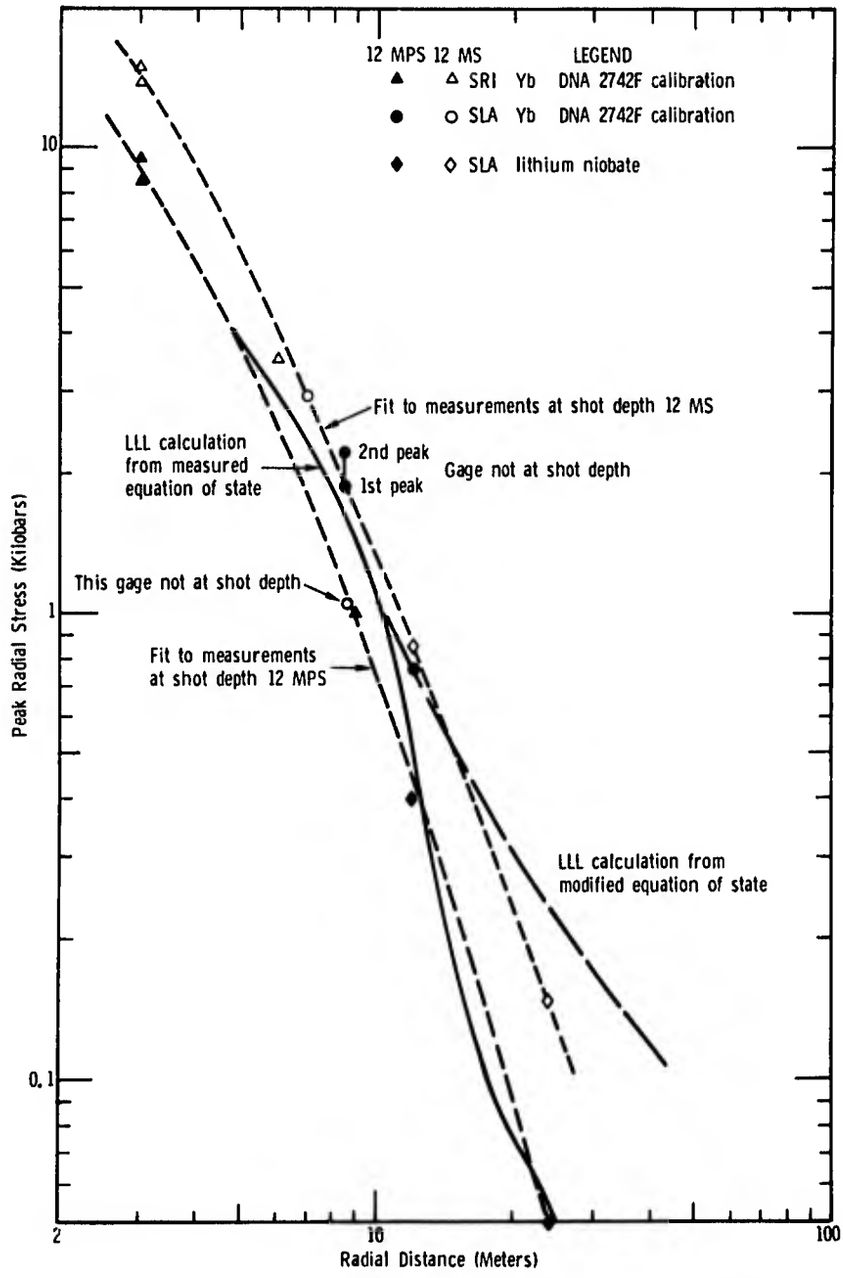

Figure 4.19 Comparison of measured peak radial stress on 12 MS and 12 MPS with the LLL pre-shot calculated stresses

Figure 4.19 provides still further evidence of the differences attributable to medium variances between the sites for 12 MPS and 12 MS. The difference is still more striking if one examines the great divergence in wave forms by comparing Fig. A-6 with E-7 or E-8 and A-7 with E-9.

Free-Field Ground Motion

Free-field ground-motion measurements made with accelerometers at shot depth and half-shot depth are summarized in Table 4.3. Records of the measurements, together with velocity-time plots obtained from first integrations and displacement-time plots from second integrations, are reproduced in Appendix F.

At the half-shot-depth station (6-6), signal arrival time agrees with that of the stress gages at the same location. Records from both gages (Figs. F-1 and F-2) exceeded band edge at values more than twice those for 12 MS at the same station. The first pulse discontinued after only 0.25 msec, and there was evidence of no motion for the next 0.75 msec, followed by a longer period of motion. These records yielded no useful information.

The fact that the records were beyond band edge is a direct result of differences between the sites of 12 MS and 12 MPS. On 12 MS, gages of the same type at the same locations, having calibration steps of 2000 and 5016 g's for the low- and high-range gages respectively, gave peak accelerations of 6500 g's. As a result, the calibration steps for 12-MPS were changed to 5032 and 6565 g's. With these values at about 60 % of band edge, the channels would have been capable of recording more than 8400 and 10900 g's respectively. Measured peaks were limited at 15,800 g's in one case (see Table 4.3), indicating that peak accelerations must have been more than three times what they were for the same location on 12 MS.

Results from the 12-meter station at shot depth were unsatisfactory for a number of reasons. The low-range gage (Fig. F-3) gave a record that shows no signal at all at the time the shock wave is expected. The record for the high-range gage (Figs. F-4 and F-5) shows a pronounced spike at the time the shock wave is expected. The duration of the acceleration pulse at about 6 msec is less than 0.2 msec, after which the record shows a return to zero until about 7.5 msec when there are additional signals. The source of signals at that time is obscure, and the shape of the pulses appears erratic. It was concluded that only arrival times at this station are valid data.

Records from the 24-meter station are doubted for the following reason. Both horizontal gages show an initial negative (inward) acceleration. This might result from gage polarity being reversed, but the record is presented as taken. The low-range horizontal gage (Figs. F-6 and F-7) had a very short acceleration and an unexplained excursion to band edge between 28 and 30 msec. The high-range gage record (Figs. F-8 and F-9) is similar except for the excursion to band edge. The vertical acceleration record (Figs. F-10 and F-11) looks credible and results in a very small peak velocity. The tangential record (Figs. F-12 and F-13) had a negative excursion beyond band edge, indicating a peak acceleration in excess of 300 g's.

A

TABLE 4.3

Summary of Acceleration Measurements at Shot Depth
ESSEX I 12 MPS 20 September 197
21,594 Pounds Nitromethane Buried 12 Meters Deep,

Accelerometer Designation	Accelerometer Orientation	Distance (m)	Depth (m)	Gage Range	Gage Limit (g's)	Gage Sensitivity	Calibration Step (g's)
6-6 AR-LO	Radial	6	6	Low	10,000	High	5,032
				Low	10,000	Low	5,032
6-6 AR-HI	Radial	6	6	High	20,000	High	6,565
				High	20,000	Low	6,565
12-12 AH-LO	Horizonta	12	12	Low	5,000	High	1,513
				Low	5,000	Low	1,513
12-12 AH-HI	Horizontal	12	12	High	10,000	High	2,536
				High	10,000	Low	2,536
24-12 AH-LO	Horizontal	24	12	Low	200	High	99
				Low	200	Low	99
24-12 AH-HI	Horizontal	24	12	High	1,000	High	497
				High	1,000	Low	497
24-12 AV	Vertical	24	12		200	High	97
					200	Low	97
24-12 AT	Tangential (Horizontal)	24	12		200	High	98
					200	Low	98
36-12 AH-LO	Horizontal	36	12	Low	200	High	99
				Low	200	Low	99
36-12 AH-HI	Horizontal	36	12	High	200	High	100
				High	200	Low	100
36-12 AV	Vertical	36	12		200	High	100
					200	Low	100
36-12 AT	Tangential (Horizontal)	36	12		200	High	60
					200	Low	60

* Reading Accuracy for time is ± 0.01 milliseconds
(L) Limited
(a) Signal limited by band edge
(b) No signal from this gage
(c) Record is of doubtful validity
(d) Signal from surface return

B

TABLE 4.3

ɜration Measurements at Shot Depth and Half Shot Depth
ESSEX I 12 MPS 20 September 1973
itromethane Buried 12 Meters Deep, Partially Stemmed

Gage Sensitivity	Calibration Step (g's)	Arrival Time* (msec)	Peak Acceleration (g's)	Time of Peak* (msec)	Peak Velocity (m/sec)	Time of Peak* (msec)
High	5,032	3.55	>10,000(a)		>45	
Low	5,032	3.55	>12,000(a)		>50	
High	6,565	3.55	>13,200(a)			
Low	6,565	3.55	>15,800(a)			
High	1,513	(b)				
Low	1,513	(b)				
High	2,536	6.05	8,650(c)	6.10		
Low	2,536	6.00	13,000(c)	6.10		
High	99	13.6	-186	13.95		
Low	99	13.7	-290	13.95		
High	497	13.5	410	13.95		
Low	497	13.5	>290 (L)	13.95		
High	97	13.6	89	14.75	0.28	17
Low	97	13.6	94	14.75	0.28	17.0
High	98	13.6	>200 (L)			
Low	98	13.6	>300 (L)			
High	99	21.5	14.5	22.9	0.2	23.9
			25.0	26.0	0.54	27.0
			45.0(d)	36.5	1.50	39.5
Low	99	21.7	15.0	22.9	0.18	23.9
			25.0	26.0	0.53	27.0
			44.0(d)	36.5	1.49	39.5
High	100	21.8	13.0	23.0	0.18	23.9
			22.0	26.1	0.50	27.0
			41.0(d)	36.7	1.35	39.6
Low	100	~22.0	14.0	22.8	0.18	23.9
			23.0	26.0	0.49	27.0
			44.0(d)	36.6	1.34	39.5
High	100	22.0	+3.0	24	-0.02	23.3
			-7.0	26	-0.10	27.1
			-5.5(d)	36	-0.19	38.0
Low	100	22.0	+3.0	24	-0.014	23.3
			-7.0	26	-0.09	27.1
			-6.0(d)	36	-0.14	38.1
High	60	21.3	-34.5	22.6	-0.39	23.5
			+47.0	26.2	+0.54	27.5
			+53.5 (d)	36.8	+0.70	37.8
Low	60	21.3	-35.0	22.6	-0.4	23.5
			+47.0	26.4	+0.54	27.5
			+53.0(d)	36.8	+0.69	37.8

Before continuing to the results at 36 meters, certain things are worth pointing out about measurements at the three stations discussed so far. All radial motions are characterized by very short acceleration pulses. These are followed by a return to zero acceleration for some span of time. Thus there remains a possibility that the records are valid in spite of their seeming otherwise. This possibility is strengthened if one notes that the horizontal displacement at m is 14.7 cm (from the high-range gage) at 65 msec, as compared with 14 cm at the same time from the fully stemmed shot. This would indicate that residual displacements on the two shots could be similar even though the motion sequence required to reach that displacement was quite different. Note also that the particle velocity at 65 msec was about 2.3 msec for 12 MS and 2.7 m/sec for 12 MPS. In neither case did the velocity return to zero by the time of cable break, which for 12 MPS occurred at about 200 msec.

The most telling argument that the records from the three closest stations are not credible is that the signatures are so different from those at 36 m, where the records are quite credible. Records from the two horizontal radial gages (Figs. F-14 through F-17) are very much alike. They show two early positive-peak accelerations at about 23 and 26 msec, followed by a much larger peak at 36.5 msec, which is attributed to a return from the surface. The integrals of these records (velocity-time) are quite different from those of 12 MS in that the velocity record of that shot goes to an initial peak of over 2 m/sec immediately after shock arrival, then drops to about 1 m/sec for about 15 msec before beginning a climb to over 2 m/sec as a result of the return signal from the surface. The corresponding record for 12 MPS goes initially to only a peak of 0.2 m/sec as a result of the signal returning from the surface. (The reader is invited to compare Fig. F-16 with Fig. B-18.) The important point to be made is that the first peak from 12 MPS, which is the one with which calculation is to compared, is only 1/10 the corresponding peak from 12 MS.

In Fig. F-22 a 3-second integration of the 36-12 high-range high-sensitivity channel shows that a peak outward displacement of 24.5 cm occurred at about 0.25 sec, rebounded to about 8 cm by 0.7 sec, and remained relatively constant thereafter.

The records from the vertical accelerometer (Figs. F-18 and F-19) show four downward velocity peaks, two from direct shock and two from the surface return, each larger than the preceding peak. The initial tangential motion (Figs. F-20 and F-21) is negative (counterclockwise) followed by two positive (clockwise) acceleration peaks, the second larger than the first, and later by a series of peaks associated with surface return. The initial velocity is negative, and the negative peak is followed by a positive peak 3.8 msec later.

A 3-second integration of the high sensitivity of the tangential accelerometer (Fig. F-22) shows a peak clockwise displacement of 15.8 cm at about 0.3 sec, followed by a counterclockwise recovery by 0.7 sec to 2.2 cm with a subsequent gradual restoration to the original position, which may or may not be real.

In Fig. 4.20 the vector sum of the particle velocities of the three components is presented versus time. If the measured density of 1.996 gm/cc for Unit 6 is used with the shock velocity of 1.45 m/msec from Fig. 4.14, together with the vector sum particle velocity of the first peak at about 24 msec, to compute peak stress, the results are as shown by the circle in Fig. 4.21. The peak stress from measured radial particle velocity falls below the scale of the plot at 5.8 bars. The peak stress determined from the vector sum falls quite close to an extension of the "a" line. Note that if the plotted circle is carried back to Fig. 4.19, the vector sum value is in excellent agreement with that calculated by LLL for what they designate the Z0 medium.[19]

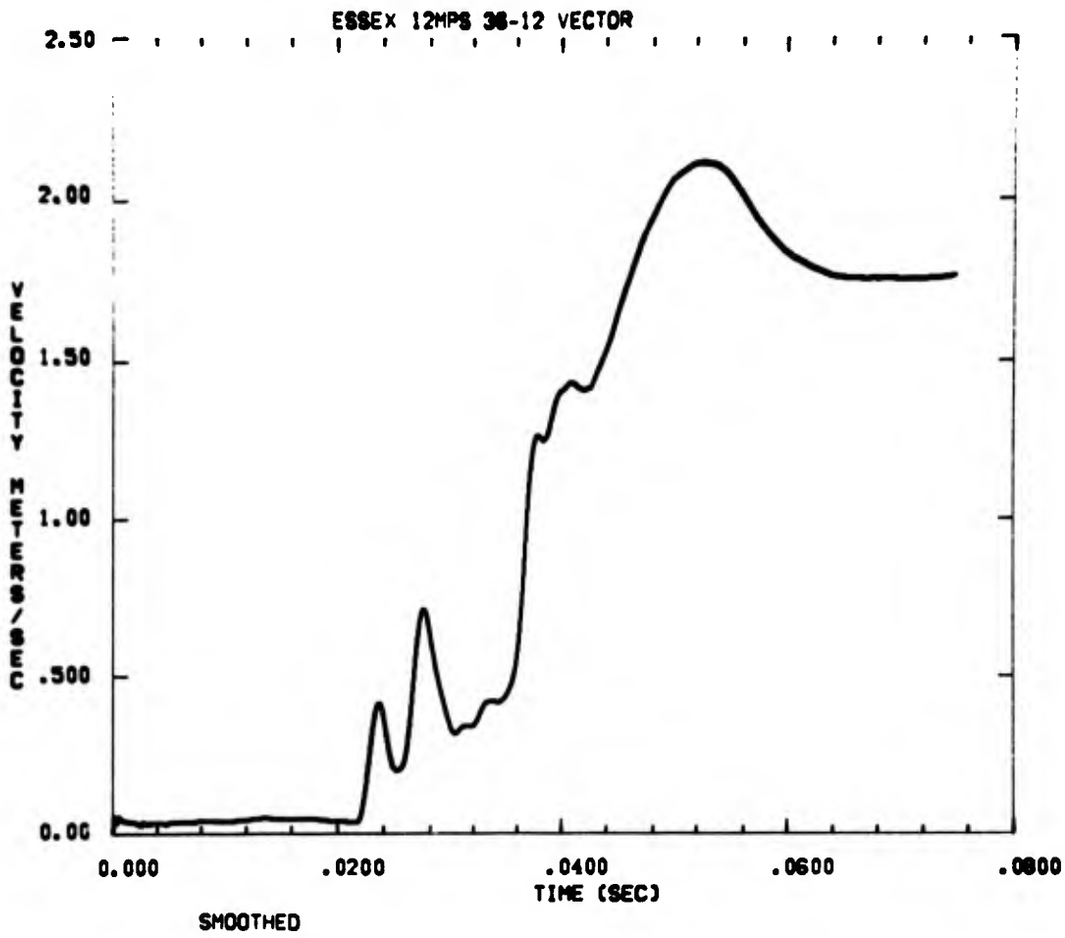

Figure 4.20 Vector sum of radial, vertical, and tangential components of velocity as a function of time at the 36-meter station

Surface-Motion Instrumentation

Table 4.4 summarizes the results of surface-motion measurements. Records of the measurements, together with their first and second integrations appear in Appendix G.

At the near-surface-zero station the low-range vertical accelerometer gave an excellent record for both sensitivities (Figs. G-1 and G-2). The high-range gage failed at 7.7 msec, and appears to have an invalid period from about 6.8 to 7.6 msec (Fig. G-3). Surface motion to about

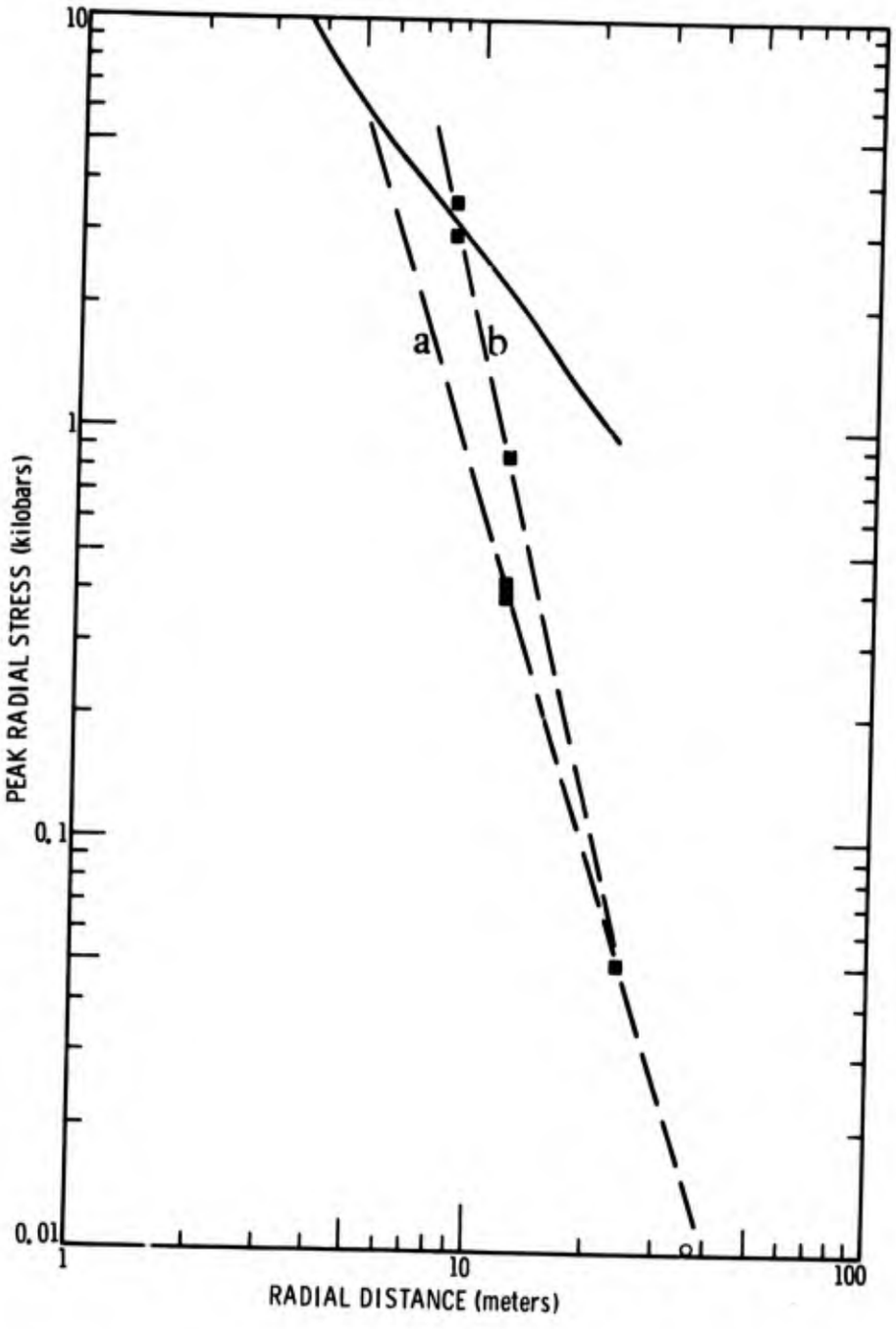

Figure 4.21 Comparison of peak radial stress measured in 12 MPS with pre-shot calculated values

A

TABLE 4.4

Summary of Surface Accelerati
ESSEX I 12 MPS 20 Sept
21,594 Pounds Nitromethane Buried 12 Met

Accelerometer Designation	Accelerometer Orientation	Distance (m)	Depth (m)	Gage Range	Gage Limit	Gage Sensitivity	Calibra (g'
0-0 AV-LO	Vertical	2/3	2/3	Low	10,000	High	2
				Low	10,000	Low	2
0-0 AV-HI	Vertical	2/3	2/3	High	20,000	High	3
				High	20,000	Low	3
0-0 AH	Horizontal	2/3	2/3		5,000	High	
					5,000	Low	
9-0 AV	Vertical	9	2/3		10,000	High	
					10,000	Low	
12-0 AV	Vertical	12	2/3		5,000	High	
					5,000	Low	
12-0 AH	Horizontal	12	2/3		1,000	High	
					1,000	Low	
24-0 AV	Vertical	24	2/3		1,000	High	
					1,000	Low	
24-0 AH	Horizontal	12	2/3		1,000	High	
					1,000	Low	

(L) Limited

B

TABLE 4.4

ary of Surface Acceleration Measurements
ESSEX I 12 MPS 20 September 1973
itromethane Buried 12 Meters Deep, Partially Stemmed

Gage Sensitivity	Calibration Step (g's)	Arrival Time (msec)	Peak Acceleration (g's)	Time of Peak (msec)	Peak Velocity (m/sec)	Time of Peak (msec)
High	2,500	4.5	4,400	6	67	90
Low	2,500	4.5	5,180	5.8	67	90
High	3,446	5.0	5,470	6.6	Failure at 7.7 msec	
Low	3,446	5.0	5,640	5.7	Failure at 7.7 msec	
High	977	4.6	1,800	5.3	8.1 26.7	6.0 11.3
Low	977	4.6	5,000	5.3	13.4 23.5	6.0 11.3
High	410	9.8	> 800 (L)	---		37
Low	410	9.8	> 1,720 (L)	---		37
High	250	10.6	470	11.1	30.6	400
Low	250	10.8	745	11.1	30.6	400
High	151	11.0	> 300 (L)	11.3		
Low	151	11.1	633	11.2	13.8	630
High	20	17.0	21.8	23.4		
			35.6 (L)	35.9	5.7	62
Low	20	17.0	21.9	23.4		
			38.3	35.9	5.75	62
High	50	17.0	12.0	40.0	2.77	85
Low	50	17.0	11.8	40.0	2.87	85

360 msec, when the signal stopped because of cable breakage, is shown in Fig. G-4. Both the low-range vertical accelerometer record and that for the horizontal accelerometer (Figs. G-5 and G-6) show a small signal starting at about 2.25 msec and peaking at about 2.5 msec, which is attributed to motion induced by the jet moving up the open hole. Since initial motion on the vertical gage is upward rather than downward, it is inferred that air-slap after blast emerges from the open hole is not the mechanism.

The record from the horizontal gage (Figs. G-7, G-8, and G-9) was limited by band edge on a negative excursion. After recovery, there is a return to carrier frequency for almost 1 msec, followed by an instantaneous jump to over 1000 g's. Thereafter the record appears quite good. To get an improved displacement-time function, the velocity over the 1-msec interval has been adjusted by the amount of the negative excursion after 50 msec. This allows a better approximation of displacement-time with the implicit assumption that velocity should be zero at about 50 msec. The assumption is based on an expectation that horizontal velocity should certainly be small between the time the shock wave has passed (about 25 msec) and the time mound growth becomes appreciable.

Vertical accelerations at the 9-meter station had positive and negative peaks limited by band edge (Figs. G-10 and G-11). As a result both peak velocities and displacements are below true values.

Except as noted below, excellent records were obtained from the vertical and horizontal accelerometers at the 12-meter station (Figs. G-12 through G-15). The record from the high-sensitivity channel of the horizontal gage was slightly limited by band edge. Three-second double integrations yield the trajectory indicated by the circles in Fig. 4.22. The trajectory is inconsistent with the ejecta plume observed by photography. An adjusted trajectory obtained in the same manner as discussed in Chapter 3 is shown for comparison only. Also shown is the trajectory for 12 MS. The larger trajectory appears to have been caused either by the two gages failing to return to zero by a small amount, or by a small baseline shift after signal arrival, of the type described in Appendix R. The amount of either, which could account for the difference between this trajectory and that for 12 MS, is indeed small. For the vertical gage it amounts to 0.29 % of half band width and 0.04 % of gage range, and for the horizontal gage 0.4 and 0.2 % respectively. In view of the inaccuracy of the unadjusted trajectory, the adjusted trajectory is qualitative only.

Figures G-16 through G-19 show vertical and horizontal motions at the 24-meter station. The vertical acceleration is characterized by a double peak, the second larger than the first. The double peak is also perceptible on the record of horizontal acceleration. The trajectory of the instrument canister, without correction for tilt, is shown in Fig. 4.23.

Note in Figs. G-16 and G-17 that the high and low sensitivities of the vertical gage give quite similar results, while the high and low sensitivities of the horizontal gage (Figs. G-18 and 19) are quite different on the 3-sec records. This appears to result from a baseline shift during the signal on the low-sensitivity channel and not on the high. (See App. R for a discussion of baseline shifts and their treatment.) This was the first case encountered where there was a shift in the baseline of

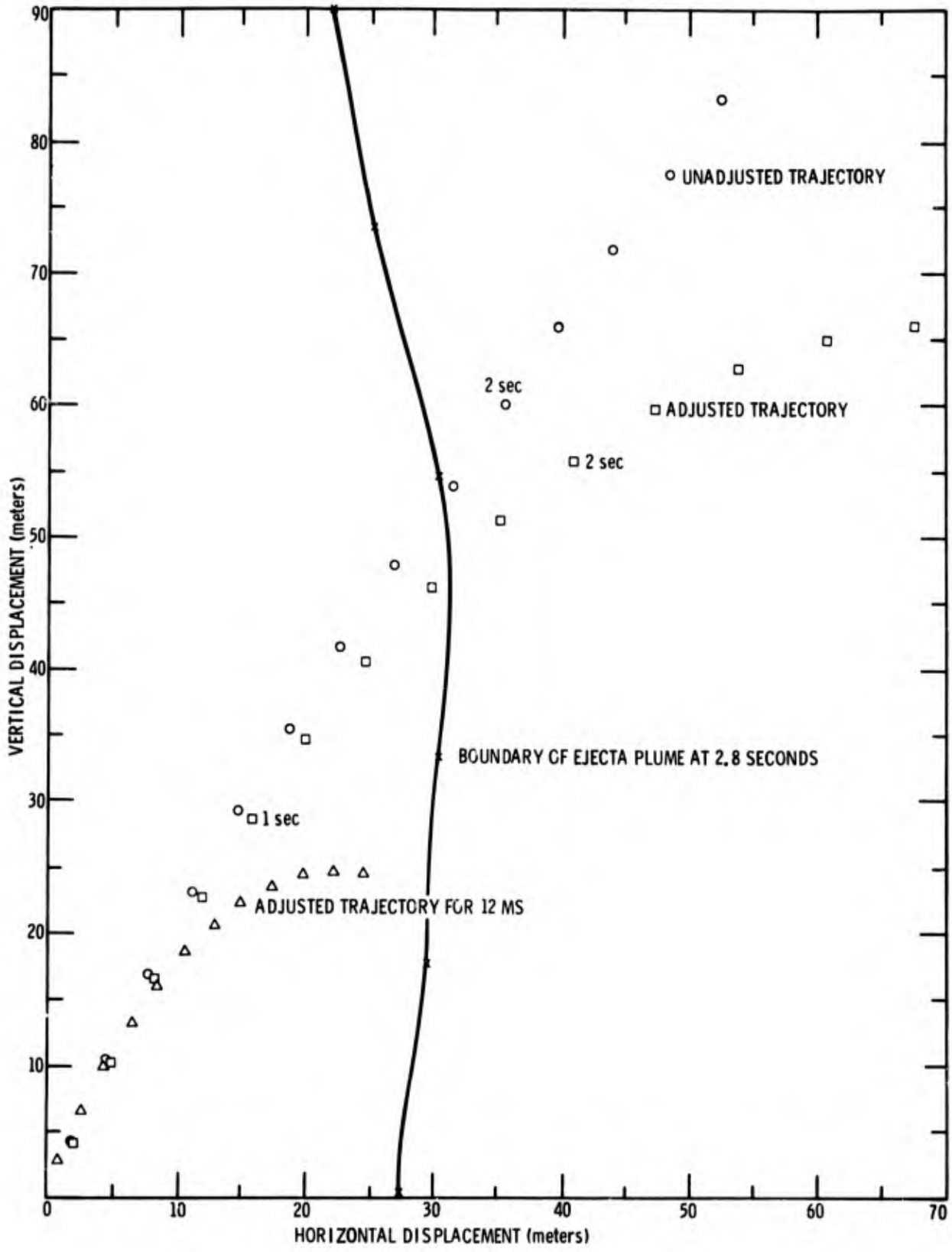

Figure 4.22 Canister trajectory for the 12-meter station of 12 MPS compared with that of 12 MS

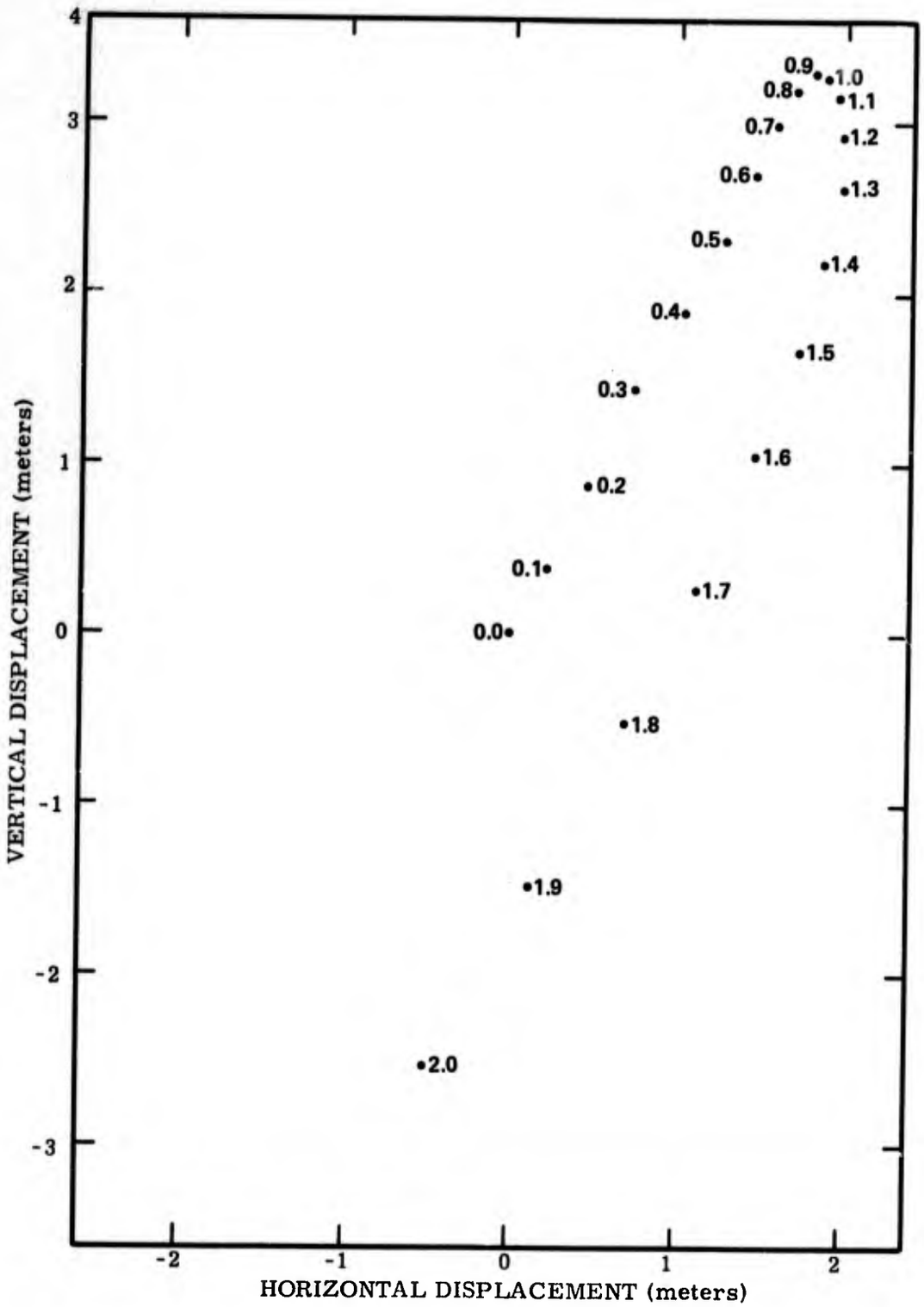

Figure 4.23 Canister trajectory for the 24-meter station, 12 MPS

one channel and not in the other from the same gage. This would appear to implicate the voltage-controlled oscillator (VCO) rather than either the gage or the recording system. It should be observed that the difference between the high- and the low-sensitivity channels amounts to only 0.2 g, which is 0.2 % of band width for the high-sensitivity channel and only 0.075 % for the low-sensitivity channel. Perhaps as important, it is only 0.02 % of gage range. A judgment is made here that the low-sensitivity channel is the incorrect one, so the trajectory in Fig. 4.24 is based on the high-sensitivity channel.

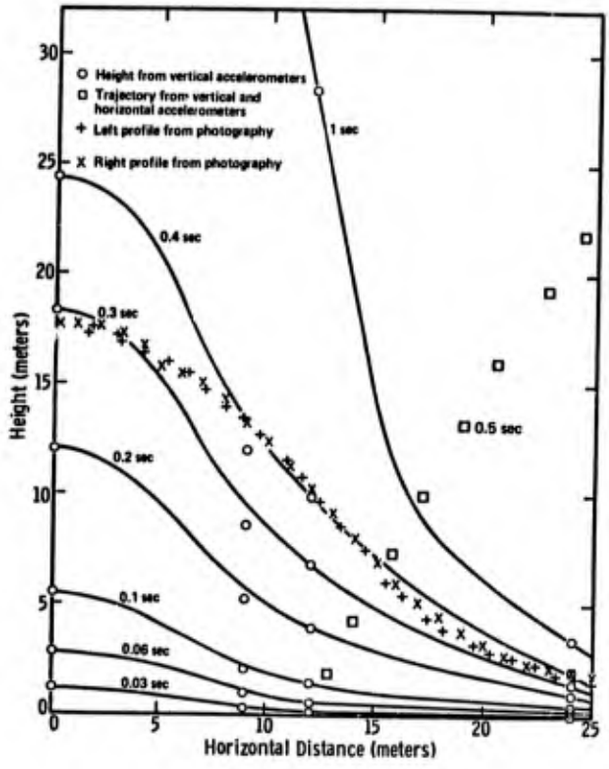

Figure 4.24 Mound profile - 12 MPS

Comparison of Fig. 4.23 with Fig. 3.16 shows that the peak vertical displacement of 12 MPS is more than twice that of 12 MS, and that at 1 sec the horizontal displacement is only slightly smaller. After 1 sec the record shows the trajectory to be continuously downward and inward, and this trend continues until cable failure at about 3 sec. An increasing downward and inward velocity may be the result of canister rotation, and since rotation at late times cannot be determined, its effect cannot be removed. If the indication that the ground surface did not pause or come to rest at or above the original level is qualitatively correct, it suggests a ground failure mechanism that would account for the crater radius for the partially stemmed shot being greater than for the stemmed shot and being beyond the 24-0 station. The mechanism suggested is that of the ground rising and falling in both shots. In the relatively unsaturated medium of the stemmed shot the upthrust material settled back to where it was supported on stable material, leaving the surface above the original ground level. In the relatively saturated medium of the partially stemmed shot

the upthrust material settled back on unstable material, possibly liquified by the impact, and the upthrust, together with the unstable material, sloughed into the crater.

In Figure 4.24 is a mound profile for 12 MPS constructed from displacement of the vertical accelerometer. The fact that the values for the 9-0 station fall below the profile is accounted for by the fact that the record was limited by band edge, and full displacement after time of limiting (around 12 msec) was not obtained. Again, a profile from the motion picture photograph at 0.3 sec has been superimposed for comparison. As can be seen, values from vertical and horizontal accelerometers at the 12-0 station and from the vertical accelerometers at the 0-0 station are in good agreement with photographic data.

Figure 4.25 compares surface vertical acceleration versus radial distance for 12 MPS with that for 12 MS. The attenuation rate is greater for 12 MPS. Perhaps more interesting is the comparison at the surface zero station, where for 12 MPS the peak values are in agreement with those from other stations, whereas, for 12 MS the peak accelerations fall well above those indicated by the other stations and below the peaks for 12 MPS. This is a further indication of differences in medium between the two shots. It shows also that the grout was a better match for 12 MPS than for 12 MS, and suggests that propagation in the grout of 12 MS was reduced by refraction into the lower-velocity medium surrounding the grout.

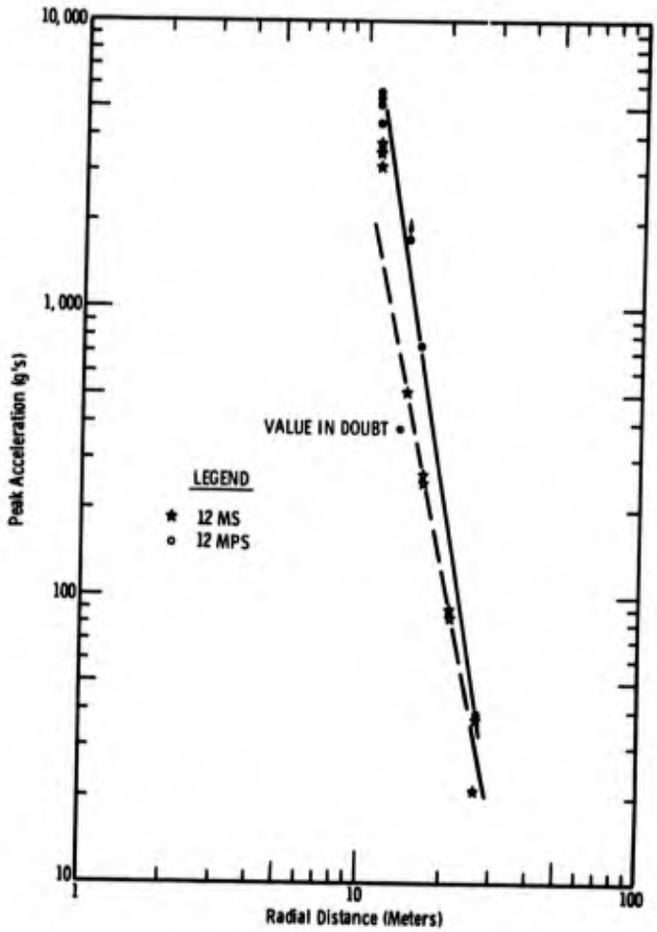

Figure 4.25 Comparison of vertical surface acceleration versus distance for 12 MS and 12 MPS

Figure 4.26 shows that there is little difference between the two shots in late-time peak velocities, despite significant differences at early times.

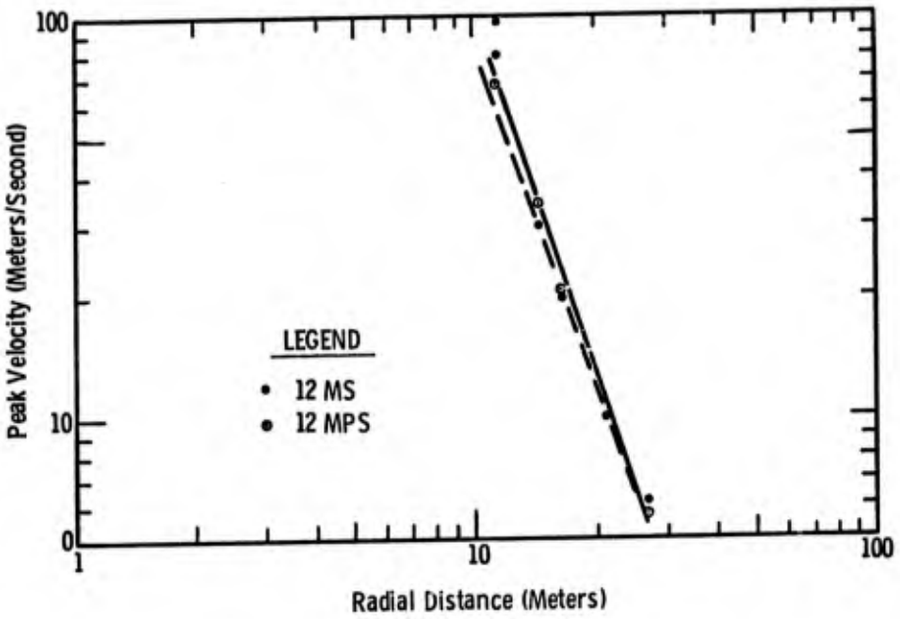

Figure 4.26 Comparison of vertical peak surface velocity versus distance for 12 MS and 12 MPS

Surface Displacement from Photography

Table 4.5 lists the cameras used to record the surface motion and flare from 12 MPS. Figure 4.27 shows the plan view of the camera station and reference markers with respect to SGZ. In Fig. 4.28 the displacement derived from accelerometer 0-0 AV-LO is compared with the vertical displacement of SGZ determined from photography. The flare obscures SGZ for a period of time (depending on camera and exposure), accounting for the loss of photography information at early times. As in the case of 12 MS (Fig. 3.23), displacement determined from photography lags behind that determined from the accelerometer.

At 9 m (Fig. 4.29), displacement from the accelerometer lags that from photography because accelerometer displacement is derived from double integration of an acceleration record in which peaks were limited. At the 12-meter station (Fig. 4.29), displacement from photography lags that from the accelerometer for about 130 msec, after which that from photography departs from the accelerometer displacement for the same reasons it did for 12 MS.

Comparison with photography for 12 MPS supports confidence in the acceleration measurements, just as it did in 12 MS.

TABLE 4.5

Summary of Camera Coverage - 12 MPS

	Timing (cps)	Camera Speed (fps)	Lens	Film	Field of View Height (ft)	Field of View Width (ft)	f Stop
1) Fastax 16 mm	1000	4000	15 in.	2479	13	18	5.6
2) Fastax 16 mm	1000	4000	10 in.	2479	20	27	4.5
3) Hycam 8 mm	1000	12000	10 in.	Plus X	20	27	11
4) Hycam 8 mm	1000	12000	6 in.	Plus X	17	44	6.3
5) Fastax 8 mm	1000	12000	6 in.	2475	17	44	7.7
6) Hycam 16 mm	1000	7000	6 in.	Plus X	33	44	16
7) Fairchild 16 mm	1000	1000	3 in.	2496	67	89	4
8) Fastax 16 mm	1000	1000	3 in.	2496	67	89	4
9) Hycam 16 mm	1000	7000	3 in.	Plus X	67	89	8
10) Fastax 16 mm	1000	4000	2 in.	EF	100	133	2.8
11) Milliken 16 mm	100	500	1 in.	EF	200	266	5.6
12) Milliken 16 mm	100	128	10 mm	EF	450	666	8
13) Milliken 16 mm	100	500	1 in.	EF	1200	1600	6.3
14) Milliken 16 mm	100	128	15 mm	EF	1714	2285	11

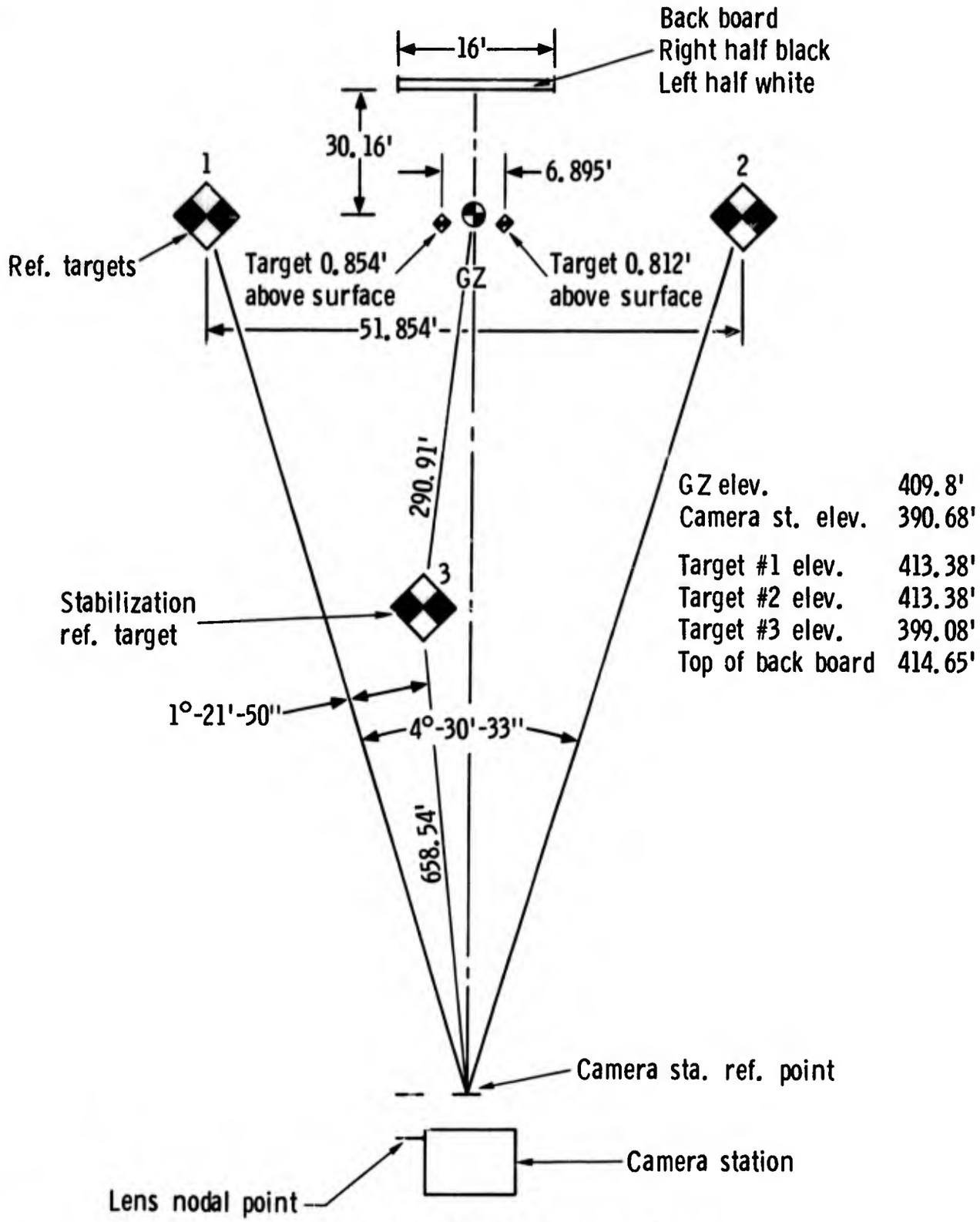

Figure 4.27 Plain view of camera layout

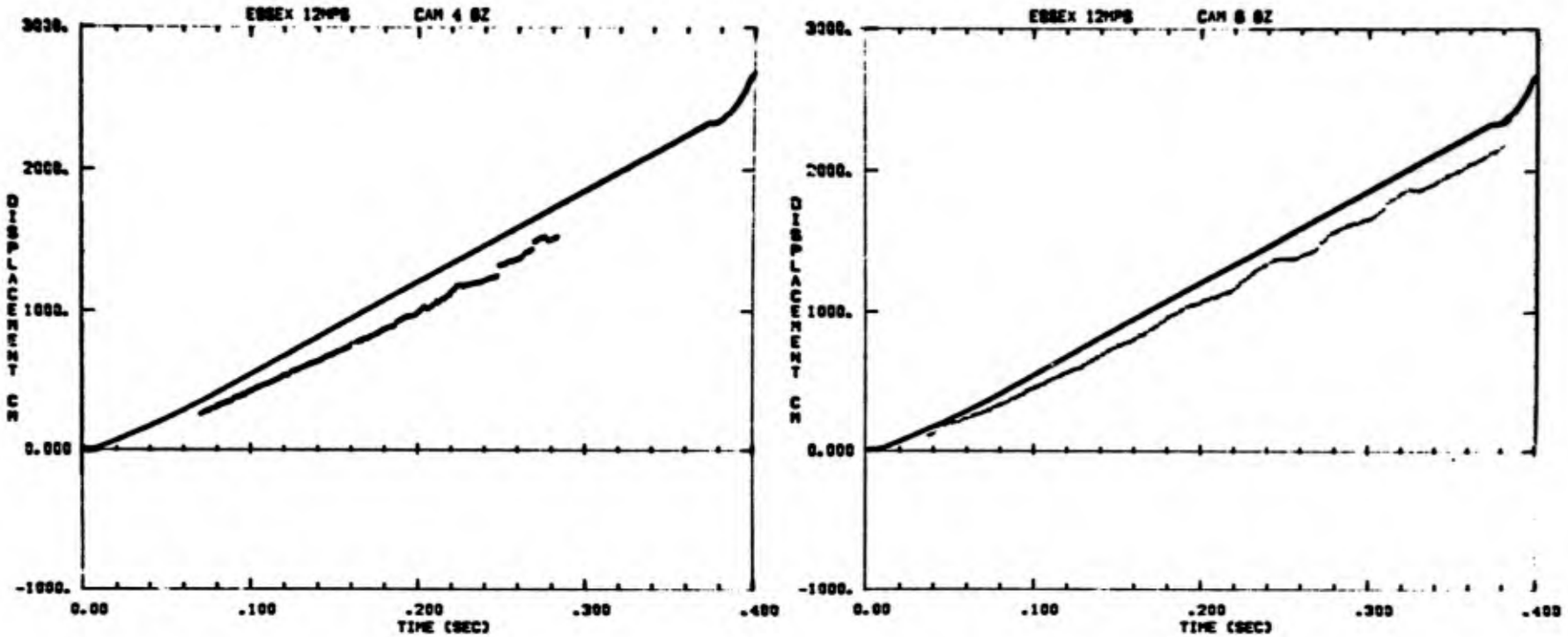

Figure 4.28 Comparison of surface zero vertical displacements from photography with those from accelerometers

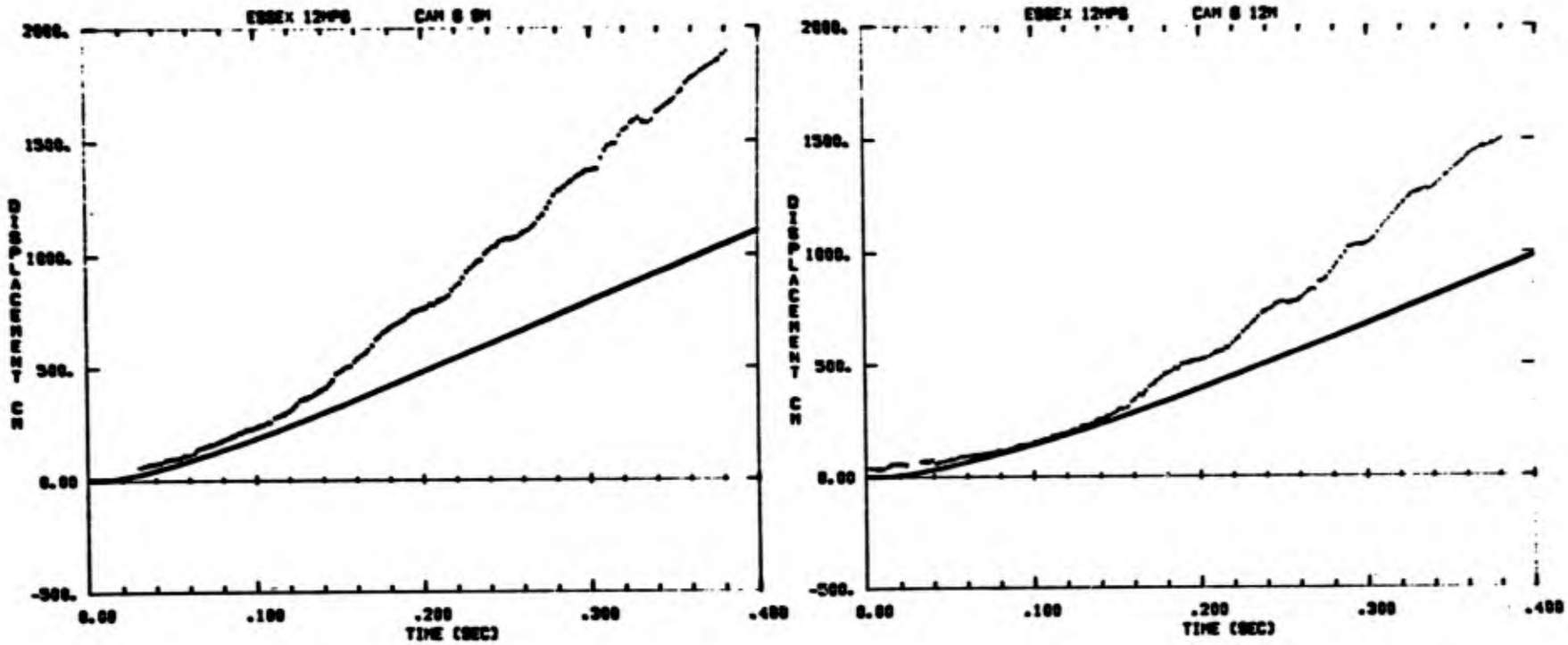

Figure 4.29 Comparison of vertical surface motion at 9 and 12 meters determined by photography with that from the vertical component of acceleration

Airblast Measurements

Results of airblast measurements are summarized in Tables 4.6 and 4.7, and the records are reproduced in Appendix H. Sandia measurements were made at three stations generally east of the shot at distances of 731, 2202, and 5307 meters. SL also recorded airblast from gages installed by BRL at three stations--20, 40, and 80 feet (6.1, 12.2, and 24.4 m)--from SGZ along an azimuth of 60°.

Waveforms measured at the SL stations were quite similar to those from 12 MS except for the large peak overpressure resulting from the flare up the open 7-inch (17.8-cm) diameter hole. This flare spike is superimposed on the regular ground-shock-induced peak. More information will be presented in Chapter 7. Here it is sufficient to say that peak overpressure from the flare of 12 MPS was 2.7 to 4.2 times the ground-shock-induced peaks from 12 MS, the difference not being constant with range. The impulse in the same pulse of 12 MPS was only 1.2 to 1.5 times that in the corresponding pulse of 12 MS. Gas-venting peak overpressure of 12 MPS was 1.75 times that of 12 MS over the range of measurements. Similarly, impulse in the gas-venting pulse was about 1.25 times larger.

The larger pressure and impulse in the first pulse was to be expected in view of the open hole. If all other things had been equal for the two shots, it would have been expected that peak overpressure and impulse of the gas-venting pulse would have been equal or slightly less for the shot with the open hole, to the extent that energy in cavity gases had been lost up the hole. The times of the gas-venting peaks for the two shots are not appreciably different for the two shots, so the higher peak overpressures are not a result of early venting while cavity gases were under higher pressure. The most probable explanation is that cavity gases of 12 MPS were under higher pressure at the time of venting simply because the cavity was smaller than that of 12 MS when venting occurred. This again could be attributed to differences in medium between the two sites.

Records of BRL measurements show a gage or cable failure for one of the two gages at 6.1 m, and the record from the other gage does not appear valid (Fig. H-4). No record was obtained from one of the two gages at 24.4 m. The record from one of the two gages at 12.2 m appears to be invalid after peak overpressure, and there is reason to question whether peak overpressure was measured. The other gage at 12.2 m was limited by band edge. At the one-psi level, BRL-2 (Fig. H-5) has a duration of 8.6 msec. The ground-shock-induced pulse arrives at 15.6 msec, and the limited spike at 28.9 msec. The spike is attributed to the flare pulse originating at SGZ at 2 msec and traveling horizontally 12.2 m in 26.9 msec. Since pulse duration is 8.6 msec, it must be assumed that contributions of the two pressure pulses seen in the pipe have merged by arrival at the 12.2-m station. Since the peak of BRL-2 was limited, there remains a possibility that a two-peak structure of the spike was missed. That the spike had a single peak, however, is confirmed by BRL-3 (Fig. H-6).

TABLE 4.6

Summary of Airblast Mea
(Metric Units)
ESSEX I 12 MPS 20
21,594 Pounds Nitromethane Buried 12 Mete

Gage Designation	SLA 1-LO	SLA 1-HI	SLA 2-LO	SLA 2-HI	SL
Gage Range	Low	High	Low	High	L
Gage Sensitivity	High	Low	High	Low	Hi
Distance (km)	731.	731.	2202.	2202.	5
Azimuth (rad)	1.484	1.484	1.412	1.412	1.
Time of Arrival of Grcund-Shock-Induced Pulse (s)	2.04	2.04	6.27	6.27	1
Flare Peak Pressure (Pa)	328.2	318.5	131.0	128.2	2
Time of Flare Peak Pressure (s)	2.079	2.079	6.300	6.300	1
Time of Crossover (s)	2.330	2.332	6.589	6.589	1
Flare Impulse (Pa-s)	13.58	13.38	4.551	4.447	1
Negative Peak Pressure (Pa)	78.60	86.18	24.75	25.51	1
Time of Negative Peak (s)	2.667	2.668	6.874	6.871	1
Time of Crossover (s)	2.954	2.954	7.170	7.154	1
Negative Impulse (Pa-s)	23.37	24.06	7.171	7.239	3
Gas Venting Peak Pressure (Pa)	77.91	81.36	27.51	27.37	9
Time of Gas Venting Peak Pressure (s)	3.130	3.130	7.325	7.34	1
Time of Crossover (s)	3.312	3.312	7.517	7.518	1
Gas Venting Impulse (Pa-s)	15.58	15.24	5.323	5.261	2

BRL-1 failed at 0.01 seconds

(L) Limited

B

TABLE 4.6

mmary of Airblast Measurements
(Metric Units)
X I 12 MPS 20 September 1973
ethane Buried 12 Meters Deep, Partially Stemmed

SLA 2-HI	SLA 3-LO	SLA 3-HI	BRL 1A	BRL 2	BRL 2A	BRL 3
High	Low	High	High	Low	High	Low
Low	High	Low	Low	High	Low	High
2202.	5307.	5307.	6.096	12.192	12.192	24.384
1.412	1.538	1.538	1.047	1.047	1.047	1.047
6.27	15.15	15.15	.0095	.0136	.0150	.0256
128.2	20.82	20.20	>104,800 (L)	>10,135 (L)	18,616.	>9646. (L)
6.300	15.234	15.234	.0107 & .0126	~.032	.0292	.0621
6.589	15.615	15.625	.0158	.253	>.037	.2269
4.447	1.972	1.958		>524.	>117.	288.2
25.51	10.69	10.41	40631.			1370.
6.871	15.843	15.829	.0234			.6731
7.154	16.149	16.148				.9446
7.239	3.365	2.868				543.3
27.37	9.101	9.032				1465.
7.34	16.29	16.28				1.139
7.518	16.800	16.801				1.421
5.261	2.082	2.096				376.5

A

TABLE 4.7
Summary of Airblast Measu
(English Units)
ESSEX I 12 MPS 20 Septe
21,594 Pounds Nitromethane Buried 12 Meters

Gage Designation	SLA 1-LO	SLA 1-HI	SLA 2-LO	SLA 2-HI	SLA 3-LO
Gage Range	Low	High	Low	High	Low
Gage Sensitivity	High	Low	High	Low	High
Distance (Ft)	2399.	2399.	7224.	7224.	17411.
Azimuth (Degrees)	85.	85.	80.9	80.9	88.1
Time of Arrival of Ground-Shock-Induced Pulse (Sec)	2.04	2.04	6.27	6.27	15.15
Flare Peak Pressure (PSI)	.0476	.0462	.0190	.0186	.00302
Time of Flare Peak Pressure (Sec)	2.079	2.079	6.300	6.300	15.235
Time of Crossover (Sec)	2.330	2.332	6.589	6.589	15.615
Flare Impulse (PSI-Sec)	.00197	.00194	.000660	.000645	.000286
Negative Peak Pressure (PSI)	.0114	.0125	.00359	.00370	.00155
Time of Negative Peak Pressure (Sec)	2.667	2.668	6.874	6.871	15.843
Time of Crossover (Sec)	2.954	2.954	7.170	7.154	16.149
Negative Impulse (PSI-Sec)	.00339	.00349	.00104	.00105	.000488
Gas Venting Peak Pressure (PSI)	.0113	.0118	.00399	.00397	.00132
Time of Gas Venting Peak Pressure (Sec)	3.130	3.130	7.325	7.34	16.29
Time of Crossover (Sec)	3.312	3.312	7.517	7.518	16.800
Gas Venting Impulse (PSI-Sec)	.00226	.00221	.000772	.000763	.000302

BRL 1 Failed at 0.01 Seconds
(L) Limited

B

TABLE 4.7
Summary of Airblast Measurements
(English Units)
SSEX I 12 MPS 20 September 1973
itromethane Buried 12 Meters Deep, Partially Stemmed

2-HI	SIA 3-LO	SIA 3-HI	BRL 1A	BRL 2	BRL 2A	BRL 3
h	Low	High	High	Low	High	Low
	High	Low	Low	High	Low	High
4.	17411.	17411.	20.	40.	40.	80.
9	88.1	88.1	60.0	60.0	60.0	60.0
7	15.15	15.15	.0095	.0136	.0150	.0256
86	.00302	.00293	>15.2 (L)	>1.47 (L)	2.70	>1.399 (L)
00	15.235	15.235	.0107 & .0126	∿.032	.0292	.0621
89	15.615	15.625	.0158	.253	>.037	.2269
0645	.000286	.000284		>.076	>.017	.0418
370	.00155	.00151	5.893			.1987
71	15.843	15.829	.0234			.6731
54	16.149	16.148				.9446
105	.000488	.000416				.0788
397	.00132	.00131				.2125
4	16.29	16.28				1.139
18	16.800	16.801				1.421
0763	.000302	.000304				.0546

Flare Pulse

With the detonation of a charge below an open hole, combustion products are incandescent upon emergence from the hole, often to a brightness that obscures photography at ordinary exposures until the gases have cooled. In the case of 12 MPS the incandescent flare was a possible source of information concerning whether the open hole pinched off. To photograph the flare two cameras (Nos. 6 and 9, see Table 4.5), with high-density filters, were used. Figure 4.30 shows six selected frames from camera 9, together with the time of each frame and the height of the flare at each time. The gas up the open hole arrived at the ported pressure gage at 2.03 msec; ground shock arrived at the 0-0 accelerometer at 4.5 to 4.6 msec. The ported pressure measurement recorded considerable impulse between 6 and 8 msec.

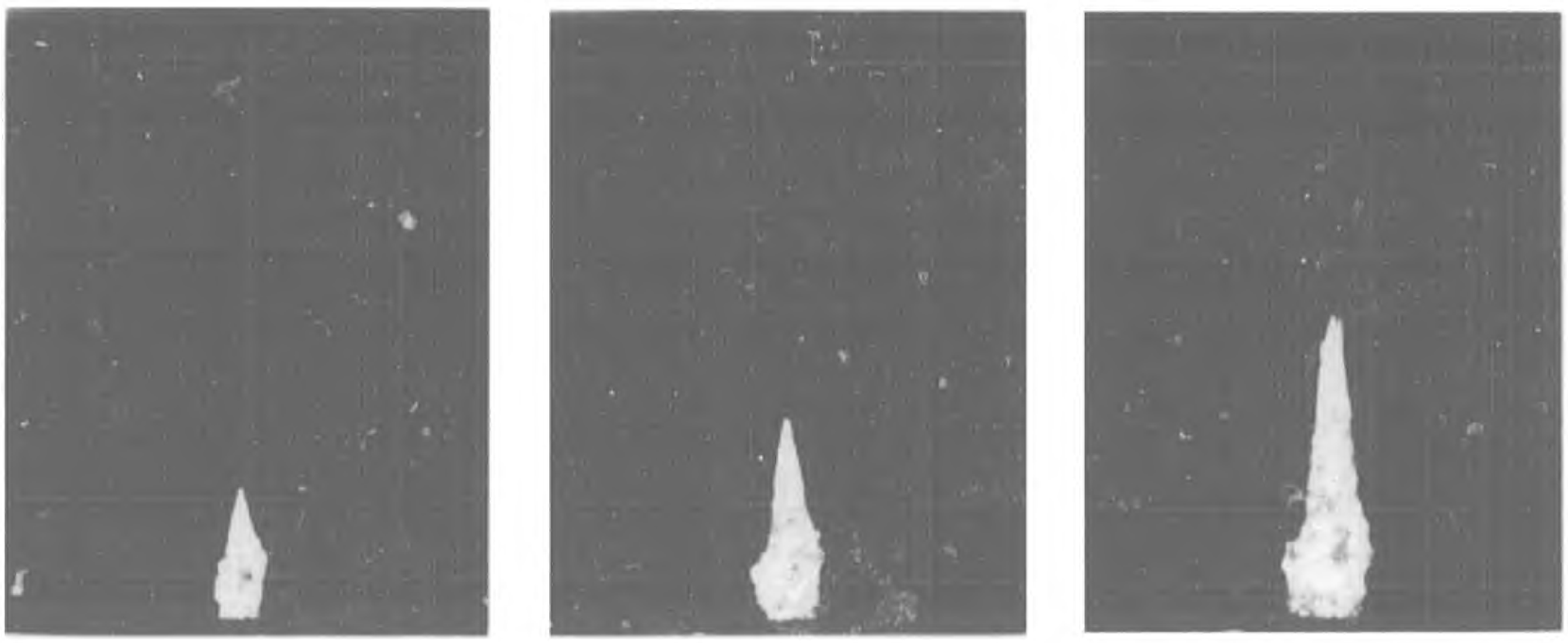

Frame 6
Time 3.086 msec Height 4.05 m

Frame 10
Time 3.658 msec Height 6.40 m

Frame 16
Time 4.517 msec Height 9.53 m

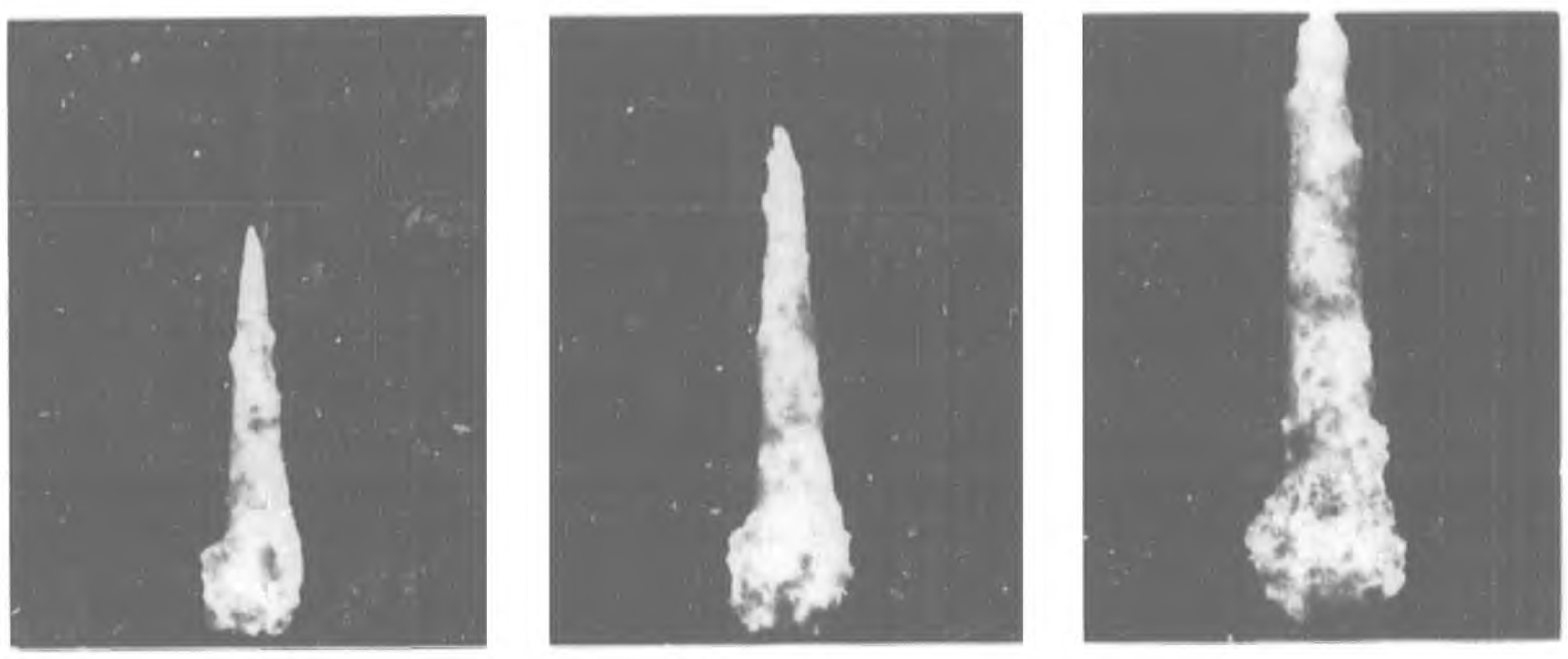

Frame 24
Time 5.662 msec Height 12.76 m

Frame 40
Time 7.952 msec Height 16.92 m

Frame 80
Time 13.677 msec Height 20 m

Figure 4.30 Profiles of flare

There is nothing in the uninterrupted sequence of high-speed photographs of the flare that could be related either to effect of ground shock on the flare or to interaction between pressure impulse and the flare. Vertical displacement of the flare top with time (Fig. 4.31) shows that the velocity of the top decreases without interruption. A similar plot of flare width showed no change in velocity of expansion that could be identified with a pressure feature. If the flare had two components, one from gas before the hole pinched off and the other from cavity gases after pinchoff (if the hole had re-opened), an increase in velocity attributed to the second component could be expected, in flare width if not in flare height. Absence of a change in velocity that could be associated with the impulse in the record of the ported pressure gage could be taken as evidence that the impulse between 6 and 8 msec in that record was due to a cause other than re-opening of the hole to cavity gases.

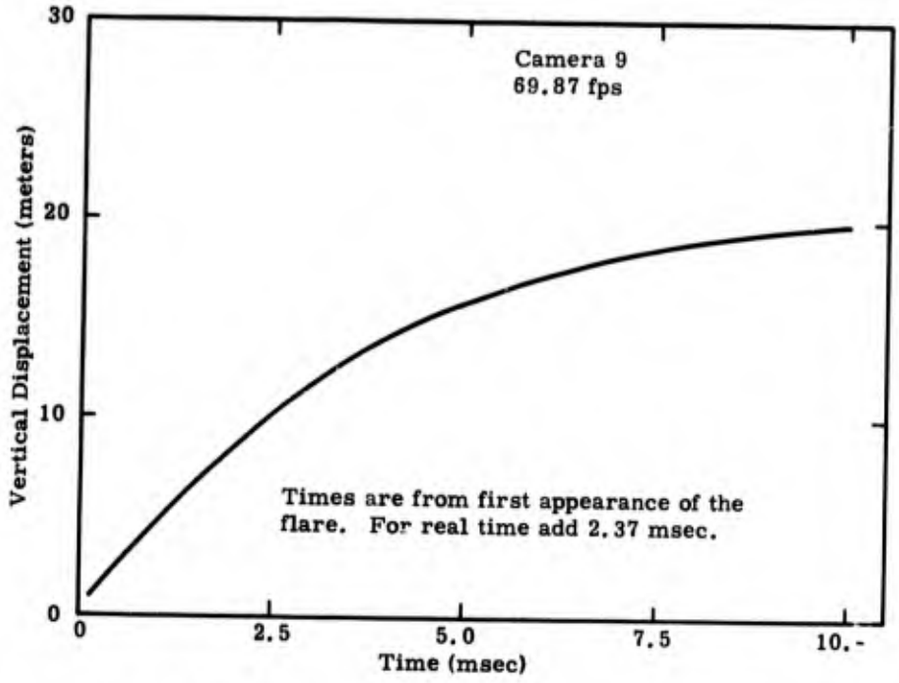

Figure 4.31 Vertical displacement of top of flare versus time

The observation to be made here is that neither photography of the flare nor the ported pressure measurement provided conclusive evidence as to whether the open hole pinched off. Additional evidence from the more distant airblast measurements is presented in Chapter 7.

CHAPTER 5

RESULTS OF THE 6-METER STEMMED EVENT

There were 45 gages installed on the 6-meter stemmed event. An excellent record was obtained from the single Slifer. Records were obtained from all 10 of the stress gages, and only one failed to give a peak stress. Some of the high-sensitivity channels were limited. All of the 12 accelerometers at shot depth and half-shot depth provided records, but one was not credible and 15 of the remaining 23 channels were limited either by band edge or by peak accelerations beyond gage range. Of the 10 surface accelerometers, one was limited by band edge or gage range, and two crystal accelerometers received an electrical pulse at shock arrival time which prevented recording of the pulse in one case and degraded the record in the other.

Records from 6 SLA airblast gages were excellent. Three of the 6 BRL gages gave usable records.

Gage Range and Set Range

Gage ranges for the 6-meter stemmed shot had been selected before going to the field and without benefit of experience with the Ft. Polk medium. In view of the great difference in media at the sites of the two 12-m shots, it was decided to go into the 6-m stemmed shot with the set ranges determined before going to the field. Table 5.1 summarizes the set ranges for low- and high-sensitivity channels and shows the peak values expected. Comparison with Table 3.1 indicates the differences in pre-shot predictions for the 6- and 12-m stemmed shots.

Location of Measurements

Figure 5.1 shows the location of the near-surface and sub-surface stress and acceleration measurements. A single Slifer was located 0.57 m from the vertical axis of the charge.

Slifer Time of Arrival

Figures 5.2 through 5.4 show the plot of frequency versus time, calibration curves of frequency versus cable length, and conversion into radial distance versus time. The Slifer provided an excellent record. The shock velocity in the grout between 4.5 and 5.5 m was about 1.7 m/msec, which, as will be seen, is somewhat greater than the velocity in the medium. In Fig. 5.4 the record beyond 4 msec and about 6 m is not shown because the charge was only 6 m deep. However, in Fig. 5.2 it is seen that just after 4 msec there is a break at about 9.4 m. Since a 12-m Slifer was used for the 6-m shot, there was another 6 m of Slifer above ground. The normal installation is for the Slifer to emerge normal to the ground surface, to curve upward and outward, then downward until some portion is lying on the ground. Although no record was kept of the point of contact with the ground, the break at 9.4 m suggests the contact was there.

TABLE 5.1

Planned Set Ranges Based On Expected Ground Motion and Stresses for 6 MS

6-METER STEMMED

Gage	R Meters	DOB Meters	Expected	Low Sensitivity	High Sensitivity
σ - SY-1	6	3	3 (kb)	2.5 (kb)	1.5 (kb)
σ - SY-2	6	3	3	5.0	2.5
σ - SY-3	6	6	4	3.0	2.0
σ - SY-4	6	6	4	5.0	3.0
σ - SL-5	6	6	4	5.0	3.0
σ - SL-1	12	6	1	0.5	0.1
σ - SL-2	12	6	1	1.0	0.5
σ - SY-5	12	6	1	1.0	0.5
σ - SL-3	24	6	0.1	0.15	0.05
σ - SL-4	24	6	0.35	0.5	0.15
a_h	12	6	1500 (g)	1500 (g)	500 (g)
a_h	12	6	1500	5000	1500
a_h	24	6	200	200	70
a_h	24	6	200	1000	200
a_h	24	6	200	200	70
a_v	24	6	200	200	70
a_t					
a_h	36	6	50	60	20
a_h	36	6	50	150	60
a_h	36	6	50	150	20
a_v	36	6	50	150	20
a_t					
a_r	5	3	20000	20000	5000
a_r	5	3	20000	40000	20000
a_v	2/3	2/3	40000	40000	10000
a_v	2/3	2/3	40000	100000	40000
a_v	9	2/3	20000	60000	6000
a_h	9	2/3	10000	15000	6000
a_v	12	2/3	10000	30000	3000
a_h	12	2/3	5000	15000	1500
a_v	18	2/3	7500	20000	1500
a_h	18	2/3	7500	20000	1500
a_v	24	2/3	5000	15000	1500
a_h	24	2/3	2500	7500	750

Slifer 1 channel
Sandia airblast 6 channels
BRL airblast 6 channels
Gages between lines were in a single hole.

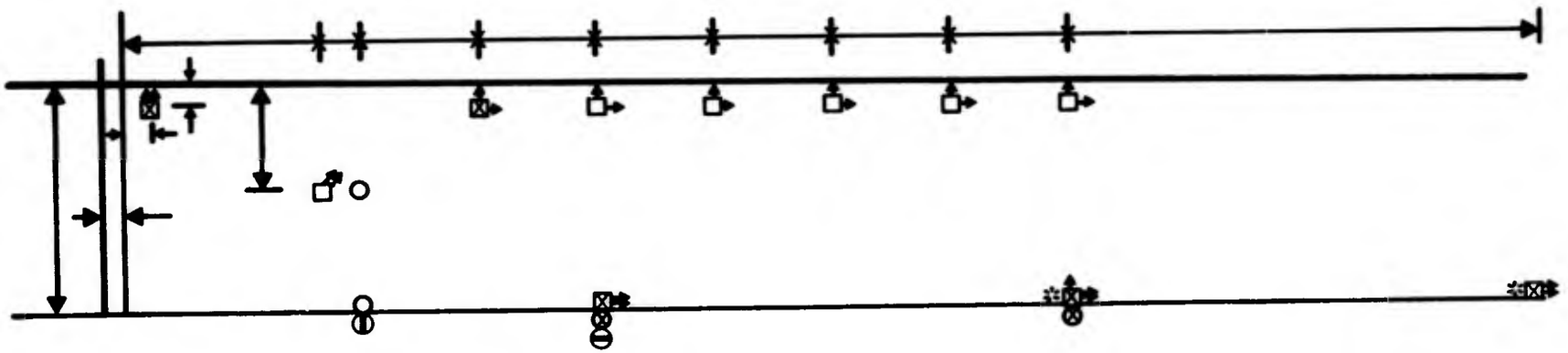

⊖ Ytterbium stress measurement (1 gage)
○ Ytterbium stress measurement (2 gages)
◐ Lithium niobate stress measurement (1 gage)
⊗ Lithium niobate stress measurement (2 gages)
Vertical acceleration measurement
Radial acceleration measurement
Horizontal acceleration measurement
Horizontal tangential acceleration measurement

} Double arrows indicate two gages

Figure 5.1 Location of stress and acceleration measurements for the 6-meter stemmed event

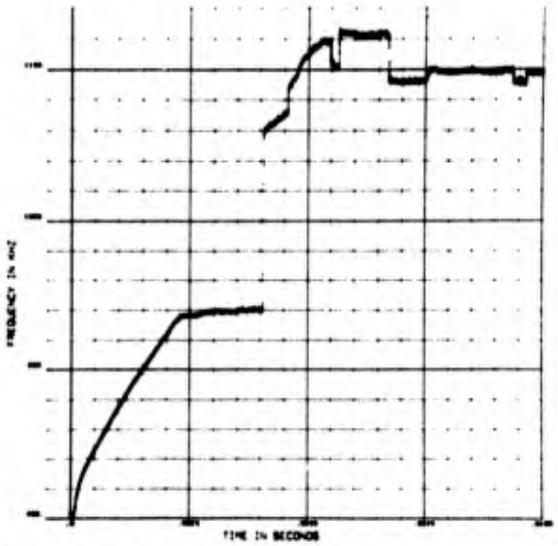

Figure 5.2 Frequency versus time for Slifer time-of-arrival measurement

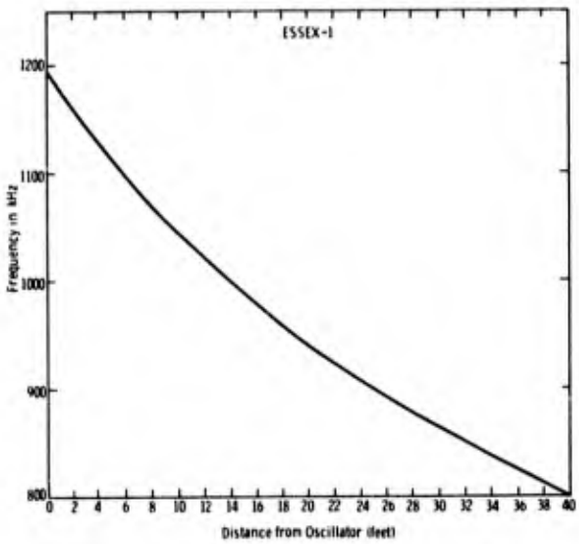

Figure 5.3 Slifer time of arrival calibration curve

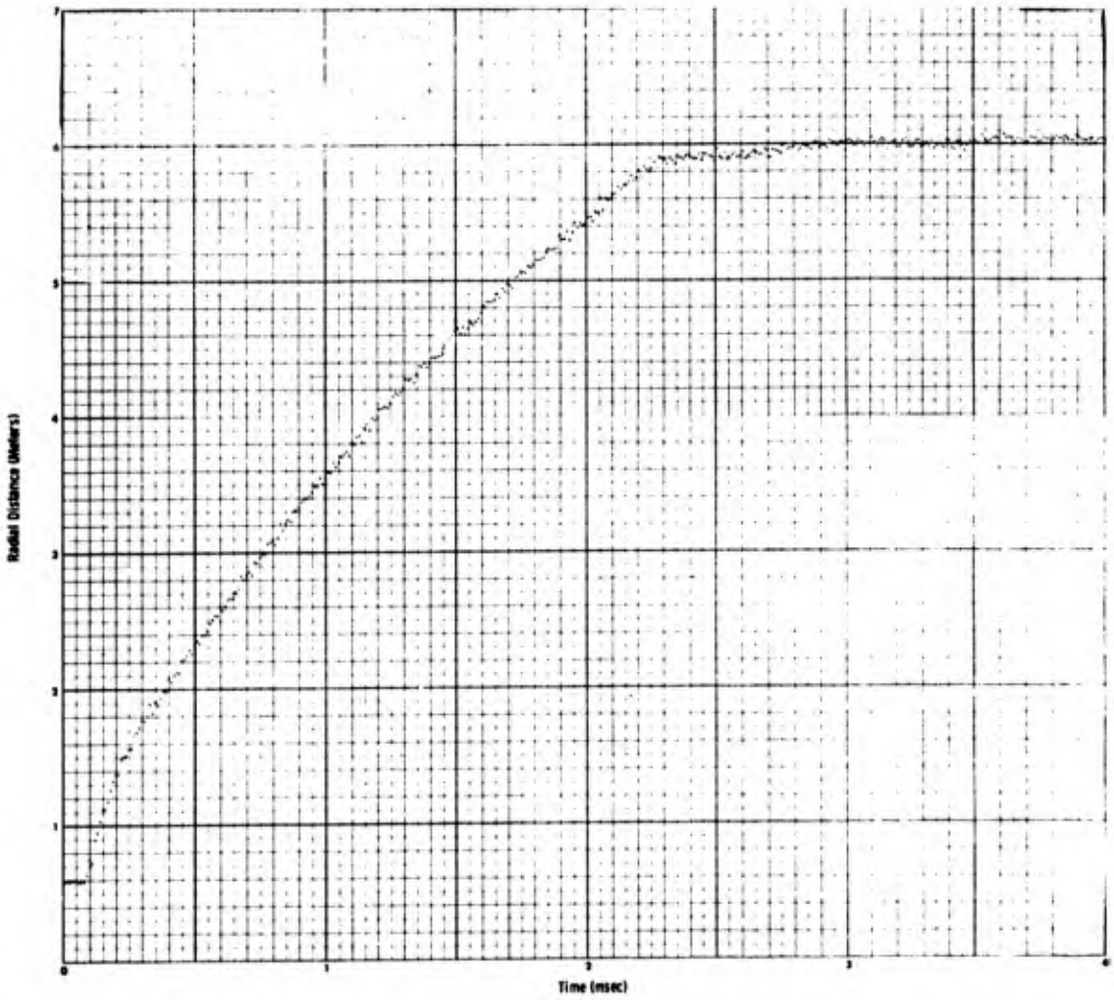

Figure 5.4 Time-of-arrival versus distance from Slifer measurement

Arrival Times at All Instrument Stations

Arrival time as measured by the Slifer is compared in Fig. 5.5 with arrival times at other instrument stations. Sonic velocities determined from stress measurements were 1.53 m/msec between 6 and 12 m and 1.57 m/msec between 12 and 24 m. Those determined from acceleration measurements were 1.63 m/msec between 12 and 24 m and 1.66 m/msec between 24 and 36 m. Since the break-away of the stress signal is more gradual than that of acceleration, it is probable that true arrival time is earlier than that read from the record.

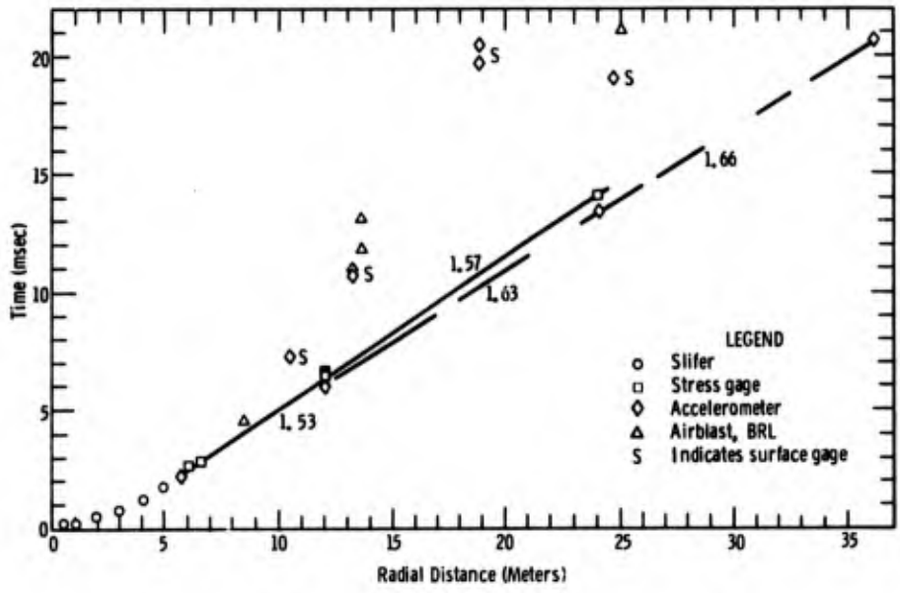

Figure 5.5 Summary plot of arrival time versus distance at all stations

Stress Measurements

Records obtained from stress measurements on the 6-m stemmed shot are reproduced in Appendix I and the principal parameters are summarized in Table 5.2. Layout and gages were the same as for the 12-m stemmed shot except that vertical dimensions were halved, a fifth ytterbium was added at the 12-m station, and a fifth lithium-niobate gage was added at the 6-m station at shot depth. Three gages at each of those locations provided an additional opportunity for comparing measurements made by the two different types of gages.

Of the 10 stress gages installed (20 records), only the lithium-niobate gage at 6 m failed to provide useful information (Fig. I-3). The two gages at the half-shot depth station failed at about 4 and 4.7 msec (Fig. I-1). The high-sensitivity channel of SY-1 had its peak limited by band edge. The low-sensitivity channel showed a peak of 2.41 kilobars, compared with 2.35 kilobars measured by the other gage (SY-2).

At the 6-m station at shot depth the record from SY-3 had a peak about 10 percent smaller than that of SY-4 at the same location (Fig. I-2).

A

TABLE 5.2

Summary of Stress Me
ESSEX I 6 MS 3 Oc
21,594 Pounds Nitromethane Buried 6

Gage Type		Distance (m)	Depth (m)	Gage Range	Gage Sensitivity	Ca St
Ytterbium	SY-1	6	3	Low Low	High Low	
	SY-2	6	3	High High	High Low	
	SY-3	6	6	Low Low	High Low	
	SY-4	6	6	High High	High Low	
	SY-5	12	6	High High	High Low	
Lithium Niobate	SL-1	12	6	Low Low	High Low	
	SL-2	12	6	High High	High Low	
	SL-3	24	6	Low Low	High Low	
	SL-4	24	6	High High	High Low	
	SL-5	6	6	High High	High Low	

* Reading accuracy for time is ± 0.01 millisecond.
(a) Limited
(b) Possibly Limited
(c) Time of peak not well defined. Limited.
(d) Direct Signal. Limited
(e) Refracted Signal
(f) Limited. Gage failed at 3.07 msec.

B

TABLE 5.2

mary of Stress Measurements
SSEX I 6 MS 3 October 1973
romethane Buried 6 Meters Deep, Fully Stemmed

ge tivity	Calibration Step (kbar)	Arrival Time* (msec)	Peak Stress (kbar)	Time of Peak* (msec)	Remarks
gh	1.5	2.82	2.11	3.09	(a)
w	1.5	2.82	2.41	3.12	(b)
gh	2.5	2.82	2.36	3.20	
w	2.5	2.81	2.35	3.22	
gh	2.0	2.49	2.54	2.81	
w	2.0	2.49	2.52	2.82	
gh	3.0	2.51	2.79	2.85	
w	3.0	2.52	2.79	2.79	
gh	0.5	6.44	0.84		(c)
w	0.5	6.45	1.02-1.25	7.90	
gh	0.1	6.38			(a)
w	0.1	6.37	0.40 ± 0.009	7.89	
gh	0.5	6.62	0.44 ± 0.05	7.91	
w	0.5	6.60	0.44 ± 0.05	7.90	
gh	0.05	13.98	0.097 ± 0.005	14.49	(d)
		(22.9)	(0.048, 0.047, 0.057)	(23.3, 25.3, 27.3)	(e)
w	0.05	14.07	0.118 ± 0.01	14.48	
gh	0.15	13.94	0.090 ± 0.011	14.49	
w	0.15	14.27	0.095 ± 0.023	14.48	
gh	2.00	2.66			(f)
w	2.00	2.65			(f)

At the 12-m station at shot depth the high-sensitivity channel of SL-1 was limited by band edge (Fig. I-5), and the low-sensitivity channel gave a peak 15 to 20% below the peak from SL-2 (Fig. I-6). Those two gages gave peaks only one-half or less of those recorded by the ytterbium gage (SY-5) at the same location (Fig. I-4). Closer examination of the time expansion of the record in that figure shows the peak stress to consist of a spike about 1.25 times the amplitude of the surrounding signal, and with a duration of only 50 microseconds. In the vicinity of the spike and again around 10 msec the record contains what appears to be ringing. This is attributed to an impedance mismatch between the grout in the instrument hole and the medium rather than to the gage, because similar fluctuations appear on the traces from the lithium-niobate gages at about the same time.

The records from the 24-m station (Figs. I-7 and I-8) show an initial spike at about 14.5 msec followed by a pronounced pulse between about 23 and 28 msec. Presumably this is a reflection or refraction from a harder layer below the shot. The pulse has three distinct spikes. If the medium has an average velocity of 1.55 m/msec (from Fig. 5.5) the sources of the spikes would be at depths of 20.6, 22.5, and 24.4 m below surface zero. The three spikes appear at the 12-m station (Figs. I-4 and I-5) and, on the same assumption noted above, indicate returns from 17.8, 19.7, and 22.3 meters. There the first of the three spikes follows the direct spike by about 8.1 msec. Comparison of Figs. I-4 and I-7 shows a much larger interval between the direct and indirect signals at the 24-m station. Since the interval between the direct and the first indirect spikes is different by only 0.75 msec, it will be noted that the larger interval is achieved at the expense of the duration of the direct pulse. At 12 m the direct pulse duration is about 5 msec, whereas at 24 m it is reduced to only about 1.5 msec. This shortening of the duration is attributed to cut-off from the rarefaction wave returning from the surface. If one uses the 1.55 m/msec average velocity cited above, the time interval between shock arrival and cut-off is 2.9 msec for the 6-3 station, 4.8 for the 6-6 station, 3.2 for the 12-6 station, and 1.9 for the 24-6 station. Average velocities to the surface and back are less than the 1.55 m/sec determined at shot depth, so actual intervals are somewhat larger.

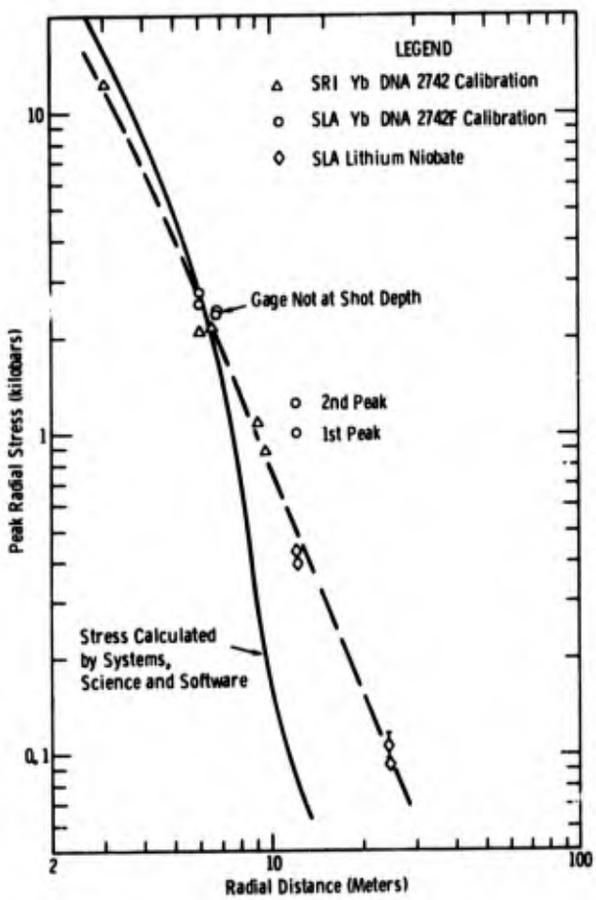

Figure 5.6 Comparison of measured and calculated stress

In Fig. 5.6 the peak radial stresses have been plotted versus radial distance for both the SL measurements and those made by SRI.

A dashed line has been drawn through the data to indicate the trend. Peak values from the

ytterbium gage at 12 m (SY-5) are discounted, not so much because they do not agree with the lithium-niobate gage peaks at the same location, but because they are not in agreement with the trend. The reason for the difference has not been determined.

The solid line in the figure represents the results of calculations done by Systems, Science, and Software.[22] Calculated and measured stresses are in quite good agreement at 2 kbars and above. Below 2 kbars the calculated values are below measured stresses, and the difference increases so that at the end of the calculated stress they are only 1/7 of the measured values.

Free-Field Ground Motion

Results of free-field ground-motion measurements made with accelerometers at shot depth and half-shot depth are summarized in Table 5.3. Records of the measurements, together with velocity-time plots from first, and displacement-time plots from second integrations are shown in Appendix J.

At the half-shot-depth station (5-3) the signal arrived at 2.23 msec and had a duration of only 0.17 msec (Figs. J-1 and J-2). On the high-sensitivity channel of the high-range gage (Fig. J-2), the signal appears to have been clipped for a reason that is not clear. On all other channels the peaks were limited by band edge. The low-sensitivity channel of the high-range gage shows a peak limited at 167,000 g. Only a 50,000-g gage was installed, so this value is not credible. If it is, peak velocity was greater then 175 m/sec. This would indicate a stress of 5 kilobars where only 2.4 was measured. The rarefaction signal from the surface arrives at the station at 4.83 msec, after which a measure of radial motion with a single orientation becomes meaningless. The very short duration suggests that the gage may not have responded to the entire ground-motion pulse.

At the closest shot-depth station (12 m), both channels of the low-range gage were limited by band edge (Fig. J-3). The low-sensitivity channel was limited at 9700 g, well above the gage range of 5000 g. The pulse appears to have a duration of only about 2 msec, with no excursion below band edge during that interval. This is in contrast to the high-range gage (Fig. J-4) where the record shows a duration of about 2.5 msec, but with several intervening excursions into negative acceleration. Considering the low-sensitivity channel, the acceleration-time record appears credible, but the integral gives some reason for doubt. The cable to the gage failed at 19 msec. The station was probably still in motion at that time and the record may be entirely valid. The slope of the velocity-time plot is quite linear and is suggestive of a baseline shift of 150 to 160 g. In view of baseline shifts encountered on other channels (see Chapters 3 and 4 and Appendix R), such a shift would not be surprising. If indeed there was a shift, it was about 0.9 percent of band width, which is in the range of or possibly a bit higher than the shifts encountered on other channels.

As in the case of the two shots discussed previously, horizontal radial, vertical, and horizontal tangential components were measured at the 24-m station at shot depth. The low-range radial gage had records limited by band edge on both sensitivities (Figs. J-5 and J-6). The peak

A

TABLE 5.3

Summary of Acceleration Measurements at
ESSEX I 6 MS 3 0
21,594 Pounds Nitromethane Buried 6

Accelerometer Designation	Accelerometer Orientation	Distance (m)	Depth (m)	Gage Range	Gage Limit (g's)	Gage Sensitivity	Calibrati Step (g'
5-3 AR-LO	Radial	5	3	Low Low	30,000 30,000	High Low	15,17 15,17
5-3 AR-HI	Radial	5	3	High High	50,000 50,000	High Low	40,09 40,09
12-6 AH-LO	Horizontal	12	6	Low Low	5,000 5,000	High Low	3,04 3,04
12-6 AH-HI	Horizontal	12	6	High High	10,000 10,000	High Low	4,96 4,96
24-6 AH-LO	Horizontal	24	6	Low Low	200 200	High Low	19 19
24-6 AH-HI	Horizontal	24	6	High High	1,000 1,000	High Low	1,00 1,00
24-6 AV	Vertical	24	6		200 200	High Low	20 20
24-6 AT	Tangential (Horizontal)	24	6		200 200	High Low	20 20
36-6 AH-LO	Horizontal	36	6	Low Low	200 200	High Low	1 1
36-6 AH-HI	Horizontal	36	6	High High	200 200	High Low	1 1
36-6 AV	Vertical	36	6		200 200	High Low	2 2
36-6 AT	Tangential (Horizontal)	36	6		200 200	High Low	

(a) See comment in text.

TABLE 5.3

ration Measurements at Shot Depth and Half Shot Depth
ESSEX I 6 MS 3 October 1973
Nitromethane Buried 6 Meters Deep, Fully Stemmed

Gage sitivity	Calibration Step (g's)	Arrival Time* (msec)	Peak Acceleration (g's)	Time of Peak (msec)	Peak Velocity (m/sec)	Time of Peak* (msec)
High	15,179	2.23	>30,000 (L)			
Low	15,179	2.18	>37,400 (L)	2.34	>42.5	2.85
High	40,096	2.23				
Low	40,096	2.23	167,000 (L?)(a)		>176	2.85
High	3,040	6.04	(L)			
Low	3,040	6.02	(L)			
High	4,966	6.04	8,710	6.10	27.5	19
Low	4,966	6.03	11,850	6.09	30.1	19
High	195	13.40	>300 (L)	13.73	>2	14.57
Low	195	13.33	291 (L)	13.71	1.96 (L)	14.57
High	1,000	13.37	365	13.59	2.17	14.54
Low	1,000	13.17	320	13.62	2.05	14.5?
High	204	13.43	>300 (L)		>3.3 (L)	15.30
Low	204	13.39	302 (L)	13.81-14.52	3.36	15.30
High	202	13.54	273	13.74	0.674	14.42
Low	202	13.54	267	13.74	0.666	14.42
High	149	20.71	312 (L)	21.12	0.715 (L)	21.29
Low	149	20.47	508 (L)	21.20	1.00 (L)	21.29
High	196	20.66	288 (L)	21.21	0.738 (L)	21.36
Low	196	20.74	289 (L)	21.21	0.746 (L)	21.34
High	200	20.74	304 (L)	21.37	1.10 (L)	21.62
Low	200	20.76	292 (L)	21.35	1.10 (L)	21.62
High	60.8	20.46	45	21.12	0.48	21.19
Low	60.8	20.41	46	21.10	0.59	21.17

velocity of 4 m/sec at about 27.5 msec from the low-sensitivity channel is not appreciably different from the one at the same time from the high-sensitivity channel of the high-range gage, which was not limited (Fig. J-7). An initial peak velocity of about 2.1 m/sec was recorded at 14.6 msec, followed by 8 msec of relatively constant (about 0.6 m/sec) velocity before arrival of the reflected and/or surface signals. A long-time integration of the record (Fig. J-21) indicates that the horizontal motion stopped at about 2.0 sec with a residual displacement of about 2.6 m.

The vertical gage at the 24-m station gave records that were limited by both gage range and band edge on both sensitivities (Figs. J-9 and J-10). If the second peak was limited at all, the limiting appears to have been small. If the rising and falling portions of the first pulse are extrapolated above the point of limiting to an intersection, a peak of about 700 g is indicated. This approximation suggests that the first peak velocity may be low by as much as 1.75 m/sec. Analysis of the long-time integration of the low-sensitivity channel (see Appendix R) suggests that the limiting of the gage by so much may have introduced a hysteresis that precludes using the long-time integration (shown in Fig. J-21) to adjust the peak velocity. It seems clear, however, that the peak vertical velocity in the first pulse is about 2.5 times the corresponding radial peak. The result of an adjustment not using the long-time integration is shown in Fig. J-24.

Both sensitivities of the tangential record were within band edge (Figs. J-11 and J-12). The initial peak velocity was 0.67 m/sec, only one-third the corresponding radial peak. The long-time integration (Fig. J-22) shows that a later peak of 1.45 m/sec occurs at about 0.30 sec; and that there is some oscillation before the ground comes to rest at about 2 sec with a residual clockwise rotation of about 100 cm.

In Fig. 5.7 the vector sum of velocity has been plotted versus time. In this plot, 1.75 m/sec has been added to the peak vertical velocity during the interval over which the acceleration peak was limited. Peak vector sum velocity was 5.2 m/sec for the first peak, most of the contribution coming from the vertical velocity rather than the radial.

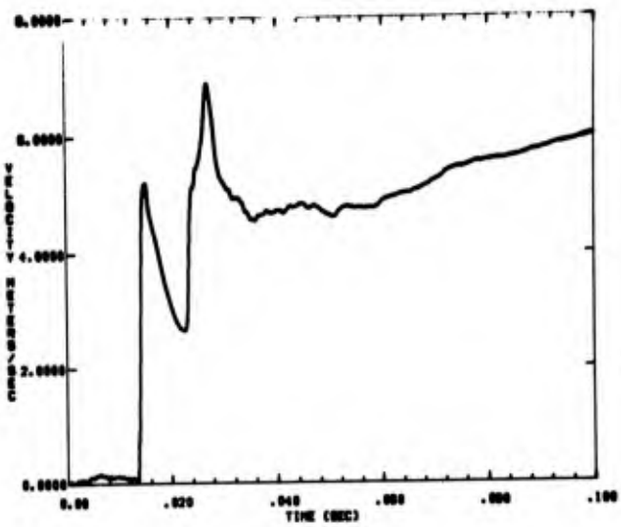

Figure 5.7 Vector sum of radial, vertical, and tangential components of velocity as a function of time at the 24-meter station

At the 36-m station, the first peak acceleration was limited by band edge on all four channels of the two radial gages (Figs. J-13 through J-16). The low-sensitivity channel of the low-range gage (Fig. J-14) appears to have been less affected by limiting than the others, giving a peak velocity of just over 1 m/sec for the first pulse. The long-time integration of the low-sensitivity channel of the high-range gage (Fig. J-22) shows a peak outward displacement of about 12 cm at about 0.3 sec, recovery of nearly all of that amount by 0.7 sec, a second outward excursion peaking at less than 5 cm at about 1.5 sec, then a residual outward displacement of about 2 cm before 3 sec.

The vertical gage at 36 m shows a record (Figs. J-17 and J-18) where the first peak acceleration could have been limited by either band edge, gage range, or both. If there was limiting, it is sufficiently small that the error in peak velocity can be disregarded. Thus, peak velocity in the first pulse was at least 1.1 m/sec. The long-time integration (Fig. J-23) shows that the peak upward displacement was nearly the same (12 cm) as the outward peak, and that it occurred slightly earlier. Extraneous noise on this channel after 1 sec made a full 3-sec integration impossible.

Figure J-17 shows a high-frequency oscillation during the negative phase of the first acceleration pulse. This same characteristic is to be observed on other records (e.g., on 12 MS: 36-12 AV; on 6 MU: 36-6 AH-LO, and possibly on 36-6 AV). Shunk[23] has observed a similar characteristic from Endevco accelerometers on other tests. Since the element to which the strain gage is bonded is prestressed to permit sensing of negative accelerations, an inadequacy in the prestressing which permits the element to chatter may be the cause.

Figures J-19 and J-20 show the high- and low-sensitivity records from the tangential gage. All peaks are within band edge and gage range, and peak velocities were quite small. The first peak was less than 0.05 m/sec clockwise, with an abrupt reversal to 0.15 m/sec counterclockwise. The signal was so small that no reasonable long-time integration could be done.

Figure 5.8 shows the vector sum of velocity at the 36-m station. In Fig. 5.9 the peak radial velocity and the vector sum peak for the 24- and 36-m stations are compared with the preshot S[3] calculated values.[22] The comparison is vague because calculated values were not extended as far as 24 m.

In Fig. 5.10 the vector sum of particle velocity as well as the measured radial particle velocity has been used, together with measured shock velocity (Fig. 5.5) and a density of 1.76 gm/cc for Unit 4, to derive a peak stress that is compared with measured peak stresses. It is worth noting that closer than 15 to 20 m the stress derived from peak

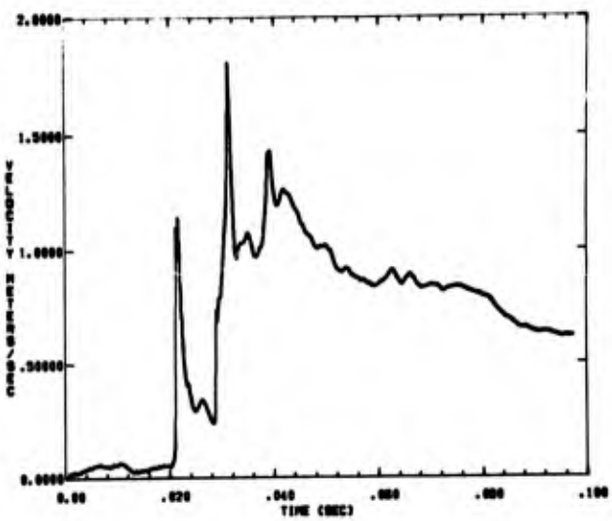

Figure 5.8 Vector sum of radial, vertical, and tangential components of velocity as a function of time at the 24-meter station

radial velocity is greater than that measured directly with the stress gages, while beyond those distances the reverse is true. The spread between the stress from radial velocity and from the vector sum is less at 36 m than at 24 m. This is because the sharp spike of the peak horizontal velocity has a very short duration and occurs during the rise of the vertical peak. The tangential component contributes little to the vector sum.

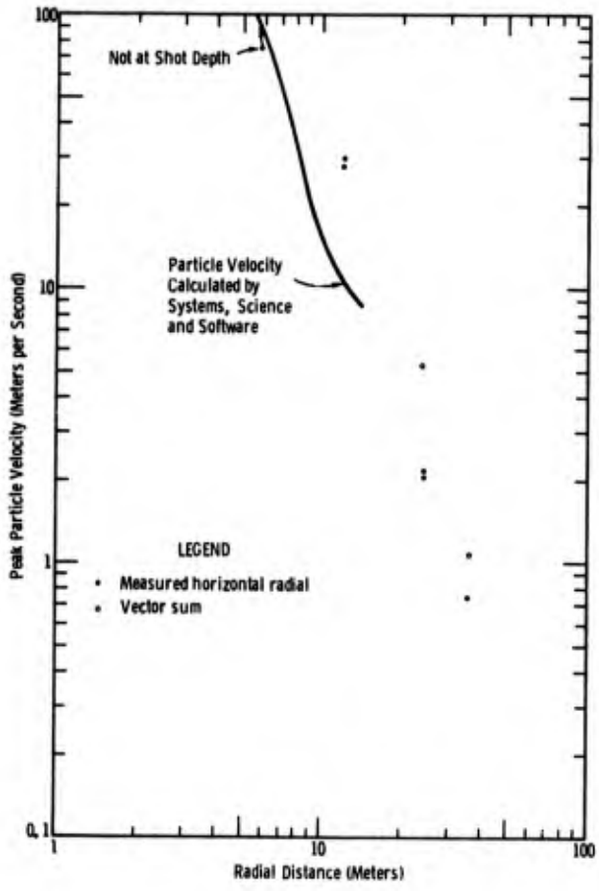

Figure 5.9 Peak particle velocities measured compared with those calculated

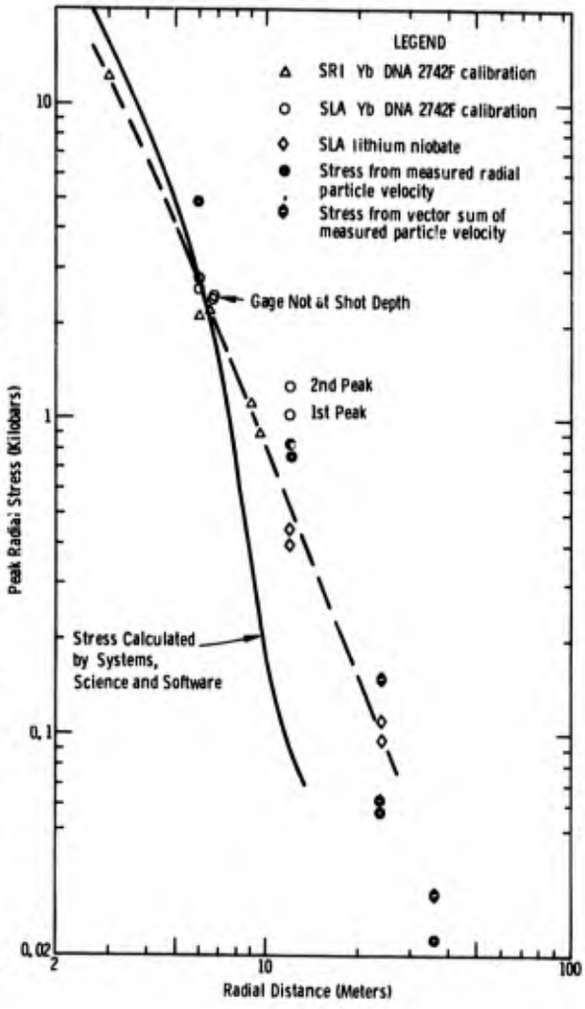

Figure 5.10 Comparison of measured stress and stress derived from particle velocity

Surface-Motion Instrumentation

The results of surface-motion measurements are summarized in Table 5.4. Records of the measurements and their first and second integrations appear in Appendix K.

Two vertical accelerometers were installed in the near-surface-zero canister. The low-range gage had a range of 50,000 g and the high-range crystal gage a range of 100,000 g. The high-sensitivity channel of the low-range gage was limited by band edge at around 40,000 g (Fig. K-1). The apparently

A

TABLE 5.4

Summary of Surface Accelerati
ESSEX I 6 MS 3 Octo
21,594 Pounds Nitromethane Buried 6 f

Accelerometer Designation	Accelerometer Orientation	Distance (m)	Depth (m)	Slant Distance** (m)	Gage Range	Gage Limit (g's)	Gage Sensitivity	Co St
0-0 AV-LO	Vertical	2/3	2/3	5.33	Low Low	50,000 50,000	High Low	
0-0 AV-HI	Vertical	2/3	2/3	5.33	High High	100,000 crystal 100,000 crystal	High Low	
9-0 AV	Vertical	9	2/3	10.43		100,000 crystal 100,000 crystal	High Low	
9-0 AH	Horizontal	9	2/3	10.43		20,000 20,000	High Low	
12-0 AV	Vertical	12	2/3	13.09		50,000 50,000	High Low	
12-0 AH	Horizontal	12	2/3	13.09		20,000 20,000	High Low	
18-0 AV	Vertical	18	2/3	18.71		30,000 30,000	High Low	
18-0 AH	Horizontal	18	2/3	18.71		20,000 20,000	High Low	
24-0 AV	Vertical	24	2/3	24.51		20,000 20,000	High Low	
24-0 AH	Horizontal	24	2/3	24.51		10,000 10,000	High Low	

**Corrected for surface elevation.

B

TABLE 5.4

of Surface Acceleration Measurements
ESSEX I 6 MS 3 October 1973
itromethane Buried 6 Meters Deep, Fully Stemmed

e)	Gage Sensitivity	Calibration Step (g's)	Arrival Time (msec)	Peak Acceleration (g's)	Time of Peak (msec)	Peak Velocity (m/sec)	Time of Peak (msec)
	High	19,915	1.55	40,000 (L)			
	Low	19,915	1.58	160,000 (L)	1.65	188 (L)	1.84
	High	80,000	1.56				
	Low	80,000	1.46				
	High	6,000	1.56				
	Low	6,000	1.54				
	High	1,493	6.79	1,847.0	9.77		
	Low	1,493	6.67	1,460.0	9.77		
	High	982	10.59	945.0	11.41		
	Low	982	10.77	1,275.0	11.40		
	High	698	10.93	763.0	11.43		
	Low	698	10.90	975.0	11.21		
	High	508	19.8	225.0	24.54		
	Low	508	20.0	285.0	24.55		
	High	498	20.5	188.0	21.88		
	Low	498	20.0	180.0	21.97		
	High	506	19.11	52.4	36.27	6	75.00
	Low	506	19.11	52.6	36.43		
	High	250	?	21.0	36.38,37.26		
	Low	250	?	?	?		

useful information from 1.5 to 3.5 msec has been expanded (Fig. K-4) to show that the first peak was limited, that the initial velocities were in excess of 60 m/sec, and that displacement in that interval was more than 8 cm. After 3.5 msec the record is useless. The low-sensitivity channel had a first peak limited by band edge at around 160,000 g, which was well beyond gage range (Fig. K-2). In addition to being limited, the record after 3.5 msec shows some characteristics that are unusual in an acceleration record, and hence are considered spurious. The crystal accelerometer failed at about 1.5 msec, which was the approximate time of shock arrival, although there may have been a recovery after 10 msec (Fig. K-3).

A single vertical crystal accelerometer at the 9-m surface station shows an abrupt negative excursion to band edge at 1.5 msec, the time the near-surface-zero crystal gage failed (Figs. K-5 and K-6). Apparently there was electrical communication between the two gages through signal-conditioning equipment. After remaining at negative band edge until about 4 msec, the channel embarked on an erratic baseline course. The true arrival of the shock wave can be seen superimposed on the erratic baseline at about 6.5 msec, continuing until about 10 msec when there is another wild negative excursion. An effort was made to linearize the erratic baseline between 6 and 10 msec to recover a signal that could be integrated. The effort was unsuccessful, in part because it was not possible to accurately estimate the baseline in a rapidly fluctuating signal.

The record from the horizontal gage at 9 m (Figs. K-7 and K-8) also shows that the gage picked up induced noise at about 1.5 msec. The noise added nothing to the integral and permitted recording of a good signal from about 6.5 msec to cable failure at around 450 msec. Discounting probable canister rotation, the gage reached a velocity of 400 m/sec and a displacement of 100 m at the time of cable failure (Fig. K-21).

At the 12-m station a vertical and a horizontal accelerometer were installed. All four channels (Figs. K-9 through K-12) picked up the induced noise at about 1.5 msec. The noise was removed by the smoothing to which the horizontal low-sensitivity channel was subjected (Fig. K-12).

Three-second double integrations of the vertical and horizontal accelerations (Fig. K-22) would ordinarily permit definition of a canister trajectory. However, in this case the vertical acceleration record shows a very large baseline shift at shock arrival, the magnitude of which could not be evaluated. Had it been possible to evaluate the shift its effect could have been removed. Since it could not, the displacement resulting from the double integration was incredible. Displacement from the double integration of the horizontal gage record is not credible. The horizontal displacement to 3 sec is about twice the length of cable to the gage, and the cable would have broken if the trajectory had had any appreciable vertical component.

When first considered, both sensitivities of the vertical and horizontal accelerometers at the 18-m station appear to have given good records (Figs. K-13 through K-16). If both records are correct, the unadjusted trajectory from long-time integrations (Fig. K-23) is as shown by the circles

in Fig. 5.11. The baseline shift on the record from the vertical gage at about 1.4 sec makes it undesirable to carry the trajectory beyond that time.

The unadjusted trajectory gives several reasons to suspect the record from the vertical gage. First, the trajectory reaches apogee at 0.8 sec. The initial angle on this shot was 46 degrees and the velocity 21.5 m/sec. Initial angles of the two 12-m canisters on the first two shots and the 18-m canister on 6 MU were close to 24 degrees; thus the angle of the trajectory of this shot appears odd. The angle would appear too small if the canister were already tilted appreciably by the time the initial angle was determined. This was about 0.3 sec on all shots, when velocity had reached an approximate peak. The unadjusted trajectory appears headed for impact at about 1.6 sec and about 22 m away, too early and too close to be consistent with the initial angle and velocity.

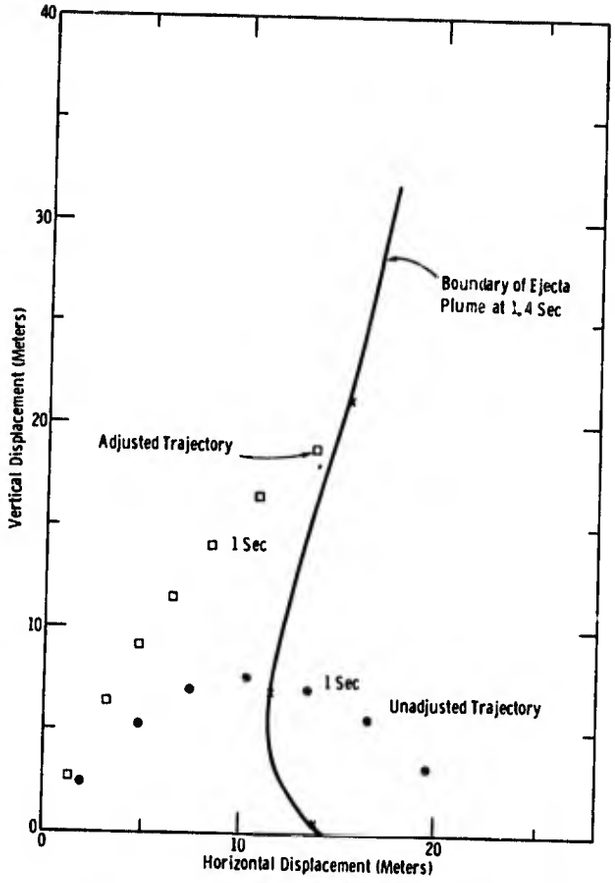

Figure 5.11 Canister trajectory for the 18-meter surface station

The other observation is that vertical velocity is zero either at apogee in its original orientation or in another orientation in which the vertical gage axis is exactly perpendicular to the actual trajectory. Since, in this case, vertical velocity is zero at 0.8 sec and negative thereafter, a valid vertical record is consistent only with counterclockwise rotation of the canister such that at 0.8 sec the vertical axis is normal to its trajectory. This hypothesis can be tested by adjusting the record with assumptions somewhat different from those used on the preceding two shots. There, it was assumed that the canister rotated clockwise, and that its tilt equalled the change in angle of the ballistic trajectory. The adjusted trajectory in each of those cases was not grossly different from a ballistic trajectory. Using this observation, a ballistic trajectory is assumed with the measured initial velocity of 21.5 m/sec but with the initial angle of 24 degrees observed on the other shots. At 0.8 sec the slope of the ballistic trajectory would have been 36.4 degrees, and for vertical velocity to have been zero, the nominally vertical axis of the gage would have had to rotate counterclockwise to 53.6 degrees at that time. The trajectory thus derived had an angle of 36.6 degrees at 0.8 sec and yielded the adjusted trajectory shown by the squares in Fig. 5.11. Also shown in the figure is the profile of the ejecta plume at 1.4 sec. Thus, the adjusted trajectory is consistent with the information obtained from high-speed photography. The purpose of what may appear to be a boot-strap procedure in obtaining an adjusted trajectory is this--that an adjustment can be made that is qualitatively correct, quantitatively approximately accurate, and is consistent with the

measurement made. Thus, the record of the vertical gage which at first appeared inaccurate can be shown to be a measurement of the environment the canister experienced.

Very good records were also obtained from the two gages at the 24-m station (Figs. K-17 through K-20). Again, canister trajectory has been determined from the long-time integrations (Figs. K-24 and K-25). The trajectory shown in Fig. 5.12 was determined from the high-sensitivity channels in each case. As in the case of the 12 MPS event where the station was within the eventual apparent crater radius, the trajectory indicates that upon downward impact of the upthrust region there was insufficient support from underlying soil and the upthrust material continued without interruption downward and into the crater. Here also, canister rotation cannot be estimated readily, and probably distorts the trajectory below the original ground level. There is one distinct difference between the trajectory of Fig. 5.12 and that of Fig. 4.23 for the 12 MPS event. In the latter, the descending portion of the trajectory was to the right of the ascending portion, whereas in Fig. 5.12 it lies to the left. This could be correct or could result from subtle baseline shifts in the horizontal acceleration record.

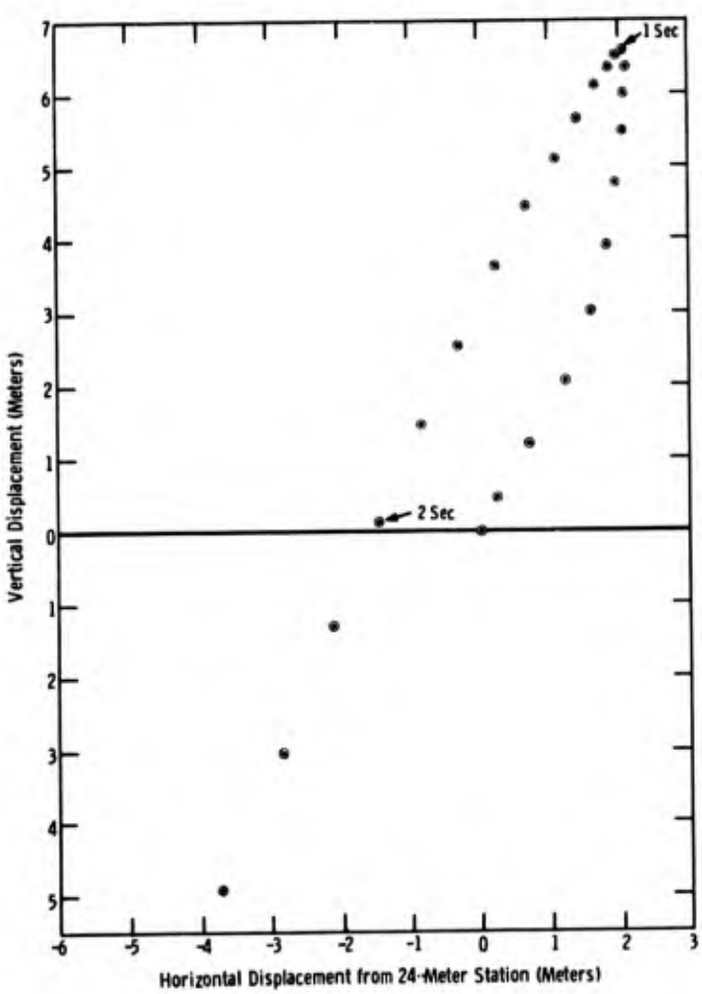

Figure 5.12 Canister trajectory for the 24-meter surface station

Surface Displacement from Photography

Table 5.5 summarizes the cameras used to record the surface motion from the 6-m stemmed shot. Figure 5.13 is a plan view of the camera station and reference markers with respect to SGZ.

TABLE 5.5

Summary of Camera Coverage 6 MS

Camera	Timing (cps)	Camera Speed (fps)	Lens	Film	Field of View				f Stop
					Height		Width		
					Feet	Metres	Feet	Metres	
1) Fastax 16 mm	1000	4000	15 in	2479	13.2	4.02	17.6	5.36	5.6
2) Fastax 16 mm	1000	4000	10 in	2479	19.8	6.04	26.4	8.05	4.5
3) Hycam 16 mm	1000	6000	10 in	2479	19.8	6.04	26.4	8.05	5.6
4) Fastax 16 mm	1000	10000	6 in	2479	16.5	5.03	44.	13.41	2.7
5) Fairchild 16 mm	1000	1000	3 in	2496	66.	20.12	88.	26.82	4.
6) Fastax 16 mm	1000	1000	3 in	2496	66.	20.12	88.	26.82	4.
7) Fastax 16 mm	1000	4000	2 in	EF	99.	30.18	132.	40.23	2.8
8) Milliken 16 mm	100	500	1 in	EF	198.	60.35	264.	80.47	5.6
9) Milliken 16 mm	100	128	10 mm	EF	495.	150.9	660.	201.2	8.
10) Milliken 16 mm	100	500	1 in	EF	600.	182.9	800.	243.8	6.3
11) Milliken 16 mm	100	128	15 mm	EF	1200.	365.8	1600.	487.7	11.

In Chapters 3 and 4 comparisons were made between the vertical displacement-time obtained from double integration of acceleration records with that obtained photographically. The previous section described the loss of vertical-acceleration records at the near-surface-zero station and the 9-m station and the large baseline shift in the vertical-acceleration record from the 12-m station which made long time-integrations useless. Displacements obtained from photographs at those stations are shown in Figs. 5.14 through 5.16. Only at the 18-m station was a record obtained that could be compared with displacements obtained photographically. The comparison is shown in Fig. 5.16. There was no evidence that the grout plug moved ahead of the surrounding ground surface as was observed on 12 MS.

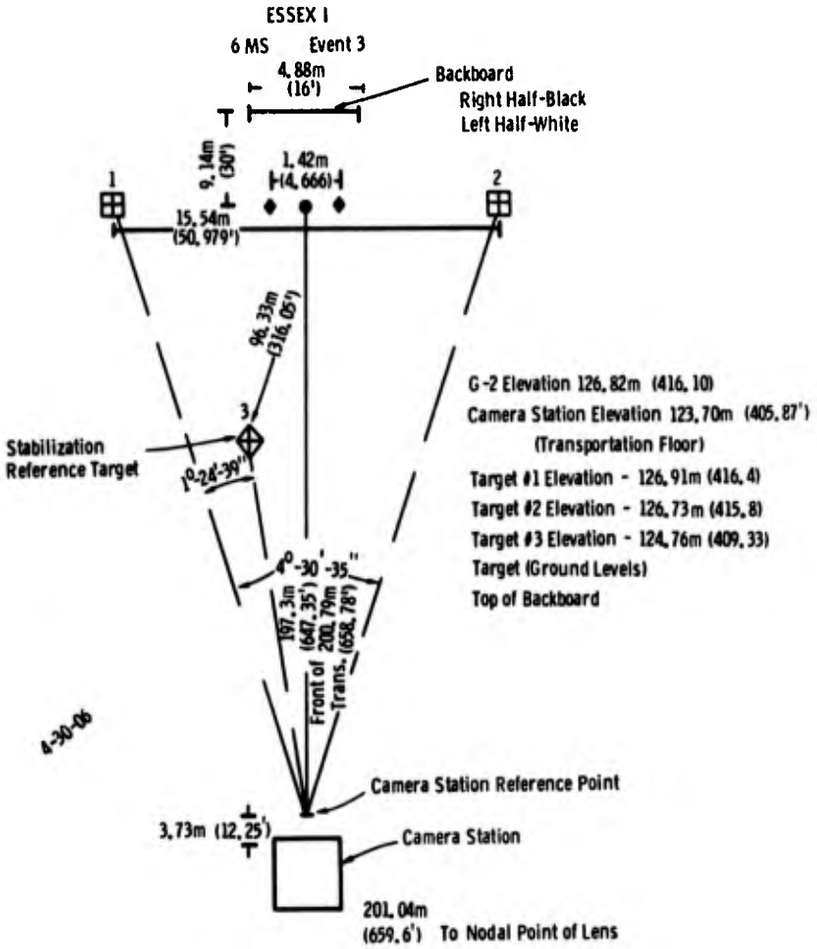

Figure 5.13 Plan view of camera layout

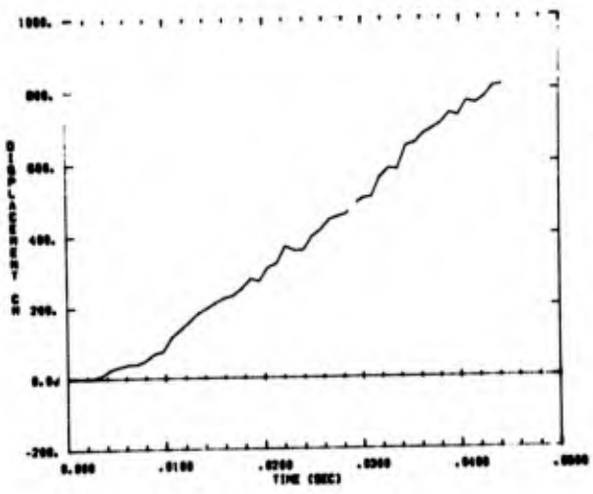

Figure 5.14a

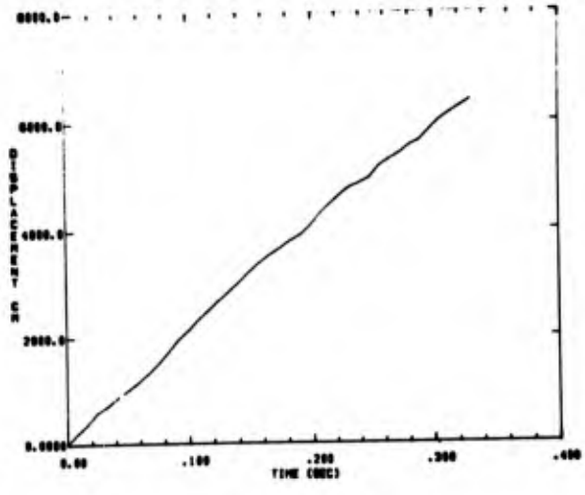

Figure 5.14b

Figure 5.14 Surface zero vertical displacements from two cameras

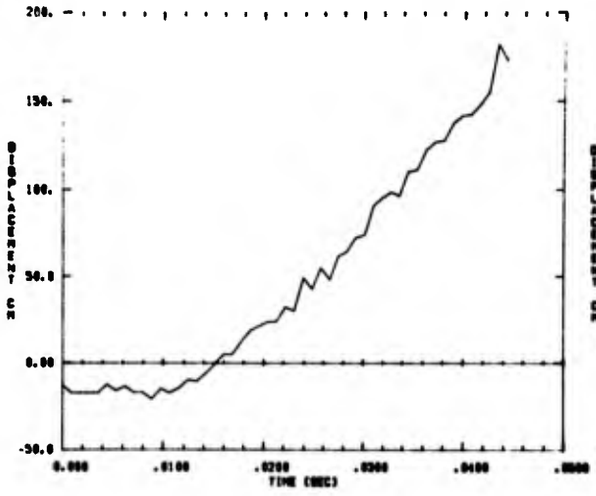

Figure 5.15a

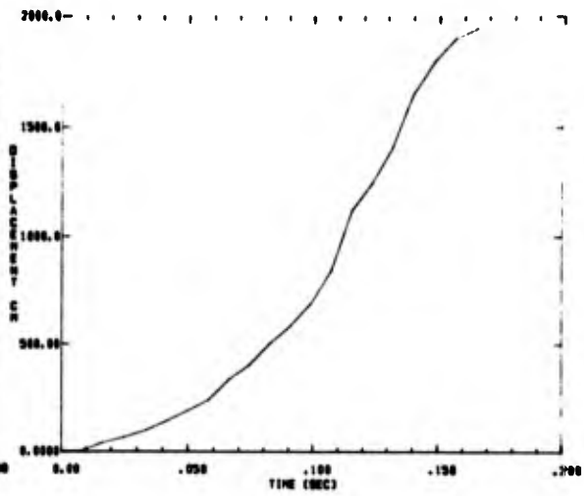

Figure 5.15b

Figure 5.15 Vertical displacement at 9 meters from two separate cameras

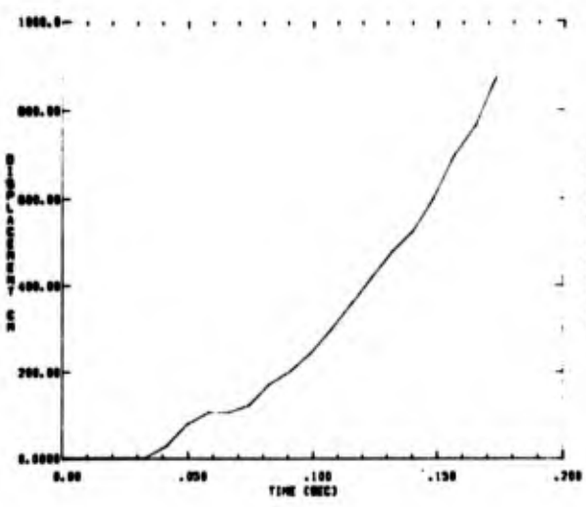

Figure 5.16a

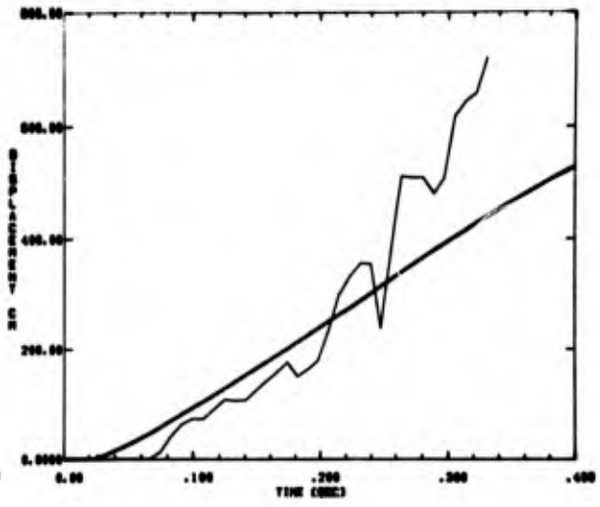

Figure 5.16b

Figure 5.16 Vertical displacement at 12 and 18 meters from photography with a comparison at 18 meters with displacement from an accelerometer

At the 24-m station, where instrumented vertical displacements were 6.5 m, no photographic displacement was obtained because all cameras with a wide enough field-of-view had an image too small to get adequate resolution.

Airblast Measurements

Results of airblast measurements are summarized in Tables 5.6 and 5.7 and the records are reproduced in Appendix L. Sandia measurements were made at three stations generally east of the shot at distances of 1.081, 2.376, and 5.893 km. SL also recorded airblast from gages installed by BRL at three stations--20, 40, and 80 feet (6.1, 12.2, and 24.4 m from SGZ along an azimuth of 90° (1.5708 radians).

Waveforms measured at the SL stations (Figs. L-1, L-2, and L-3) were as expected from a stemmed shot and were similar to those of 12 MS, consisting of a ground-shock-induced pulse and a gas-venting pulse, each following by a negative phase. The principal differences between these measurements and those on 12 MS were the larger peak pressures in both pulses as a result of the shallower burial depth of 6 MS. Also because of shallower burial, the increase in the gas-venting peak is greater than in the ground-shock-induced peak. Contrary to expectations the interval between the two peaks was nearly 50 percent longer in the case of 6 MS than in 12 MS. Ordinarily the interval decreases as charge burial depth is decreased. The fact that it didn't in this case could be attributed to the more saturated medium of 6 MS, causing the mound material to stay together longer before venting gas escaped from the expanding cavity. Arguing against this explanation is the fact that the intervals between the two peaks on 12 MS and 12 MPS were about the same even though saturation was considerably greater in the case of 12 MPS. Previous experience with stemmed shots in bearpaw shale[24] and submerged coral[25] have shown waveforms with no appreciable gas-venting pulse, presumably because the mound and cavity have continued to grow without venting until cavity pressures were too small to originate such a pulse.

Records from BRL measurements indicate either gage or cable failure for the two gages at 6.1 m and one of the two gages at 12.2 m (see Figs. L-4 and L-5). The other gage at 12.2 m recorded a peak ground-shock-induced pressure of about 150 mbar before the gage or cable failed at 0.84 sec. At the 24.4-m stations the records of both gages continue to 2.07 sec before cable failure. The records produced by both gages (BRL 3 LO and BRL 3 HI) are qualitatively similar, yet quantitatively dissimilar in certain components. The peak ground-shock-induced overpressure of BRL 3 LO was 8 percent greater than for BRL 3 HI, but the ground-shock-induced impulse was 40 percent smaller because the positive-to-negative crossover for 3 LO was nearly 100 msec earlier than for 3 HI. For the negative phase following the ground-shock-induced pulse, the peak of 3 LO was 30 percent greater than 3 HI, and the negative impulse 75 percent greater. Between 1 and 2 sec, both gages recorded (Figs. L-6 and L-7) a low-amplitude pulse of about a 500-msec duration, a small negative pulse, then a much larger amplitude pulse that continued until the cable broke. One or both of the positive pulses can be attributed to venting gas, possibly at different locations as well as times. The gas-venting peak at the three SL stations followed the ground-shock-induced peak by an average of 1.66 sec. A time of 1.66 sec after the ground-shock-induced peak at this BRL 24.4-m

A

TABLE 5.6

Summary of Airblast
(Metric Unit
ESSEX I 6MS 3
21,594 Pounds Nitromethane Buried 6

Gage Designation	SLA 1-LO	SLA 1-HI	SLA 2-LO	SLA 2-HI	SLA 3-LO
Gage Range	Low	High	Low	High	Low
Gage Sensitivity	High	Low	High	Low	High
Distance (m)	1081.	1081.	2376.	2376.	5983.
Azimuth (rad)	1.838	1.838	1.662	1.662	1.477
Time of Arrival of Ground-Shock-Induced Pulse (s)	3.074	3.074	6.760	6.762	16.922
Ground-Shock-Induced Peak Pressure (Pa)	211.7	208.9	108.2	106.9	33.44
Time of Ground-Shock-Induced Peak Pressure (s)	3.151	3.157	6.774	6.772	17.007
Time of Crossover (s)	3.257	3.259	6.934	6.935	17.135
Ground-Shock-Induced Impulse (Pa-s)	22.34	22.68	10.96	10.41	4.233
Negative Ground-Shock-Induced Peak Pressure (Pa)	135.8	142.7	57.92	59.29	24.41
Time of Negative Ground-Shock-Induced Peak Pressure (s)	3.412	3.398	7.087	7.077	17.308
Time of Crossover (s)	3.624	3.627	7.295	7.297	17.486
Negative Ground-Shock-Induced Impulse (Pa-s)	28.41	28.68	13.24	13.17	5.281
Time of Arrival of Gas Venting Pulse (s)	4.330	4.355	8.031	8.069	18.212
Gas Venting Peak Pressure (Pa)	165.5	159.3	74.46	75.15	22.75
Time of Gas Venting Peak Pressure (s)	4.783	4.788	8.473	8.472	18.649
Time of Crossover (s)	4.877	4.876	8.537	8.535	18.753
Gas Venting Impulse (Pa-s)	27.10	29.30	14.13	13.51	5.412
Negative Gas Venting Peak Pressure (Pa)	190.3	189.6	86.18	87.56	2.958
Time of Negative Gas Venting Peak Pressure (s)	4.991	4.983	8.674	8.678	18.856
Time of Crossover (s)	5.429	5.446	9.006	9.007	19.152
Negative Gas Venting Impulse (Pa-s)	29.58	30.47	13.44	13.10	5.585

B

TABLE 5.6

Summary of Airblast Measurements
(Metric Units)
SEX I 6MS 3 October 1973
itromethane Buried 6 Meters Deep, Fully Stemmed

SIA 3-LO	SIA 3-HI	BRL 1	BRL 1A	BRL 2	BRL 2A	BRL 3-LO	BRL 3-HI
Low	High	Low	High	Low	High	Low	High
High	Low	High	Low	High	Low	High	Low
5983.	5983.	6.096	6.096	12.192	12.192	24.384	24.384
1.477	1.477	1.571	1.571	1.571	1.571	1.571	1.571
16.922	16.914	.00446	.00451	.01181	.01306	.0212	~.021
33.44	31.99		20822.		15072.	7928.	7308.
17.007	17.003		.00851		.0292	.063	.071
17.135	17.133					.227	.321
4.233	4.068					641.9	1076.
24.41	24.48					3399.	2620.
17.308	17.307					.436	.459
17.486	17.487					.9	.7
5.281	5.143					964.6	551.6
18.212	18.22					1.336	1.25
22.75	22.48					16920.	16437.
18.649	18.652					2.016	2.046
18.753	18.758						
5.412	5.302						
2.958	2.916						
18.856	18.856						
19.152	19.152						
5.585	5.440						

A

TABLE 5.7
Summary of Airblast Measure
(English units)
ESSEX I 6MS 3 Octobe
21,594 Pounds Nitromethane Buried 6 Meters

Gage Designation	SLA 1-LO	SLA 1-HI	SLA 2-LO	SLA 2-HI	SLA 3-LO	SLA
Gage Range	Low	High	Low	High	Low	Hig
Gage Sensitivity	High	Low	High	Low	High	Low
Distance (Ft)	3545.	3545.	7800.	7800.	19333.	193
Azimuth (Degrees)	105.3	105.3	95.2	95.2	84.6	84.
Time of Arrival of Ground-Shock-Induced Pulse (Sec)	3.074	3.074	6.760	6.762	16.922	16.
Ground-Shock-Induced Peak Pressure (PSI)	.0307	.0303	.0157	.0155	.00485	.00
Time of Ground-Shock-Induced Peak Pressure (Sec)	3.151	3.157	6.774	6.772	17.007	17.
Time of Crossover (Sec)	3.257	3.259	6.934	6.935	17.135	17.
Ground-Shock-Induced Impulse (PSI-Sec)	.00324	.00329	.00159	.00151	.000614	.00
Negative Ground-Shock-Induced Peak Pressure (PSI)	.0197	.0207	.0084	.0086	.00354	.00
Time of Negative Ground-Shock-Induced Peak Pressure (Sec)	3.412	3.398	7.087	7.077	17.308	17.
Time of Crossover (Sec)	3.624	3.627	7.295	7.297	17.486	17.
Negative Ground-Shock-Induced Impulse (PSI-Sec)	.00412	.00416	.00192	.00191	.000766	.00
Time of Arrival of Gas Venting Pulse (Sec)	4.330	4.335	8.031	8.069	18.212	18.
Gas Venting Peak Pressure (PSI)	.0240	.0231	.0109	.0108	.00330	.00
Time of Gas Venting Peak Pressure (Sec)	4.783	4.788	8.473	8.472	18.643	18.
Time of Crossover (Sec)	4.877	4.876	8.537	8.535	18.753	18.
Gas Venting Impulse (PSI-Sec)	.00393	.00425	.00205	.00196	.000785	.00
Negative Gas Venting Peak Pressure (PSI)	.0276	.0275	.0125	.0127	.00429	.00
Time of Negative Gas Venting Peak Pressure (Sec)	4.991	4.983	8.674	8.678	18.856	18.
Time of Crossover (Sec)	5.429	5.446	9.006	9.007	19.152	19.
Negative Gas Venting Impulse (PSI-Sec)	.00429	.00442	.00195	.00190	.000810	.00

TABLE 5.7

ummary of Airblast Measurements
(English units)
SSEX I 6MS 3 October 1973
romethane Buried 6 Meters Deep, Fully Stemmed

SLA 3-LO	SLA 3-HI	BRL 1	BRL 1A	BRL 2	BRL 2A	BRL 3 LO	BRL 3 HI
Low	High	Low	High	Low	High	Low	High
High	Low	High	Low	High	Low	High	Low
19333.	19333.	20.	20.	40.	40.	80.	80.
84.6	84.6	90.	90.	90.	90.	90.	90.
16.922	16.914	.00446	.00451	.01181	.01306	.0212	~.021
.00485	.00464		3.02		2.186	1.15	1.06
17.007	17.003		.00851		.0292	.063	.071
17.135	17.133					.227	.321
.000614	.000590					.0931	.156
.00354	.00355					.493	.38
17.308	17.307					.436	.459
17.486	17.487					.9	.7
.000766	.000746					.1399	.080
18.212	18.22					1.336	1.25
.00330	.00326					2.454	2.384
18.649	18.652					2.016	2.046
18.753	18.758						
.000785	.000769						
.00429	.00423						
18.856	18.856						
19.152	19.152						
.00810	.000789						

station is in the middle of the low-amplitude pulse preceding the larger one. Two smaller peaks can be seen on the rising portion of the gas-venting pulse at the close SL station, and these may be vestiges of the smaller pulse seen at 24.4 m.

More information on airblast from this shot is included in Chapter 7.

CHAPTER 6

RESULTS OF THE 6-METER UNSTEMMED EVENT

In many respects the results from the 6-meter unstemmed event were less satisfying than from the other shots, primarily because signal levels were higher than anticipated. The three Slifers gave excellent records. Of the four ported pressure gages in the open hole, two from SL and two from BRL, only one of the latter gave a useful record. Only one of the five ytterbium gages gave a record not limited by band edge. Of six lithium-niobate gages installed, one was disconnected before shot time, and two showed records limited by band edge. Each of the remaining three showed signals induced from other lithium-niobate gages.

All four of the accelerometers installed at the two closest stations had records limited by band edge, although one record was affected very little. At 24 meters one of two radial accelerometers had records limited by band edge, and the other record appears incredible. Records from the vertical and tangential gages at 24 m appear quite good even though gage range was exceeded. The cable failed on the tangential gages and one horizontal gage shortly after peak velocity was reached. The tangential gage at 36 m gave an excellent record, but the vertical and two horizontal gage records were beyond gage range, and three horizontal channels were limited by band edge, although by amounts small enough that velocity and displacement were affected relatively little.

Of the 10 accelerometers installed at the surface stations, the horizontal gage at 12 m or its cable failed at shock arrival, the record from the vertical gage suffered a severe baseline shift, and both of the surface-zero vertical gages were limited by band edge. The horizontal gage failed shortly after achieving peak velocity. Other records were usable.

The 6 SLA airblast gages provided good records, as did 5 of the 6 BRL gages.

Gage Range and Set Range

Since the 6 MU shot was instrumented as nearly like the 6 MS shot as possible, there were few differences in set ranges, and, of course, no differences in gage ranges since gages were purchased and installed well in advance of both shots. Where gages over-ranged on the 6 MS shot it could be anticipated that they would do the same on the 6 MU shot unless there were significant differences in the medium at the two sites. Table 6.1 summarizes the set ranges for the low- and high-sensitivity channels and shows the peak values expected. Comparison with Table 5.1 will show the few changes made. As in the previous shot, set ranges for some of the accelerometers were greater than gage range.

TABLE 6.1

Planned Set Ranges Based on Expected Ground Motion and Stress for 6 MU

6 Meter Unstemmed

Gage	R Meters	DOB Meters	Expected	Low Sensitivity	High Sensitivity
σ - SY-1	6	3	3 (kb)	1.5 (kb)	0.75 (kb)
σ - SY-2	6	3	3	3.0	1.5
σ - SL-6	6	3	3	3.0	1.5
σ - SY-3	6	6	4	2.0	1.0
σ - SY-4	6	6	4	4.0	2.0
σ - SL-5	6	6	4	4.0	2.0
σ - SL-1	12	6	1	0.5	0.2
σ - SL-2	12	6	1	1.0	0.5
σ - SY-5	12	6	1	1.0	0.5
σ - SL-3	24	6	0.1	0.15	0.05
σ - SL-4	24	6	0.35	0.50	0.15
a_h	12	6	1500 (g)	5000 (g)	3000 (g)
a_h	12	6	1500	10000	5000
a_h	24	6	200	500	200
a_h	24	6	200	1500	1000
a_v	24	6	200	500	200
a_t	24	6	200	500	200
a_h	36	6	50	500	200
a_h	36	6	50	500	200
a_v	36	6	50	500	200
a_t	36	6	50	500	200
a_r	5	3	20000	40000	15000
a_r	5	3	20000	80000	40000
a_v	1-2/3	2/3	40000	80000	40000
a_v	1-2/3	2/3	40000	160000	80000
a_h	2/3	2/3	20000	60000	10000
a_v	9	2/3	20000	100000	50000
a_v	12	2/3	10000	9000	1000
a_h	12	2/3	5000	6000	700
a_v	18	2/3	7500	1500	500
a_h	18	2/3	7500	1500	500
a_v	24	2/3	5000	1500	500
a_h	24	2/3	2500	750	250

Pressure in open hole	2 channels
Slifer	3 channels
Sandia airblast	6 channels
BRL airblast	8 channels

Gages between lines were in a single hole.

Location of Measurements

Figure 6.1 shows the location of the near-surface and sub-surface stress and acceleration measurements on the unstemmed shot. Locations of Slifer and pressure measurements ported into the open hole are shown in Figure 6.2.

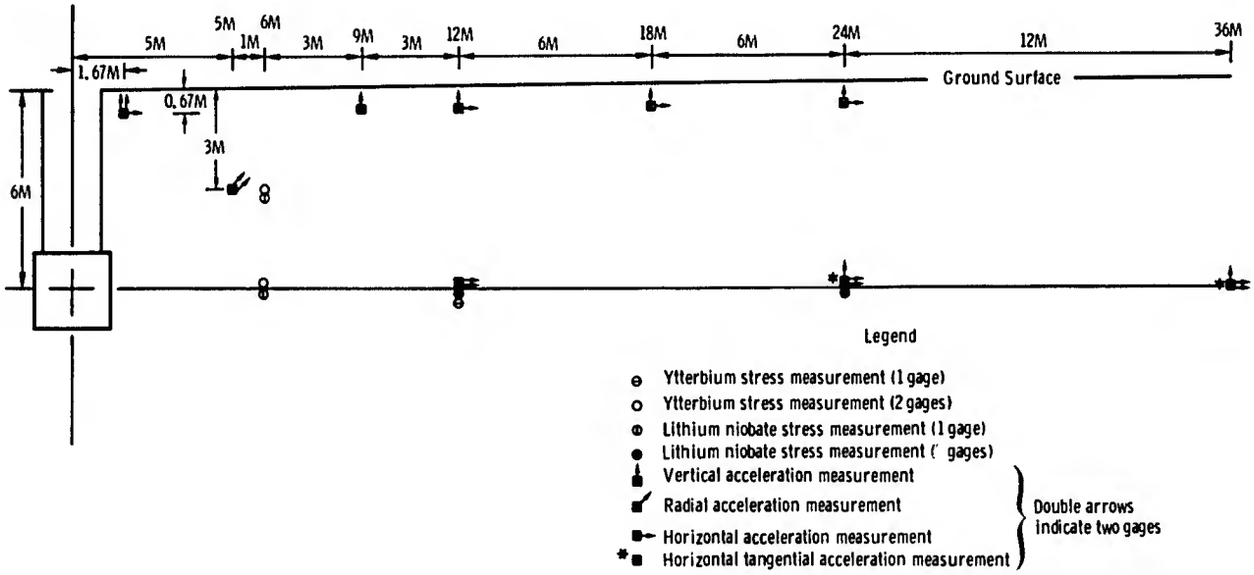

Figure 6.1 Location of stress and acceleration measurements for the 6-meter unstemmed event

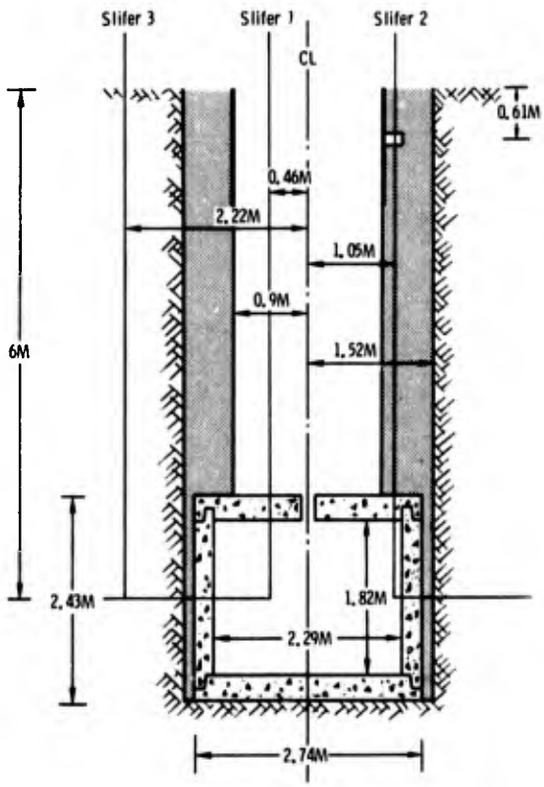

Figure 6.2

Location of Slifer and ported pressure measurements for the 6-meter unstemmed event

Slifer Time of Arrival

Figures 6.3 through 6.11 show, in order of Slifers 1, 2, and 3, the plots of frequency versus time, calibration curves of frequency versus cable length, and conversion into radial distance versus time. The three Slifers extended from shot depth to the surface and gave excellent records.

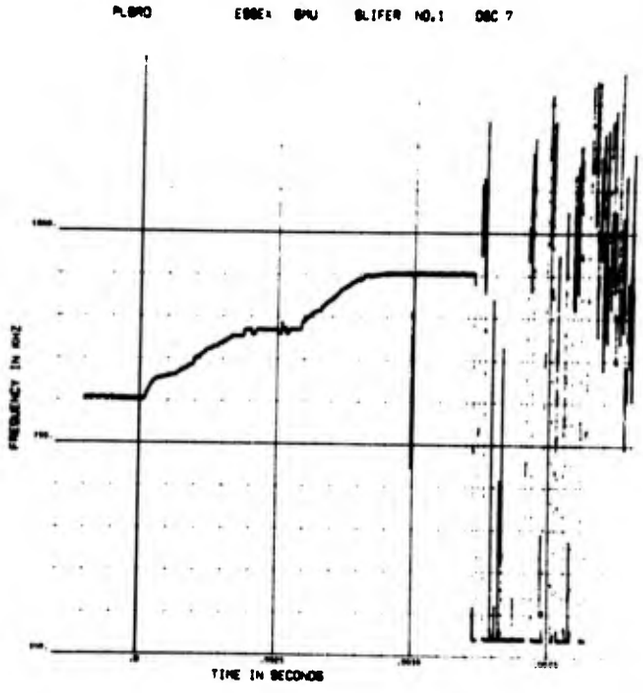

Figure 6.3

Frequency versus time for Slifer 1 time-of-arrival measurement

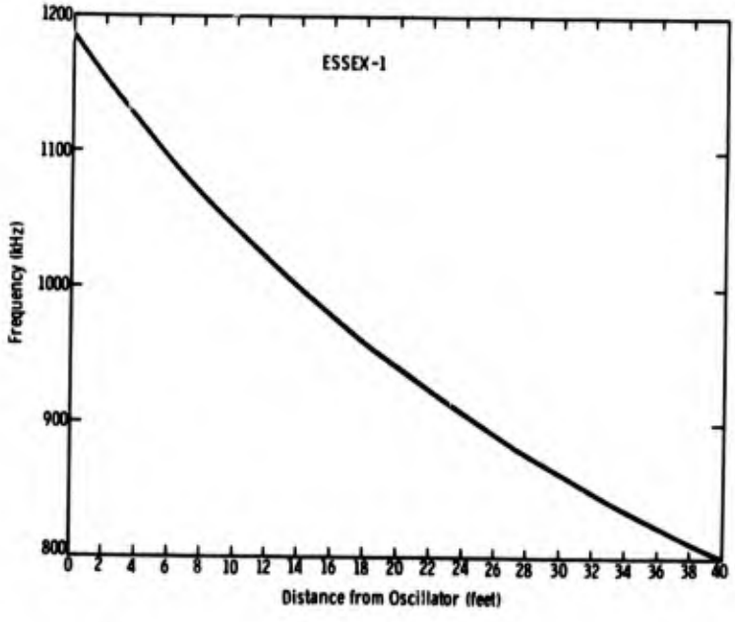

Figure 6.4

Calibration curve for Slifer 1 time-of-arrival measurement

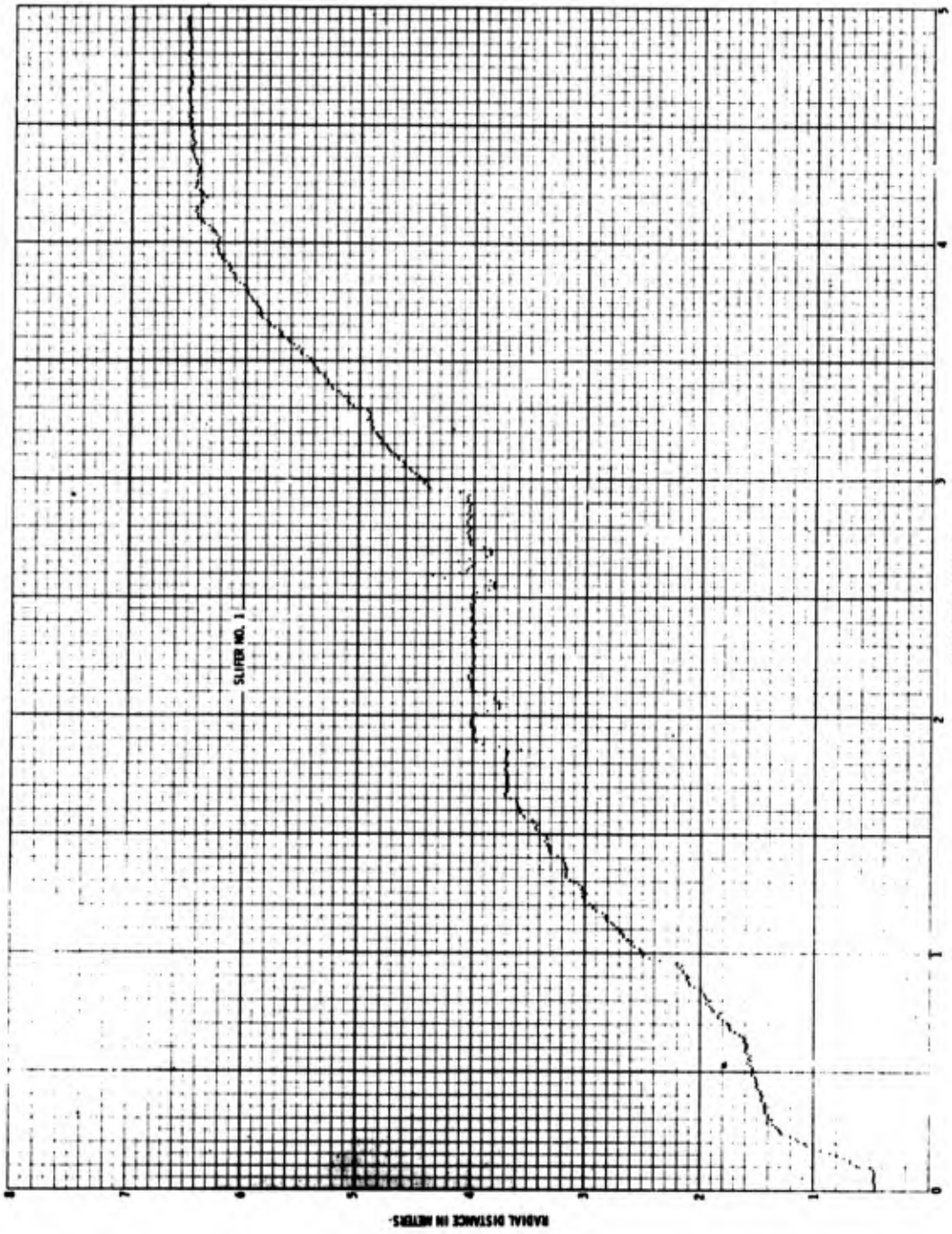

Figure 6.5 Time-of-arrival versus distance for Slifer 1 time-of-arrival measurement

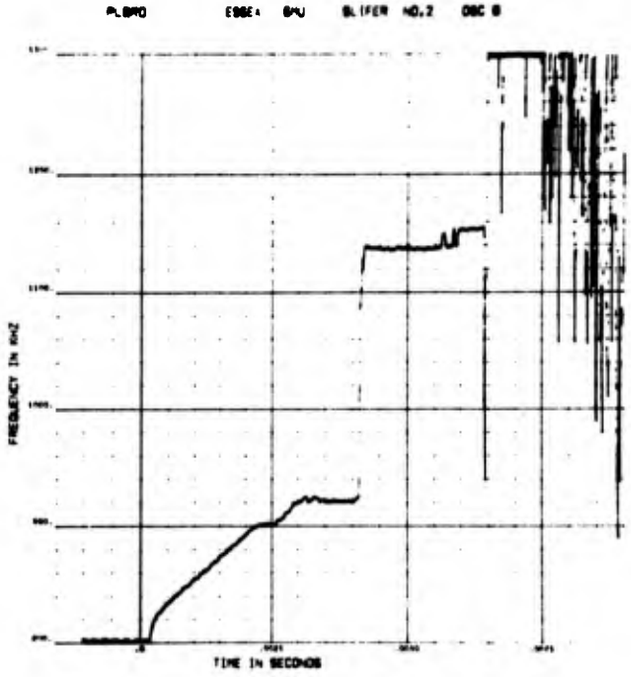

Figure 6.6 Frequency versus time for Slifer 2 time-of-arrival measurement

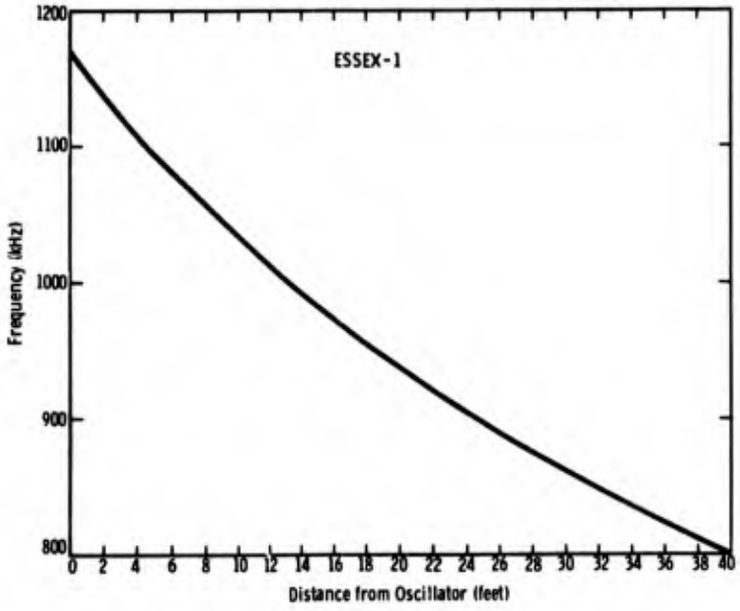

Figure 6.7 Calibration curve for Slifer 2 time-of-arrival measurement

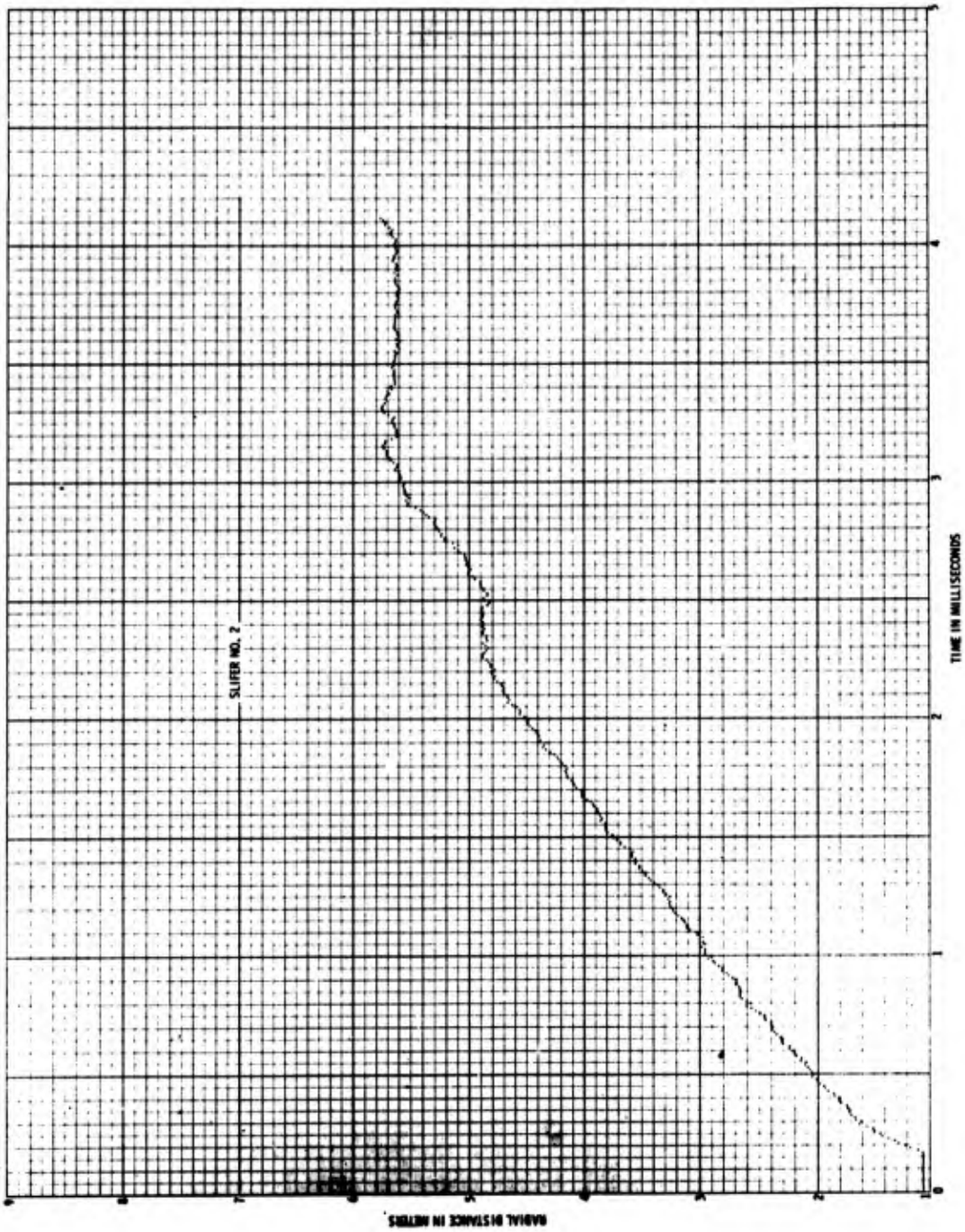

Figure 6.8 Time-of-arrival versus distance for Slifer 2 time-of-arrival measurement

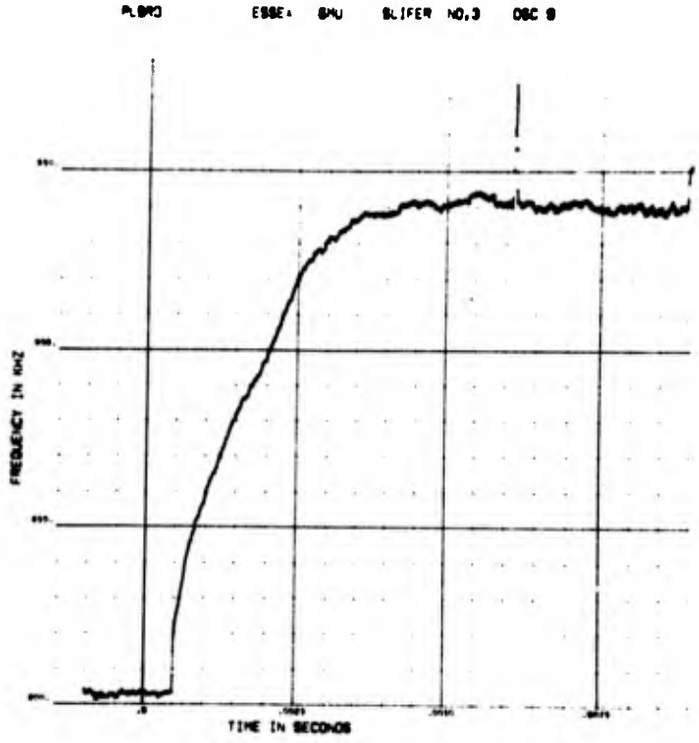

Figure 6.9 Frequency versus time for Slifer 3 time-of-arrival measurement

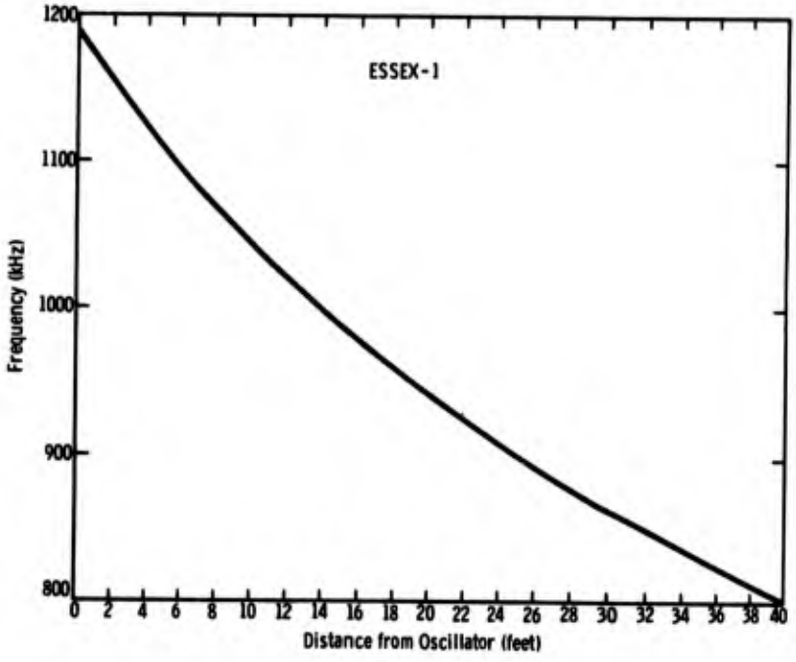

Figure 6.10 Calibration curve for Slifer 3 time-of-arrival measurement

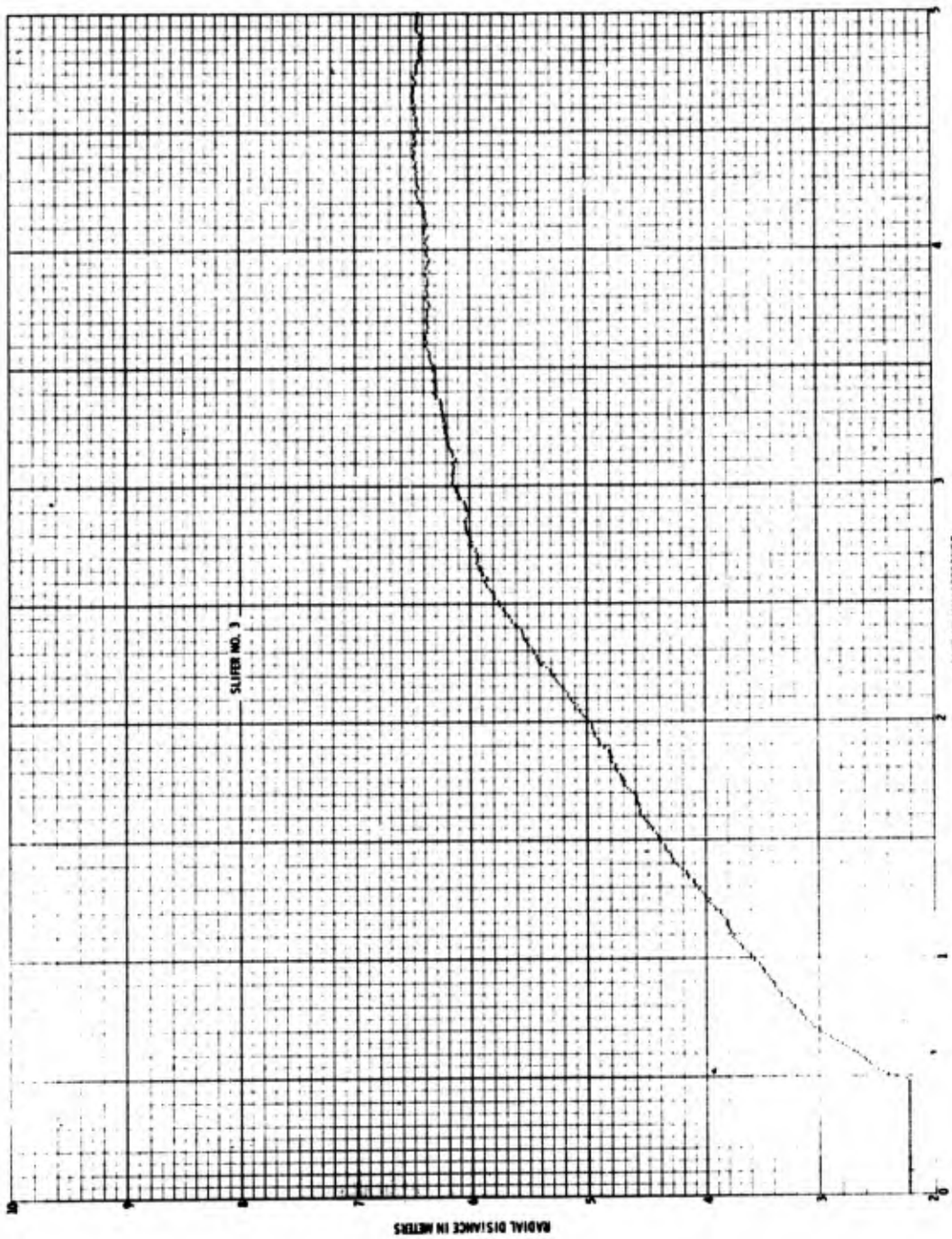

Figure 6.11 Time-of-arrival versus distance for Slifer 3 time-of-arrival measurement

Use of the 3 time-of-arrival measurements permits a very accurate reconstruction of the advance of the shock front through the soil (Slifer 3), the grout (Slifer 2), and the open hole (Slifer 1). The reconstruction is shown in Fig. 6.12. By 0.25 msec the shock front had passed through the concrete lid. The lid had a 5-inch (12.7-cm) diameter open hole designed to admit the booster assembly, which was inserted through a 4.026-inch (102.3-mm) ID steel pipe with a 0.237-inch (6-mm) thick wall that ran from the ground surface to about 1.5 feet (0.46 meters) below the top of the concrete lid. The steel pipe was supported on the top of the concrete lid by a 3/8-inch (9.5-mm) steel flange. With the booster assembly in place, the steel pipe had throughout its length a hollow thin-walled aluminum tube with a 0.75-inch (19-mm) OD to which the top of the booster was fastened. Inside the aluminum tube were three RG 213 electric cables, one Reynolds C 0.2-inch (5-mm) cable, and one 1/16-inch (1.6-mm) steel airplane cable.

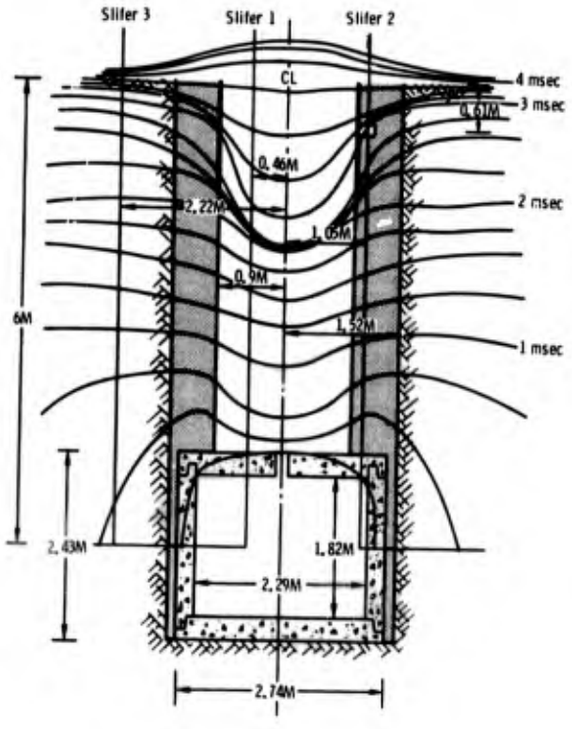

Figure 6.12 Advance of shock wave as determined from Slifer measurements

In Fig. 6.12 we have presented an interpretation of the Slifer data as it would appear if Slifer 1 had not been displaced vertically by combustion gases emerging up the open hole. This interpretation indicates that the steel flange and pipe allowed little if any flare of hot gas to escape through the hole in the concrete lid. The shock wave passing through the concrete would leave it pulverized. The pattern suggests that the shock front slowed after passing through the concrete, causing the front to lag the front in the surrounding grout and soil between 0.5 and 2.0 msec. Interpretation of Fig. 6.12 would suggest that between 2 and 2.75 msec, the shock front was slowed by a mechanism that is not obvious.

This interpretation shows that after 2.75 msec the shock front again begins advancing up the open hole so that at 4 msec, the front in the hole is in a position comparable to that in the surrounding grout and soil at about the surface level. Thereafter, the front above the hole advances more rapidly than away from the hole.

The interpretation illustrated in Fig. 6.12 is consistent with ground-shock arrival at the near-surface-zero accelerometer station. It is inconsistent with shock arrival time measured in the open hole by the ported pressure instruments, with emergence of the (nonluminescent) plume observed by photography, or with pressure observed at the closest BRL airblast station. Airblast up the open hole (see next section) peaked at 2.78 msec. Arrival time could be interpreted as

either 1.97, 2.30, or 2.55 msec. Camera 2 shows the plume emerging from the top of the hole at 2.38±0.2 msec and achieving a height of 0.42 m at 2.6±0.2, and a height of 0.98 m at 2.8±0.2 msec. Only an arrival time of 2.30 msec at the ported pressure gage is consistent with photographic data. Airblast arrived at the closest BRL airblast station at 4.57 m at 4 msec.

Figure 6.13 is a reconstruction of shock-front position that is consistent with the other measurements, in which it is assumed that the open-hole Slifer is displaced during the time span covered, and which represents the authors' judgment of how the Slifer may have moved as a function of time. In Fig. 6.13 the initial lag is still maintained until about 1.75 msec, after which the front in the hole accelerates with respect to the front in the surrounding material. The disadvantage of the postulation of Fig. 6.13 is that it does not explain the mechanism by which particle velocity behind the shock front in the open hole can transmit sufficient velocity to the Slifer to cause it to be displaced ahead of the shock front in the hole.

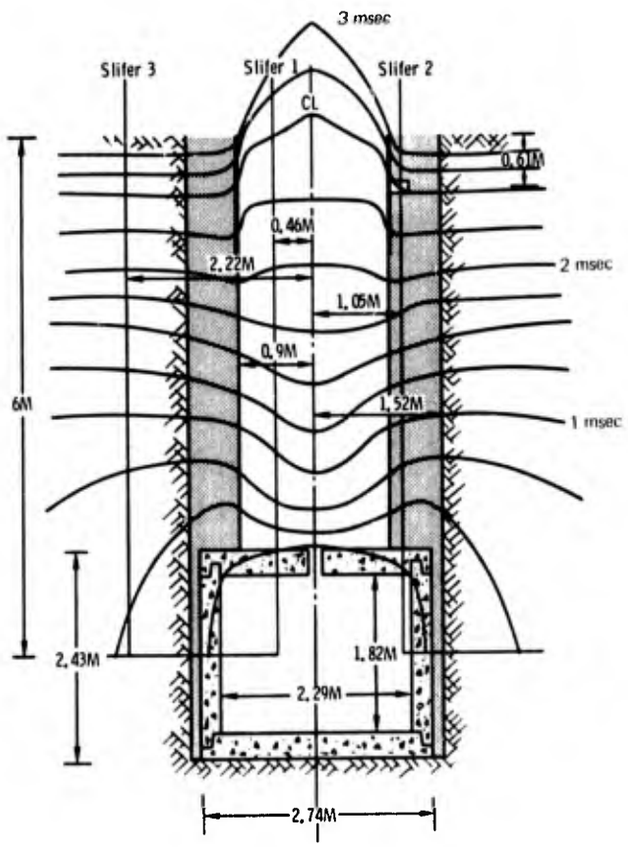

Figure 6.13

Reinterpretation of advance of shock wave as determined from Slifer measurements

Arrival Times at all Instrument Stations

Figure 6.14 shows arrival times at surface and below-ground instruments. At shot depth the shock velocity was quite uniform to 36 m at about 1.73 m/msec. This was less than for 12 MS and more than for 12 MPS and 6 MS. At the surface the average velocity was about 1.09 m/msec from the near-surface-zero station to the 24-m station except at 9 m, where for unknown reasons the

shock arrived about 1.4 msec earlier than that velocity would indicate. At the 24-m station there is no evidence of early arrival from refraction through the medium below, as occurred on 6 MS. Arrival times at BRL airblast gages are misleading since at the closest (4.57 m on the surface) the blast wave from the open hole arrives ahead of the ground shock at the surface. At the 13.4-m station on the surface the arrival is that of the same air-transmitted wave from the open hole, and its amplitude is so large that a preceding ground-shock induced pulse is not discernible.

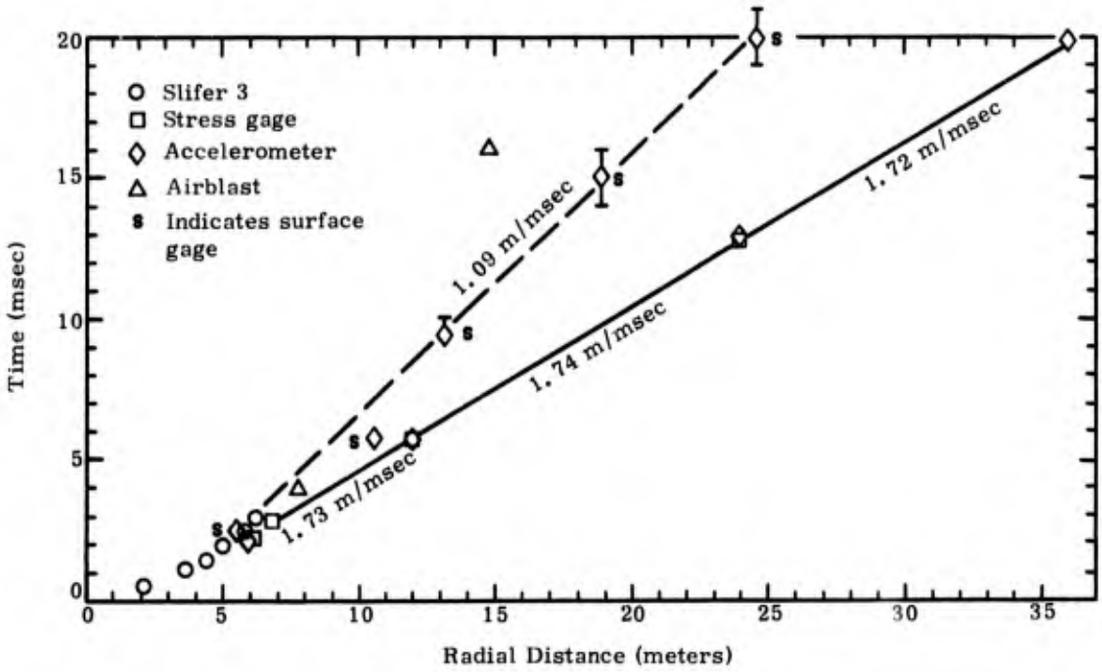

Figure 6.14 Summary plot of arrival times at all stations

Ported Pressure Measurements in Open Hole

Four pressure gages were installed with their sensing elements flush with a curved aluminum plate fitted to the wall of the hole. Two of the gages were installed by SL and recorded with two sensitivities, and the other 2 by BRL. The 4 gages were located on 4-inch (10.2-cm) centers 2 feet (0.61 m) down from the top of the hole in a 0.25-inch (6.3-mm)-thick arc of aluminum plate that extended 1.37 m into the open hole. Records from the first two are shown in Fig. 6.15, and those from the BRL gages in Fig. 6.16. All four gages or their cables failed before 3 msec. The times of failure were 2.37, 2.75, 2.82, and 2.80 for the P-1, P-2, BRL-A, and BRL-B gages, respectively.

Close examination of the record from the BRL-A gage shows some evidence of weak signals before gage or cable failure. When this portion of the record was expanded (Fig. 6.17), clear signals were revealed. By 1.3 msec the gage had recovered from an initial EM signal. Three arrivals can be identified at 1.97, 2.30, and 2.55 msec. Comparison with other data in the preceding section shows that the signal arriving at 1.97 msec is too early to be credible, and that the one at 2.30 msec

does agree with other measurements. The short negative pulse at about 2.5 msec, which interrupts an otherwise continuous rise, coincides with ground-shock arrival at the gage. A peak overpressure of 480 bars (6940 psi) is credible in view of the peak of 557 bars recorded in the open hole of 12 MPS. Whereas the pulse from that 12-m shot arrived at 2.03 msec and consisted of a sharp shock, the one from this shot at half the depth arrived at 2.30 msec. The slower average velocity can only be attributed to the effect of the mass of concrete from the lid that was accelerated by the pulse. The slower rise to a peak could also be attributed to turbulence caused by concrete particles in the pulse.

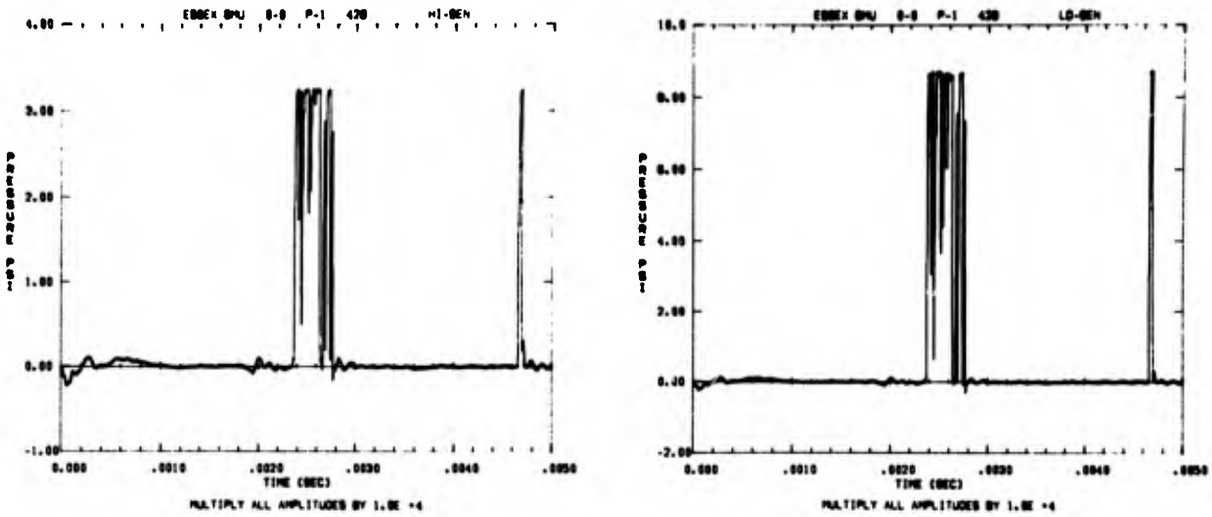

(a) (b)

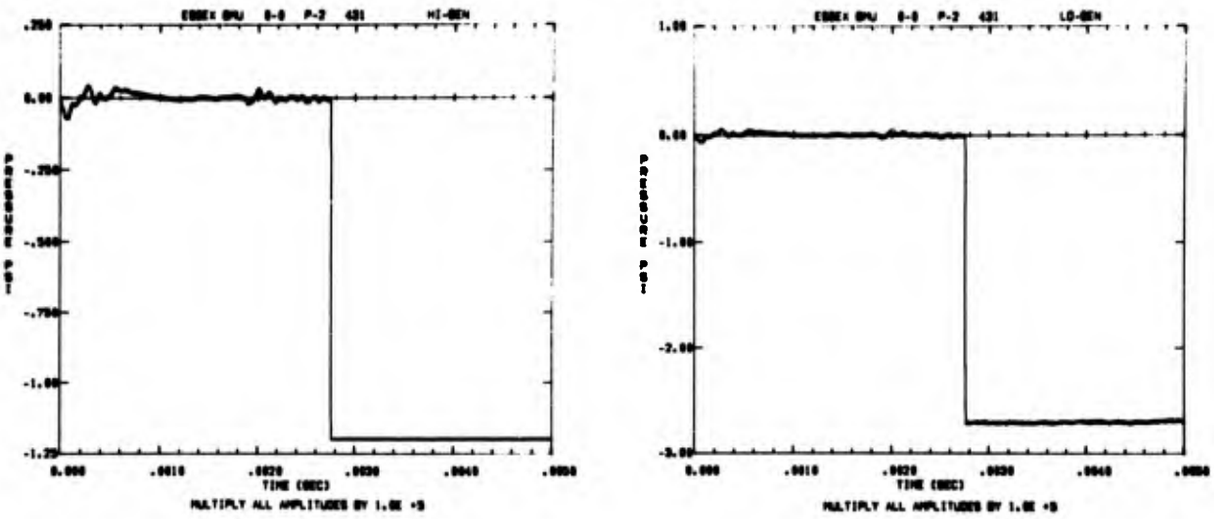

(c) (d)

Figure 6.15 Records from Sandia ported pressure measurements

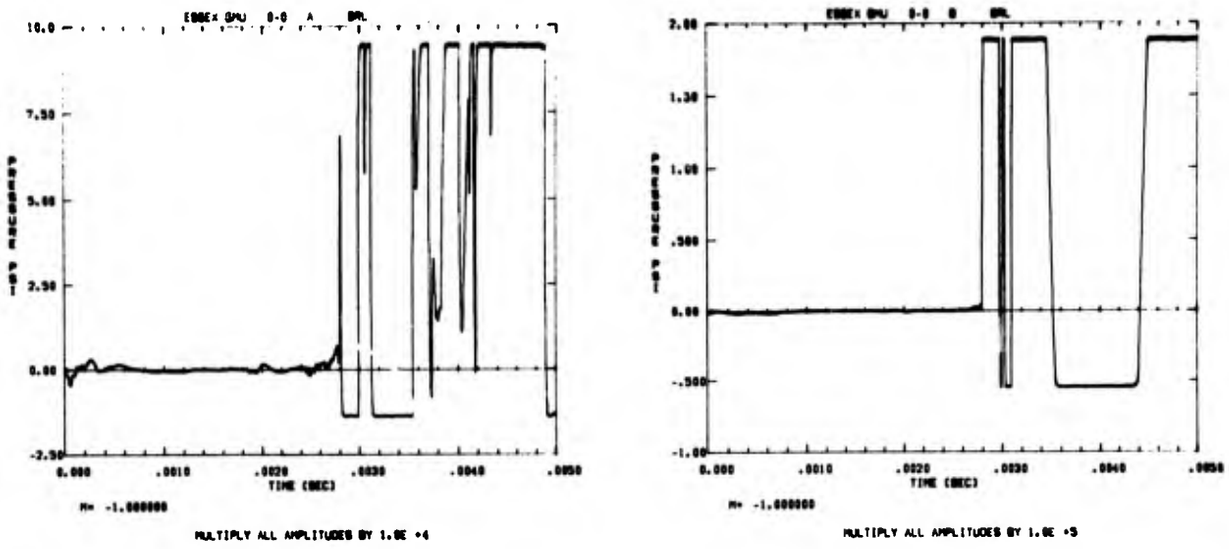

(a) (b)

Figure 6.16 Records from BRL ported pressure measurements

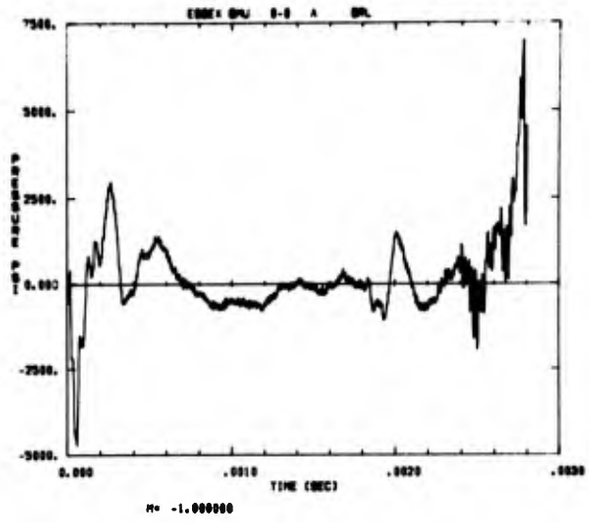

Figure 6.17 Expansion of portion of pressure measurement before gage or cable failure

Stress Measurements

Records obtained for stress measurements made on the 6 MU event are reproduced in Appendix M and the principal parameters are summarized in Table 6.2.

Stress measurements for this shot differed from the preceding ones in several ways. A total of 11 gages were installed to increase the number of direct comparisons between ytterbium and lithium-niobate gages. A large number of records were beyond band edge because expected stresses had been reduced slightly owing to smaller charge weight and to account for energy losses through the open hole. Records from the lithium-niobate gages contained signals induced by other lithium niobate-gages, degrading those records. Cross-talk between adjacent subcarriers of the recording equipment and playback equipment was excluded as a cause. A significant effort to define the cause precisely was unsuccessful. Electrical induction in the signal-conditioning package for these gages is the most likely source even though the same equipment presented no problems on the three previous shots.

A

TABLE 6.2

Summary of Stress Mea
ESSEX I 6 MU 24 Oct
17,275 Pounds Nitromethane Buried 6

Gage Type		Distance (m)	Depth (m)	Gage Range	Gage Sensitivity	Calibration Step (kbar)
Ytterbium	SY-1	6	3	Low Low	High Low	0.75 0.75
	SY-2	6	3	High High	High Low	1.50 1.50
	SY-3	6	6	Low Low	High Low	1.0 1.0
	SY-4	6	6	High High	High Low	2.0 2.0
	SY-5	12	6	High High	High Low	0.5 0.5
Lithium Niobate	SL-1	12	6	Low Low	High Low	0.2 0.2
	SL-2	12	6	High High	High Low	0.5 0.5
	SL-3	24	6	Low Low	High Low	0.05 0.05
	SL-4	24	6	High High	High Low	0.15 0.15
	SL-5	6	6	High High	High Low	2.00 2.00
	SL-6	6	3	High High	High Low	1.50 1.50

(L) Limited
(a) Limited by band edge
(b) Gage or cable failed at shock arrival
(c) Refracted signal
(d) Gage disconnected prior to detonation
(e) Numbers in parentheses are a second peak

TABLE 6.2

Summary of Stress Measurements
ESSEX I 6 MU 24 October 1973
Nitromethane Buried 6 Meters Deep, Unstemmed

Calibration Step (kbar)	Arrival Time (msec)	Peak Stress (kbar)	Time of Peak (msec)	Remarks
0.75	2.84	>1.05 (L)		(a)
0.75	2.85	>1.2 (L)		(a)
1.50	2.84	1.95	3.35	
1.50	2.83	1.93	3.34	
1.0	2.34	>1.4 (L)		(a)
1.0	2.33	>1.7		(a)
2.0	2.33	>2.89 (L)		(b)
2.0	2.33	~3 est.		(b)
0.5	5.85	>0.78		(a)
0.5	5.82	>1.23 (L)		(a)
0.2	(d)			
0.2	(d)			
0.5	5.80	0.60 (0.43)	5.95 (6.7)	(e)
0.5	5.8	0.60 (0.42)	5.83 (6.48)	(e)
0.05	12.68	>0.098 (L)		(a)
		0.062		(c)
0.05	12.65	>0.14 (L)		(a)
		0.065		(c)
0.15	12.69	>0.29 (L)		(a)
		0.008		(c)
0.15	12.85	0.40	13.235	
		0.0083		(c)
2.00	2.37	1.73	2.80	
2.00	2.35	1.82	2.46	
1.50	2.92	2.68 ± 0.2	3.3	
1.50	2.9	2.68 ± 0.2	3.31	

One of the 11 gages installed, a lithium-niobate gage at 12 m range at shot depth, became inoperative and was disconnected before shot time.

At 6 m range and half shot depth, two ytterbium and one lithium-niobate gage were installed. The low-range ytterbium gage gave a record (Fig. M-1) that was beyond band edge on both sensitivities, but the other (Fig. M-2) showed a peak stress of 1.94 kilobars on both sensitivities. The principal signal from the lithium-niobate gage was superimposed on an induced signal from SL-5 (Fig. M-2). That, together with a baseline shift that occurred sometime during the main signal, accounts for the uncertainty.

The slightly closer station, at 6 m range at shot depth, also had two ytterbium gages and one lithium-niobate gage. Here also the low-range record (Fig. M-1) was beyond band edge, and the high-range gage or its cable failed microseconds after shock arrival. The highest point on the record before failure (see Fig. M-3) would suggest a peak stress of about 3 kbars at failure, assuming a wave shape similar to that recorded by the lithium-niobate gage. The record from the latter (Fig. M-3) gave a peak of about 1.78 kbars if the electrical transients are ignored. The first half millisecond of the signal is without interference from signals induced by other gages. It appears that the next, approximately one millisecond of the record, was reduced by interference from an induced signal from SL-6. That the stress was reduced is deduced from the fact that all other induced signals on the record are negative. This record also shows a baseline shift that occurred sometime during the main signal. The remarkable thing about the records of SL-5 and SL-6 is that they show that the gage and the cable survived at the closest stations for more than 0.1 sec.

Two lithium-niobate gages (one of which was later disconnected) and one ytterbium gage were installed at the 12-m shot-depth station. The record of the latter (Fig. M-4) was limited by band edge on both sensitivities. The record from the lithium-niobate gage shows a peak of 0.6 kbars at 5.9 msec and a lower peak of 0.42 at 6.6 msec. Except for the first peak, the wave shape is similar to that of SY-2 at the half-shot-depth station. This record also gives evidence of a baseline shift.

Two lithium-niobate gages were installed at the 24-m shot-depth station. Both showed a main shock wave and a reflected shock wave. The low-range gage record had the peak of the main wave beyond band edge on both sensitivities. This gage was unique in that its record, alone of the five lithium-niobate gage records, had no induced signals (Fig. M-5). The record of the high-range gage had a peak limited by band edge on the high-sensitivity channel but within band edge on the low-sensitivity channel. There is no way to determine whether the induced signals on the other lithium-niobate records came from SY-3 or SY-4. If they came from SY-3 there is a possibility that there is a contribution to the SY-4 pulse from the SY-3 induced signal. Since on the other records the induced signal from SL-3 and/or SL-4 had the same polarity as those from SL-2, it would be in order to assume that in the record of SL-4, the induced signal from SL-3, if it exists, would have a negative polarity. Thus, if there is an induced signal from SL-3 on the main signal from SL-4 its effect would be to lower the SL-4 peak. From the estimate of induced signal amplitudes it is

believed that an induced signal would add no more than 0.034 kbar to the peak of SL-4. As will be seen below, the peak stress from SL-4 is high with respect to those from other gages even without such a contribution.

In Fig. 6.18 the peak radial stress measured by both Sandia and SRI has been plotted versus distance. The peak radial stress measured at 24 m by SL-4 is extremely high with respect to other data, and no reason has been determined. Similarly, at half shot depth, the stress measured by the ytterbium gage (SY-2) is 0.73 times that measured by the lithium-niobate gage (SL-6) at the same location. Since the medium at half shot depth can differ from that at shot depth, there is no reason to expect stresses to be comparable. Thus it is not proper to say that SY-2 is the gage in error even though it is suspect.

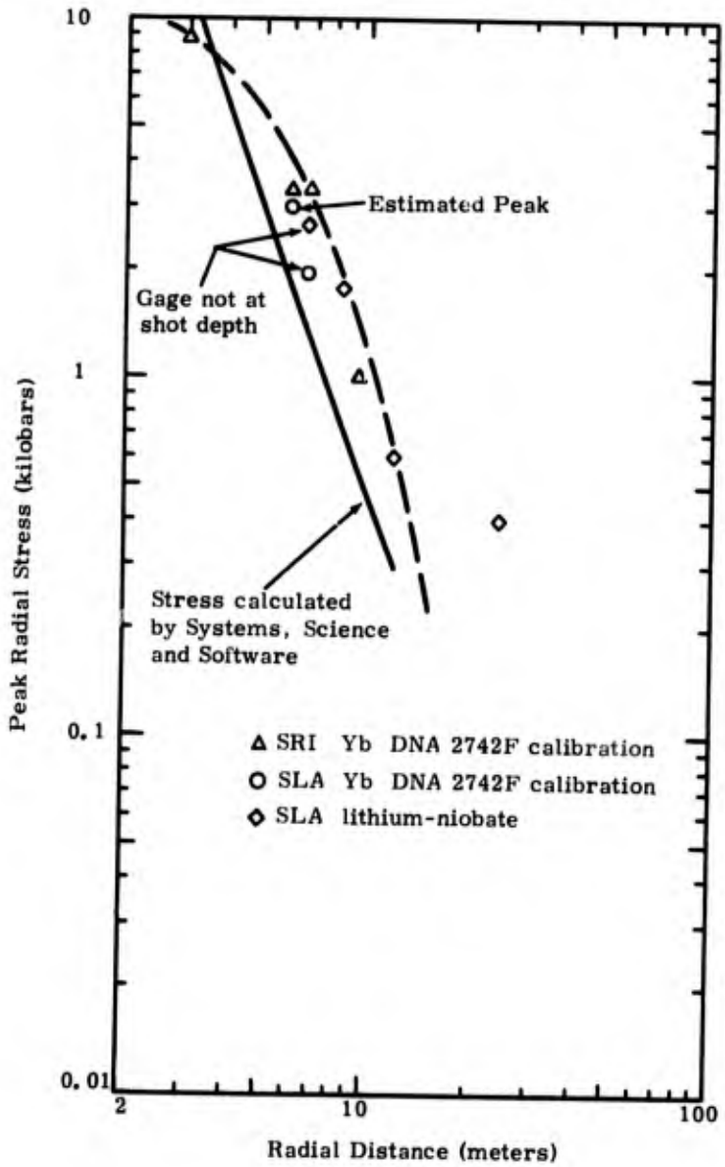

Figure 6.18 Comparison of measured and claculated stress

Free-Field Ground Motion

Significant parameters of the free-field ground-motion measurements are summarized in Table 6.3. In Appendix N the records from the accelerometers, together with their first and second integrations, are presented.

Figures N-1 and N-2 show the first 10 msec of the records from the two radial accelerometers located at 5 m and half shot depth. From the low-range gage several peaks were limited by band edge on the high-sensitivity channel. On the low-sensitivity channel, only the first peak was limited at about 80,000 g's, well beyond the 30,000-g range of the gage used. Similarily, several peaks of the high-sensitivity channel of the high-range gage were limited by band edge, and only the first peak was limited on the low-sensitivity channel. That peak was limited at about 160,000 g's, again well above the 50,000-g range of the gage used. The first pulse arrives shortly after 2 msec, and lasts only 0.2 msec. Later signals occurring after about 4 msec are attributed to refractions and returns from the surface, and make a radial measurement meaningless in the absence of measurements of other components of motion. The first pulse is of interest not only for its short duration but also because positive acceleration is followed by a return to ambient, rather than by a negative excursion. We were at first inclined to discard the record as incredible, but there was the fact, as will be seen below, that some of the radial acceleration pulses at 12 and 24 m at shot depth had similar characteristics. The low-sensitivity channel of the high-range gage indicates an initial peak velocity of greater than 210 m/sec. Nonlinearities would cause the gage to indicate a lower than actual velocity in the region above gage range, so that indicated velocity can be considered a lower limit. The gage manufacturer could offer no reason why over-ranging the gage should cause it to fail to respond to negative acceleration.

Both sensitivities of the low-range gage at the 12-m station were limited by band edge (Fig. N-3). Band edge was at 5,500 and 9,500 g's respectively for the high- and low-sensitivity channels of the 5,000-g gage. Here, too, pulse duration was only 0.2 msec and there was no appreciable negative acceleration. This is in contrast to the records from the high-range gage (Fig. N-4), where there was a pronounced negative excursion immediately following the positive pulse. Records from both sensitivities again were limited by band edge, at about 10,000 and 20,000 for the two sensitivities, the latter being twice the gage range. In this case, 0.2 msec includes the duration of both the positive and negative pulses. This is in contrast to the stress measurement, which had a duration of over 2 msec. The velocity pulse shape (Fig. N-4) resembles the stress pulse shape (Fig. M-4), as it should. The peak particle velocity, together with measured shock velocity (Fig. 6.14) and density, indicated a derived peak stress of about 0.56 kilobar, nearly equal to the measured peak stress (Fig. M-4). Thus, limiting of the acceleration peak was small and reduced the velocity peak by very little, and credence is given to the record despite the seemingly brief acceleration spike. Having two gages in the same canister, one with a negative pulse and one without, is puzzling, but since the record with the negative pulse agrees with the stress record, we conclude that for some reason the other gage was not responding to the negative signal.

A

TABLE 6.3

Summary of Acceleration Measurements at Shot
ESSEX I 6 MU 24 Octob
17,275 Pounds Nitromethane Buried 6 Me

Accelerometer Designation	Accelerometer Orientation	Distance (m)	Depth (m)	Gage Range	Gage Limit (g's)	Gage Sensitivity	Calibration Step (g's)
5-3 AR-LO	Radial	5	3	Low	30,000	High	14,894
				Low	30,000	Low	14,894
5-3 AR-HI	Radial	5	3	High	50,000	High	39,818
				High	50,000	Low	39,818
12-6 AH-LO	Horizontal	12	6	Low	5,000	High	2,987
				Low	5,000	Low	2,987
12-6 AH-HI	Horizontal	12	6	High	10,000	High	5,000
				High	10,000	Low	5,000
24-6 AH-LO	Horizontal	24	6	Low	200	High	200
				Low	200	Low	200
24-6 AH-HI	Horizontal	24	6	High	1,000	High	1,000
				High	1,000	Low	1,000
24-6 AV	Vertical	24	6		200	High	200
					200	Low	200
24-6 AT	Tangential (Horizontal)	24	6		200	High	201
					200	Low	201
36-6 AH-LO	Horizontal	36	6	Low	200	High	203
				Low	200	Low	203
36-6 AH-HI	Horizontal	36	6	High	200	High	200
				High	200	Low	200
36-6 AV	Vertical	36	6		200	High	200
					200	Low	200
36-6 AT	Tangential (Horizontal)	36	6		200	High	201
					200	Low	201

B

TABLE 6.3

tion Measurements at Shot Depth and Half Shot Depth
ESSEX I 6 MU 24 October 1973
Nitromethane Buried 6 Meters Deep, Unstemmed

ge vity	Calibration Step (g's)	Arrival Time (msec)	Peak Acceleration (g's)	Time of Peak (msec)	Peak Velocity (m/sec)	Time of Peak (msec)
h	14,894	2.18	> 30,900 (L)	2.26	>46.0	
	14,894	2.16	> 80,000 (L)	2.29	>108.0	
h	39,818	2.18	> 82,050 (L)	2.31	>113.0	
	39,818	2.16	> 159,000 (L)	2.23	>210.0	
h	2,987	5.71	> 5,530 (L)	5.86	> 8.0	
	2,987	5.71	> 9,500 (L)	5.85	>13.7	
h	5,000	5.73	> 10,730 (L)	5.80	> 9.3	
	5,000	5.71	> 20,500 (L)	5.77	>16.3	
h	200	12.78	>400 (L)		> 0.88	13.25
	200	12.83	>993 (L)	13.09	>1.39	13.23
h	1,000	12.88	> 2,230 (L)	13.15	>4.71	13.40 and later
	1,000	12.91	3,520	13.11	5.55	13.32 and later
h	200	12.79	> 386 (L)	13.14	>1.10	
	200	12.82	+551, -513	13.16, 14.12	1.18	13.40
h	201	12.79	-377, +363	13.08, 13.10	-0.43	13.13
	201	12.83	-410, +323	13.05, 13.16	-0.415	13.12
h	203	19.75	> 428 (L)	20.23	>1.58	20.43
	203	19.82	> 488 (L)	20.25	>1.60	20.43
h	200	19.84	> 383 (L)	20.36	>1.47	~20.43
	200	19.85	432	20.32	>1.51	20.55
h	200	19.84	> 349 (L)	20.33	>0.79	20.47
	200	19.77	> 319 (L)	20.31	0.76	~20.47
h	201	19.84	253	20.22	0.72	~20.5
	201	19.66	246	20.20	0.74	20.35

Since the record is a valid one, it is in order to look at the response of the gage between 10 and 20 msec. It was during that interval that rarefaction waves from the surface began to influence ground motion at the point of measurement. Figure N-5 shows acceleration, velocity, and displacement for the first 20 msec. If there was little or no rotation of the gage canister during this short time, the record indicates that after a maximum outward displacement of about 2.5 cm the direction of motion reversed and had moved inward 60 cm by 20 msec. It would be worthwhile for those doing the calculations to see if calculated ground motion is in agreement with that reported here.

Two horizontal accelerometers were installed at the 24-m station. The low-range 200-g gage (Fig. N-6) was limited by band edge at about 400 g's on the high-sensitivity and 1,000 g's on the low-sensitivity channel. Most puzzling is that the 2262C accelerometer has a mechanical stop which, for the 200-g range gage used here, should accommodate only 225 g's, yet on the low-sensitivity channel we were able to record four times that amount. The record is consistent with some of those discussed above in having a short duration; about 0.35 msec for the positive and 0.7 for the negative pulse. The cable apparently broke just after completion of the negative pulse. The record from the high-range (1,000-g) gage (Figs. N-7 and N-8) is in contrast to the low-range gage record and is consistent with others discussed above in having no negative pulse. The high-sensitivity channel was limited by band edge, but the low-sensitivity channel was not, and gave a peak of 3,500 g's. After the positive pulse the signal returned to zero where it remained until about 48 msec, when a pronounced negative excursion appeared. This excursion is attributed to a reflection from below, which coincides timewise with a similar positive excursion appearing on the record of the vertical gage at the same location, and is also like that record in having the excursion in one direction only. Here, again, were two gages in the same canister, one with a negative phase and one without, and again, we give credence to the one with a negative phase. The puzzling point about the high-range gage is that it failed to record a negative pulse associated with direct shock transmission, yet recorded faithfully one associated with the reflected signal. Since the positive pulse appears valid, there is no reason to doubt the peak velocity, even though velocity does not decrease following the peak. Using the measured peak particle velocity, measured shock velocity, and density, the derived peak stress is about 0.2 kilobar. Compare this with the measured stress of 0.4 kilobar shown in Fig. M-6. The note on the figure points out that the 0.4-kilobar level could include a contribution from an induced signal from the companion stress gage at the same station. A comparison of the derived stress with measured stress indicates that the stress measured by SL-4 does indeed include a contribution from SL-3.

The plus-3-sec record from the low-sensitivity channel of the high-range gage is not shown. It did contain a signal at about 0.35 sec that was even stronger than the initial pulse and had all the characteristics of an acceleration record. The same signal appears on the vertical gage record at the same station, so the gages were responding to some motion of the canister. Since no comparable signal was seen at the 36-m station, a reflected wave is an unlikely source. A remaining possibility is canister movement induced by ground motions jerking on the hardened cable to the canister.

The vertical gage at the 24-m station (Figs. N-9 and N-10) gave a record that was limited by band edge on the high-sensitivity channel but not on the low. The peaks from the low-sensitivity channel, about ±500 g's, were beyond the 200-g range of the gage, so could have been limited by gage range. At about 47 msec there was a reflected signal that was positive (upward) only and that had an amplitude over twice that of the direct signal. The long-time record shows other strong signals at 0.375 and 0.7 sec, the first of which was seen on the record of the horizontal gage and the second not.

The tangential accelerometer record shows an initial counterclockwise motion followed by a clockwise return (Fig. N-11). The cable failed about 1.5 msec after signal arrival. Only the negative peak of the high-sensitivity channel was limited by band edge, but all four peaks were beyond range of the 200-g gage used.

Vector sum of velocity versus time for the 24-m station is shown in Fig 6.19, and has been carried only to the time of cable failure on two of the three gages used. Peak vector sum velocity was 1.85 m/sec, of which the major amount, 1.56 m/sec, was contributed by the radial component. Thus at this station, departures from spherical shock propagation as a result of medium inhomogeneities were small relative to those on other shots.

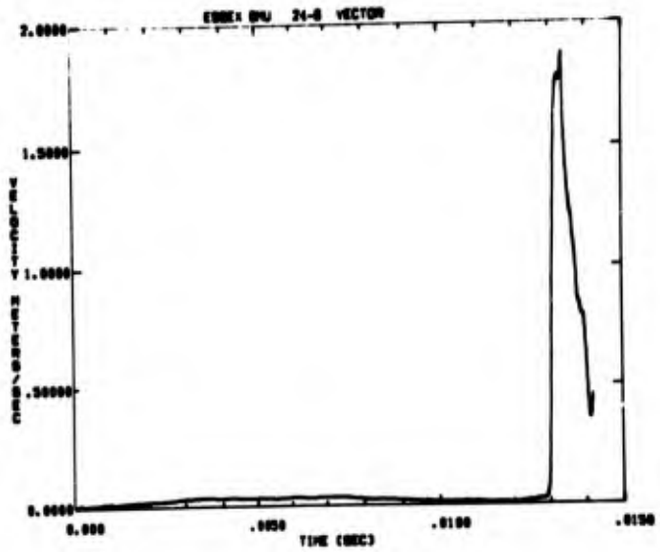

Figure 6.19 Vector sum of radial, vertical, and tangential components of velocity as a function of time at the 24-m station

Two horizontal radial accelerometers were installed at the 36-m station. All four channels (Figs. N-12 through N-15) indicated peaks greater than the 200-g range of the gages used. Both sensitivities of the low-range gage and the high-sensitivity channel of the high-range gage were limited by band edge. The low-sensitivity channel of the high-range gage indicated a peak velocity

of 1.5 m/sec. Since this is comparable to the peak velocity recorded on the other three channels, it is concluded that band-edge limiting did not degrade those records appreciably and that gage over-ranging would affect all four channels equally and by an amount that would be small because of the short duration of the acceleration pulse.

Peak vertical accelerations also were beyond gage range (Figs. N-16 and N-17), and again the effect is judged small for the same reason. The high-sensitivity channel was limited slightly by band edge. Peak vertical velocity was about half the horizontal radial.

Horizontal tangential accelerations were within band edge and only slightly beyond gage range (Figs. N-18 and N-19). Initial peak velocity was comparable to the vertical peak.

Three-second records of the three components are shown in Figs. N-20 and N-21. The records indicate that motion at 36 m had essentially ceased by 1.5 sec.

Vector sum of velocity versus time is shown in Fig. 6.20. Here the peak was 1.79 m/sec. Since this is essentially the same as at the 24-m station, it suggests that peak-limiting may have been more severe there than at 36 m. Most of the vector sum contribution in Fig. 6.20 came from the radial component, attesting to nearly spherical shock propagation.

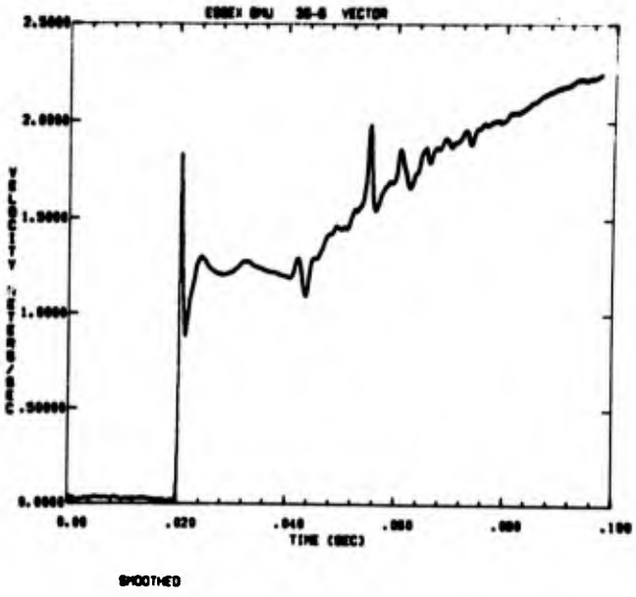

Figure 6.20 Vector sum of radial, vertical, and tangential components of velocity as a function of time at the 36-m station

Figure 6. 21 compares measured particle velocities with those calculated.

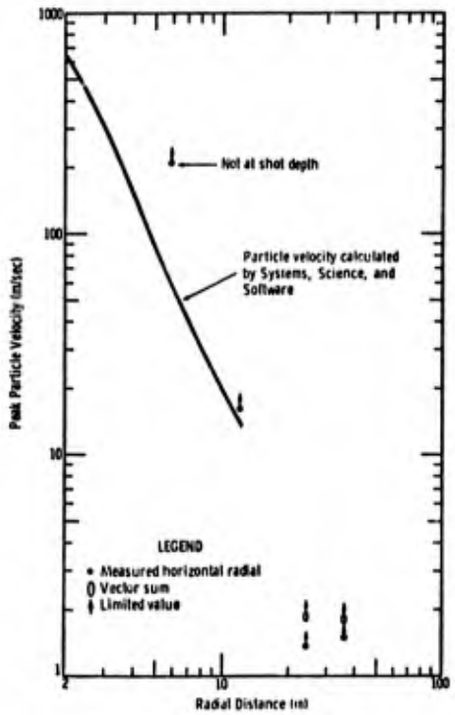

Figure 6. 21 Peak particle velocities measured compared with those calculated

Directly measured peak stresses are compared in Fig. 6. 22 with those derived from peak particle velocities. The stress from peak velocity at half-shot depth is about 3 times larger than that measured directly, in spite of the fact that the record was limited by both band edge and gage range; hence this comparison allows the acceleration record to be judged inaccurate. As noted earlier, agreement at the 12-m station is excellent, confirming that any limiting of the acceleration record was indeed minor. At 24 m the gage with a valid negative phase, though limited, shows values below the trend, indicating that the effect of limiting was severe. From this record with no negative phase, if it is assumed that peak velocity was unaffected, a derived stress above the trend is indicated. All records from 36 m were limited, but it may be assumed that values of peak stress derived from the acceleration records indicate a lower limit. A line through all measurements based on that assumption and judgment is shown in the figure.

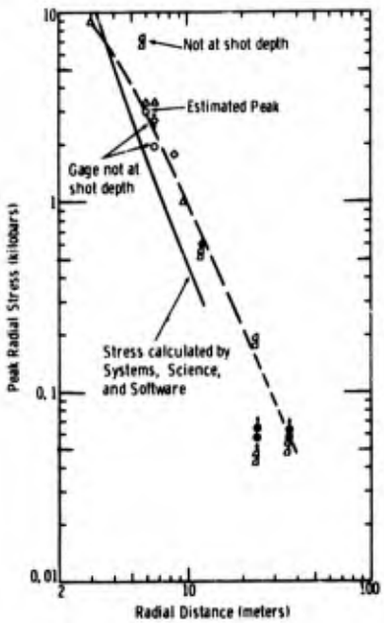

LEGEND

△ SRI Yb DNA 2742F calibration.

○ SLA Yb DNA 2742F calibration.

◇ SLA lithium-niobate.

◭ Stress from measured radial particle velocity.

● Stress from vector sum of measured particle velocity. Double values of ◭ and ● are for densities of 1. 84 and 1. 99 gm/cc for geologic Units 2 and 5, respectively.

Figure 6. 22 Comparison of measured stress and stress derived from peak particle velocity

Surface-Motion Instrumentation

Table 6.4 summarizes surface-motion measurements. Copies of the records and their first and second integrations constitute Appendix O.

Two vertical accelerometers and one horizontal accelerometer were installed at the near-surface zero station. The size of the open hole required that the station be at 1.67 rather than 0.67 m horizontally from SGZ. All four channels of vertical acceleration were beyond band edge (Figs. O-1 and O-2), all had early cable failures, and the two gages provided signals with different durations. Indicated peak acceleration and velocity are not credible. The cable to the horizontal gage survived for only 0.5 msec after shock arrival (Fig. O-3), but provided a good signal to that time with a peak acceleration of about 10,000 g's and a peak velocity of about 10 m/sec. Early cable failures at this station prevented long-time integrations for mound trajectory.

A single vertical accelerometer at 9 m showed peak acceleration of almost 30,000 g's and a peak velocity of almost 70 m/sec at 9 msec (Fig. O-4). It is interesting to compare the acceleration signal for this unstemmed shot with that at the same station on the 6-m stemmed shot (Fig. K-5). Although there the acceleration was superimposed on a transient baseline, the two acceleration signatures are similar.

The vertical accelerometer at the 12-m station showed a peak acceleration preceded by electrical noise which, as in the case of the 6-m stemmed event, can be attributed to arrival at the near-surface-zero station (Fig. O-5). The nature of the record is such that a substantial baseline shift shortly after peak is suspected even though it cannot be identified. Existence of a shift is deduced from the fact that the displacement derived from the 3-sec integration is about 1,000 times the length of the cable from the gage to the junction box. The horizontal gage at the same station experienced failure or cable breakage at signal arrival (Fig. O-6).

A vertical and a horizontal accelerometer were installed at the 18-m station. All signals were within band edge and were very noisy because measured accelerations were such a small percentage of band width (Figs. O-7 and O-8). Vertical and horizontal acceleration peaks were ill-defined because of the noise. Fortunately, integrations suffered little from the noise. Three-second integrations of the vertical and horizontal accelerations (Fig. O-11) permit the canister trajectory to be estimated. The estimation, without any adjustment, is shown by the circles in Fig. 6.23. It is assumed in this unadjusted trajectory that the canister did not rotate. A trajectory that reverses its horizontal direction and moves back into the ejecta plume seems unusual, and this motion may be a result of canister rotation after 2 sec. The unadjusted trajectory was compared with the boundary of the ejecta plume at 2.0 and 2.6 sec as obtained from high-speed photography. This plume had a very strong vertical component, and it can be seen from comparison with Fig. 5.8 that at 1.4 sec the plume from 6 MS had already spread horizontally as much as it had by 2.6 sec on 6 MU. Thus, the trajectory is not an unreasonable one in the light of photographic measurements.

A

TABLE 6.4

Summary of Surface Acceleratio
ESSEX I 6 MU 24 October
17,275 Pounds Nitromethane Buried 6 Me

Accelerometer Designation	Accelerometer Orientation	Distance (m)	Depth (m)	Slant Distance (m)	Gage Range	Gage Limit (g's)	Gage Sensitivity
0-0 AV-LO	Vertical	1-2/3	2/3	5.59	Low Low	50,000 50,000	High Low
0-0 AV-HI	Vertical	1-2/3	2/3	5.59	High High	100,000 crystal 100,000 crystal	High Low
0-0 AH	Horizontal	1-2/3	2/3	5.59		50,000 50,000	High Low
9-0 AV	Vertical	9	2/3	10.52		100,000 crystal 100,000 crystal	High Low
12-0 AV	Vertical	12	2/3	13.19		50,000 50,000	High Low
12-0 AH	Horizontal	12	2/3	13.19		20,000 20,000	High Low
18-0 AV	Vertical	18	2/3	18.83		30,000 30,000	High Low
18-0 AH	Horizontal	18	2/3	18.83		20,000 20,000	High Low
24-0 AV	Vertical	24	2/3	24.63		20,000 20,000	High Low
24-0 AH	Horizontal	24	2/3	24.63		10,000 10,000	High Low

(a) Failed at 7.91 msec

(b) Failed at 7.26 msec

(c) Failed at 9.68 msec

(d) Indeterminate

(e) Values not credible

B

TABLE 6.4

ry of Surface Acceleration Measurements
SSEX I 6 MU 24 October 1973
Nitromethane Buried 6 Meters Deep, Unstemmed

Limit 's)	Gage Sensitivity	Calibration Step (g's)	Arrival Time (msec)	Peak Acceleration (g's)	Time of Peak (msec)	Peak Velocity (m/sec)	Time of Peak (msec)
,000	High	40,283	2.50	>78,500			
,000	Low	40,283	2.55	>300,000 (e)	~2.80	>1,220 (e)	3.11 (a)
,000 tal	High	100,000	2.99	>16,000		>5,000 (e)	(b)
,000 tal	Low	100,000	2.92	>300,000 (e)		>8,200 (e)	>7.0
,000	High	10,000	2.52	10,000	2.64	10	2.73
,000	Low	10,000	~2.55	11,300	2.62	11.8	2.72
,000 tal	High	50,000	5.75	>27,400	6.00	68.5	9.1
,000 tal	Low	50,000	5.62	(d)	6.19	65	9.15
000	High	1,000	9.77	>2,000	~11.23		
000	Low	1,000	9.43	~1,500			
,000	High	696	9.50				(c)
,000	Low	696	9.54				(c)
,000	High	500	~15	~99	24.87		
,000	Low	500	~15	~140	~25		
,000	High	466.7	~15	~25	~25		
,000	Low	466.7	(d)	(d)	(d)	(d)	
000	High	500	~20	~30		2.22	~49
000	Low	500	~20	~32	~27		
000	High	246.7	~20	(c)	~27	2.20	50
000	Low	246.7	~25	(d)			

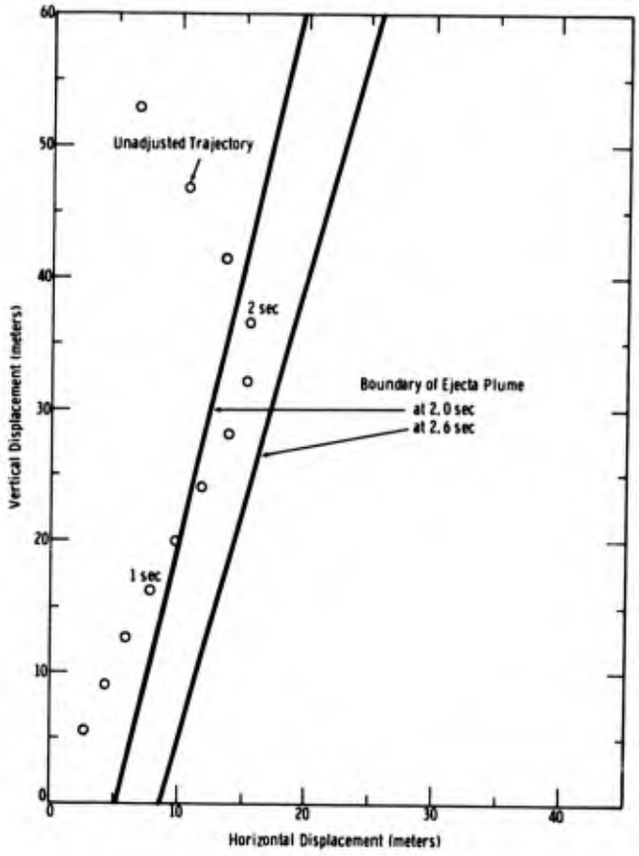

Figure 6.23 Canister trajectory for the 18-meter surface station

An attempt at adjustment using a ballistic trajectory in the same manner as was done on 6 MS yielded an adjusted trajectory that was in such great disagreement with the photography that it was discarded. It is obvious from the unadjusted trajectory that the horizontal component is too large from about 1 to 2.2 sec, and too small thereafter. However, since the trajectory is not changing in a characteristic manner, no assumption is available on which a logical adjustment can be based. It is difficult to believe the canister moved inward after 2 sec, and by trial-and-error, based on arbitrary assumptions of canister rotation, one could probably produce an adjusted trajectory that remained a small distance inside the boundary of the ejecta plume.

Records from both sensitivities of the vertical and horizontal accelerometers at the 24-m station have been included in Figs. O-9, O-10, O-12, and O-13. This has been done to illustrate a point. Note in Fig. O-12 that the second integration yields displacement-time curves that are essentially the same for both sensitivities of vertical acceleration. This is in contrast to the horizontal component, where at cable failure at 2.4 sec the high-sensitivity record integrates to a displacement of 10.96 m, whereas the low-sensitivity record shows 22.1 m. Although this is a difference of a factor of 2, it comes about from a baseline shift of only 0.95 g. This would amount to 0.22 percent of half band width for the high-sensitivity gage but only 0.07 percent for the low-sensitivity

gage. Since such a shift is a more stringent requirement for the low-sensitivity channel, it is judged that the high-sensitivity channel is the more credible.

Figure 6.24 shows the trajectory obtained from the high-sensitivity channels of both components. The figure shows an upthrust of about 1.3 m at about 0.6 sec, followed by a fall that continues through the point of origin and downward into the crater, indicating again the instantaneous shear failure of the material. After the canister has passed through its original position, canister rotation is highly probable, so the trajectory is qualitatively correct even if not quantitatively so. It can be noted, however, that even without correction for canister rotation, its position at 2.4 sec when the cable broke is 14 m from the origin, whereas the cable had an estimated 15 m of slack. This makes the trajectory seem credible.

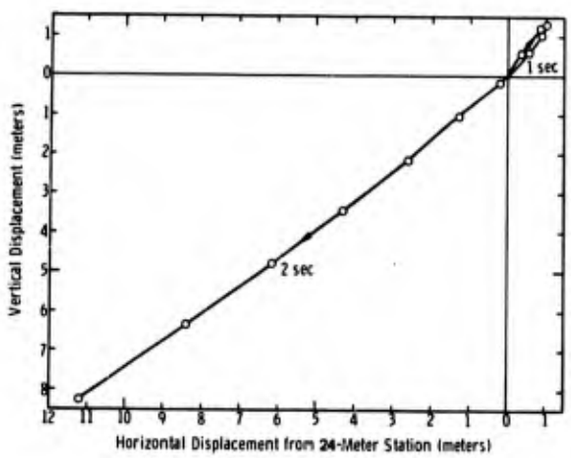

Figure 6.24 Canister trajectory for 24-meter surface station

Surface Displacement from Photography

Table 6.5 summarizes the cameras used to record surface motion and the plume emerging from the open hole. Figure 6.25 shows the plan view of the camera station and reference markers with respect to SGZ.

On the 12-m partially stemmed shot the material emerging from the open hole was highly incandescent, over-exposing film with normal lens openings and requiring lens filters for resolution of the flare. On the 6-m unstemmed shot, none of the material emerging from the larger open hole was luminescent. Adequate resolution was obtained with customary exposures, and film from cameras with lens filters was useless. The incandescent flare observed on 12 MPS could have been enhanced by reflections from the aluminum tubing that lined the hole. An incandescent flare was observed on the M-9 unstemmed shot and the M-16 partially stemmed shot of the Middle Course II series, where no aluminum tubing was involved. It is speculated here that pulverized material from the concrete lid over the explosive cooled the gases below the point of incandescence by the time the plume emerged from the hole.

TABLE 6.5

Summary of Camera Coverage 6 MU

Camera	Timing (cps)	Camera Speed (fps)	Lens	Film	Field of View				f Stop
					Height		Width		
					Feet	Metres	Feet	Metres	
Fastax 16 mm	1000	4000	6 in.	Plus X	20.4	6.22	27.2	8.29	8.0
Fastax 16 mm	1000	4000	6 in.	Plus X	20.4	6.22	27.2	8.29	16.0
Hycam 16 mm	1000	4000	6 in.	Plus X	20.4	6.22	27.2	8.29	13.5
Hycam 16 mm	1000	4000	5 in.	Plus X	24.5	7.47	32.7	9.97	16.0
Fastax 16 mm	1000	8000	4 in.	Plus X	15.5	4.72	40.9	12.47	11.0
Hycam 16 mm	1000	12000	3 in.	Plus X	20.5	6.25	54.5	16.61	16.0
Fastax 16 mm	1000	1200	3 in.	Plus X	20.5	6.25	54.5	16.61	16.0
Fairchild 16 mm	1000	1000	3 in.	Plus X	40.9	12.47	54.5	16.61	4.0
Fastax 16 mm	1000	1000	3 in.	Plus X	40.9	12.47	54.5	16.61	5.6
Hycam 16 mm	1000	12000	2 in.	Plus X	30.6	9.33	81.8	24.93	11.4
Fastax 16 mm	1000	1200	2 in.	Plus X	31.0	9.45	81.8	24.93	12.0
Fastax 16 mm	1000	4000	2 in.	EF	61.3	18.68	81.8	24.93	4.0
Milliken 16 mm	100	500	1 in.	EF	122.7	37.40	163.6	49.87	5.6
Milliken 16 mm	100	128	10 mm	EF	306.7	93.48	409.0	124.7	8.0
Milliken 16 mm	100	500	1 in.	EF	600.0	182.9	800.0	243.8	11.0
Milliken 16 mm	100	128	15 mm	EF	1200.0	365.8	1600.0	487.7	6.3

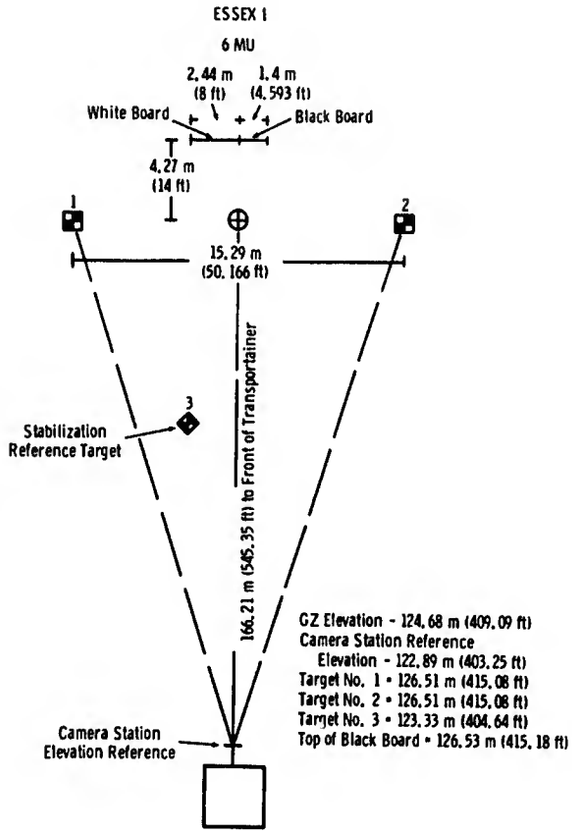

Figure 6.25 Camera station (plan view)

Figure 6.26 shows development of the plume. The sequence starts at 1.8 msec and runs at a rate of about 0.9 msec per frame. Later development is shown in Fig. 6.27. The plume reached a height of 95 m at about 75 msec. Figure 6.28 shows the displacement-time history of the top of the plume. The initial velocity of the plume as measured by Camera 4 was about 2000 m/sec. Camera 7 indicates a lower initial velocity because of inaccuracy of ground-surface profile definition on the film with the larger field of view. After 8 msec, however, the velocity is about 1800 m/sec, approaching that seen by Camera 4.

Vertical displacement of the ground surface, obtained from Cameras 4 and 7, is shown in Fig. 6.29 for a point near SGZ. The plume emerging from the open hole prevented observation precisely at ground zero. The base of the plume spread horizontally for a short distance over the surface. The point read was the intersection of the surface and the base of the plume and may represent a point a few meters in front of SGZ. Figures 6.30 and 6.31 show vertical displacement at 9, 12, 18, and 24 m. In the latter two cases, a comparison is made with displacement derived from the vertical accelerometer at that distance. Particularly at 24 m, the resolution from a camera with a wide enough field of view to include that station results in considerable inaccuracy where maximum displacements are as small as 1 to 3 m. At these stations displacements from the accelerometers are preferred.

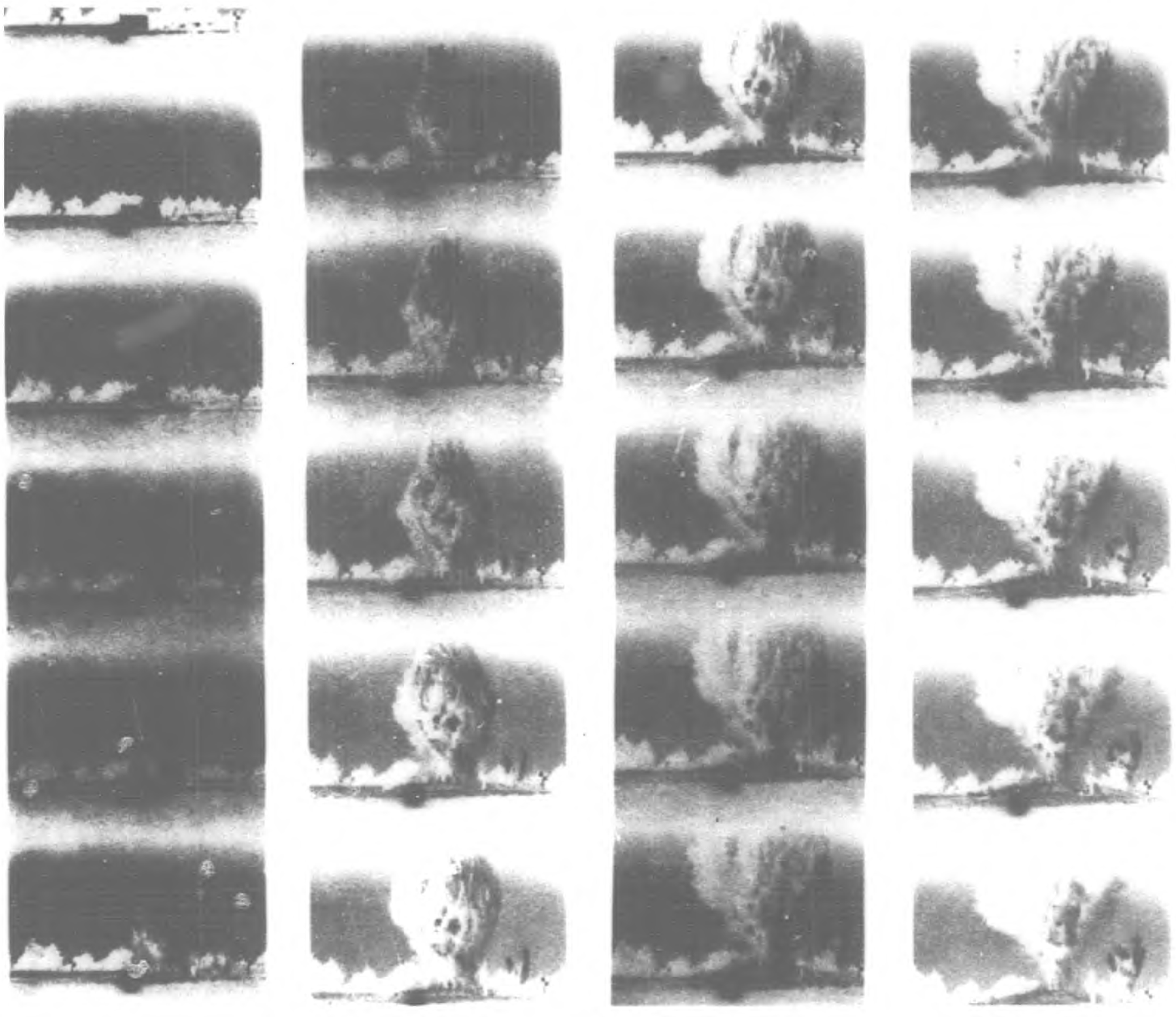

Figure 6.26 Early development of plume

Figure 6.27 Later development of plume from 0.058 sec to 0.082 sec

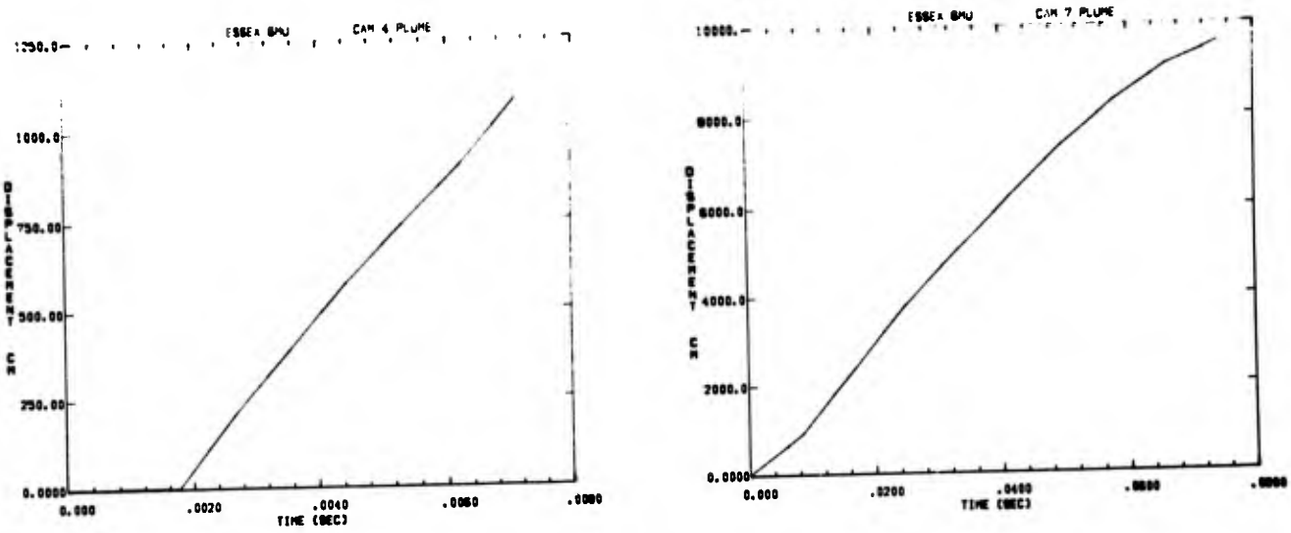

Figure 6.28 Vertical displacement of plume top from two separate cameras

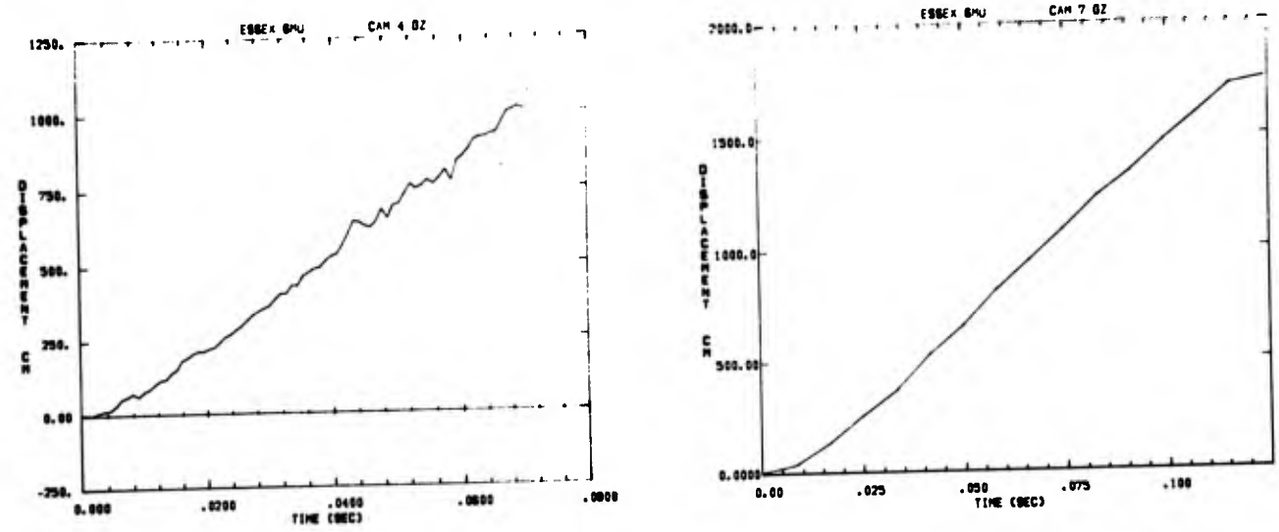

Figure 6.29 Vertical displacement of base of plume from two separate cameras

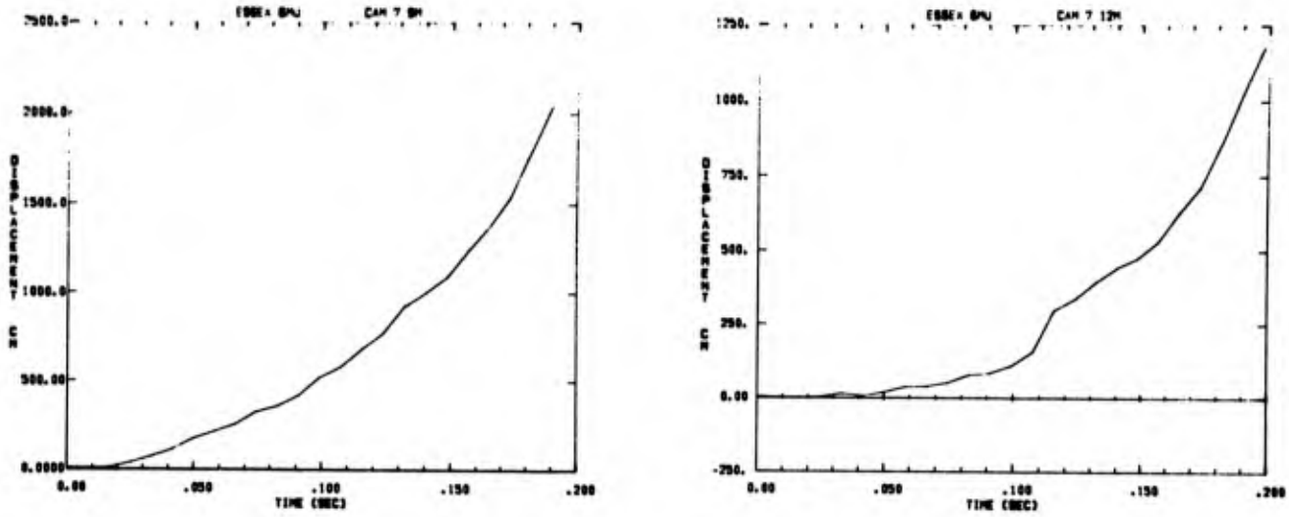

Figure 6.30 Vertical displacement of ground surface at 9 and 12 meters

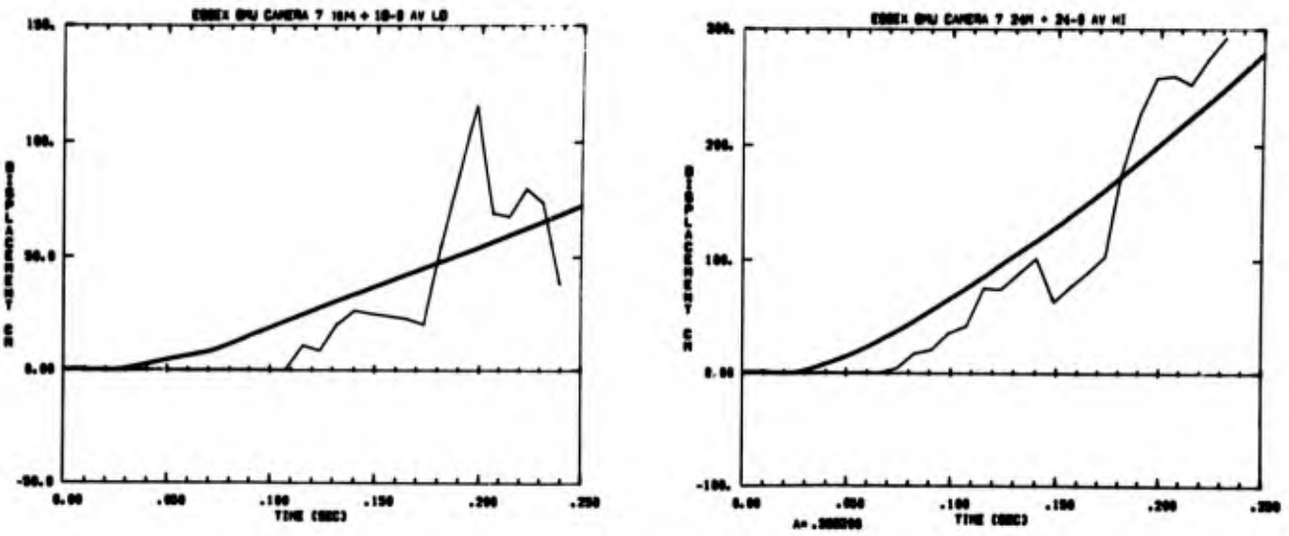

Figure 6.31 Vertical displacement from photography of ground surface at 18 and 24 meters, compared with that from accelerometers

With results from all shots in hand, it is in order at this point to make comparisons with the earlier shots. In Fig. 6.32 the surface-zero displacement versus time from camera data is presented for all four shots. The results are precisely what might have been predicted. First, there was essentially no difference between the two 12-meter shots, indicating that 12 MPS behaved as a stemmed shot and that the small open hole had no appreciable effect on surface motion. Surface motion for 6 MS was more than three times that for the 12-meter shots, as would be expected because of the shallower burial depth. By comparison with 6 MS, 6 MU shows noticeably less displacement, indicating that appreciable energy was lost up the large open hole, and was thus not available for kinetic energy in the ground.

Fig. 6.33 shows the height of the smoke plume as a function of time for the two unstemmed shots. The one from 12 MPS rises relatively slowly and stops rising at about 45 m. The plume from 6 MU rises rapidly and was still rising when its top went beyond the frame of the pictures. In the plot for 12 MPS there would have been a point at 0.04 second, but at that time the plume occupied so small a portion of the frame that a height could not be determined. For the same reason, the height at 0.08 second is somewhat uncertain.

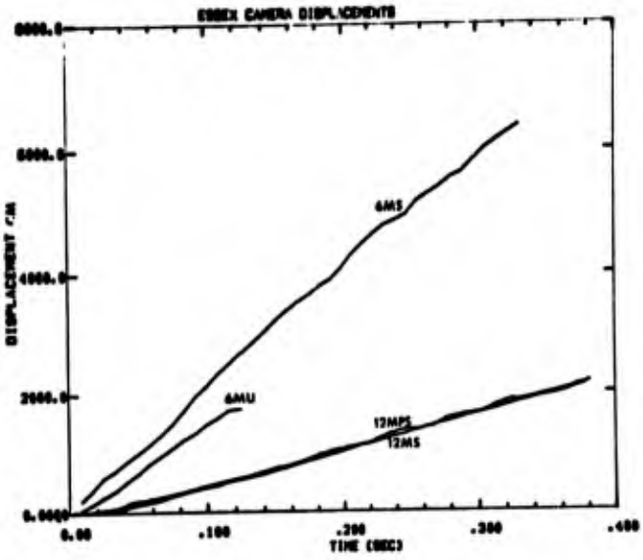

Figure 6.32

Comparison of ground-zero surface displacements from each of the four shots

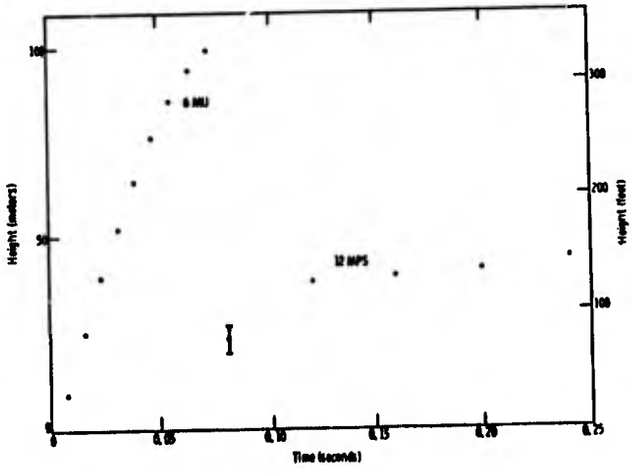

Figure 6.33

Height of smoke plume for 12 MPS and 7 MU versus time

Airblast Measurements

Tables 6.6 and 6.7 summarize the results of airblast measurements, and the records are reproduced in Appendix P. Sandia measurements were made at three stations generally east of the shot at distances of 0.987, 2.314, and 5.878 km (3238, 7592, and 19285 feet). Sandia also recorded airblast from gages installed by BRL at 4.57, 10.67, 13.41, 17.07, 26.21, and 167.63 m (15, 35, 44, 56, 86, and 550 feet). Gages were not all on the same azimuth, the azimuths being 1.087, 1.136, 1.222, 1.168, 1.222, and 1.222 rad, respectively. There was one gage at each station except for Station 5, where there were two.

Waveforms at the SL stations (Figs. P-1, P-2, and P-3) were as would be expected from a shot with a large open hole; each had a large flare* spike superimposed on the regular ground-shock-induced peak. At Station SLA-2 the negative pulse following the gas-venting pulse was especially small, apparently because of interference with another pulse arriving along a different path. While more information will be presented in Chapter 7, it is pointed out here that the flare peak overpressure was three to four times that of the ground-shock-induced peak of 6 MS, whereas the impulse from both the flare and the ground-shock induction of 6 MU was less than that in the ground-shock-induced impulse of 6 MS. Thus, although the spike produced much higher peak overpressures, it contained little impulse. Both gas-venting peak overpressure and gas-venting impulse of 6 MU were less than those of the 6-m stemmed shot. This suggests that gases escaping up the open hole reduce gas reservoir pressure, which eventually erupts through the mound.

No record was obtained for the BRL second station, and BRL Station 6 has a record all but obscured by what appears to be about 60-Hz noise on the carrier (see Fig. P-6). The signal can be seen more clearly on the impulse-time plot at about 450 msec. The record from the closest BRL station (Fig. P-4) shows signal arrival at 4 msec and gage failure at 4.7 msec. Arrival time is consistent with arrival time for a ground-shock-induced pulse, but the peak overpressure recorded is much too high to be consistent with ground-surface particle velocities. If the gage was not malfunctioning, the signal must have come from a flare pulse. Since peak pressure in the open hole appears to have been about 480 bars (6940 psi), attenuation of such a short-duration pulse to about 100 bars (1430 psi) at 4.57 m (15 feet) is credible. A plot of overpressure-distance along the BRL line indicates a different attenuation rate between the first two stations than beyond.

*We use the word "flare" to identify pulses from gases emerging up the open hole, even though the emerging material was not incandescent.

A

TABLE 6.6

Summary of Airblast Me
(Metric Unit
ESSEX I 6 MU 24
17,275 Pounds Nitromethane Buried 6

Gage Designation	SIA 1-LO	SIA 1-HI	SIA 2-LO	SIA 2-HI	SIA 3-LO
Gage Range	Low	High	Low	High	Low
Gage Sensitivity	High	Low	High	Low	High
Distance (m)	987.	987.	2314.	2314.	5878.
Azimuth (rad)	1.515	1.515	1.517	1.517	1.417
Time of Arrival of Flare Pulse (s)	2.803	2.803	6.559	6.559	16.880
Flare Peak Pressure (Pa)	810.8	872.2	457.1	451.6	95.84
Time of Flare Peak Pressure (s)	2.809	2.809	6.566	6.566	16.899
Time of Crossover (s)	2.858	2.859	6.793	6.791	17.126
Flare Impulse (Pa-s)	19.58	20.75	9.239	9.308	2.799
Negative Peak Pressure (Pa)	122.0	158.6	56.05	57.50	19.93
Time of Negative Peak Pressure (s)	3.101	3.149	6.913	6.913	17.264
Time of Crossover (s)	3.353	3.354	7.094	7.095	17.516
Negative Impulse (Pa-s)	20.75	21.99	8.756	9.101	3.185
Time of Arrival of Gas Venting Pulse (s)	3.670	3.669	7.448	7.448	17.767
Gas Venting Peak Pressure (Pa)	134.4	162.7	67.78	67.02	17.31
Time of Gas Venting Peak Pressure (s)	3.742	3.742	7.554	7.529	17.891
Time of Crossover (s)	3.891	3.889	7.655	7.654	17.989
Gas Venting Impulse (Pa-s)	21.10	21.86	11.17	10.07	2.930
Negative Peak Pressure (Pa)	79.29	96.53	36.82	45.78	11.10
Time of Negative Peak Pressure (s)	4.000	3.968	7.759	7.755	18.094
Time of Crossover (s)	4.134	4.135	7.879	7.875	19.3
Negative Impulse (Pa-s)	7.515	8.894	3.241	3.723	2.854

TABLE 6.6

mary of Airblast Measurements
(Metric Units)
I 6 MU 24 October 1973
tromethane Buried 6 Meters Deep, Unstemmed

-HI	SLA 3-LO	SIA 3-HI	BRL 1	BRL 3	BRL 4	BRL 5	BRL 5A
	Low	High	Low	Low	Low	Low	High
	High	Low	High	High	High	High	Low
	5878.	5878.	4.572	13.411	17.069	26.213	26.213
	1.417	1.417	1.087	1.222	1.168	1.222	1.222
	16.880	16.881	.004	.0303	.0392	.0608	.0623
	95.84	94.46		60026.	33908.	23959.	25407.
	16.899	16.899		.0306	.0395	.0611	.0643
	17.126	17.126				.1008	.0788
	2.799	2.820				242.0	234.4
	19.93	20.89				47250.	3178.
	17.264	17.259				.3333	.0861
	17.516	17.452					
	3.185	3.110					
	17.767	17.767					
	17.31	16.13					
	17.891	17.869					
	17.989	17.989					
	2.930	3.075					
	11.10	13.17					
	18.094	18.094					
	19.3	19.6					
	2.854	2.606					

A

TABLE 6.7

Summary of Airblast Me
(English Units
FSSEX I 6MU 24
17,275 Pounds Nitromethane Buried

Gage Designation	SLA 1-LO	SLA 1-HI	SLA 2-LO	SLA 2-HI	SLA 3-LO
Gage Range	Low	High	Low	High	Low
Gage Sensitivity	High	Low	High	Low	High
Distance (Ft)	3238.	3238.	7592.	7592.	19285.
Azimuth (Degrees)	86.8	86.8	86.9	86.9	81.2
Time of Arrival of Flare Pulse (Sec)	2.803	2.803	6.559	6.559	16.880
Flare Peak Pressure (PSI)	.1176	.1265	.0663	.0655	.0139
Time of Flare Peak Pressure (Sec)	2.809	2.809	6.566	6.566	16.899
Time of Crossover (Sec)	2.858	2.859	6.793	6.791	17.126
Flare Impulse (PSI-Sec)	.00284	.00301	.00134	.00135	.000406
Negative Peak Pressure (PSI)	.0177	.0230	.00813	.00834	.00289
Time of Negative Peak Pressure (Sec)	3.101	3.149	6.913	6.913	17.264
Time of Crossover (Sec)	3.353	3.354	7.094	7.095	17.516
Negative Impulse (PSI-Sec)	.00301	.00319	.00127	.00132	.000462
Time of Arrival of Gas Venting Pulse (Sec)	3.670	3.669	7.448	7.448	17.767
Gas Venting Peak Pressure (PSI)	.0195	.0236	.00983	.00972	.00251
Time of Gas Venting Peak Pressure (Sec)	3.742	3.742	7.554	7.529	17.891
Time of Crossover (Sec)	3.891	3.889	7.655	7.654	17.989
Gas Venting Impulse (PSI-Sec)	.00306	.00317	.00162	.00146	.000425
Negative Gas Venting Peak Pressure (PSI)	.0115	.0140	.00534	.00664	.00161
Time of Negative Peak Pressure (Sec)	4.000	3.968	7.759	7.755	18.094
Time of Crossover (Sec)	4.134	4.135	7.879	7.875	19.3
Negative Impulse (PSI-Sec)	.00109	.00129	.00047	.00054	.000414

B

TABLE 6.7

mary of Airblast Measurements
(English Units)
I 6MU 24 October 1973
Nitromethane Buried 6 Meters Deep, Unstemmed

I	SLA 3-LO	SLA 3-HI	BRL 1	BRL 3	BRL 4	BRL 5	BRL 5A
	Low	High	Low	Low	Low	Low	High
	High	Low	High	High	High	High	Low
	19285.	19285.	15.0	44.0	56.0	86.0	86.0
	81.2	81.2	62.3	70.0	66.9	70.0	70.0
	16.880	16.881	.004	.0303	.0392	.0608	.0623
	.0139	.0137		8.706	4.918	3.475	3.685
	16.899	16.899		.0306	.0395	.0611	.0643
	17.126	17.126				.1008	.0788
	.000406	.000409				.0351	.0340
	.00289	.00303				6.853	.461
	17.264	17.259				.3333	.0861
	17.516	17.452					
	.000462	.000451					
	17.767	17.767					
	.00251	.00234					
	17.891	17.869					
	17.989	17.989					
	.000425	.000446					
	.00161	.00191					
	18.094	18.094					
	19.3	19.6					
	.000414	.000378					

CHAPTER 7

AIRBLAST

Two subjects are treated in this chapter. First, the results of airblast measurements on five surface and near-surface bursts of 1000-pound (453.6-kg) spheres of cast TNT made for the Air Force Weapons Laboratory (AFWL) are reported. Second, the results of the Essex I airblast measurements are analyzed further and the suppression of airblast as an indicator of suppression of radioactivity is examined further.

AFWL Series

Table 7.1 summarizes the five shots in the AFWL series. On each shot airblast was measured by two gages at each of three stations. The distances from the shots to the stations and the principal parameters measured are summarized in Tables 7.2 through 7.5. Records of airblast measurements are presented in Appendix Q.

TABLE 7.1

Summary of AFWL Shots

Event	Date	Time	Temperature (°C)	Wind Direction	Wind Velocity (m/sec)	Charge Location
AFWL-1	9-24-73	12:44	28.33	S	3.58	
AFWL-2	9-25-73	09:41	26.67	SE	3.58	
AFWL-3	9-27-73	12:50	29.44	ESE	1.79	
AFWL-4	9-26-73	13:40	30.56	SE	2.68	
AFWL-5	9-29-73	12:38	26.11	SE	0.45	

In Figs. 7.1 through 7.4 the peak overpressures, positive-phase impulses, peak negative pressures, and negative impulses are plotted versus distance for the five shots. Lines connect the data at each station. Ordinarily the data from both the high- and low-range gages are in excellent agreement. Where there was a disparity the reason was sought. If one was found it served as a basis for biasing the line in favor of one of the two data points. If no reason was obvious, lines were fit between values for the low- and high-range gages.

A

TABLE 7.2

Summary of Airblast Uni
(Metric Units)

Shot Number	Gage Designation	Gage Range	Gage Sensitivity	Distance (m)	Azimuth (rad)	Time of Arrival of Pulse (s)*	Peak Overpressure (Pa)	Ti Peak O (
1	STA 1-LO	Low	High	302.	1.90	.8065	2662.	
	STA 1-HI	High	Low	302.	1.90	.8065	2457.	
	STA 2-LO	Low	High	1180.	1.65	3.2815	677.	3
	STA 2-HI	High	Low	1180.	1.65	3.2820	675.	3
	STA 3-LO	Low	High	3006.	1.30	8.4420	252.	8
	STA 3-HI	High	Low	3006.	1.30	8.4420	260.	8
2	STA 1-LO	Low	High	380.	2.12	1.0190	2243.	1
	STA 1-HI	High	Low	380.	2.12	1.0190	2093.	1
	STA 2-LO	Low	High	1229.	1.73	3.4300	828.	3
	STA 2-HI	High	Low	1229.	1.73	3.4305	734.	3
	STA 3-LO	Low	High	3017.	1.34	8.5245	221.	8
	STA 3-HI	High	Low	3017.	1.34	8.5250	240.	8
3	STA 1-LO	Low	High	393.	2.70	1.0470	2256.	1
	STA 1-HI	High	Low	393.	2.70	1.0470	2053	1
	STA 2-LO	Low	High	1114.	1.89	3.0945	809.	3
	STA 2-HI	High	Low	1114.	1.89	3.0950	678.	3
	STA 3-LO	Low	High	2832.	1.38	8.0015	203.	8
	STA 3-HI	High	Low	2832.	1.38	8.0015	211.	8
4	STA 1-LO	Low	High	422.	2.52	1.1245	2437.	1
	STA 1-HI	High	Low	422.	2.52	1.1245	2291.	1
	STA 2-LO	Low	High	1184.	1.86	3.2840	780.	3
	STA 2-HI	High	Low	1184.	1.86	3.2840	712.	3
	STA 3-LO	Low	High	2910.	1.38	8.1715	254.	8
	STA 3-HI	High	Low	2910.	1.38	8.1710	260	8
5	STA 1-LO	Low	High	393.	2.28	1.0700	1632.	1
	STA 1-HI	High	Low	393.	2.28	1.0700	1553.	1
	STA 2-LO	Low	High	1213.	1.78	3.4335	474.	3
	STA 2-HI	High	Low	1213.	1.78	3.4340	375.	3
	STA 3-LO	Low	High	2979.	1.36	8.5065	121.	8
	STA 3-HI	High	Low	2979.	1.36	8.5065	128.	8

* Reading accuracy for time is ±.0005 second

B

TABLE 7.2

Summary of Airblast Units
(Metric Units)

Peak Overpressure (Pa)	Time of Peak Overpressure (s)*	Time of Crossover (s)*	Positive Impulse (Pa - s)	Negative Peak Overpressure (Pa)	Time of Negative Peak Overpressure (s)*	Time of Crossover (s)*	Negative Impulse (Pa - s)
2662.	.8095	.8450	44.7	1126.	.8790	.9345	49.5
2457.	.8090	.8455	43.1	1098.	.8783	.9155	46.5
677.	3.2900	3.3245	13.0	314.	3.3785	3.4040	15.2
675.	3.2903	3.3235	12.3	322.	3.3775	3.4045	14.5
252.	8.4625	8.4875	6.28	148.	8.5443	8.5760	8.83
260.	8.4615	8.4865	6.47	159.	8.5430	8.5755	9.10
2243.	1.0220	1.0613	42.3	916.	1.1150	1.1790	47.3
2093.	1.0220	1.0620	41.4	941.	1.1147	1.1805	47.0
828.	3.4365	3.4790	14.3	308.	3.5520	3.5650	16.7
734.	3.4370	3.4800	13.4	292.	3.5528	3.5650	16.0
221.	8.5400	8.5885	5.27	112.	8.6550	8.6780	6.12
240.	8.5385	8.5888	5.57	122.	8.6528	8.6780	6.46
2256.	1.0500	1.0953	45.5	768.	1.1423	1.2120	42.9
2053	1.0505	1.0920	39.6	920.	1.1435	1.2120	56.4
809.	3.0990	3.1455	18.1	308.	3.2070	3.2785	19.6
678.	3.1020	3.1460	15.9	283.	3.2035	3.2790	17.4
203.	8.0140	8.0640	5.85	105.	8.1223	8.1730	6.29
211.	8.0118	8.0635	6.17	115.	8.1206	8.1730	6.69
2437.	1.1280	1.1733	44.9	699.	1.2105	1.2995	42.3
2291.	1.1280	1.1715	43.6	713.	1.2105	1.3270	44.0
780.	3.2895	3.3375	17.0	271.	3.3820	3.4720	17.7
712.	3.2910	3.3378	16.2	252.	3.3723	3.4725	17.2
254.	8.1880	8.2225	6.17	81.	8.2788	8.3500	5.94
260	8.1890	8.2225	6.39	94.	8.2860	8.3480	6.10
1632.	1.0748	1.1160	36.7	891.	1.1735	1.2045	43.3
1553.	1.0768	1.1170	37.5	1020.	1.1733	1.2040	42.3
474.	3.4440	3.4880	14.4	3	3.5515	3.5815	16.0
375.	3.4425	3.4873	11.6	259.	3.5425	3.5798	13.0
121.	8.5193	8.5650	3.99	96.	8.6398	8.6570	4.36
128.	8.5253	8.5640	4.17	121.	8.6400	8.6540	4.51

TABLE 7.3

Summary of Airblast Measure
(Metric Units)

Shot Number	Gage Designation	Gage Range	Gage Sensitivity	Distance (Ft)	Azimuth (Degrees)	Time of Arrival of Pulse (sec)*	Peak Overpressure (PSI)	Time of Peak Overpre (sec)*
1	Sta 1-LO	Low	High	992.	108.8	.8065	.3861	.8095
	Sta 1-HI	High	Low	992.	108.8	.8065	.3564	.8090
	Sta 2-LO	Low	High	3873.	94.4	3.2815	.0982	3.2900
	Sta 2-HI	High	Low	3873.	94.4	3.2820	.0979	3.2903
	Sta 3-LO	Low	High	9863.	74.7	8.4420	.0365	8.4625
	Sta 3-HI	High	Low	9863	74.7	8.4420	.0377	8.4615
2	Sta 1-LO	Low	High	1245.	121.7	1.0190	.3253	1.0220
	Sta 1-HI	High	Low	1245.	121.7	1.0190	.3035	1.0220
	Sta 2-LO	Low	High	4031.	99.0	3.4300	.1201	3.4365
	Sta 2-HI	High	Low	4031.	99.0	3.4305	.1065	3.4370
	Sta 3-LO	Low	High	9897.	76.8	8.5245	.0321	8.5400
	Sta 3-HI	High	Low	9897.	76.8	8.5250	.0348	8.5385
3	Sta 1-LO	Low	High	1290.	154.8	1.0470	.3272	1.0500
	Sta 1-HI	High	Low	1290.	154.8	1.0470	.2978	1.0505
	Sta 2-LO	Low	High	3655.	108.2	3.0945	.1173	3.0990
	Sta 2-HI	High	Low	3655.	108.2	3.0950	.0984	3.1020
	Sta 3-LO	Low	High	9292.	79.1	8.0015	.0294	8.0140
	Sta 3-HI	High	Low	9292.	79.1	8.0015	.0306	8.0118
4	Sta 1-LO	Low	High	1383.	144.5	1.1245	.3534	1.1280
	Sta 1-HI	High	Low	1383.	144.5	1.1245	.3323	1.1280
	Sta 2-LO	Low	High	3885.	106.5	3.2840	.1132	3.2895
	Sta 2-HI	High	Low	3885.	106.5	3.2840	.1032	3.2910
	Sta 3-LO	Low	High	9548.	79.2	8.1715	.0368	8.1880
	Sta 3-HI	High	Low	9548.	79.2	8.1710	.0377	8.1890
5	Sta 1-LO	Low	High	1288.	130.9	1.0700	.2367	1.0748
	Sta 1-HI	High	Low	1288.	130.9	1.0700	.2253	1.0768
	Sta 2-LO	Low	High	3980.	101.9	3.4335	.0687	3.4440
	Sta 2-HI	High	Low	3980.	101.9	3.4340	.0544	3.4425
	Sta 3-LO	Low	High	9772.	77.8	8.5065	.0175	8.5193
	Sta 3-HI	High	Low	9772.	77.8	8.5065	.0185	8.5253

* Reading Accuracy is ± .0005 seconds.

B

TABLE 7.3

y of Airblast Measurements
(Metric Units)

ure	Time of Peak Overpressure (sec)*	Time of Crossover (sec)*	Positive Impulse (PSI-sec)	Negative Peak Overpressure (PSI)	Time of Negative Peak Overpressure (sec)*	Time of Crossover (sec)*	Negative Impulse (PSI-Sec)
	.8095	.8450	.00649	.1633	.8790	.9345	.00718
	.8090	.8455	.00625	.1593	.8783	.9155	.00675
	3.2900	3.3245	.00188	.0456	3.3785	3.4040	.00220
	3.2903	3.3235	.00178	.0467	3.3775	3.4045	.00210
	8.4625	8.4875	.000911	.0215	8.5443	8.5760	.00128
	8.4615	8.4865	.000938	.0230	8.5430	8.5755	.00132
	1.0220	1.0613	.00614	.1328	1.1150	1.1790	.00686
	1.0220	1.0620	.00600	.1365	1.1147	1.1805	.00681
	3.4365	3.4790	.00207	.0446	3.5520	3.5650	.00242
	3.4370	3.4800	.00195	.0423	3.5528	3.5650	.00232
	8.5400	8.5885	.000765	.0162	8.6550	8.6780	.000887
	8.5385	8.5888	.000808	.0177	8.6528	8.6780	.000937
	1.0500	1.0953	.00660	.1114	1.1423	1.2120	.00622
	1.0505	1.0920	.00575	.1334	1.1435	1.2120	.00818
	3.0990	3.1455	.00263	.0447	3.2070	3.2785	.00284
	3.1020	3.1460	.00231	.0411	3.2035	3.2790	.00253
	8.0140	8.0640	.000848	.0152	8.1223	8.1730	.000912
	8.0118	8.0635	.000895	.0167	8.1206	8.1730	.000970
	1.1280	1.1733	.00651	.1014	1.2105	1.2995	.00614
	1.1280	1.1715	.00632	.1034	1.2105	1.3270	.00643
	3.2895	3.3375	.00247	.0393	3.3820	3.4720	.00256
	3.2910	3.3378	.00235	.0365	3.3723	3.4725	.00250
	8.1880	8.2225	.000895	.0118	8.2788	8.3500	.000861
	8.1890	8.2225	.000927	.0136	8.2860	8.3480	.000885
	1.0748	1.1160	.00532	.1292	1.1735	1.2045	.00628
	1.0768	1.1170	.00544	.1480	1.1733	1.2040	.00614
	3.4440	3.4880	.00209	.0459	3.5515	3.5815	.00232
	3.4425	3.4873	.00168	.0375	3.5425	3.5798	.00189
	8.5193	8.5650	.000578	.0139	8.6398	8.6570	.000633
	8.5253	8.5640	.000605	.0175	8.6400	8.6540	.000654

TABLE 7.4

Summary of Airblast En
(Metric Units)

Shot Number	Gage Designation	Gage Range	Gage Sensitivity	Distance (m)	Azimuth (rad)	Positive Phase Energy Flux (hPa^2 - s)
1	STA 1-LO	Low	High	302.	1.90	7.444
	STA 1-HI	High	Low	302.	1.90	6.684
	STA 2-LO	Low	High	1180.	1.65	0.5552
	STA 2-HI	High	Low	1180.	1.65	0.5120
	STA 3-LO	Low	High	3006.	1.30	0.1155
	STA 3-HI	High	Low	3006.	1.30	0.1227
2	STA 1-LO	Low	High	380.	2.12	5.961
	STA 1-HI	High	Low	380.	2.12	5.557
	STA 2-LO	Low	High	1229.	1.73	0.7074
	STA 2-HI	High	Low	1229.	1.73	0.6123
	STA 3-LO	Low	High	3017.	1.34	0.07829
	STA 3-HI	High	Low	3017.	1.34	0.0818
3	STA 1-LO	Low	High	393.	2.70	6.251
	STA 1-HI	High	Low	393.	2.70	5.029
	STA 2-LO	Low	High	1114.	1.89	0.9108
	STA 2-HI	High	Low	1114.	1.89	0.6883
	STA 3-LO	Low	High	2832.	1.38	0.07934
	STA 3-HI	High	Low	2832.	1.38	0.08376
4	STA 1-LO	Low	High	422.	2.52	6.541
	STA 1-HI	High	Low	422.	2.52	6.109
	STA 2-LO	Low	High	1184.	1.86	0.8110
	STA 2-HI	High	Low	1184.	1.86	0.7107
	STA 3-LO	Low	High	2910.	1.38	0.1115
	STA 3-HI	High	Low	2910	1.38	0.1197
5	STA 1-LO	Low	High	393.	2.28	3.993
	STA 1-HI	High	Low	393.	2.28	3.846
	STA 2-LO	Low	High	1213.	1.78	0.4953
	STA 2-HI	High	Low	1213.	1.78	0.3109
	STA 3-LO	Low	High	2979.	1.36	0.03527
	STA 3-HI	High	Low	2979.	1.36	0.03532

B

TABLE 7.4

mary of Airblast Energy
(Metric Units)

Positive Phase Energy Flux (hPa^2 - s)	Negative Phase Energy Flux (hPa^2 - s)	Total Energy Flux (hPa^2 - s)	Postive Phase Energy (MJ)	Negative Phase Energy (MJ)	Total Energy (MJ)
7.444	4.160	11.65	105.0	58.66	164.3
6.684	3.808	10.55	94.26	53.70	148.8
0.5552	0.3632	0.9317	119.4	78.08	200.3
0.5120	0.3252	0.8509	110.1	69.90	182.9
0.1155	0.1036	0.2372	161.0	144.4	330.7
0.1227	0.1090	0.2510	171.1	151.9	349.9
5.961	3.052	9.080	132.1	67.61	201.1
5.557	3.071	8.652	123.1	68.03	191.7
0.7074	0.3813	1.098	164.3	88.54	255.0
0.6123	0.3451	0.9650	142.2	80.15	224.1
0.07829	0.05182	0.1317	109.6	72.54	184.3
0.0818	0.05586	0.1450	123.5	78.20	203.0
6.251	2.187	8.462	149.4	52.25	202.2
5.029	3.275	8.414	120.2	78.26	201.0
0.9108	0.4302	1.345	174.7	82.52	258.0
0.6883	0.3403	1.032	132.0	65.29	197.9
0.07934	0.04697	0.1274	98.36	58.23	157.9
0.08376	0.05068	0.1360	103.8	62.82	168.5
6.541	2.115	8.652	180.0	58.20	238.1
6.109	2.230	8.319	168.1	61.34	228.9
0.8110	0.3085	1.112	176.1	66.99	243.6
0.7107	0.2909	1.003	154.3	63.17	217.8
0.1115	0.03513	0.1483	146.2	46.07	194.5
0.1197	0.03917	0.1607	157.0	51.37	210.7
3.993	2.833	6.845	94.59	67.11	162.2
3.846	2.657	6.513	91.10	62.95	154.3
0.4953	0.3694	0.8699	112.0	83.55	196.8
0.3109	0.2377	0.5467	70.32	53.76	123.7
0.03527	0.02809	0.06370	48.10	38.31	86.86
0.03532	0.02943	0.06560	48.16	40.12	89.45

A

TABLE 7.5

Summary of Airblast Ener
(Metric Units)

Shot Number	Gage Designation	Gage Range	Gage Sensitivity	Distance (Ft)	Azimuth (Degrees)	Positive Phase Energy Flux (PSI^2 - Sec)
1	STA 1-LO	Low	High	992.	108.8	.001566
	STA 1-HI	High	Low	992.	108.8	.001406
	STA 2-LO	Low	High	3873.	94.4	.0001168
	STA 2-HI	High	Low	3873.	94.4	.0001077
	STA 3-LO	Low	High	9863.	74.7	.00002429
	STA 3-HI	High	Low	9863.	74.7	.00002581
2	STA 1-LO	Low	High	1245.	121.7	.001254
	STA 1-HI	High	Low	1245.	121.7	.001169
	STA 2-LO	Low	High	4031.	99.0	.0001488
	STA 2-HI	High	Low	4031.	99.0	.0001288
	STA 3-LO	Low	High	9897.	76.8	.00001647
	STA 3-HI	High	Low	9897.	76.8	.00001855
3	STA 1-LO	Low	High	1290.	154.8	.001315
	STA 1-HI	High	Low	1290.	154.8	.001058
	STA 2-LO	Low	High	3655.	108.2	.0001916
	STA 2-HI	High	Low	3655.	108.2	.0001448
	STA 3-LO	Low	High	9292.	79.1	.00001669
	STA 3-HI	High	Low	9292.	79.1	.00001762
4	STA 1-LO	Low	High	1383.	144.5	.001376
	STA 1-HI	High	Low	1383.	144.5	.001285
	STA 2-LO	Low	High	3885.	106.5	.0001706
	STA 2-HI	High	Low	3885.	106.5	.0001495
	STA 3-LO	Low	High	9548.	79.2	.00002345
	STA 3-HI	High	Low	9548.	79.2	.00002519
5	STA 1-LO	Low	High	1288.	130.9	.000840
	STA 1-HI	High	Low	1288.	130.9	.000809
	STA 2-LO	Low	High	3980.	101.9	.0001042
	STA 2-HI	High	Low	3980.	101.9	.0000654
	STA 3-LO	Low	High	9772.	77.8	.00000742
	STA 3-HI	High	Low	9772.	77.8	.00000743

B

TABLE 7.5

ry of Airblast Energy
(Metric Units)

Positive Phase Energy Flux (PSI^2 - Sec)	Negative Phase Energy Flux (PSI^2 - Sec)	Total Energy Flux (PSI^2 - Sec)	Positive Phase Energy ($In\text{-}Lb/10^6$)	Negative Phase Energy ($In\text{-}Lb/10^6$)	Total Energy ($In\text{-}Lb/10^6$)
.001566	.000875	.00245	929.2	519.2	1454.
.001406	.000801	.00222	834.3	475.3	1317.
.0001168	.0000764	.000196	1056.0	691.0	1773.
.0001077	.0000684	.000179	974.2	618.7	1619.
.00002429	.00002179	.0000499	1425.0	1278.0	2927.
.00002581	.00002292	.0000528	1514.0	1344.0	3097.
.001254	.000642	.00191	1169.0	598.4	1780.
.001169	.000646	.00182	1090.0	602.1	1696.
.0001488	.0000802	.000231	1454.0	783.7	2257.
.0001288	.0000726	.000203	1259.0	709.4	1984.
.00001647	.00001090	.0000277	970.1	642.0	1632.
.00001855	.00001175	.0000305	1093.0	692.1	1797.
.001315	.000460	.00178	1322.0	462.4	1789.
.001058	.000689	.00177	1064.0	692.6	1779.
.0001916	.0000905	.000283	1546.0	730.4	2284.
.0001448	.0000716	.000217	1169.0	577.8	1751.
.00001669	.00000988	.0000268	870.5	515.3	1398.
.00001762	.00001066	.0000286	919.1	556.0	1492.
.001376	.000445	.00182	1593.0	515.2	2107.
.001285	.000469	.00175	1488.0	542.9	2026.
.0001706	.0000649	.000236	1558.0	592.9	2156.
.0001495	.0000612	.000211	1366.0	559.1	1928.
.00002345	.00000739	.0000312	1294.0	407.8	1722.
.00002519	.00000824	.0000338	1390.0	454.7	1865.
.000840	.000596	.00144	837.2	594.0	1435.
.000809	.000559	.00137	806.3	557.1	1365.
.0001042	.0000777	.000183	991.6	739.4	1742.
.0000654	.0000500	.000115	622.4	475.8	1094.
.00000742	.00000591	.0000134	425.7	339.1	768.8
.00000743	.00000619	.0000138	426.3	355.1	791.7

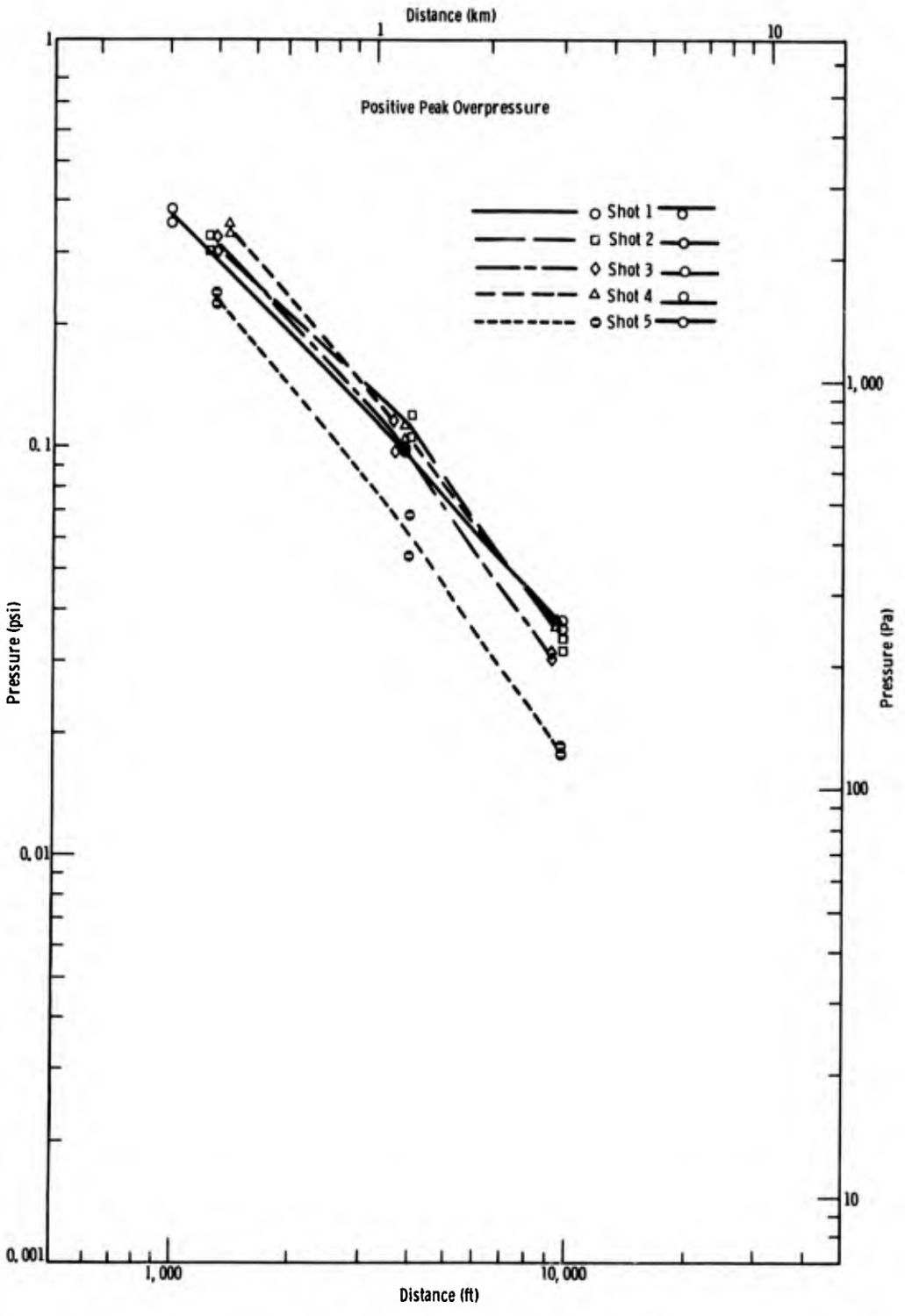

Figure 7.1 Peak overpressure versus distance for AFWL shots

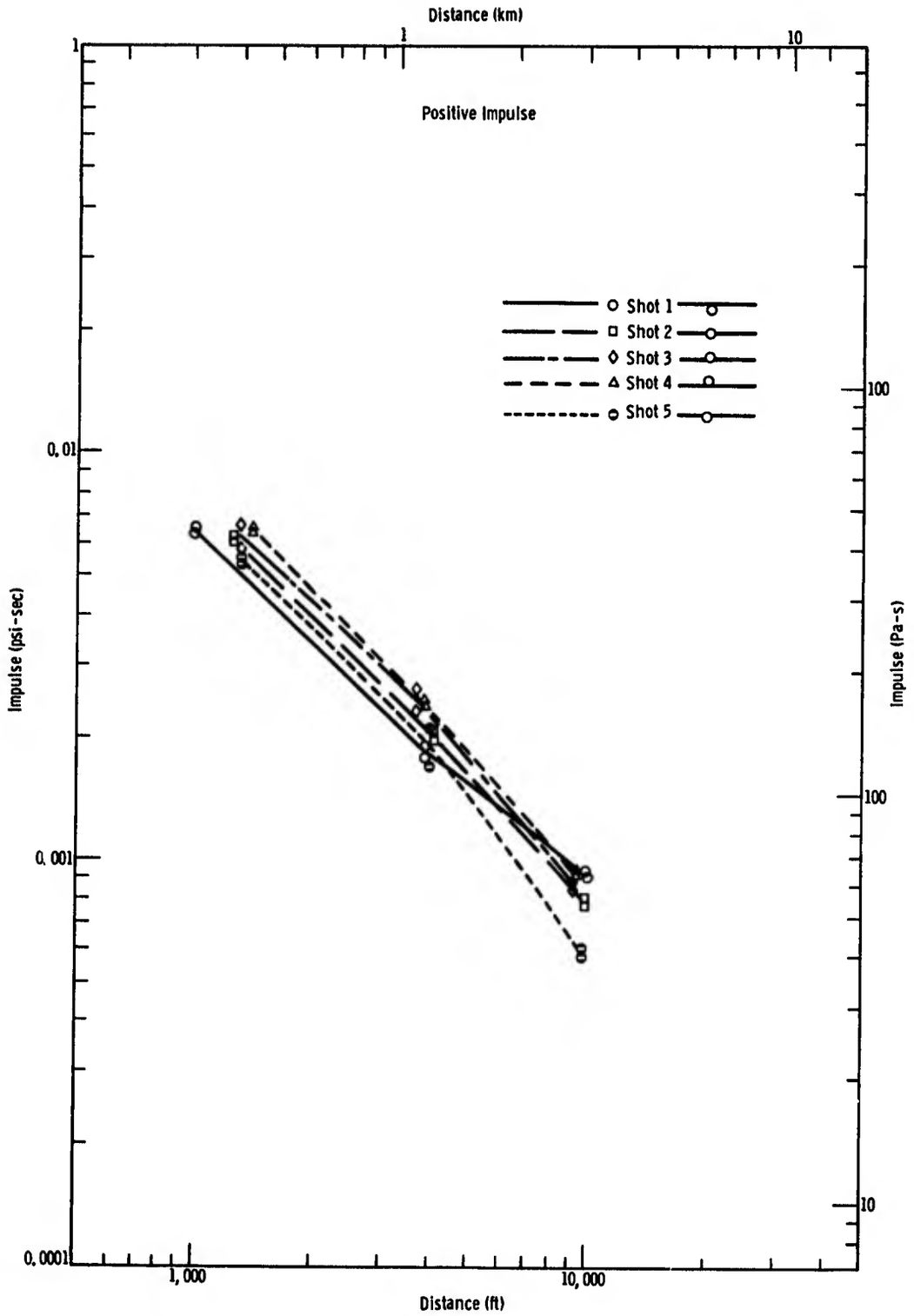

Figure 7.2 Positive impulse versus distance for AFWL shots

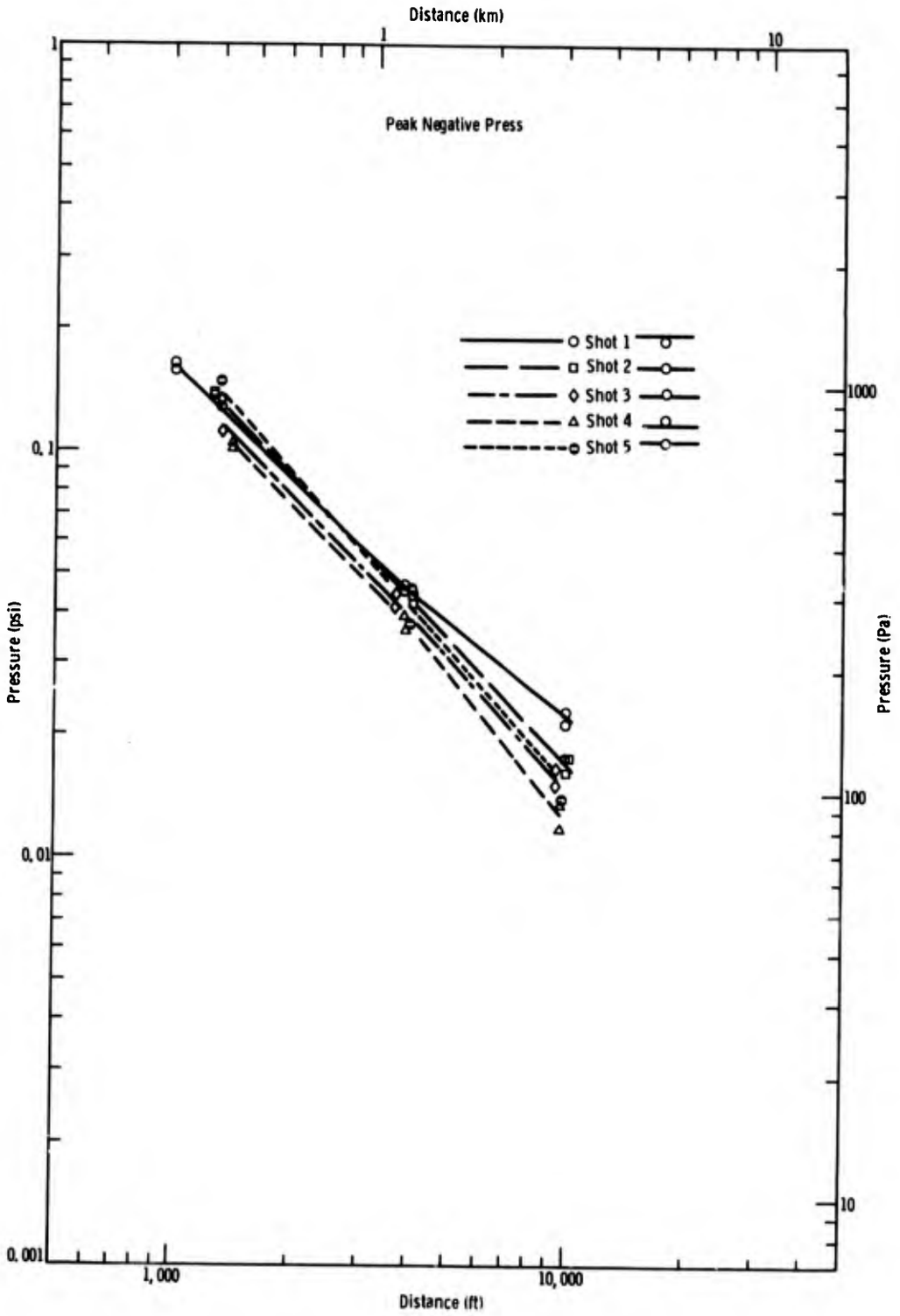

Figure 7.3 Peak negative pressure versus distance for AFWL shots

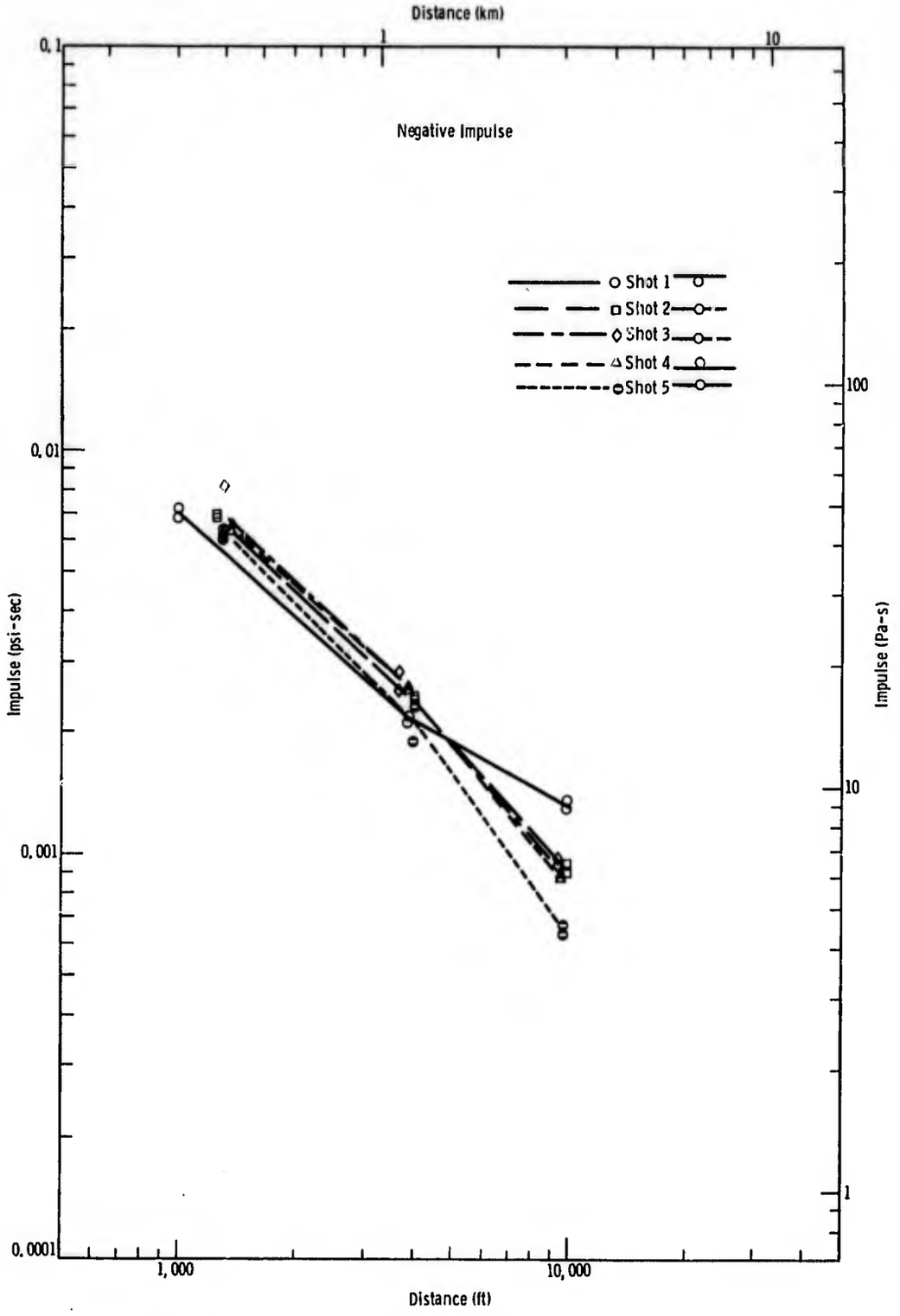

Figure 7.4 Negative impulse versus distance for AFWL shots

If all shots had been detonated under the same meteorological conditions, airblast values should decrease as the position of the charge changes from above ground to below ground; that is, in the following shot order: 4, 3, 2, 5, and 1 (see Table 7.1). If one chooses a distance such as 2,000 feet over which meteorological effects should be smaller than at larger distances, one finds that the actual order for peak overpressure is 4, 2, 3, 1, and 5. Shot 5 peak overpressures are distinctly lower than the others, which differ relatively little. The order for positive-phase impulse, which is a less erratic parameter than peak overpressure, is (Fig. 7.2) 4, 3, 2, 5, and 1 at the same distance--precisely the order that would be expected. Except for shot 1, the order remains the same for positive-phase impulse over the range in which measurements were made. Shot 1 had the largest impulse at the farthest station, presumably because of ducting of focusing meteorology. At 2000 feet the largest impulse is only 34% greater than the smallest. Stated another way, positive-phase impulse from a charge tangent above surface and one tangent below surface was 17% greater and 17% smaller, respectively, than that from a charge half-buried. Trends for peak negative pressure and negative-phase impulse were not nearly as distinct. Attenuation rates of all parameters with distance were close to R^{-1}, not allowing for minor discontinuities in rates.

Three of the 5 shots had charge placement positions exactly the same as those for three of the shots of the Diamond Ore series.[26] It is interesting to make direct comparisons of the peak overpressures and positive-phase impulses of the two series.

Before the Diamond Ore data were added they were scaled from the Fort Peck ambient conditions to those of the Fort Polk series. Ambient temperature was that measured at each site. Ambient pressure was not measured at either site, so standard-atmosphere pressures for the elevation of each site were used. This makes the comparison inaccurate by the amount of day-to-day fluctuations in ambient pressure at the two sites. It is noted that in each case the rate of attenuation is different for otherwise comparable burst conditions.

The results of the comparisons are shown in Figs. 7.5 through 7.10. In each of the figures the airblast parameter from the shots at Fort Peck tends to fall below that at Fort Polk. The differences may result from (1) the fact that ambient airpressure at either or both sites was different from that given by the standard-atmosphere tables, or (2) differences in the explosive used in the two series. Spheres used at Fort Peck were cast by Hawthorne Ordnance Depot while those for Fort Polk were cast by or for the Defence Research Establishment, Suffield, Alberta, Canada. There were differences in charge diameters in the two cases, presumably as a result of differences in charge density, possibly plus minor chemical differences.

Tables 7.4 and 7.5 summarize energy in the airblast from the five shots. Energy flux is the integral of p^2t, and is shown for the positive phase in Fig. 7.11 and for the negative phase in Fig. 7.12. That for the total pulse has not been plotted, but is available from the tables. Note in Fig. 7.11 that the energy flux at 2000 feet follows the sequence of the peak overpressure (Fig. 7.2) rather than the orderly sequence of charge position followed by the positive impulse (Fig. 7.3).

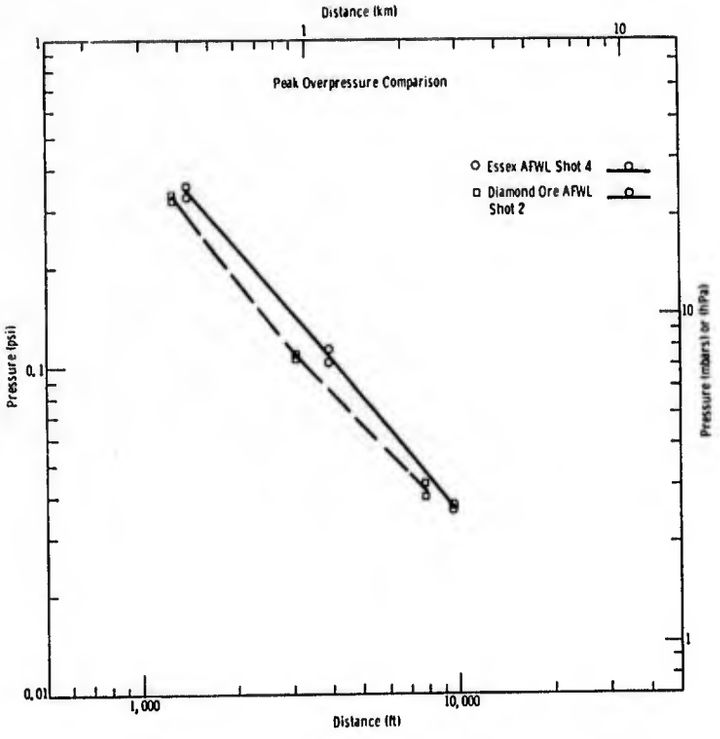

Figure 7.5

Comparison of peak overpressure from Essex and Diamond Ore

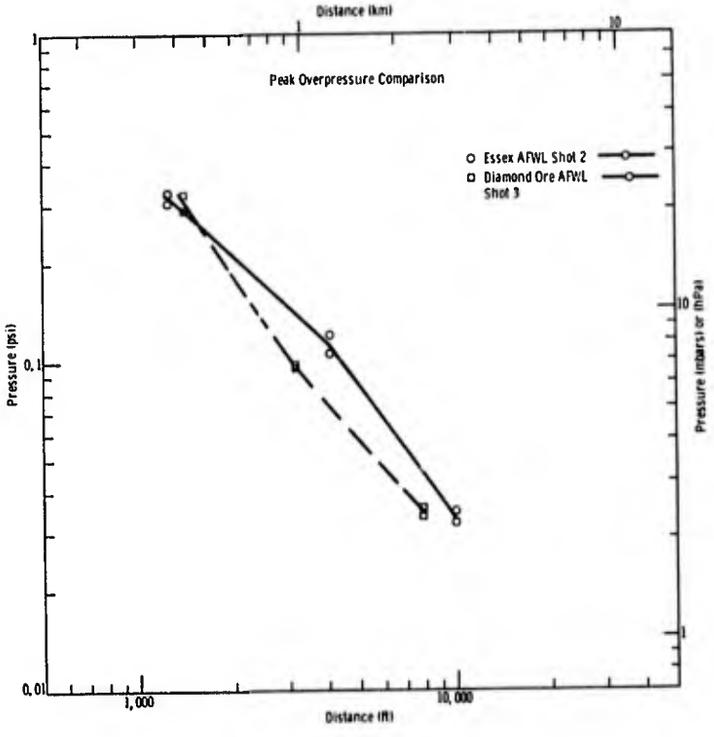

Figure 7.6

Comparison of peak overpressure from Essex and Diamond Ore

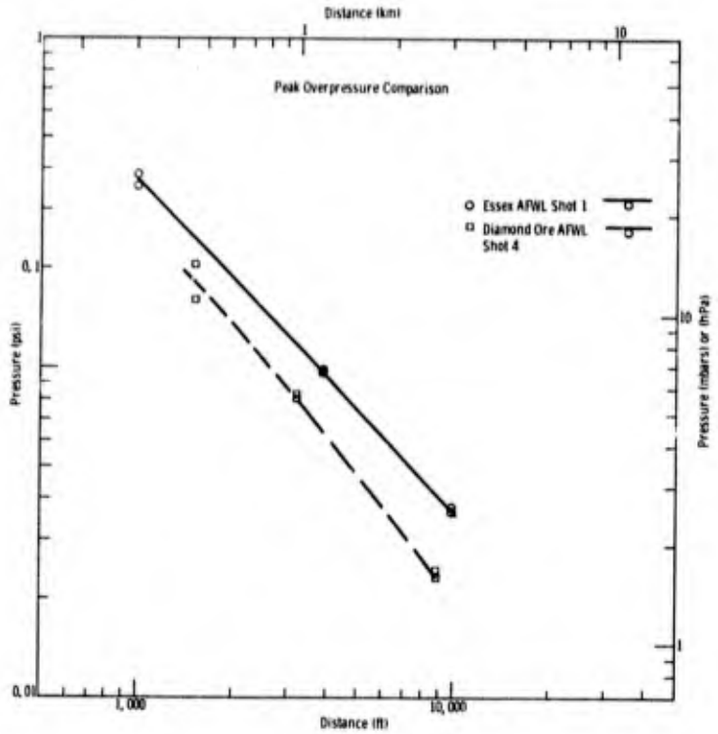

Figure 7.7

Comparison of peak overpressure from Essex and Diamond Ore

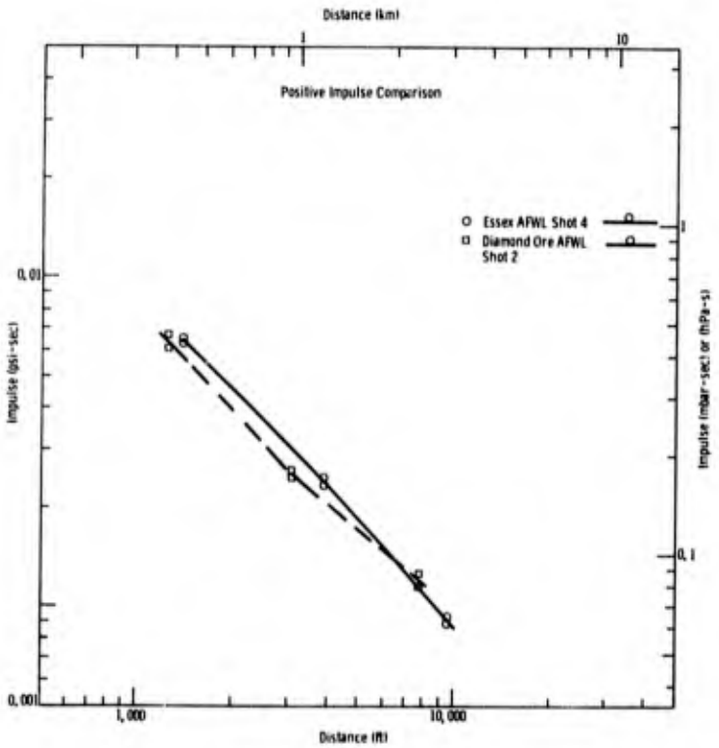

Figure 7.8

Comparison of positive impulse from Essex and Diamond Ore

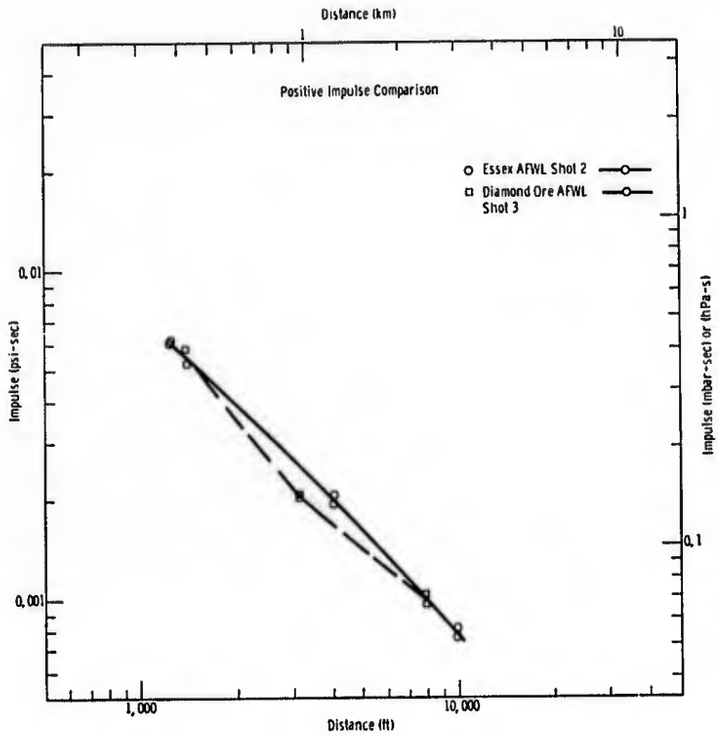

Figure 7.9

Comparison of positive impulse from Essex and Diamond Ore

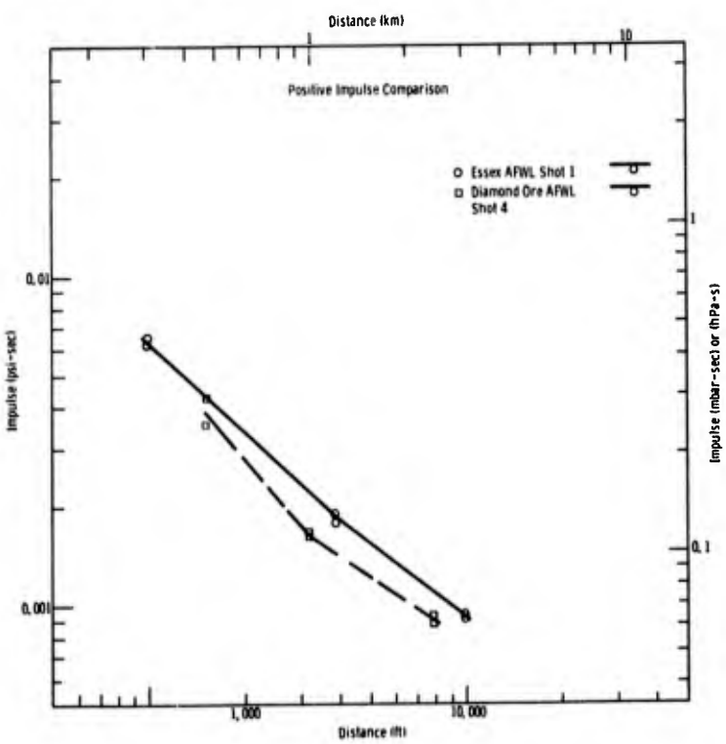

Figure 7.10

Comparison of positive impulse from Essex and Diamond Ore

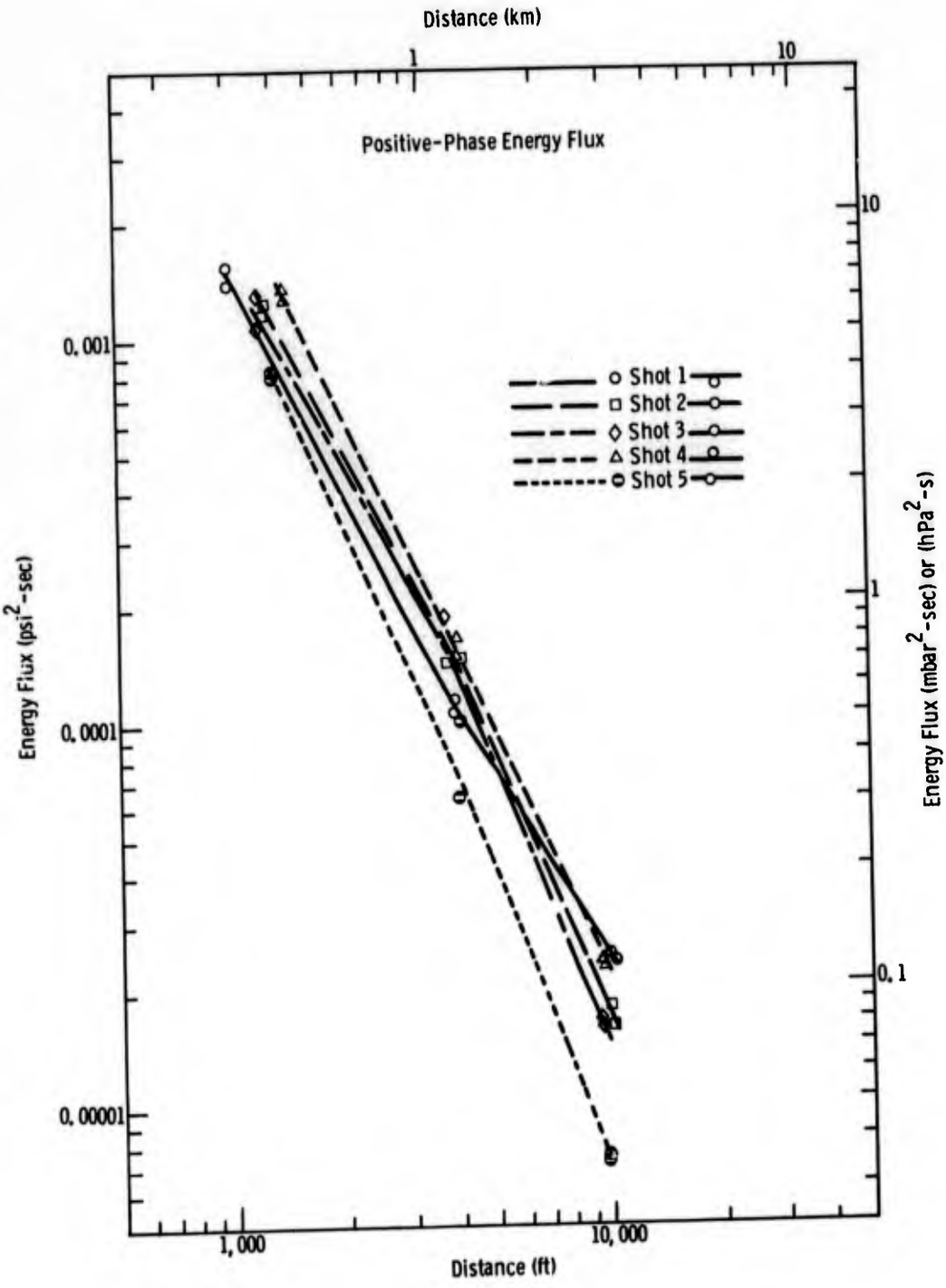

Figure 7.11 Energy flux in the positive phase versus distance

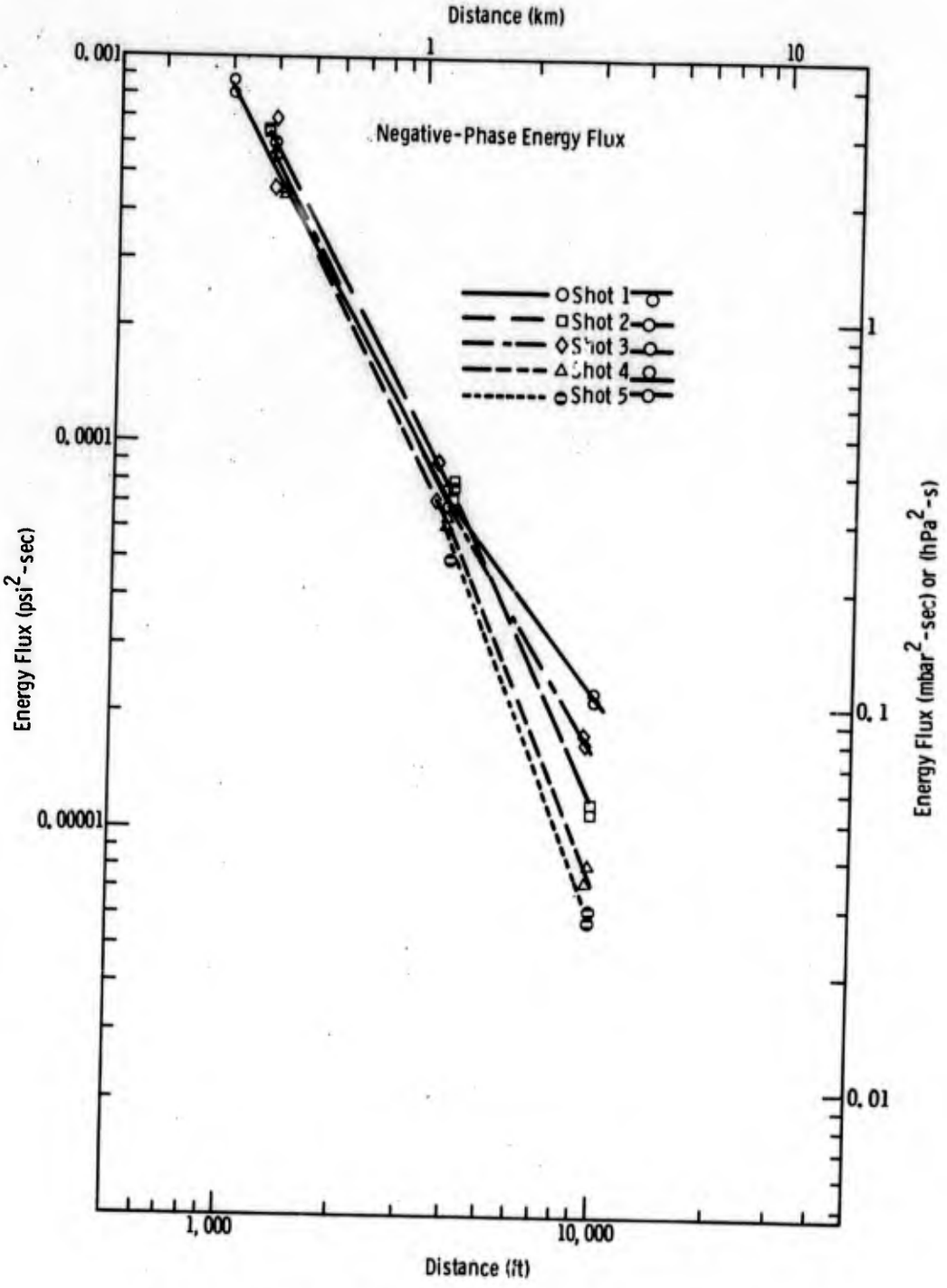

Figure 7.12 Energy flux in the negative phase versus distance

In an infinite homogeneous atmosphere a hemispherical propagation of the airblast envelope from surface and near-surface bursts can be assumed, and the energy flux integrated over the surface of the hemisphere will give energy in the airblast components or in the total airblast wave. If the atmosphere were indeed homogeneous, energy in the airblast wave would be constant as a function of distance except for minor irreversible energy losses. Thus, plots of energy versus distance are an appropriate means of examining effects of meteorology, possible gage measurement inconsistencies, and charge position. Later it will be seen that the energy in the positive phase of AFWL-2 is used to determine airblast suppression from the four charges of the Essex series.

Figures 7.13, 7.14, and 7.15 show energy in the positive and negative phases, and the total airblast wave as a function of distance. The trends with charge position are the same as for energy flux, as they should be, but the trends are more obvious from Fig. 7.13 than, for example, from Fig. 7.11. Positive-phase energy from AFWL-1, which should have been the smallest at all distances, is actually the largest at the farthest station, and is probably an indication of a focusing meteorological structure, or a ducting structure, which prevented hemispherical expansion of the airblast envelope. Positive-phase energy from AFWL-5 is very small at the farthest station, probably indicating a structure that refracted airblast upward away from the ground surface.

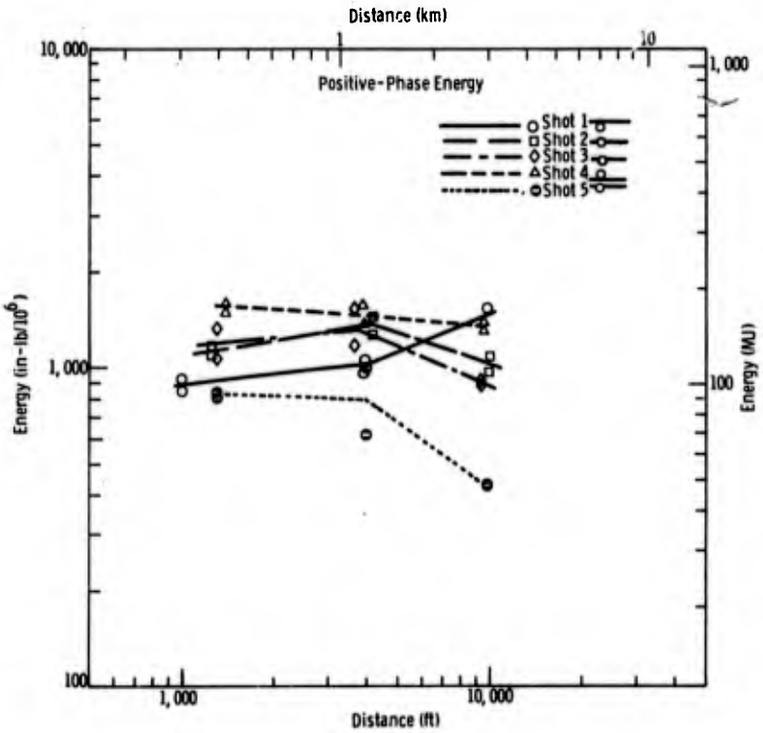

Figure 7.13 Positive-phase energy versus distance

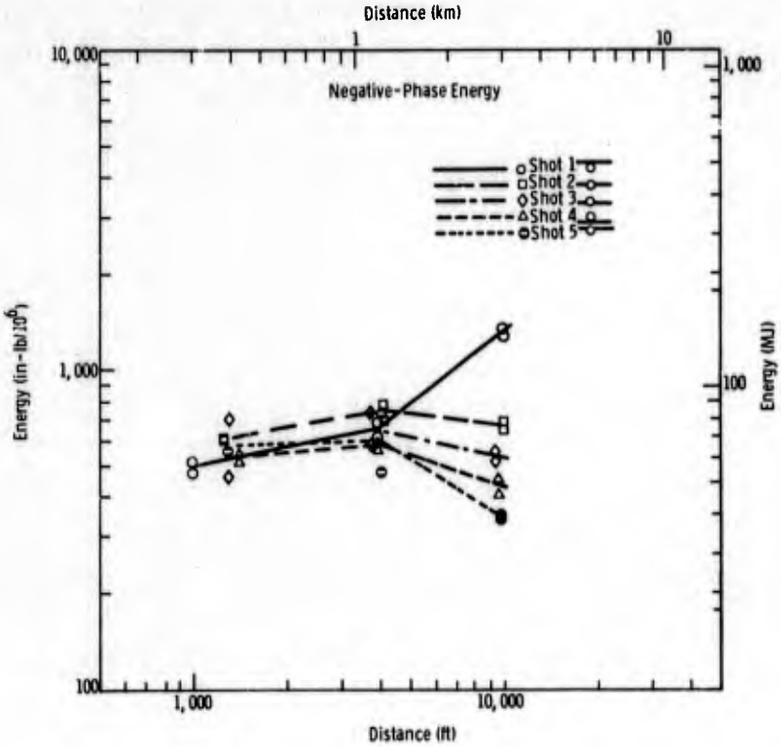

Figure 7.14

Negative-phase energy versus distance

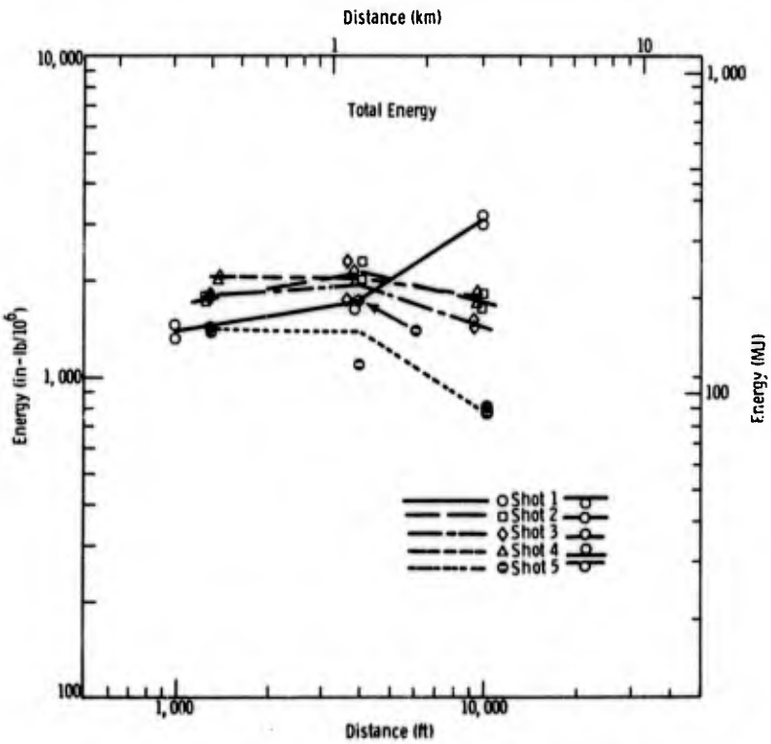

Figure 7.15

Total airblast energy versus distance

The purpose of AFWL in requesting and funding airblast measurements was not made clear, especially in view of past measurements on two similar series.[26,27] Because differences in charge placement with respect to the surface are small, the resulting differences in airblast are subtle. The effects of meteorology, on the other hand, are substantial, and tend to override those resulting from charge position. If in the future the effects of charge position over a small vertical range on airblast are an important objective, it is recommended that all shots be fired during a short period of time on a single day to take advantage of meteorology that is common to all.

Airblast Suppression

In the report on Project Middle Course II,[28] suppression of airblast as a function of charge burial depth and stemming was suggested as a reasonable analogue for suppression of residual radiation from nuclear explosions by burial depth and stemming. The basis for the hypothesis was that explosion gases are the source of both residual radiation and that portion of the airblast wave caused by venting gases. Accordingly, this section first provides further discussion of airblast from the four Essex shots, and then relates those results to airblast and residual radiation suppression.

Tabular summaries of peak overpressure, negative pressure, and positive- and negative-phase impulses were included in tables in each of the four preceding chapters: Tables 3.7 and 3.8 for 12 MS; Tables 4.6 and 4.7 for 12 MPS; Tables 5.6 and 5.7 for 6 MS; and Tables 6.6 and 6.7 for 6 MU. Airblast energy data are summarized in Tables 7.6 through 7.13.

Figure 7.16 presents the ground-shock-induced peak overpressures as a function of distance for the four shots. Note that for the partially stemmed and unstemmed shots the peak has been labeled "flare overpressure." This is because the pressure caused by detonation gases escaping up the open hole as an incandescent flare cause overpressures that coincide timewise with the ground-shock-induced overpressures, are superimposed on them, and the two are inseparable without an assumption. The assumption is that between two shots, one stemmed and one unstemmed, there are no other differences (such as medium differences), and the ground-shock-induced contribution of the stemmed shot can be subtracted from the combined contribution of the unstemmed shot to yield the contribution of gases escaping through the open hole. It is this contribution which must be added to that of the gas-venting pulse to determine the total contribution of explosion gases of unstemmed shots. It is clear from the figure that peaks from 6 MU are greater than from 6 MS and those from 12 MPS greater than those from 12 MS. The same is true for the impulse from the first pulse for the two 12-m shots, but in the case of the 6-m shots, the impulse from the stemmed shot is greater than from the unstemmed shot. This makes the assumption stated above unusable and says that the flare contributes a negative value to escaping gases. What has happened in fact is that the differences in media between the sites of the two shots are so great that the effect of these differences overrides the effect of stemming. Another contributing factor is the negative spike that immediately follows the positive spike from the flare pulse, thus reducing the impulse during the ground-shock-induced phase. In what follows we have attributed to the flare all impulse that occurs

on 6 MU during the time its overpressure exceeds the overpressure on 6 MS. Because this process is not precise, we have not bothered to take into account differences caused by 6 MU having a smaller charge weight than 6 MS, or by the fact that distances to the stations were not the same for the two shots.

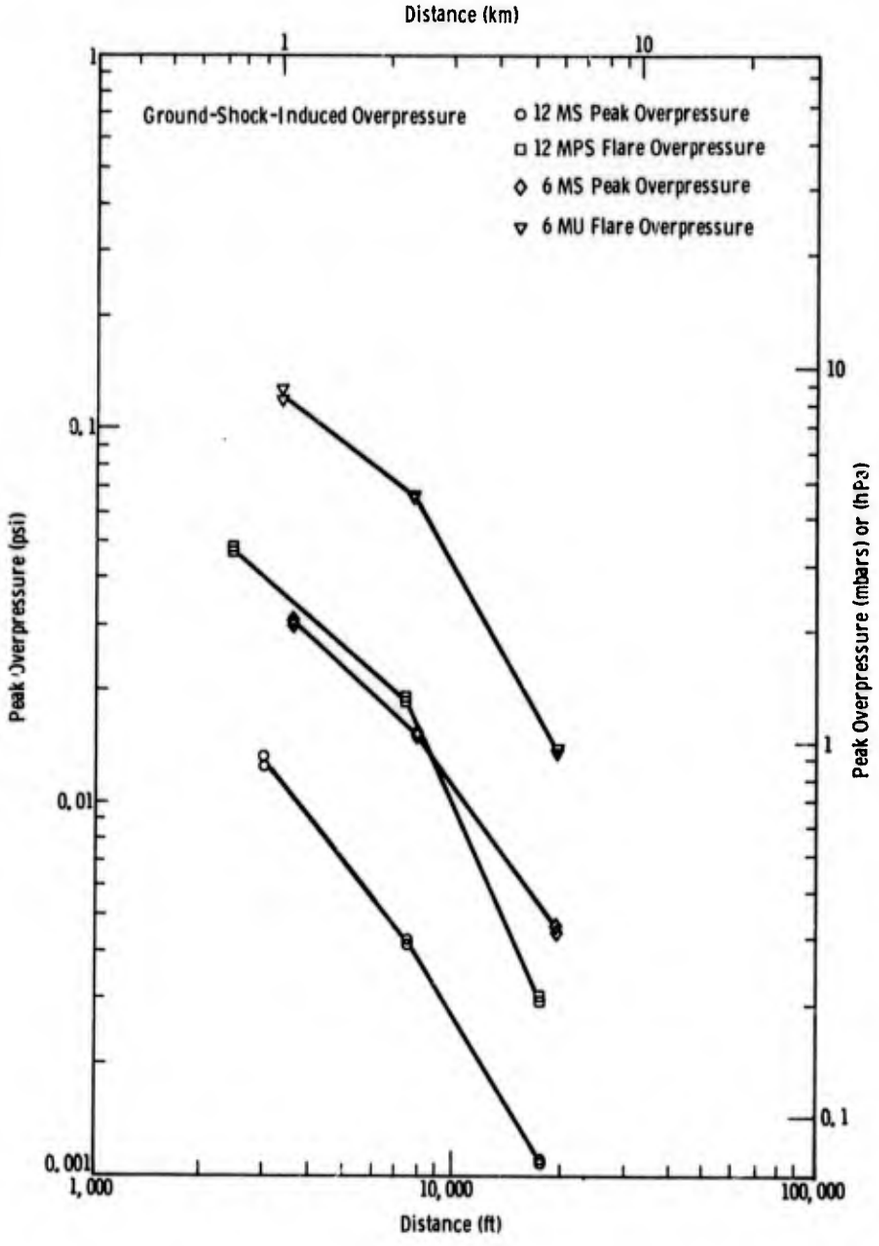

Figure 7.16 Ground-shock-induced peak overpressure versus distance

Notice in Figs. 7.16 and 7.17 that attenuation rates with distance are relatively more uniform for impulse than for peak overpressure, especially on the unstemmed shots. This is because meteorological effects on short-duration pressure spikes are much more pronounced.

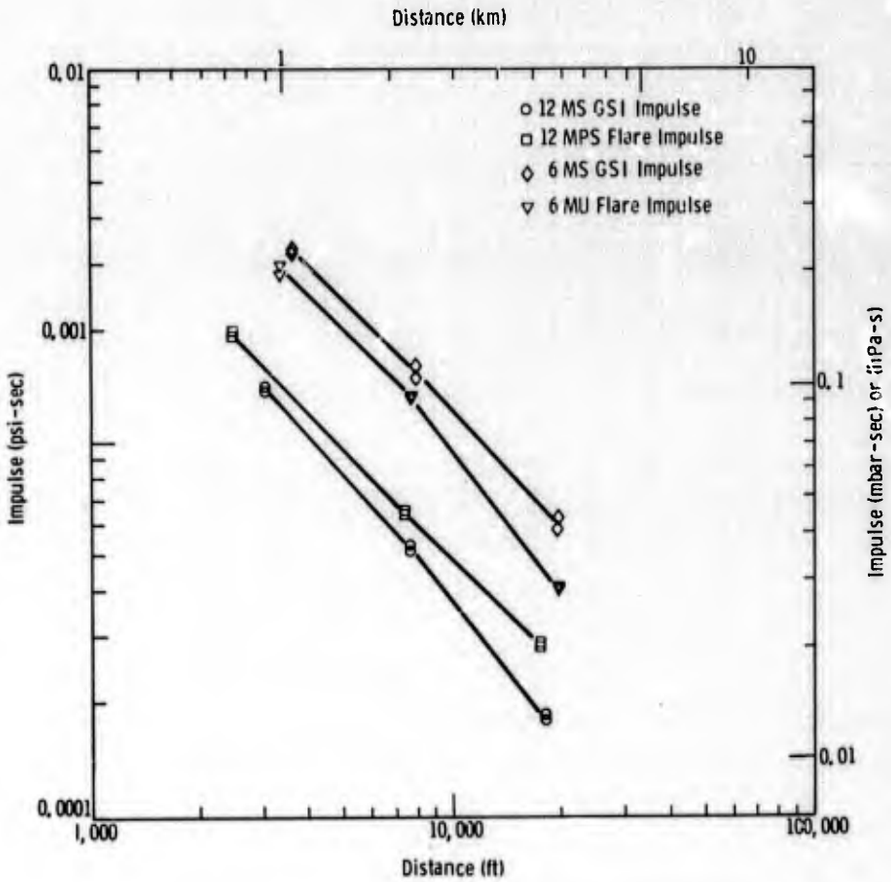

Figure 7.17 Ground-shock-induced impulse versus distance

A

TABLE 7.6

Summary of Airblast E
(Metric Units)
ESSEX I 12 MS 23 Aug
21,594 Pounds Nitromethane Buried 12 Mete

Gage Designation	SLA 1-LO	SLA 1-HI	SLA
Gage Range	Low	High	Lo
Gage Sensitivity	High	Low	Hi
Distance (km)	.903	.903	2.
Azimuth (rad)	1.962	1.962	1.
Ground-Shock-Induced Energy Flux (Pa^2-s)	508.7	480.1	58.
Negative Pulse Energy Flux (Pa^2-s)	532.4	499.1	89.
Gas Venting Energy Flux (Pa^2-s)	204.4	194.9	35.
Total Energy Flux (Pa^2-s)	1322.	1241.	19
Ground-Shock-Induced Energy (MJ)	6.435	6.074	4.7
Negative Pulse Energy (MJ)	6.736	6.315	7.2
Gas Venting Energy (MJ)	2.586	2.466	2.8
Total Energy (MJ)	16.72	15.70	15.

TABLE 7.6

Summary of Airblast Energy
(Metric Units)
EX I 12 MS 23 August 1973
methane Buried 12 Meters Deep, Fully Stemmed

SLA 2-LO	SLA 2-HI	SLA 3-LO	SLA 3-HI
Low	High	Low	High
High	Low	High	Low
2.283	2.283	5.417	5.417
1.602	1.602	1.616	1.616
58.47	55.62	6.227	6.275
89.85	84.14	12.17	12.65
35.18	34.23	4.611	4.659
195.4	186.3	24.39	25.15
4.727	4.497	2.835	2.856
7.264	6.803	5.539	5.755
2.844	2.767	2.099	2.121
15.80	15.06	11.10	11.45

A

TABLE 7.7

Summary of Airblast En
(Metric Units)
ESSEX I 12 MS 23 Augu
21,594 Pounds Nitromethane Buried 12 M

Gage Designation	SLA 1-LO	SLA 1-HI	SLA 2-
Gage Range	Low	High	Low
Gage Sensitivity	High	Low	High
Distance (Ft)	2963.	2963.	7490.
Azimuth (Degrees)	112.4	112.4	91.8
Ground-Shock-Induced Energy Flux (PSI^2-Sec)	.0000107	.0000101	.0000
Negative Pulse Energy Flux (PSI^2-Sec)	.0000112	.0000105	.0000
Gas Venting Energy Flux (PSI^2-Sec)	.0000043	.0000041	.0000
Total Energy Flux (PSI^2-Sec)	.0000278	.0000261	.0000
Ground-Shock-Induced Energy (In-Lb/10^6)	56.96	53.76	41.84
Negative Pulse Energy (In-Lb/10^6)	59.62	55.89	64.29
Gas Venting Energy (In-Lb/10^6)	22.89	21.82	25.17
Total Energy (In-Lb/10^6)	148.0	138.9	139.8

B

TABLE 7.7

ummary of Airblast Energy
(Metric Units)
EX I 12 MS 23 August 1973
romethane Buried 12 Meters Deep, Fully Stemmed

SLA 2-LO	SLA 2-HI	SLA 3-LO	SLA 3-HI
Low	High	Low	High
High	Low	High	Low
7490.	7490.	17772.	17772.
91.8	91.8	92.6	92.6
.00000123	.00000117	.000000131	.000000132
.00000189	.00000177	.000000256	.000000266
.00000074	.00000072	.000000097	.000000098
.00000411	.00000392	.000000513	.000000529
41.84	39.80	25.09	25.28
64.29	60.21	49.02	50.94
25.17	24.49	18.58	18.77
139.8	133.3	98.24	101.3

A

TABLE 7.8

Summary of Airblast Ener
(Metric Units)
ESSEX I 12 MPS 20 Sept
21,594 Pounds Nitromethane Buried 12 Mete

Gage Designation	SLA 1-LO	SLA 1-HI	SLA 2-
Gage Range	Low	High	Low
Gage Sensitivity	High	Low	High
Distance (km)	.7311	.7311	2.2017
Azimuth (rad)	1.484	1.484	1.412
Flare Energy Flux (Pa^2-s)	1526.	1469.	233.4
Negative Pulse Energy Flux (Pa^2-s)	1293.	1350.	136.9
Gas Venting Energy Flux (Pa^2-s)	908.0	893.7	110.8
Total Energy Flux (Pa^2-s)	3727.	3717.	481.1
Flare Energy (MJ)	12.57	12.10	17.44
Negative Pulse Energy (MJ)	10.66	11.13	10.23
Gas Venting Energy (MJ)	7.48	7.37	8.27
Total Energy (MJ)	30.7	30.6	35.9

B

TABLE 7.8

ary of Airblast Energy
(Metric Units)
12 MPS 20 September 1973
thane Buried 12 Meters Deep, Partially Stemmed

	SLA 2-LO	SLA 2-HI	SLA 3-LO	SLA 3-HI
	Low	High	Low	High
	High	Low	High	Low
	2.2017	2.2017	5.3066	5.3066
	1.412	1.412	1.538	1.538
	233.4	219.6	18.49	17.83
	136.9	127.9	25.91	23.58
	110.8	107.4	12.45	12.26
	481.1	455.4	56.86	53.62
	17.44	16.41	8.03	7.74
	10.23	9.56	11.25	10.23
	8.27	8.03	5.41	5.32
	35.9	34.0	24.7	23.3

TABLE 7.9

Summary of Airblast Ener
(Metric Units)
ESSEX I 12 MPS 20 Se
21,594 Pounds Nitromethane Buried 12 Meters

Gage Designation	SLA 1-LO	SLA 1-HI	SLA 2-I
Gage Range	Low	High	Low
Gage Sensitivity	High	Low	High
Distance (Ft)	2399.	2399.	7224.
Azimuth (Degrees)	85.	85.	80.9
Flare Energy Flux (PSI^2-Sec)	.0000321	.0000309	.00000
Negative Pulse Energy Flux (PSI^2-Sec)	.0000272	.0000284	.00000
Gas Venting Energy Flux (PSI^2-Sec)	.0000191	.0000188	.00000
Total Energy Flux (PSI^2-Sec)	.0000784	.0000782	.00001
Flare Energy (In-Lb/10^6)	111.3	107.14	154.37
Negative Pulse Energy (In-Lb/10^6)	94.31	98.47	90.55
Gas Venting Energy (In-Lb/10^6)	66.22	65.18	73.25
Total Energy (In-Lb/10^6)	271.8	271.1	318.2

B

TABLE 7.9

Summary of Airblast Energy
(Metric Units)
ESSEX I 12 MPS 20 September 1973
romethane Buried 12 Meters Deep, Partially Stemmed

-HI	SLA 2-LO	SLA 2-HI	SLA 3-LO	SLA 3-HI
	Low	High	Low	High
	High	Low	High	Low
	7224.	7224.	17411.	17411.
	80.9	80.9	88.1	88.1
09	.00000491	.00000462	.000000389	.000000375
84	.00000288	.00000269	.000000545	.000000496
88	.00000233	.00000226	.000000262	.000000258
82	.00001012	.00000958	.000001196	.000001128
	154.37	145.25	71.04	68.49
	90.55	84.57	99.53	90.58
	73.25	71.05	47.85	47.11
	318.2	301.2	218.4	206.0

A

TABLE 7.10

Summary of Airblast En
(Metric Units)
ESSEX I 6 MS 3
21,594 Pounds Nitromethane Buried 12 Mete

Gage Designation	SLA 1-LO	SLA 1-HI	SLA 2
Gage Range	Low	High	Low
Gage Sensitivity	High	Low	High
Distance (km)	1.0805	1.0805	2.37
Azimuth (rad)	1.838	1.838	1.66
Ground-Shock-Induced Energy Flux (Pa^2-s)	3613.	3708.	827.
1st Negative Pulse Energy Flux (Pa^2-s)	2805.	2852.	599.
Gas Venting Energy Flux (Pa^2-s)	2424.	2472.	537.
2nd Negative Phase Energy Flux (Pa^2-s)	3518.	3565.	751.
Total Energy Flux (Pa^2-s)	12359.	12645.	2710
Ground-Shock-Induced Energy (MJ)	65.14	66.84	72.2
1st Negative Phase Energy (MJ)	50.56	51.42	52.2
Gas Venting Energy (MJ)	43.70	44.56	46.8
2nd Negative Phase Energy (MJ)	63.42	64.28	65.5
Total Energy (MJ)	222.8	227.9	236.

B

TABLE 7.10

Summary of Airblast Energy
(Metric Units)
X I 6 MS 3 October 1973
omethane Buried 12 Meters Deep, Fully Stemmed

	SLA 2-LO	SLA 2-HI	SLA 3-LO	SLA 3-HI
	Low	High	Low	High
	High	Low	High	Low
	2.3774	2.3774	5.8927	5.8927
	1.662	1.662	1.477	1.477
	827.2	774.9	98.40	93.65
	599.0	584.7	99.83	96.03
	537.2	499.1	70.83	68.45
	751.1	713.1	114.6	111.2
	2710.	2572.	384.1	369.4
	72.20	67.63	52.76	50.21
	52.28	51.04	53.53	51.49
	46.89	43.57	37.97	36.71
	65.55	62.23	61.43	59.64
	236.5	224.5	205.9	198.1

TABLE 7.11

Summary of Airblast Energy
(Metric Units)
ESSEX I 6 MS 3 October 1973
21,594 Pounds Nitromethane Buried 6 Meters Deep, F

Gage Designation	SLA 1-LO	SLA 1-HI	SLA 2-LO
Gage Range	Low	High	Low
Gage Sensitivity	High	Low	High
Distance (Ft)	3545.	3545.	7800.
Azimuth (Degrees)	105.3	105.3	95.2
Ground-Shock-Induced Energy Flux (PSI^2-Sec)	.000076	.000078	.0000174
1st Negative Phase Energy Flux (PSI^2-Sec)	.000059	.000060	.0000126
Gas Venting Energy Flux (PSI^2-Sec)	.000051	.000052	.0000113
2nd Negative Phase Energy Flux (PSI^2-Sec)	.000074	.000075	.0000158
Total Energy Flux (PSI^2-Sec)	.000260	.000266	.0000570
Ground-Shock-Induced Energy (In-Lb/10^6)	576.5	591.6	639.0
1st Negative Phase Energy (In-Lb/10^6)	447.5	455.1	462.7
Gas Venting Energy (In-Lb/10^6)	386.8	394.4	415.0
2nd Negative Phase Energy (In-Lb/10^6)	561.3	568.9	580.2
Total Energy (In-Lb/10^6)	1972.	2017.	2093.

B

TABLE 7.11

Summary of Airblast Energy
(Metric Units)
SSEX I 6 MS 3 October 1973
ltromethane Buried 6 Meters Deep, Fully Stemmed

-HI	SLA 2-LO	SLA 2-HI	SLA 3-LO	SLA 3-HI
	Low	High	Low	High
	High	Low	High	Low
	7800.	7800.	19333.	19333.
	95.2	95.2	84.6	84.6
78	.0000174	.0000163	.00000207	.00000197
0	.0000126	.0000123	.00000210	.00000202
2	.0000113	.0000105	.00000149	.00000144
5	.0000158	.0000150	.00000241	.00000234
6	.0000570	.0000541	.00000808	.00000777
	639.0	598.6	467.0	444.4
	462.7	451.7	473.8	455.7
	415.0	385.6	336.1	324.9
	580.2	550.8	543.7	527.9
	2093.	1987.	1822.8	1752.9

A

TABLE 7.12

Summary of Airblast
(Metric Unit
ESSEX I 6MU 24 Oct
17,275 Pounds Nitromethane Buried

Gage Designation	SLA 1-LO	SLA 1-HI	S
Gage Range	Low	High	L
Gage Sensitivity	High	Low	H
Distance (km)	.987	.987	2
Azimuth (rad)	1.515	1.515	1
Flare Pulse Energy Flux (Pa^2-s)	10411.	11884.	2
1st Negative Pulse Energy Flux (Pa^2-s)	1716.	1930.	3
Gas Venting Energy Flux (Pa^2-s)	1749.	1959.	4
2nd Negative Pulse Energy Flux (Pa^2-s)	396.0	432.1	7
Total Energy Flux (Pa^2-s)	14261.	16210.	1
Flare Pulse Energy (MJ)	93.64	106.90	2
1st Negative Pulse Energy (MJ)	15.44	17.36	3
Gas Venting Energy (MJ)	15.74	17.62	3
2nd Negative Pulse Energy (MJ)	3.56	3.89	1
Total Energy (MJ)	128.3	145.8	1

B

TABLE 7.12

Summary of Airblast Energy
(Metric Units)
ESSEX I 6MU 24 October 1973
ds Nitromethane Buried 6 Meters Deep, Unstemmed

-HI	SIA 2-LO	SLA 2-HI	SLA 3-LO	SLA 3-HI
	Low	High	Low	High
	High	Low	High	Low
	2.314	2.314	5.878	5.878
	1.517	1.517	1.417	1.417
	2448.	2453.	193.5	189.2
	334.7	360.8	38.74	38.13
	454.5	404.1	35.65	36.70
	72.26	97.93	9.793	7.178
	3313.	3318.	277.6	271.4
	201.50	201.89	102.75	100.48
	27.54	29.70	20.58	20.25
	37.40	33.26	18.93	19.49
	5.95	8.06	5.20	3.81
	272.7	273.1	147.4	144.2

TABLE 7.13

Summary of Airblast Ene
(Metric Units)
ESSEX I 6MU 24 October
17,275 Pounds Nitromethane Buried 6 Mete

Gage Designation	SLA 1-LO	SLA 1-HI	SLA 2-
Gage Range	Low	High	Low
Gage Sensitivity	High	Low	High
Distance (Ft)	3238.	3238.	7592.
Azimuth (Degrees)	86.8	86.8	86.9
Flare Pulse Energy Flux (PSI^2-Sec)	.000219	.000250	.00005
1st Negative Pulse Energy Flux (PSI^2-Sec)	.0000361	.0000406	.00000
Gas Venting Energy Flux (PSI^2-Sec)	.0000368	.0000412	.00000
2nd Negative Pulse Energy Flux (PSI^2-Sec)	.00000833	.00000909	.00000
Total Energy Flux (PSI^2-Sec)	.000300	.000341	.00006
Flare Pulse Energy (In-Lb/10^6)	828.8	946.1	1783.4
1st Negative Pulse Energy (In-Lb/10^6)	136.6	153.7	243.8
Gas Venting Energy (In-Lb/10^6)	139.3	155.9	331.1
2nd Negative Pulse Energy (In-Lb/10^6)	31.5	34.4	52.6
Total Energy (In-Lb/10^6)	1135.	1291.	2414.

B

TABLE 7.13

Summary of Airblast Energy
(Metric Units)
SSEX I 6MU 24 October 1973
s Nitromethane Buried 6 Meters Deep, Unstemmed

-HI	SLA 2-LO	SLA 2-HI	SLA 3-LO	SLA 3-HI
	Low	High	Low	High
	High	Low	High	Low
	7592.	7592.	19285.	19285.
	86.9	86.9	81.2	81.2
50	.0000515	.0000516	.00000407	.00000398
406	.00000704	.00000759	.000000815	.000000802
412	.00000956	.00000850	.000000750	.000000772
0909	.00000152	.00000206	.000000206	.000000151
41	.0000697	.0000698	.00000584	.00000571
	1783.4	1786.9	909.4	889.3
	243.8	262.8	182.1	179.2
	331.1	294.3	167.6	172.5
	52.6	71.3	46.0	33.7
	2414.	2417.	1305.	1276.

Figure 7.18 shows peak gas-venting overpressure versus distance, and gas-venting impulse is shown in Fig. 7.19. The order for the four shots is the same for overpressure as for impulse.

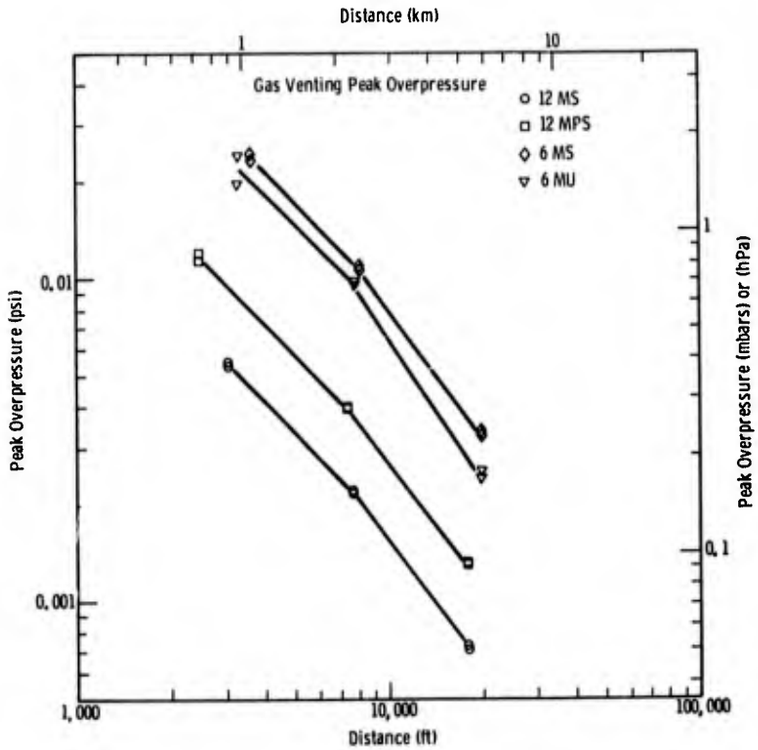

Figure 7.18

Gas venting peak overpressure versus distance

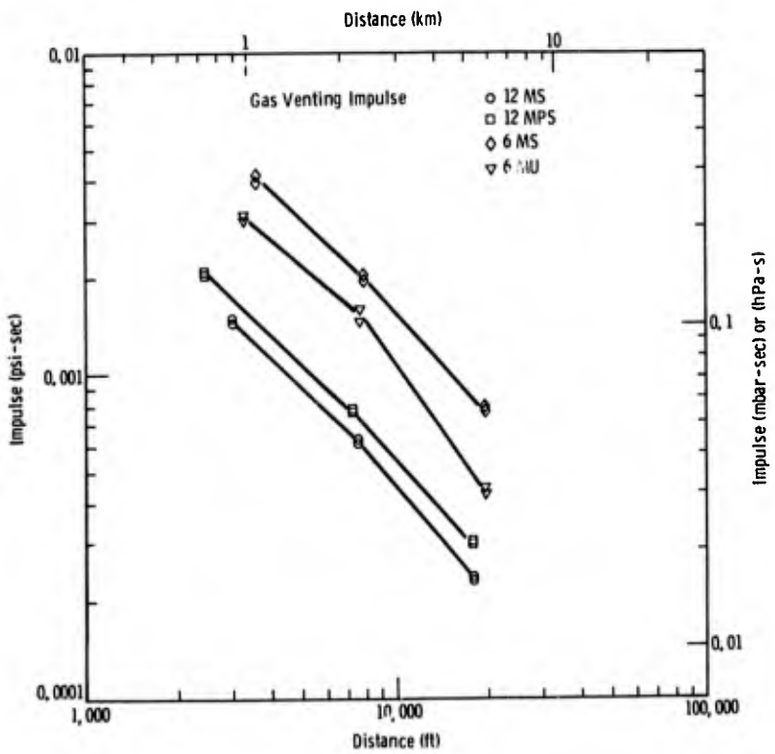

Figure 7.19

Gas venting impulse versus distance

However, whereas the overpressure difference between the 6-m shots is small, and for the 12-m shots is larger, the reverse is true for impulse. If the medium for the two 12-m shots had been exactly the same, and if the 12-MPS open hole had pinched off quickly, both peak overpressure and impulse would be the same except that in 12 MPS they would be slightly smaller by the amount that cavity pressure had been reduced by the earlier escape of gas up the open hole. The fact that gas-venting overpressure and impulse for 12 MPS are larger than for 12 MS indicates that medium effects completely overrode the small effect of the open hole. In the case of the two 6-meter shots the peak overpressure and impulses from the stemmed shot were larger than from the unstemmed shot, as would be expected. However, in view of the large effect of medium differences on the 12-meter shots, it must be observed that if medium differences had been as great on the 6-meter shots, the effect of the large open hole on 6 MU could have been much greater than is indicated by the information shown in Figs. 7.18 and 7.19.

Energy flux versus distance is shown in Figs. 7.20 and 7.21 for the ground-shock-induced pulse and the gas-venting pulse, respectively. The order for the four shots in Fig. 7.21 for the gas-venting pulse is the same as for peak overpressure (Fig. 7.18) and impulse (Fig. 7.19). Because of the large open hole on 6 MU, the energy in the combined ground-shock-induced and flare pulses is larger (Fig. 7.20) than for the unstemmed shot at the same depth, whereas the reverse was true in Fig. 7.21.

The trends displayed by Figs. 7.20 and 7.21 are more apparent in Figs. 7.22 and 7.23 where energy in those components of the blast wave have been obtained by integrating the energy flux over the surface of the hemispherical airblast envelope. Energy for the negative pulses and the entire airblast wave is shown in Figs. 7.24 and 7.25, again as a function of distance. If there had been no differences in medium at the sites of the four shots, the total energy in Fig. 7.25 would have been the same for 12 MS and 12 MPS, the total energy for 6 MU would have been 85% of that of 6 MS because of the smaller charge weight of 6 MU, and the difference between the energy of the two 12-meter shots and that of 6 MS could have been attributed to differences in burial depth. All shots show energy measured at the second station to be more than would be indicated by a straight-line interpolation between the first and third stations. The much larger energy at the second station on the 6 MU shot is attributed to possible meteorological focusing resulting from a stronger-than-usual inversion. This cannot be verified, since atmospheric soundings measured only wind direction and speed.

Having presented the airblast from buried and surface bursts, it is in order for us to examine airblast suppression as a function of charge burial and stemming. Airblast suppression for Project Middle Course II data[28] was determined at a distance of 2,000 feet from 1-ton charges. To be consistent, we will consider airblast from a 1,000-pound surface burst at a distance of $2,000 \times (0.5)^{1/3} = 1,587$ feet. At that distance the half-buried (true surface) burst (AFWL 2) had a positive-phase impulse of 0.0049 psi-sec, and a positive-phase energy of 1,200 in-lb/10^6. (We will ignore the small differences that may result from using different types of explosives.) This will correspond to a positive-phase impulse of 0.0133 psi-sec at 4,308 feet from a 10-ton surface

burst, or 0.0126 psi-sec at 4,082 feet from an 8.5-ton surface burst. For the same distances and charge weights, the positive-phase energies would be 24,000 and 20,400 in-lb/10^6. This permits determination of airblast suppression, as shown in Table 7.14. Since the media in which the stemmed and unstemmed shots were detonated were different, one can approximate what the suppression would have been if they had been detonated in the same medium. This involves assuming that medium does not affect the flare (probably a valid assumption), and that the gas that escapes up the open hole does not appreciably decrease the reservoir of gas in the cavity. This latter assumption is probably reasonable for the 12-meter shots where the hole was quite small and may have pinched off, but it causes overestimation of airblast suppression, and is probably in considerable error in the case of the 6-meter shots.

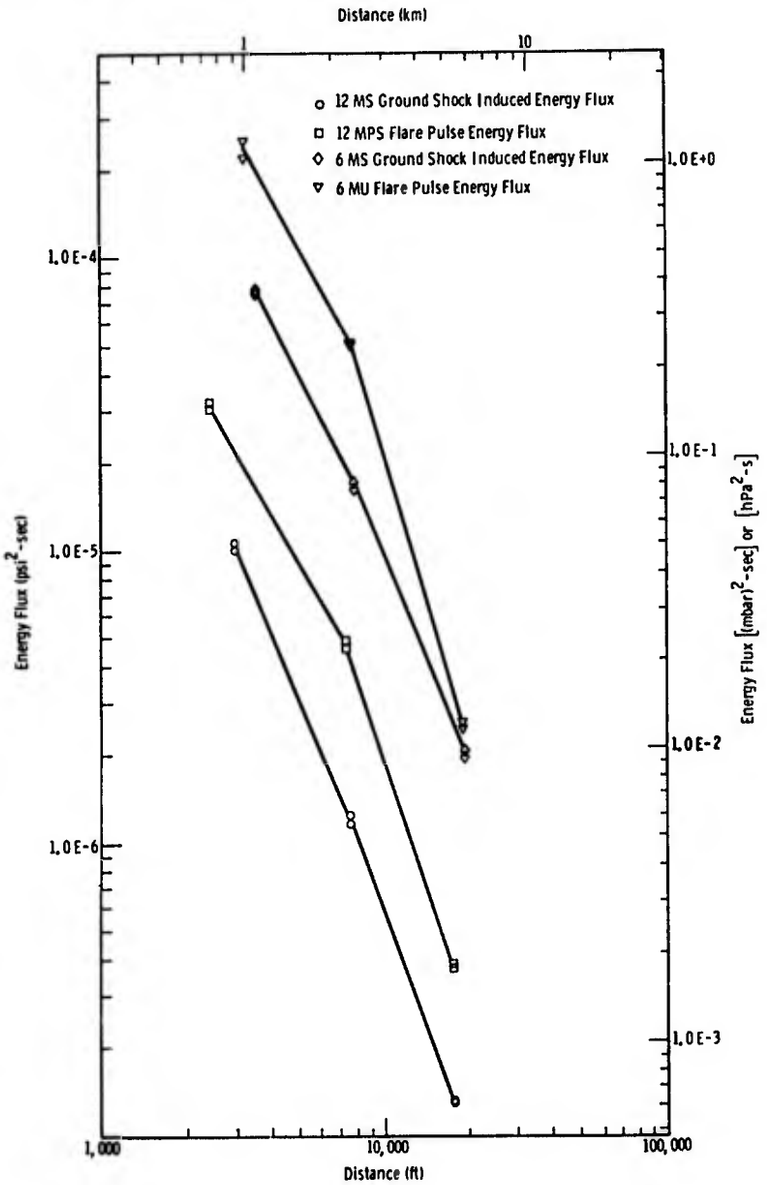

Figure 7.20 Ground-shock-induced energy flux versus distance

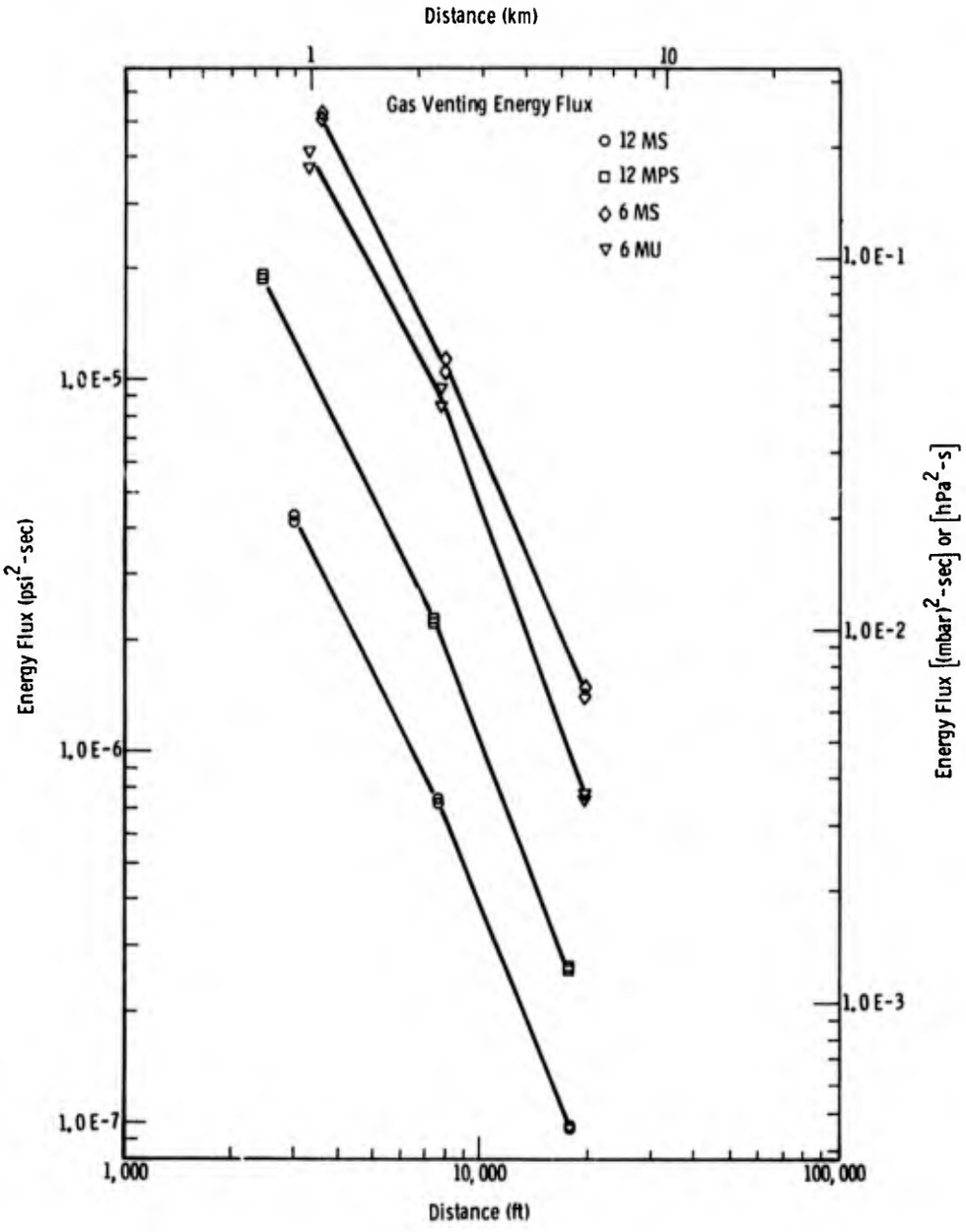

Figure 7.21 Gas venting energy flux versus distance

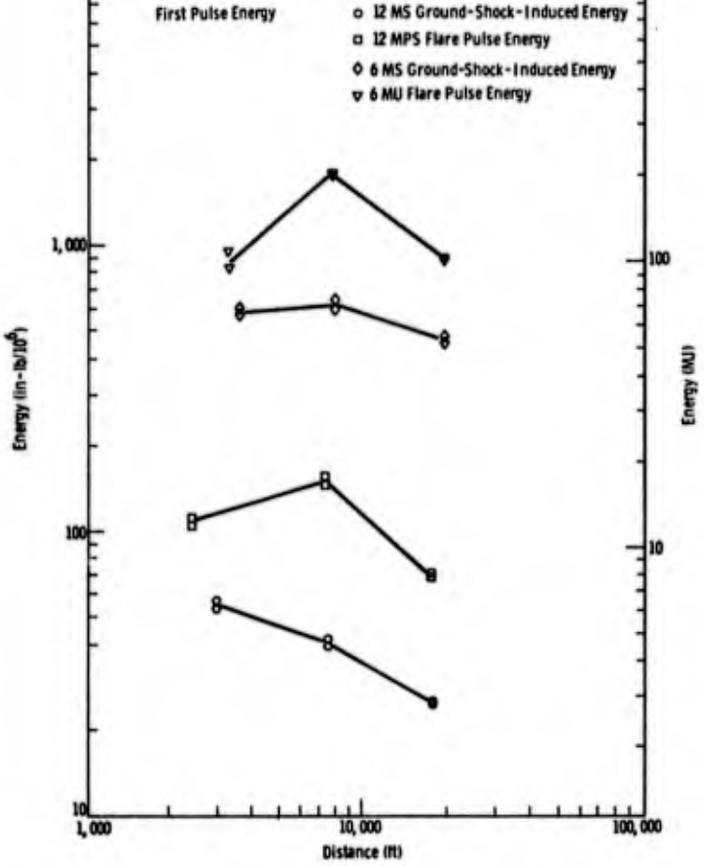

Figure 7.22

Ground-shock-induced energy versus distance

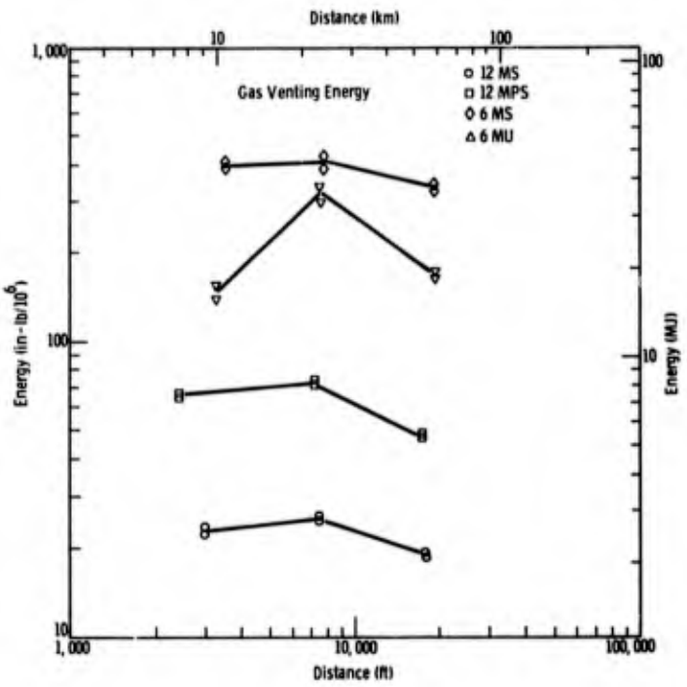

Figure 7.23

Gas venting energy versus distance

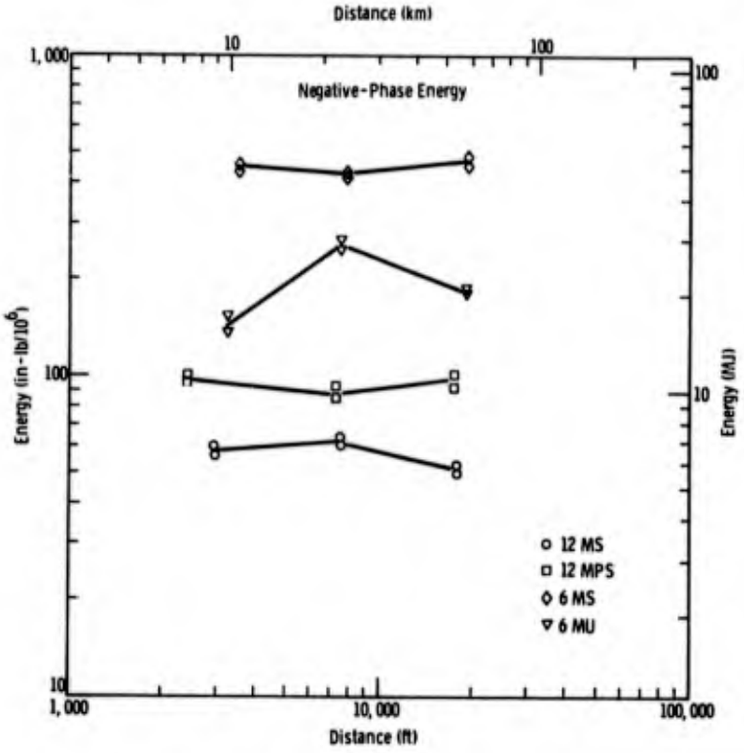

Figure 7. 24

Negative-phase energy versus distance

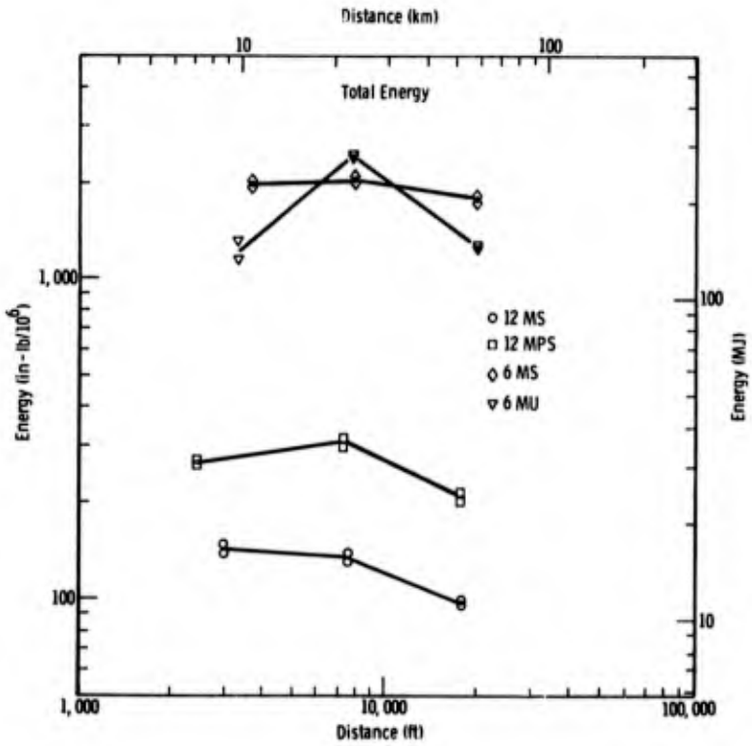

Figure 7. 25

Total airblast energy versus distance

TABLE 7.14

Determination of airblast suppression

	12 MS		12 MPS		6 MS		6 MU	
	Impulse (psi-sec)	Energy (in-lb/10^6)	Impulse (psi-sec)	Energy (in-lb/10^6)	Impulse (psi-sec)	Energy (in-lb/10^6)	Impulse (psi-sec)	Energy (in-lb/10^6)
Gas Venting Pulse	0.00105	23.5	0.00125	70	0.0035	390	0.0026	155-180[a]
Flare Pulse Contribution			0.00026	85			0.0012	305-375[a]
Total	0.00105	23.5	0.00151	155	0.0035	390	0.0038	460-555[a]
Equivalent Surface Burst	0.0133	24,000	0.0133	24,000	0.0133	24,000	0.0126	20,400
Ratio: Total/Surface	0.079	0.00098	0.114	0.0065	0.263	0.0163	0.302	0.0225-0.0272[a]
Gas Venting Pulse[b]	0.00105	23.5			0.0035	390		
Flare Pulse Contribution[b]	0.00026				0.0014[c]			
Total[b]	0.00131				0.0049			
Equivalent Surface Burst	0.0133				0.0133			
Ratio: Total/Surface[b]	0.098				0.368			

(a) The smaller number is from interpolation between Station 1 and 3.

(b) Recalculation to estimate effect if unstemmed shot had been fired in the same medium as stemmed shot.

(c) Scaled from 8.5 to 10 tons.

Figure 7.26 is taken directly from the Middle Course II report.[28] The curves represent the median and the upper and lower limits of radioactivity suppression with scaled charge burial depth for nuclear cratering explosions. Charge burial has been scaled by the cube root of charge yield, multiplied by the density of the overburden above the charge. Airblast-suppression data are from the M-series of Middle Course II and the B-series of Project Trinidad.[27] In adding the Essex data, scaled burial depth was obtained by using averages for densities weighted according to thickness of each geological unit reported to be above the charge by Ehrgott and Stanley.[29]

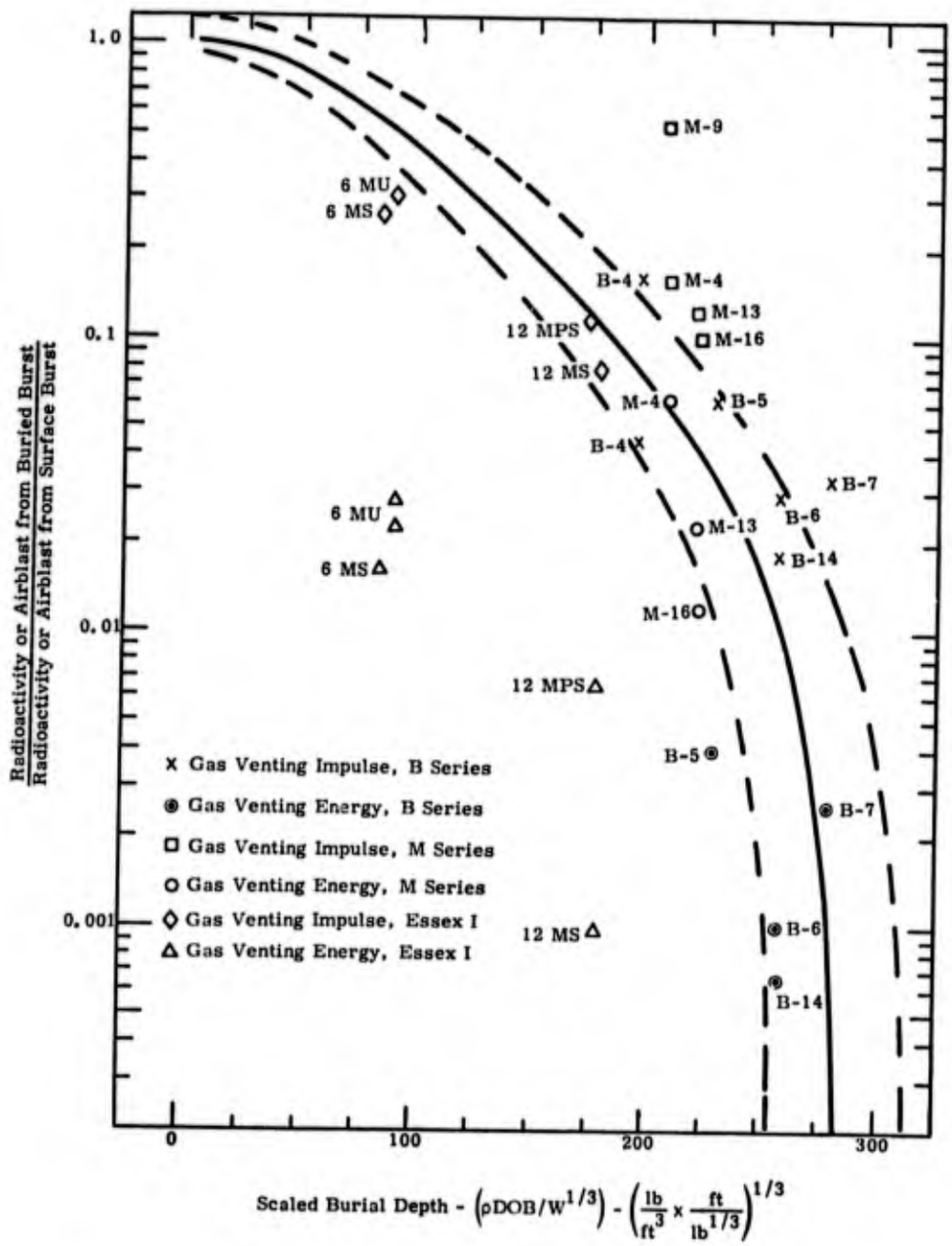

Figure 7.26 Comparison of radioactivity suppression with burial depth against suppression of airblast gas-venting impulse and energy with burial depth

Suppression of Essex airblast impulse was slightly less than would have been expected from the Middle Course and Trinidad results. The B- and M-series used aluminized ammonium nitrate slurry, the AFWL shots were TNT, and the Essex shots were gelled nitromethane. Difference in explosives for the surface bursts could account for only a small difference in blast suppression; they would cause the Essex suppression factors to be about 3 percent higher than those of the B and M series. Differences attributable to the different explosives used for the buried charges cannot be evaluated with information now available. As important as these difference may be, differences in medium that are not accounted for by simple differences in density may be of even greater importance. There is earlier evidence[24, 25, 30] that some wet media greatly diminish or eliminate the gas-venting pulse, apparently because, as the mound grows without rupture, the cavity continues to expand without venting until cavity pressure drops nearly to ambient by the time venting would otherwise occur. Proper accounting for medium differences and better understanding of their effects on airblast may bring Essex suppression into better agreement with that from the other events.

Figure 7.26 also shows suppression of airblast energy from the Essex experiments. For all shots the energy suppression is much greater than suppression of residual radioactivity on the nuclear events. Before Essex data were added to the figure it appeared that airblast-impulse suppression values were on the upper edge of the spread in radioactive suppression data, whereas airblast-energy suppression was on the lower edge. Now it appears that airblast-energy suppression is not a good analogue, and that it only seemed to be because of coincidences having to do with scaled burial depths and suppression values for the B and M series. For the two 6-m shots the difference in energy suppression was about the same as impulse suppression; for the 12-m shots, the energy of the stemmed shot was suppressed much more than that of the partially stemmed shot. The reason is found by comparing the waveforms of the gas-venting pulses (Figs. D-1 and H-1) of the two shots. The amplitude of the pulse of the stemmed shot is considerably less than that of the partially stemmed shot. It is not clear whether the differences are more of those caused by differences in medium or whether they are a result of differences in meteorology.

The results depicted in Fig. 7.26 lead to the conclusion that suppression of impulse of the venting gas is a reasonable analogue to suppression of radioactivity from nuclear explosions, and that the analogue could probably be improved considerably with better understanding of the effect of medium on the gas-venting pulse. In this connection, it should be pointed out that medium effects on suppression of radioactivity are not well understood either, since only a limited number of materials and especially a limited range of moisture contents have been involved in nuclear cratering explosions.

CHAPTER 8

CONCLUSIONS AND RECOMMENDATIONS

It has become customary in reports of this kind to treat conclusions and recommendations in separate sections. Here we depart from that tradition by stating a series of conclusions and then underlining the recommendations that arise logically from those conclusions. We treat separately the recommendations that deal with planning and operational considerations, instrument performance, the medium, and analysis and evaluation of the data.

So that the conclusions and recommendations can appear in proper perspective, it is in order to quote the objectives of the Essex I series.[31]

> b. Technical Objectives. The technical objectives of Project ESSEX, ESSEX I, and ESSEX I, Phase 1, are listed below:
>
> (1) ESSEX.
> (a) Determine the most effective combination of placement and yield to produce barriers and obstacles in a given terrain or geology while minimizing collateral effects.
> (b) Develop methods to estimate the damage to structural targets as a function of yield and location of burst.
> (c) Define that particular combination of minimum yield and best placement that will produce a desired effect.
> (d) Define the governing troop safety criteria and the extent of collateral effects as a function of yield and placement.
> (2) ESSEX I.
> (a) Provide, through numerical calculations and field experiments, a method of simulating nuclear-produced cratering detonations by using high explosives.
> (b) Develop a numerical capability for predicting ADM cratering effects.
> (c) Develop a fallout simulation technique using non-radioactive material.
> (d) Determine the applicability of present high-explosive scaling relationships to low-yield nuclear devices.
> (e) Determine the effects of geology, depth of burial, stemming conditions, yield, and emplacement hole size on:
> 1 obstacle size and shape (considering lip height, crater radius and depth, and side slope angle)
> 2 continuous and discrete ejecta deposition patterns
> 3 ground shock
> 4 nuclear radiation from fallout
> 5 dynamic pressure and peak airblast overpressure from troop safety levels to structural damage levels (to include tree blowdown)
> (f) Determine and demonstrate effectiveness of craters as obstacles or barriers through mobility trials on site.
> (g) Determine troop safety/standoff distances.
> (h) Provide a means of estimating the time required to bypass, breach, or repair an obstacle or barrier created by a nuclear cratering detonation.

(i) Determine the best combination of placement and yield to produce a given crater in a given terrain and geologic media.
(j) Develop and optimize linear cratering techniques (size, shaping) and compare the results to a like crater produced by a larger single nuclear detonation.
(k) Determine methods of tying in craters to natural barriers to optimize obstacle effectiveness.
(l) Determine the feasibility of creating landslides as barriers to mobility considering both the tactical environment and the effect levels required.
(m) Determine collateral effects data for use in targeting studies conducted in ESSEX II-VII.

(3) ESSEX, Phase 1.
(a) Verify, through field experiments, a numerical method of simulating nuclear-produced craters by using high explosives.
(b) Develop a numerical capability for predicting ADM cratering effects.
(c) Determine the effect of a selected geology, depth of burial, varied stemming conditions (full stemming, partial stemming, and no stemming), and two emplacement hole sizes on:
1 obstacle size and shape (considering lip height, crater radius and depth, and side slope angle)
2 continuous and discrete ejecta deposition patterns
3 ground shock
4 nuclear radiation from fallout
5 dynamic and peak airblast overpressures from troop safety levels to structural damage levels (to include tree blowdown)
(d) Demonstrate obstacle effectiveness of the resultant craters.
(e) Determine troop safety standoff distances.
(f) Determine applicability of present HE scaling relationships to low-yield ADM's.
(g) Evaluate a fallout simulation technique using nonradioactive materials.
(h) Determine collateral effects data for use in targeting studies conducted in ESSEX II-VII.

The program objectives are quoted to emphasize that Essex I, Phase 1 had multiple objectives. As is often the case with such programs, the different objectives are not always compatible. The principal purpose of the measurements reported here was to meet objectives (3) (a) and (b) by providing information against which hydrodynamic codes used for numerical simulation could be checked and verified. This can be done best in a very uniform medium. Other objectives, apparently, led to the choice of a site with a medium that was realistic from the viewpoint of tactical employment of ADM's. The authors have concluded that the goal of verifying numerical simulation by hydrodynamic codes could have been better met if the medium had been chosen for great uniformity, without regard for its tactical significance. In the following sections we support this conclusion by establishing the reliability of the measurements and by evaluating the effects of medium differences.

Planning and Operations

Instruments were purchased on the basis of pre-shot predictions, which were based for the most part on hydrodynamic calculations. Peak surface acceleration fell off faster with distance from ground zero than predicted, and instruments at the outer stations were often used at only a

small percentage of gage range. At shot depth the reverse was true; peak acceleration attenuated with distance less rapidly than predicted. In this case, gages at the outer stations were frequently over-ranged. Therefore, if further experiments of this type are to be conducted in an untried medium, it is recommended that one shot be fielded as a calibration event sufficiently ahead of the rest of the series that measurement results from the calibration shot can be used in selecting instrumentation. This recommendation is made despite the fact that the results of 12 MS misled us into making changes in set ranges for 12 MPS that should not have been made.

Hydrodynamic calculations normally yield stress and particle velocity as a function of time. Peak acceleration is then obtained from the derivative of the rise of the particle velocity-time pulse. However, the rise of a calculated particle velocity pulse is strongly dependent on the artifices used in a code to attempt to approximate the shock physics. These artifices include, but are not limited to, artificial viscosity and zone size. To the extent possible with the measurements reported here, it is recommended that those making hydrodynamic calculations attempt to match the acceleration characteristics of some of these measurements by tailoring the related artifices to better reproduce measured results.

The Ft. Polk medium consists of interstratified sands, silts, and clays, and mixtures of those constituents. For the purposes of Essex I, Phase 1, the soils were categorized into six equation-of-state units. If this categorization is too gross, it may not be possible to act upon the above recommendation from the measurements reported here. If so, it is recommended that the sponsors conduct at least one shot of the type reported here, with comparable instrumentation, in as homogeneous a medium as can be found.

To emplace the explosive container in saturated soil it was found necessary to "dewater" the formation at shot depth. This was done by pumping from several wells a few feet from the emplacement hole. After the charge was stemmed, monitoring in a nearby hole indicated that the water had returned to equilibrium. However, there was no measure of other possible changes in the medium such as migration of fines. For future experiments of this type, if the charge cannot be emplaced without dewatering, it is recommended that samples be obtained shortly before shot time to determine whether the medium has become appreciably different than the samples obtained for equation-of-state determinations.

The success of the three-second single and double integrations of surface acceleration records in producing trajectories was not recognized until long after field activities had been completed and the data were being analyzed. It would have been especially helpful in evaluating the accuracy of the trajectories if the terminal position of the canister had been known. By this time, however, craters had been backfilled and the areas around them cleared. It is recommended that on future events a special effort be made to determine terminal position of gage canisters and that the test area not be cleared until data have been analyzed and reported.

Instrument Performance

Lithium-niobate stress gages were used for the first time on this Essex series. They performed very well. Induced signals from other gages of the same type on the 6 MU event are attributed to the signal-conditioning equipment rather than to the gage, even though the mechanism by which the signals were induced is unknown. The gage has the advantage of linear response on loading and unloading, together with a strong electrical output.

Ytterbium gages performed much as had been expected. A lower rate of survival of gages or cables resulted simply from the fact that the ytterbium gages were used for high-stress measurements and lithium niobate for low stresses in places where the electrical output of the ytterbium gages was insufficient.

There were cases of inconsistency in measurement-- 12 MS, SL-1, and -2; 12 MPS, SL-2 and SY-5; and 6 MS, SY-5 and SL-1 and -2; in each case, the gage underlined was considered to have the more reliable record by comparison with stress-distance relationships from other gages on the same shot. These unresolved inconsistencies do not implicate one gage type more than the other; we have concluded that they are a result of human error, the nature of which has not been identified.

In view of linearity during unloading and the strong electrical output of the lithium-niobate gage, it appears to be a promising addition to existing stress-measuring systems. It is recommended that the lithium-niobate gage be evaluated further on other explosive tests.

Four piezoelectric accelerometers were used, two on 6 MS and two on 6 MU. Both gages on 6 MS failed to give usable records. On 6 MU one gage record was limited and the other gave a good record. The reason for the failure on 6 MS has not been determined, so we make no recommendation concerning the piezoelectric gages.

All other accelerometers were piezoresistive and performed especially well. There were a few cases, as noted earlier, where the gages did not appear to respond properly in the negative phase. On 6 MU, the gage sometimes appeared to fail to respond at all to negative acceleration. No reason was obvious. With these two exceptions the gages functioned remarkably well, as evidenced by comparison with other measurements. The first of the comparisons was the especially good agreement between several long-time double integrations of acceleration records and ground-surface displacements versus time measured with high-speed photography. A baseline shift that occurred after signal arrival on a number of records was usually of the order of 0.25 % or less of bandwidth and gage range, which is well within the manufacturer's specifications. We were not able to determine conclusively whether the shift was due to the gage or to associated VCO's and amplifiers. If it resulted from failure of the gage to return precisely to zero, the amount of the shift is so small that the gage cannot be faulted. Nonetheless, we recommend that an effort be made to determine whether the shift is due to failure of the gage to return to zero, and if so, we suggest that the value of the gage for these kinds of applications would be enhanced if the accuracy of the return to zero can be improved.

The second comparison was on 6 MU at the 12-meter station, where there was very good agreement between stress derived from the first integration of the acceleration record and the stress record measured directly.

Not only did all the Slifer time-of-arrival measurements give excellent results, but their accuracy was far better than we had expected. Because the Slifers worked so well, and because time of arrival is a parameter that can be compared with calculated values, it is recommended that Slifer measurements be continued on experiments of this type.

Ported pressure measurements were made inside the open holes of 12 MPS and 6 MU. Failure of gages or cables at early times on both shots merely evidences the harsh environment in which the measurements were attempted. The uncertainty of the interpretation of the record obtained on 12 MPS does not reflect on gage performance. We conclude that our experience with these gages on the two shots is insufficient for gage evaluation.

All pressure gages used for measuring above-ground airblast were of a proven type and performed as expected.

High-speed photography provided a graphic record of surface motion, mound growth, and venting. Most important, it supplied a record of surface displacement that compared quite well with displacement derived from double integration of acceleration records, which gave confidence in double integration of those records for times up to three seconds.

The success of the Essex measurements should be attributed not only to the end instruments, but to the entire system. Special canisters to protect accelerometers, and hydraulic hose to protect cables, improved cable survival and probably increased the time before gage and cable failures, although the environment above 2 kilobars remains harsh in terms of instrument and cable survival. Special credit for data retrieval goes to the three-tiered redundancy described in Chapter 1, especially in view of pre-shot uncertainties in expected ground motion and of the medium differences discussed in the following section. An overall view of the instrumentation effort appears in Table 8.1, which presents results of all measurements made on the four Essex shots, together with notation of a successful measurement, the cause of an unsuccessful record, the duration of recording before gage or cable failure, and other pertinent remarks. From the table the outcome of each channel measured can be assessed. Table 8.2 condenses the Table 8.1 overview to what amounts to a score sheet for the instrumentation effort. The table summarizes the number of measurements of each type made and the number that were successful, and indicates the reasons for unsuccessful measurements. Several points can be made from Table 8.2, backed up by Table 8.1. For most of the ground-motion measurements where the output of a gage was recorded at two sensitivities, the success rate was moderate. The second column of Table 8.2 indicates data losses from both channels of a gage. Because of the redundancy of two gages at a given location, the third column shows that there were very few locations at which measurements were made where at least one successful record was not obtained. The analysis also shows that the largest number of losses were due to the record being limited by band edge. Table 8.2 notes the cases where limiting was so severe that the record consititutes a loss. Comparison of the two tables distinguishes between cases where band-edge limiting caused the record to be a loss and those where it did not. Frequently the loss of a peak could be recovered, or limiting was so small that overall results were not appreciably degraded. Limiting by band edge is a direct result of large variations in medium together with pre-shot uncertainties in the level of motion to be measured. There were only 10 gages (20 channels) that gave records judged to be unreliable, usually because of unexplained instrument response. Table 8.1 also notes those accelerometers where gage range was exceeded. Above the nominal range, gage output becomes increasingly nonlinear. Fortunately, excursions into the nonlinear range ordinarily consisted of very short-duration spikes, inaccuracies in the acceleration peaks contributed negligible error to first and second integrations, and degradation of velocity and displacement measurements was discernible barely if at all.

TABLE 8.1

Summary of ESSEX Records

	Distance (m)	[illegible] Hi Sen	[illegible] Lo Sen	[illegible] Remarks	[illegible] Hi Sen	[illegible] Lo Sen	[illegible] Remarks	[illegible] Hi Sen	[illegible] Lo Sen	[illegible] Remarks	[illegible] Hi Sen	[illegible] Lo Sen	[illegible] Remarks
Stress Gages													
SY-1	8.5 a	L	G	b 13	L,O	L,O	b 2.4	L	G	b 1.2	L,O	L,O	
SY-2	8.5 a	G	G	b 10.5	G	G	b 2.4	G	G	b 1.9	G	G	b 1.0
SL-6	8.5 a										G	G	g
SY-3	6 or 7	L,O	L,O	b 1.1	O	O	b O	G	G	b 1.9	L,O	L,O	
SY-4	6 or 7	G	G	b 0.25	O	O	b O	G	G	b 0.4	G	G	b 0.15, h
SL-5	6 or 7				O	O	b O	L,O	L,O	b 0.4	G	G	g
SY-5	12				G	G		L	G	d	L,O	L,O	b 17.5
SL-1	12	L,O	G	c,d	U	U		L,O	G		D	D	
SL-2	12	G	G		G	G	d	G	G		G	G	b 17.
SL-3	24	NR	NR		G	G		L	G	c,f	L,O	L,O	i
SL-4	24	G	G	c	G	G		G	G	f	L,O	L	i
Accelerometers													
Radial low	6-6,5-3	L,O	G	b 2.5	L,O	L,O		L,O	L,O		L,O	L,O	j
Radial high	6-6,5-3	G	G	b 2.5	L,O	L,O		L,O	L,U		L,O	L,O	j
Horizontal low	12	L,O	L,O	b 0.3	NS	NS		L,O	L,O		L,O	L,O	j, k
Horizontal high	12	L,O	L,O	b 0.3	U	U		G	G	b 13	L,O	L	j
Horizontal low	24	L,O	L	j	U	U		L	[illegible]	j	L,O	L	j
Horizontal high	24	L,O	L	j	U	U	b 180	G	[illegible]	b 2700	G	G	j,k
Vertical	24	L,O	L	j	G	G		L,O	L	j	L	L	j
Tangential	24	L,O	G	j	L,O	L,O		G	G	b 2300, j	G	G	b 1.2, j
Horizontal low	36	L,O	L,O		G	G	f	L	L	j	L	L	j
Horizontal high	36	L,O	L	j	G	G	f	L	L	j	L	L	j
Vertical	36	L,O	L	j	G	G	f	L	L	j	L	L	j
Tangential	36	L,O	G	b 2950	G	G	f	G	G		L	L	j
Vertical low	0-0	L,O	G	b 400	G	G	b 360	L	G	h	L,O	L,O	b 6.5
Vertical high	0-0	G	G	b 400	G	G	b 2.7	U	U		L,O	L,O	b 4.5
Horizontal	0-0				G	G	b 350, f				G	G	b 0.5, f
Vertical	9-0	G	G	b 1600, f	L,O	O	b 2950	U	U		G	G	f
Horizontal	9-0							G	G	b 450			
Vertical	12-0	G	G	b 2400, f	G	G	b 2950	G	G	b > 3000, f	G	G	l
Horizontal	12-0	G	G	b 2400, f	L	G	b 2950	G	G	b > 3000, f	U	U	b 0.5
Vertical	18-0	G	G	b 2200, f				G	G	b 1800, f	G	G	b > 3000, f
Horizontal	18-0							G	G	b 1800, f	G	G	b > 3000, f
Vertical	24-0	G	G	b 2900	L	G	b 2700	G	G	b 2700, f	G	G	b 2400, f
Horizontal	24-0	G	G	b 2900, f	G	G	b 2950, f	G	G	b 2700, f	G	G	b 2400, f
Slifers													
1		G			G			G			G		
2					G		m				G		
3					G						G		
Ported Pressure Gages													
P1 low					U						O	O	
P2 high					G		b 8				O	O	
BRL A											G		b 0.3
BRL B											O		
Airblast													
SLA 1		G	G		G	G		G	G		G	G	
SLA 2		G	G		G	G		G	G		G	G	
SLA 3		G	G		G	G		G	G		G	G	
BRL 1		G	G	b 300	G	G		L	G	b 4	G		b 0.7
BRL 2		G	G	b 1300	L	G	l	L	G		NR		
BRL 3		G	G	b > 5000, f	L	D		G	G	b 2070	G		
BRL 4											G		
BRL 5											G	G	
BRL 6											G		f

a At half shot depth.
b Gage or cable failure at ___msec after shock arrival. If no time is cited for failure, the gage and cable survived through the period of useful data.
c Record sustained and emp-induced baseline shift.
d Record does not agree with record of other gage or gages at the same location.
f Record noisy because of low signal amplitude, especially for low sensitivity channel.
g Value of the record is reduced by interference from induced signal from another gage.
h Peak value only.
j Peak exceeded nominal range of gage.
k Record indicates gage did not respond to negative signal.
l Gage underwent major baseline shift.
m Gage damaged during construction.

D Gage disconnected before shot time.
G Good record.
L Peak limited by band edge.
NR No record.
NS No signal on record.
O No useable data.
U Unreliable measurement.
} Gages paired at same location.

TABLE 8.2

Digest of Essex Instrumentation (all shots)

(First number is number installed, second number represents useful data returned)

	Channels	Gages	Locations
Stress	78 - 49[a]	39 - 26[b]	16 - 15[c]
Acceleration at shot depth	96 - 53[d]	48 - 32[e]	16 - 10[f]
Acceleration at surface	72 - 59[g]	36 - 31[h]	20 - 20
Slifer	8 - 8	8 - 8	8 - 8
Ported pressure	8 - 2[i]	6 - 2[j]	2 - 2
BRL airblast	24 - 22[k]	24 - 22[l]	15 - 14[m]
SLA airblast	24 - 24	24 - 24	12 - 12
Total for four Essex shots	310 - 217	185 - 145	89 - 81
AFWL airblast	30 - 30	30 - 30	15 - 15
Total for Essex series	340 - 247	215 - 175	104 - 96

Summary of data losses

	(a)	(b)	(c)	(d)	(e)	(f)	(g)	(h)	(i)	(j)	(k)	(l)	(m)
Limited by band edge	17	7		35	12	4	7	2					
Unreliable data	8	4	1	6	3	2	6	3					
Deleted before shot	2	1									1	1	
No record	2	1									1	1	1
No signal				2	1				6	4			
Total	29	13	1	43	16	6	13	5	6	4	2	2	1

Of a total of 340 channels installed, 247 (73%) provided useful data. Of the 215 gages used, at least one usable record was obtained from each of 175 (81%). And, most important, of the 104 locations from which information was desired, at least one useful record was obtained from each of 96 (92%).

Measurements made on the four shots provided a number of checks for internal consistency. Where two like gages at the same location provided records, a measure of the differences attributable to gages of the same type was obtained. Where stress gages of different types were installed at the same location they provided a check of one against the other. Where a stress and an acceleration measurement were made at the same location, stress derived from the first integration of the acceleration record made it possible to check stress against the acceleration measurement. Where acceleration records from gages at shot depth could be singly and doubly integrated to quiescence, confidence in the measurement could be established. Where this could be done for gages near the surface, the displacement could be compared directly with surface motion observed with high-speed

photography. We believe the Essex measurements to constitute a set that is unusual if not unique in these checks for internal consistency, and it is recommended that a similar instrumentation philosophy (i.e., redundance) be used on similar future experiments.

Medium Effects

There were differences in medium within single sites as well as between sites. Site selection was based on an exploratory hole drilled at or near each ground zero. Vertical stratigraphy was determined from each hole, and the material was categorized as one of six equation-of-state units. Interfaces between units were determined from the samples. Not all units appeared at each site.

The subtle medium differences that existed at each shot site appear to have been greater for 12 MS than for the other shots. Exploratory drilling had revealed a layer at shot depth that was more competent than the surrounding material, and could be characterized as a weak siltstone. Later drilling of instrument holes showed that this layer extended at shot depth along the azimuth at which the SLA measurements were made. Instrument holes drilled on another azimuth only 20^{o} clockwise from the first did not encounter the more competent layer at shot horizon, indicating that the layer dipped below the horizon in that direction. Measured sonic velocity at the shot horizon in this layer was about 2 m/msec, well above that used for design of the stemming grout.

These differences within the same site were reflected in the measurements. Accelerations at shot depth were greater than predicted, resulting in numerous records with peaks limited by band edge. Signals recorded from accelerometers, stress gages, and Slifers out to 9 meters from the vertical axis through the charge are consistent with refractions outward from the grout column into the surrounding lower-velocity medium, and later back from the surrounding medium into the column.

Where there are differences between measured and calculated parameters, they can be ascribed to an inaccurate measurement or an inaccurate calculation. The redundancy used here of two gages of each type and two types of gages at some locations was an effort to reduce measurement inaccuracy as much as possible--an effort we believe to have been fruitful. Calculation inaccuracies may be caused by inadequacy of the code itself (mathematical modeling, numerics, etc.) or by inadequacy of input describing the medium. If this input is accurate, the results of precise measurements can be used to improve the code. Code verification demands precise measurements and accurate description of the medium. Even if we grant inaccuracies in a code, their extent and type can be evaluated only to the extent of uncertainties about the accuracy with which the medium is described. Thus, we believe that the precision with which the medium is described is the essence of code verification. This precision, in turn, has two components: the accuracy with which equation-of-state measurements are made from soil samples, and whether the number of samples obtained is sufficient to describe the medium in a macroscopic sense. Therefore, if the experiment were to be repeated under the same circumstances (a non-uniform medium), we would recommend that equation-of-state measurements be obtained from numerous samples obtained in the vicinity where measurements are to be made, especially at the lower stress levels. Figure 3.12 well illustrates the need for accurate information at these levels. The stresses calculated by LLL above 1 kilobar agree well with (though are slightly below) measured stresses. This is to be expected because code inaccuracies increase

with distance and subtle differences in equations of state are relatively less important at the high stress level. Below 1 kilobar, LLL calculated stress versus distance using both the equation of state from samples recovered from the exploratory hole (solid curve), and later a modified equation of state that was more nearly in agreement with the competent layer at the charge horizon (long dashed curve). At 25 meters there is almost a factor of four between the two curves.

The upper LLL curve agrees well with peak stress derived from the vector sum of three measured components of particle velocity. The vector sum is a more accurate representation when shear velocities are small than when they are large. A lower limit is obtained from peak radial velocity alone. The fact that acceleration measurements made at 36 meters provided a consistent set with three-second first integrations which, like acceleration, had returned to quiescence, and second integrations that show a constant residual displacement, leads to confidence in the stress derived from acceleration measurements. The peak stress measured directly at 24 meters falls below derived stress, and we conclude that the former is the better of the two.

We conclude that the nonuniform medium significantly reduced the accuracy with which numerical simulation could be verified for the reasons cited above, especially at lower stress levels. In any future test where measurements are made for code verification purposes, it is recommended that the tests be done in a homogeneous medium. Further, it is recommended that measurements not be made if the medium is as heterogeneous as that at Ft. Polk unless the number of locations at which equation-of-state determinations are made is sufficiently large to thoroughly represent the heterogeneity. Even so, it will be quite some time before numerical-simulation techniques reach the point where results of measurements in heterogeneous media are useful in refining numerical codes. Although numerical-simulation techniques have reached the point where measurements in heterogeneous stratified media can be compared with calculated values, the precision required to detect differences that would be useful in refining numerical codes is not as easily achieved as in a homogeneous medium.

The principal purpose of the 12 MPS event was to evaluate, by direct comparison with the 12 MS shot, the effect of a small-diameter open hole on ground motion and cratering. It was expected that the bottom of the hole would pinch off quite early and that the differences would be small and associated with loss of a small portion of energy up the open hole. While it appears that the hole did pinch off, neither photography, ported pressure measurements, nor airblast provided conclusive proof that it did so. The effects of the open hole were indeed small, as had been expected, but medium differences at the two sites were so great as to grossly obscure the effects of differences in stemming. The effects of medium differences are made evident by comparing for the two shots the measured stresses, ground-motion measurements at shot depth and on the surface, mound growth, and, especially, airblast. It is recommended that no further experimental attempt be made to assess the effect of the partial stemming of penetrator emplacement unless both a partially stemmed and a fully stemmed identical shot can be done in as homogeneous a medium as can be found.

Airblast

Airblast measurements made on the AFWL 1,000-pound surface and near-surface bursts were consistent. Because differences in height of burst and depth of burst were small (± 1 charge radius), the differences in airblast are especially subtle. We conclude that when such measurements are made under conditions of different meteorology for each shot that meteorological effects exceed and

obscure the effects of charge position. Therefore, it is recommended that airblast measurements not be made in the future on such near-surface series unless the shots can be detonated at intervals of a few minutes to remove meteorology as a variable.

Airblast measurements were made on the four buried shots for the purpose of evaluating suppression of airblast as an analogue of suppression of radioactivity. The differences in airblast suppression between the stemmed and partially stemmed 12-meter shots were overridden by effects of the differences in medium. Even so, we were able to determine that the gas escaping from the small open hole constituted less than 20 percent of the total gas-venting impulse. We conclude from a comparison of suppression of airblast on the two stemmed shots with suppression of radioactivity from nuclear cratering events that the suppression of gas-venting impulse is a reasonable analogue of suppression of radioactivity, and recommend that investigation of this analogue be pursued on future shots as an alternative to a radioactivity simulant.

References

1. Military Engineering with Nuclear Explosives, DASA 1669, Nuclear Cratering Group, U. S. Corps of Engineers, Livermore, California, June 1966.
2. Project Tank Trap, Technical Report No. 17, U. S. Army Engineer Nuclear Cratering Group, Livermore, California, and Land Locomotion Laboratory, U. S. Army Tank-Automotive Command, Warren, Michigan, June 1969.
3. Blackmon, C. A., and A. A. Rula, Event Dial Pack, Project LN309: Effectiveness of Craters as Barriers to Mobility, Miscellaneous Paper M-71-4, U. S. Army Engineer Waterways Experiment Station, Vicksburg, Mississippi, March 1971.
4. Caudle, W. N., A. Y. Pope, R. L. McNeill, and B. E. Margason, The Feasibility of Rapid Soil Investigations Using High-Speed, Earth-Penetrating Projectiles, SC-R-68-1736, Sandia Laboratories, New Mexico, August 1967.
5. Colp, John L., Terradynamics: A Study of Projectile Penetration of Natural Earth Materials, SC-DR-68-215, Sandia Laboratories, Albuquerque, New Mexico, June 1968.
6. Young, C. Wayne, "Depth Prediction for Earth-Penetrating Projectiles," Journal of the Soil Mechanics and Foundations Division, Proceedings of the American Society of Civil Engineers, pp. 803-817, May 1969.
7. Young, C. W., Empirical Equations for Predicting Penetration Performance in Layered Earth Materials for Complex Penetrator Configurations, SC-DR-72 0523, Sandia Laboratories, Albuquerque, New Mexico, December 1972.
8. Heusinkveld, M., and F. Holzer, "A Method of Continuous Shock Front Position Measurement," Review of Scientific Instruments, 35, 1105-1107, 1963.
9. Smith, C. W., D. E. Grady, L. Seaman, and C. F. Petersen, Constitutive Relations from IN SITU Lagrangian Measurements of Stress and Particle Velocity, DNA 2883I, Stanford Research Institute, Menlo Park, California, January 1972.
10. Ginsberg, M. J., Calibration and Characterization of Ytterbium Stress Transducers, DNA 2742F, Stanford Research Institute, Menlo Park, California, October 1971.
11. Graham, R. A., "Strain Dependence of the Piezoelectric Polarization of Z-Cut Lithium Niobate," Solid State Communications, Vol. 12, pp. 503-506, 1973.
12. Graham, R. A., "Pressure Dependence of the Piezoelectric Polarization of Lithium Niobate," 1973 Ultrasonics Symposium, Monterey, California, November 4-6, 1973.
13. Graham, R. A., and R. D. Jacobson, "Lithium Niobate Stress Gauge for Pulsed Radiation Deposition Studies," Applied Physics Letters, to be published.
14. Vortman, L. J., and J. W. Long, Methods of Processing, Evaluating, and Recovering Airblast Data, SC-RR-72 0634, Sandia Laboratories, Albuquerque, New Mexico, December 1973.
15. Vortman, L. J., 20-Ton HE Cratering Experiments in Desert Alluvium, Project Stagecoach, SC-4596(RR), Sandia Laboratories, Albuquerque, New Mexico, May 1962.
16. Vortman, L. J., 20-Ton and 1/2-Ton High Explosive Cratering Experiments in Basalt Rock, SC-4675(RR), Sandia Laboratories, Albuquerque, New Mexico, August 1962.
17. Perret, W. R., A. J. Chabai, J. W. Reed, and L. J. Vortman, Project Scooter, Sandia Laboratories, Albuquerque, New Mexico, October 1963.
18. Memorandum from B. Mather, Waterways Experiment Experiment Station to Director, Explosive Excavation Research Laboratory, Subject: "Grout Design for ESSEX I at Fort Polk," April 26, 1973.
19. Letter from J. B. Bryan and Donald E. Burton, Lawrence Livermore Laboratory, to Major Richard Gates, Explosive Excavation Research Laboratory, August 14, 1973.
20. Verbal communication with R. C. Bass, Sandia Laboratories, Albuquerque, New Mexico.
21. Verbal communication with L. D. Tyler, Sandia Laboratories, Albuquerque, New Mexico.

22. Written communication with T. R. Blake, Systems, Science and Software, La Jolla, California, May 3, 1974.

23. Verbal communication with R. A. Shunk, Science Applications, Inc., Albuquerque, New Mexico.

24. Cress, J. P., J. E. Lattery, J. B. Andrews, F. F. Warden, and L. J. Vortman, Project Pre-Gondola III, Phase I, Summary Report, PNE 1114, U. S. Army Engineer Nuclear Cratering Group, Livermore, California, April 1970.

25. Vortman, L. J., Airblast from Project Tugboat Detonations, SC-RR-70-541, Sandia Laboratories, Albuquerque, New Mexico, November 1970.

26. Vortman, L. J., Airblast Measurements, Project Diamond Ore, Phase IIB, SLA-73-0353, Sandia Laboratories, Albuquerque, New Mexico, to be published.

27. Vortman, L. J., Airblast from Project Trinidad Detonations, SC-RR-71 0056, Sandia Laboratories, Albuquerque, New Mexico, July 1971.

28. Vortman, L. J., Project Middle Course II Airblast and Surface Motion, SC-RR-72 0342, Sandia Laboratories, Albuquerque, New Mexico, December 1972.

29. Ehrgott, J. Q., and R. L. Stanley, Material Property Investigation for Essex I, Test Site at Ft. Polk, Louisiana, U. S. Army Engineer Waterways Experiment Station, Vicksburg, Mississippi, July 1973.

30. Keefer, J. M., W. F. Jackson, and D. P. Lefevre, Close-in Airblast from a Row of Buried Charges, Ballistic Research Laboratories, Aberdeen Proving Ground, Maryland; also chapter in Project PreGondola II, Summary Report, PNE 1112, U. S. Army Corps of Engineers, Nuclear Cratering Group, Livermore, California, February 1971.

31. Harvey, William T., Technical Concept, Project Essex, Phase I, U. S. Army Engineer Waterways Experiment Station, Explosive Excavation Research Laboratory, Livermore, California, undated.